Innovative Solutions for Slope Stability Reinforcement and Characterization: Vol. III

Final Report
December 2005

Sponsored by
the Iowa Highway Research Board
(IHRB Project TR-489)
and
the Iowa Department of Transportation
(CTRE Project 03-127)

ctre
Center for Transportation
Research and Education

IOWA STATE
UNIVERSITY

Iowa State University's Center for Transportation Research and Education is the umbrella organization for the following centers and programs: Bridge Engineering Center • Center for Weather Impacts on Mobility and Safety • Construction Management & Technology • Iowa Local Technical Assistance Program • Iowa Traffic Safety Data Service • Midwest Transportation Consortium • National Concrete Pavement Technology Center • Partnership for Geotechnical Advancement • Roadway Infrastructure Management and Operations Systems • Statewide Urban Design and Specifications • Traffic Safety and Operations

About the PGA

The mission of the Partnership for Geotechnical Advancement is to increase highway performance in a cost-effective manner by developing and implementing methods, materials, and technologies to solve highway construction problems in a continuing and sustainable manner.

Disclaimer Notice

The contents of this report reflect the views of the authors, who are responsible for the facts and the accuracy of the information presented herein. The opinions, findings, and conclusions expressed in this publication are those of the authors and not necessarily those of the sponsors.

The sponsors assume no liability for the contents or use of the information contained in this document. This report does not constitute a standard, specification, or regulation.

The sponsors do not endorse products or manufacturers. Trademarks or manufacturers' names appear in this report only because they are considered essential to the objective of the document.

Non-discrimination Statement

Iowa State University does not discriminate on the basis of race, color, age, religion, national origin, sexual orientation, gender identity, sex, marital status, disability, or status as a U.S. veteran. Inquiries can be directed to the Director of Equal Opportunity and Diversity at Iowa State University, (515) 294-7612.

Technical Report Documentation Page

1. Report No. IHRB Project TR-489	2. Government Accession No.	3. Recipient's Catalog No.	
4. Title and Subtitle Innovative Solutions for Slope Stability Reinforcement and Characterization: Vol. III		**5. Report Date** December 2005 **6. Performing Organization Code**	
7. Author(s) Mark Thompson, David J. White, and Vernon R. Schaefer		**8. Performing Organization Report No.** CTRE Project 03-127	
9. Performing Organization Name and Address Center for Transportation Research and Education Iowa State University 2901 South Loop Drive, Suite 3100 Ames, IA 50010-8634		**10. Work Unit No. (TRAIS)** **11. Contract or Grant No.**	
12. Sponsoring Organization Name and Address Iowa Highway Research Board Iowa Department of Transportation 800 Lincoln Way Ames, IA 50010		**13. Type of Report and Period Covered** Final Report **14. Sponsoring Agency Code**	
15. Supplementary Notes Visit www.ctre.iastate.edu for color PDF files of this and other research reports			

16. Abstract

Soil slope instability concerning highway infrastructure is an ongoing problem in Iowa, as slope failures endanger public safety and continue to result in costly repair work. Volume I of this current study summarizes research methods and findings, while Volume II provides procedural details for incorporating into practice an infrequently-used testing technique–borehole shear tests. Volume III of this study of field investigation of fifteen slopes in Iowa demonstrates through further experimental testing how lateral forces develop along stabilizing piles to resist slope movements.

Results establish the feasibility of an alternative stabilization approach utilizing small-diameter pile elements. Also, a step-by-step procedure that can be used by both state and county transportation agencies to design slope reinforcement using slender piles is documented. Initial evidence of the efficiency and cost-effectiveness of stabilizing nuisance slope failures with grouted micropiles is presented. Employment of the remediation alternative is deemed more appropriate for stabilizing shallow slope failures.

Overall, work accomplished in this research study included completing a comprehensive literature review on the state of the knowledge of slope stability and slope stabilization, the preparation and performance of fourteen full-scale pile load tests, the analysis of load test results, and the documentation of a design methodology for implementing the technology into current practices of slope stabilization. Recommendations for further research include monitoring pilot studies of slope reinforcement with grouted micropiles, supplementary experimental studies, and advanced numerical studies.

17. Key Words	18. Distribution Statement		
alternative stabilization approach—borehole shear testing—grouted micropiles—lateral soil movement—load transfer—remedial measures—slope stability—small-diameter pile—soil slope instability	No restrictions.		
19. Security Classification (of this report)	**20. Security Classification (of this page)**	**21. No. of Pages**	**22. Price**
Unclassified.	Unclassified.	247	NA

INNOVATIVE SOLUTIONS FOR SLOPE STABILITY REINFORCEMENT AND CHARACTERIZATION: VOL. III

Final Report
December 2005

Principal Investigator
David J. White
Assistant Professor, Iowa State University

Co-Principal Investigator
Vernon R. Schaefer
Professor, Iowa State University

Research Assistant
Mark J. Thompson
Iowa State University

Sponsored by
the Iowa Highway Research Board
(IHRB Project TR-489)

Preparation of this report was financed in part
through funds provided by the Iowa Department of Transportation
through its research management agreement with the
Center for Transportation Research and Education,
CTRE Project 03-127.

A report from
Center for Transportation Research and Education
Iowa State University
2901 South Loop Drive, Suite 3100
Ames, IA 50010-8632
Phone: 515-294-8103
Fax: 515-294-0467
www.ctre.iastate.edu

TABLE OF CONTENTS

LIST OF FIGURES

LIST OF TABLES

ACKNOWLEDGMENTS

The Iowa Department of Transportation and the Iowa Highway Research Board sponsored this study under contract TR-489. The authors are grateful for the sponsorship.

The authors would like to thank the following persons: Gary Kretlow Jr. (Iowa DOT) and Robert Stanley (Iowa DOT), for their help in collecting desk information on the slope failures; Dr. Muhannad Suleiman and Bhooshan Karnik (CH2M Hill), for their help during part of the field work; Donald Davidson Jr., Matt Birchmier, and Sherry Voros, for their help in the laboratory work; and Scott Schlorholtz, for his advice in the XRD tests.

The authors also would like to acknowledge the following undergraduate students: Ashley Schwall, who performed the XRD tests; Martinique Martineau, Matz D. Jungmann, Andy S. Floy, Jesse J. Clark, Christopher E. Milner, and Michael K. Richardson who helped in field tests.

The findings, opinions, recommendations, and conclusions expressed in this report are those of the authors and do not necessarily reflect the views of the sponsor and administrations.

EXECUTIVE SUMMARY

Soil slope instability concerning highway infrastructure is an ongoing problem in Iowa, as slope failures endanger public safety and continue to result in costly repair work. This research consists of field investigations addressing both the characterization and reinforcement of such slope failures. The research methods and findings of these investigations are summarized in Volume 1 of this report. Research details of the independent characterization and reinforcement investigations are provided in Volumes 2 and 3, respectively. Combined, the field investigations offer guidance on identifying the factors that affect slope stability at a particular location and also on designing slope reinforcement using pile elements for cases where remedial measures are necessary.

Research Summary

Characterization of slope failures is complicated, because the factors affecting slope stability can be difficult to discern and measure, particularly soil shear strength parameters. Extensive research has been conducted on slope stability investigations and analysis. The current research, however, focused on applying an infrequently-used testing technique comprised of the Borehole Shear Test (BST). This in-situ test rapidly provides effective (i.e., drained) shear strength parameter values of soil. Using the BST device, fifteen Iowa slopes (fourteen failures and one proposed slope) were investigated and documented. Particular attention was paid to highly weathered shale and glacial till soil deposits, which have both been associated with slope failures in the southern Iowa drift region. Conventional laboratory tests, including direct shear tests, triaxial compression tests, and ring shear tests were also performed on undisturbed and reconstituted soil samples to supplement BST results. The shear strength measurements were incorporated into complete evaluations of slope stability using both limit equilibrium and probabilistic analyses.

Remediation of slope failures requires stabilization alternatives that address causes of slope instability. Slope reinforcement using pile elements can be an effective method of remediation in preventing slope movements in weak soils where enhanced drainage does not provide adequate stability. Soil load transfer to pile elements from the downslope soil movement as occurs in slope failures is a complex soil–structure interaction problem. Soil–structure interactions for small-diameter, grouted pile elements subject to lateral soil movement were investigated by conducting full-scale pile load tests, in which piles installed through a shear box into stable soil were loaded by uniform lateral translation of soil. Instrumentation of the shear boxes and pile reinforcement indicated the load distributions that developed along the piles. The load test analyses which followed the pile load tests support the claim that the distributed loads which are mobilized during pile loading depend on the relative displacement between the soil and pile elements. The reliable estimation of these load distributions is important, because the influence of piles on the global stability of the slope depends directly on the pile loading condition.

Research Conclusions

The following conclusions were drawn from slope stability case histories:

- The Borehole Shear Test often measures peak shear strength parameters, which are generally not operative for a slope failure, and sometimes measures the soften shear strength when the measurements are taken near the slip surface. Factors of safety for case histories of slope failures calculated using BSTs were generally greater than unity.
- The ring shear test using reconstituted samples gives residual shear strength parameter values corresponding to relatively large shear displacements. Factors of safety for case histories of slope failures calculated using ring shear test results were generally less than unity.
- Back calculated shear strengths for slope failures that provided factors of safety equal to unity were generally between shear strengths from ring shear tests and Borehole Shear Tests. Slope failures can be attributed to soil softening or progressive failure and may have been caused by high water tables.
- For some slope failures, the use of the BST are useful in better estimating the operative (or the mobilized) shear strength in conjunction with the residual shear strength and back calculated shear strength.
- For the slope failures, the glacial tills generally have lower clay fraction and lower plasticity index than the clay shales. All the tills are classified as low plasticity clay (CL) according to Unified Soil Classification System, while most of the shales are classified as high plasticity clay (CH).
- The peak BST results for the slope failures show that, the glacial tills and the clay shales have similar average values of effective friction angle, which are 22.5^{o} and 22.1^{o}, respectively; but the glacial tills have considerably lower average value of effective cohesion (11.6 kPa) than the clay shales (17.7 kPa). However, the glacial tills have higher residual shear strength (residual friction angle of 8.4^{o} to 26.9^{o}) than the clay shales (residual friction angle of 6.2^{o} to 15.1^{o}).
- Sensitivity analyses showed that soil shear strength is the most sensitive parameter affecting factors of safety. Water table location additionally has a significant influence on slope stability.
- Probabilistic slope stability analyses are useful when a relatively large amount of input parameters are available, such as shear strengths obtained from BSTs. The probability of slope failure is evaluated based on statistical distribution of soil shear strengths.

The following conclusions were drawn from investigating pile reinforcement:

- The installation of slender piles in weak soils offers considerable resistance to lateral soil movement, with improvement factors from the load tests ranging from 1.2 to 6.6. Improvement factors are defined as a ratio of peak loads for reinforced tests and unreinforced tests.

- Pile section moment capacities were mobilized, indicating that a "flexible" pile failure mode was achieved. The depth of maximum moment and pile failure ranged from 1.8 to 5.4 pile diameters below the shear plane.
- The relative soil-pile displacement at the soil surface indicates the behavioral stages of small-diameter piles as (1) mobilization of soil shear stresses and elastic bending of pile, (2) mobilization of pile concrete compressive strength, and (3) incipient pile failure due to pile moment capacity mobilization. The behavioral characteristics of slender piles are controlled by structural pile behavior through moment-curvature relationships as much as they are by soil behavior.
- Displacement-based lateral response analysis methods which use soil p-y curves accurately predict the deflection and bending moment of piles subject to lateral soil movement. From these pile behavior characteristics, pile shear may be calculated and applied to the limit equilibrium equation for evaluating global stability of reinforced slopes.

Recommendations for Implementation

The research findings are expected to benefit civil and geotechnical engineers of government transportation agencies, consultants, and contractors dealing with slope stability, slope remediation, and geotechnical testing in Iowa. In-situ BST measurements provide reliable, site-specific soil parameters for design applications which can lead to substantial cost savings over using empirical estimations for critical soil properties. As the BST is an alternative to expensive and time-consuming laboratory testing, the device is particularly useful in obtaining relatively large amounts of data necessary for probabilistic analyses. Procedures for incorporating Borehole Shear tests into practice are documented in Volume 2 of this report. Nevertheless, some training may be required for effective and appropriate use. The BST is primarily intended to test cohesive soils. The device can produce erroneous results in gravelly soils. Additionally, the quality of boreholes affects test results, and disturbance to borehole walls should be minimized before test performance. A final limitation of widespread Borehole Shear testing may be its limited availability, as only about 4 to 6 test devices are currently being used in Iowa.

The research presented in Volume 3 demonstrates with experimental testing how lateral forces develop along stabilizing piles to resist slope movements. This report then documents a step-by-step procedure that can be used by both state and county transportation agencies to design slope reinforcement using slender piles. A state department of transportation may develop training seminars for all local transportation agencies to provide further guidance in using the proposed design method. This effort may be coordinated with the authors and might be extended so far as to conduct a pilot study to demonstrate the intended process of designing and evaluating the reinforcement solution. While slope reinforcement with slender piles by county transportation agencies is encouraged, such action is recommended to be coordinated with the state department of transportation. This organization can document all such remediation projects to better guide counties using successful and unsuccessful experiences, as the DOT will have working knowledge of other unstable slope characteristics and corresponding reinforcement designs. The proposed slope reinforcement solution has not yet been demonstrated at an Iowa slope failure site. As a result, difficulty in scheduling and

bidding a pile reinforcement project and evaluating the effectiveness of the measure may impede successful implementation. Obtaining experience and feedback through data collection or visual inspection, however, will promote incorporation of the research findings into standard slope remediation practice.

Successful implementation of innovative slope stability reinforcement and characterization solutions can be evaluated by documenting the number of slopes reinforced with pile elements and those investigated using BST measurements, respectively. Cost savings of incorporating Borehole Shear testing into site investigation practice will be made evident by comparing costs corresponding to designs for geostructures making use of accurate and reliable soil properties (obtained from BST measurements) to those designs using estimated soil properties and higher factors of safety. Calculating long-term cost savings of slope reinforcement using piles considering maintenance costs associated with alternatives and the cost for rebuilding a failed drainage remediation, for example, can indicate the progress and consequences of implementation.

INTRODUCTION

Failures of slopes occur throughout the world and contribute to economic losses. These losses, intuitively proportional to the magnitude of failure, are direct and indirect costs to individuals and institutions. Direct costs include the replacement and maintenance of structures and transportation facilities. Indirect costs include loss of tax revenues on properties devalued as a result of slope failures and loss of industrial and agricultural productivity due to the damage of land (Spiker and Gori 2003). The impact of slope failures on these losses is often undervalued. The U.S. Geological Survey (Spiker and Gori 2003) estimates that the United States, every year, experiences in excess of $1 billion in damages and approximately 50 deaths; worldwide, slope failures cause 100's of billions of dollars in damage and 100's of thousands of deaths. More locally, the annual cost for remediation and maintenance of slopes often exceeds state and county transportation budgets. The U.S. Geological Survey is leading a newly-developed, 10-year plan to "substantially reduce the risk of loss of life, injuries, economic costs, and destruction of natural and cultural resources caused by landslides and other ground-failure hazards" (Spiker and Gori 2003). Current understanding of such socioeconomic losses justifies the allocation of funds needed for slope stability research.

The immediate need for slope stability research and the development of new remediation technologies is evidenced by a survey of Iowa county engineers conducted in 2001. The data show that 80 percent of the responding counties have experience slope stability problems. Table 1 provides the percent of Iowa counties having experienced the presented slope failure conditions (e.g. frequency, soil type, etc). Select survey results are shown graphically in Figure 1.

Research Problem Statement

Slope instability continues to pose problems for highway systems in Iowa. Failures occur on both new embankment foreslopes and cut backslopes. The failures occur because identifying factors that affect stability at a particular location, such as soil shear strength values, ground water surface elevations, and negative influences from construction activities are often difficult to discern and measure. Once a failure occurs or a potential failure is identified, highway agencies need information and knowledge of which methods of remediation will be most effective to stabilize the slope. Ideally, these stability problems can be discovered and addressed before a slope failure occurs. When remediation is necessary, however, options are needed that give consideration to the remediation goals, cost constraints, environmental constraints, schedule constraints, and constructability. Newly-developed technologies for the repair of nuisance slope failures and maintenance of state transportation infrastructure are ideally simple, rapid, and cost-effective.

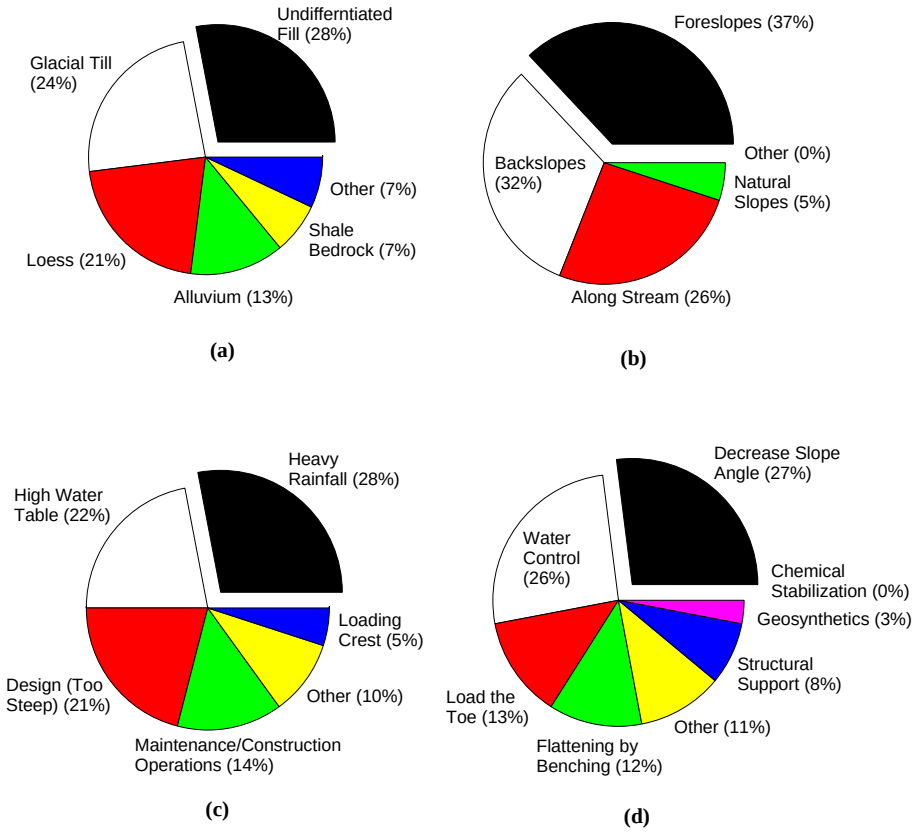

Figure 1. Conditions of Iowa slope failures (Lohnes et al. 2001)

Table 1. Conditions of Iowa slope failures (Lohnes et al. 2001)

Landslide Frequency	**1 - 5**	**6 - 10**	**11 - 15**	**15 +**	—
	44%	25%	14%	17%	—
Soil Types	**Fill**	**Glacial Till**	**Loess**	**Alluvium**	**Shale Bedrock**
	28%	24%	21%	13%	7%
Landslide Location	**Foreslope**	**Backslope**	**Along Stream**	**Natural Slope**	—
	37%	32%	26%	5%	—
Probable Causes	**Heavy Rainfall**	**High Water Table**	**Poor Design**	**Human Activity**	**Loading Crest**
	28%	22%	21%	14%	5%
Slope Angle	**< 1:1**	**1:1 - 2:1**	**2:1 - 3:1**	**3:1 - 4:1**	**> 4:1**
	18%	49%	29%	3%	1%
Slope Height	**1 - 10 ft**	**11 - 20 ft**	**21 - 30 ft**	**> 30 ft**	—
	25%	41%	21%	13%	—
Remediation / Preventative Method	**Flattening**	**Water Control**	**Load Toe**	**Benching**	**Structural Support**
	27%	26%	13%	12%	8%

Research Goal

Development of Slope Reinforcement Technology

Research was conducted to develop a new innovation in slope stabilization for Iowa soil conditions. The research group conceived small-diameter, grouted columns that are easily and rapidly constructed. The slope stabilization alternative was to be sufficiently developed to implement into current slope reinforcement practices of state and county transportation agencies in Iowa.

Technical Problem

Load Transfer of Piles Subject to Lateral Soil Movement

Soil load transfer to relatively stiff pile elements from the downslope soil movement as occurs in a slope failure is a complex soil-structure interaction problem. The downslope soil movement of slope failures induces lateral load distributions along stabilizing piles that vary with soil type, pile size, pile spacing, and relative movement between the pile and soil. The reliable estimation of these load distributions and resolution of the technical problem are important, because the influence of piles on the global stability of a reinforced slope depends directly on the pile loading condition.

Lateral soil movement described herein refers to the movement associated with slope failures, as opposed to the movement associated with settling embankments, excavation operations, or tunneling operations. The applicability of piles for stabilization of the latter movement is beyond the scope of the research and not considered.

Preceding Research Investigations

Several investigators (e.g. Broms 1964, Reese *et al* . 1974, Ito and Matsui 1975, Poulos 1995) have studied the interaction of piles subject to lateral soil movement. Methods of design and analysis for pile stabilization exhibit significant differences, suggesting that the stabilizing mechanisms are not fully understood. The present research aims to evaluate an existing analytical method, focusing on the applicability of the method to slender, small-diameter micropiles. Full-scale pile load tests facilitate the evaluation and subsequent recommendation for application of the method.

Research Objectives

Interpret Loads Induced by Lateral Soil Movement

Soil-structure interactions for small-diameter piles subject to lateral soil movement are investigated by conducting full-scale pile load tests. Proposed pile load tests are conducted in a manner similar to large-scale direct shear tests, where piles installed through a shear box into existing ground are loaded by uniform lateral translation of soil. Instrumented shear boxes aid the evaluation of stress-strain relationships of "reinforced" soil. Instrumentation of pile reinforcement (i.e. strain gauges) provides bending moment profiles and offers evidence of the distributed loads developed along the pile. The determination of loads induced by lateral soil movement and characterization of load transfer is the principal objective for resolving the technical problem and achieving the overall research goal.

Measure Material Properties of Soil and Pile Elements

Soils are complicated engineering materials because the material properties are highly variable and must often be estimated for geotechnical engineering design and analysis. Common laboratory tests to evaluate soil shear strength parameters for slope stability analyses include direct shear tests and triaxial compression tests, considering drained and/or undrained conditions. Because laboratory tests can be expensive and time consuming, the Iowa Borehole Shear Test (BST) is an alternative in-situ test that provides shear strength parameters on an effective stress or drained basis. High quality shear strength parameters, obtained from the aforementioned tests, are principal inputs for evaluating slope stability, with and without reinforcement.

The material properties associated with pile elements are less variable than soil and are predicted to a higher degree of certainty with fewer laboratory tests. Although combining concrete and reinforcing steel to achieve a more effective composite material complicates the

evaluation of engineering properties, established methods are available for predicting the performance of the composite material.

Knowledge of soil and pile material properties is necessary for the analysis of pile load tests and facilitates the prediction of pile behavior with analytical and finite element methods.

Predict Pile Behavior Associated with Lateral Soil Movement

The prediction of pile behavior associated with downslope soil movement is important to the development of the proposed remediation technology. The potential implementation of the technology requires that design engineers use existing resources (e.g. analytical methods, computer software) to reproduce the response of a pile subject to the loading conditions of slope reinforcement. The development of the SDGM stabilization design methodology, for example, relies on closed-form analytical methods to predict pile behavior including maximum moment and shear forces. The design method also incorporates conventional limit equilibrium methods to determine the factor of safety against slope instability. The research project evaluated an existing analytical model and the ability of the model to predict pile loading conditions. The research project employed computer software (LPILE) to identify and calibrate the pile response subject to the physically-imposed boundary conditions of the pile load tests.

Develop Slope Reinforcement Design Methodology

The implementation of pile stabilization requires a rational procedure for designing micropiles and the micropile stabilization system for given slope failure conditions. The design procedure for slope reinforcement draws upon concepts of existing remediation methods, but demonstrates the unique behavior of soil reinforced by grouted micropiles. The research objective is particularly important, because technical literature offers little guidance to engineers designing pile-stabilized slopes.

Research Significance

Development of Slope Remediation Technology

Research funded by the Iowa Highway Research Board was conducted with the primary goal of developing the aforementioned slope remediation alternative. Demonstration of the stability of pile-stabilized slopes, inclusive of a reliable design methodology, assists state transportation agencies with incorporating pile stabilization systems into slope remediation practices. In many cases, pile stabilization may be more effective and more appropriate than conventional stabilization practices (i.e. excavation, drainage).

Continuation of Research on Piles Subject to Lateral Soil Movement

The present research follows the work of Reese *et al* . (1974), Ito and Matsui (1975), and Poulos (1995). The full-scale pile load tests of controlled soil type, pile size, and pile spacing

offer a unique data set that explores the respective influences on piles subject to lateral soil movement. Every effort was made to perform research that was collectively innovative and practical.

Report Organization

Chapter 1 provides an introduction to the problem of slope instability and the use of small-diameter micropiles for the stabilization of shallow slope failures. The research goals and objectives are discussed with a focus on how the investigation resolves the technical issues associated with pile-stabilized slopes. In addition to the benefits of the research project, the section provides a framework for how the research findings will be implemented.

Chapter 2 presents a background on pile stabilization. The principal objective of the literature review is to demonstrate the need for research in this area of slope remediation. Understanding the existing state-of-knowledge reveals considerations that are important to the development of the remediation technology and use of grouted micropiles, in particular.

Chapter 3 details the conception, preparation, and performance of experimental tests for characterizing load transfer of piles subject to lateral soil movement. The chapter offers an overview of grouted micropiles and explains the development of the comprehensive testing program. The testing program, which includes laboratory and field tests, is completed to satisfy the research objectives of measuring properties of engineering materials and evaluating the loads induced on piles subject to uniform lateral translation of soil. Additionally, results from laboratory testing are presented in Chapter 3.

Chapter 4 provides the results from load tests on piles subject to lateral soil movement. The material of the chapter supports the discussion of results and design methodology of the subsequent chapters. The following load test results are presented:

- Shear box load-displacement relationship
- Pile head load-displacement relationship
- Relative displacement of shear box and pile head
- Photogrammetry
- Shear box rotation and tilt
- Pile bending moment distributions
- Soil sampling with in-situ testing devices

Chapter 5 presents the load test analysis, which was performed to: (1) evaluate the finite difference lateral response analysis method proposed by Reese and Wang (2000) and (2) verify the predicted structural performance of piles under the loading condition of slope reinforcement. The analysis was accomplished by comparing observed behavior of pile load tests with predicted behavior from numerical model of piles subject to horizontal soil movement. The analysis additionally evaluates the applicability of the method to grouted micropile stabilization in Iowa soils.

Chapter 6 establishes a protocol for designing pile-stabilized slopes, making use of the preceding load test data and results. The design method incorporates limit states of the matrix soil and the proposed pile, such that the design method is based on failure of the soil or structural failure of the pile. The design method extends the determination of the resisting force of a single pile to the determination of the influence of multiple piles on global slope stability. The proposed design method involves evaluating the stability of a failing slope with common limit equilibrium methods and using prepared design charts for calculating a new factor of safety for the pile-stabilized slope.

Chapter 7 presents the conclusions of the research investigation. The conclusions address the research goals and objectives, and indicate the successes for each phase of the research project.

Chapter 8 provides recommendations regarding how the research is to be implemented in the immediate and long-term future. The author recommends that the design methodology be further explored by means of pilot studies of stabilizing slope failures in Iowa. The implementation of the design method and process of slope monitoring provides critical evidence as to whether the proposed remediation alternative is an effective and viable option for slope stabilization in Iowa.

BACKGROUND

Introduction

Slope stability is a basic subject of geotechnical engineering. Slope stabilization with pile elements, however, is a specialized subject of geotechnical engineering and the focus of only limited research. The purpose of the background is to summarize important concepts of pile stabilization. The background is divided into three sections, including (1) complicating issues of pile stabilization; (2) review of design methods for slope stabilization with piles, and (3) case histories of slope stabilization with small-diameter piles.

Complicating Issues of Pile Stabilization

Stabilization of unstable slopes with pile elements is complicated by factors affecting pile performance under the loading conditions of slope reinforcement and factors controlling the influence of piles on global slope stability. The research group acknowledges the following complicating issues of pile-stabilized slopes:

- Prediction of load distributions along piles – The load development on piles subject to downslope soil movement, presented earlier as the research technical problem, is important; because the influence of piles on the global stability of an unstable slope depends directly on the loading. This issue is the focus of performed experimental and analytical work and is addressed throughout this document.
- Influence of soil type – Understanding the influence of soil type is important for designing pile stabilization. The engineering properties of soil – soil shear strength parameters, in particular – control the stability of the unreinforced slope and the required reinforcement capacity. Stress-strain behavior of slope soils and the determination of an ultimate soil pressure profile with depth facilitate the development of limit resistances considering failure of soil above the failure surface, failure of soil due to insufficient anchorage, and structural failure of the pile elements.
- Influence of pile size and spacing – The influence of pile size and spacing on slope and pile stability of reinforced slopes is evidenced by the dependence of pile behavior on the reinforcement parameters. Load-displacement (p-y) curves, which are used to relate pile displacement and soil response, are most reliably back-calculated from pile load tests and are found to vary with pile size and spacing.
- Pile orientation – The orientation of piles with respect to slope and failure surfaces affects the performance of reinforcement and the influence of reinforcement on slope stability. The resultant stabilizing force of a pile does not necessarily act in the same direction as the failure surface, and only one directional component of the force acts to oppose slope movement. Also of consequence, skin friction achieved by pile elements potentially reduces the normal stress between the unstable and stable soil masses, resulting in reduced soil shear resistance. The research group recognizes, however, that the stabilization potential of slender pile elements is optimized by

altering the inclination of the piles to develop axial loads (i.e. tension or compression), reducing the loads responsible for pile bending. Heavily-reinforced piles may benefit from mobilization of tension, whereas lightly-reinforced piles may benefit from mobilization of compression. The research group performing tests on soil displacement grouted micropiles, for this study, did not evaluate the influence of pile orientation on pile behavior. The pile and the resistance developed along the pile were perpendicular and parallel to the shear plane, respectively. Battered (i.e. non-vertical) piles accept axial loads due to the mobilization of skin friction along the length of piles subject to soil movement. The performance of pile load tests on battered piles is the next most important task for improving remediation with soil displacement grouted micropiles.

- Truncation of piles – The truncation of piles likely increases the capacity of the reinforcement system. Aside from potential reductions in the total applied load on the pile, the moment development in a truncated pile is reduced due to the shortened moment-arm on which the load acts. This benefit is particularly important for slope stabilization with slender pile elements, because the moment capacity of the pile sections controls the failure mode of the stabilization system.
- Soil arching – Soil arching refers to the transfer of loads from weak elements to strong, stiff elements. The phenomenon is applicable to pile-stabilized slopes, where deforming soil indirectly transfers load to stiff pile elements. Soil arching is generally regarded as a contributor to the capacity of the slope reinforcement. Unfortunately, designers of pile stabilization do not fully understand the conditions necessary for soil arching to occur or the quantitative effects of soil arching on the stability of reinforced slopes.
- Stress concentrations – The loads developed on piles subject to downslope movement are induced by displacement. The imposition of displacement compatibility between piles and adjacent soil result in stress concentrations of which current design methodologies fail to consider. The difference in stiffness between soil and steel-reinforced concrete involve a requisite difference in mobilized stresses, for a given displacement.

The preceding issues of pile-stabilized slopes, several of which are addressed by the current research project, are illustrated in Figure 2.

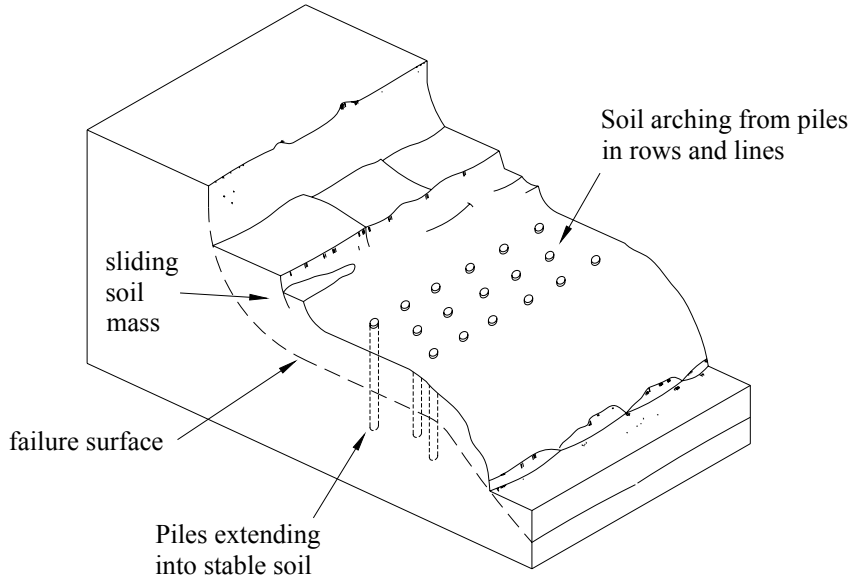

(a)

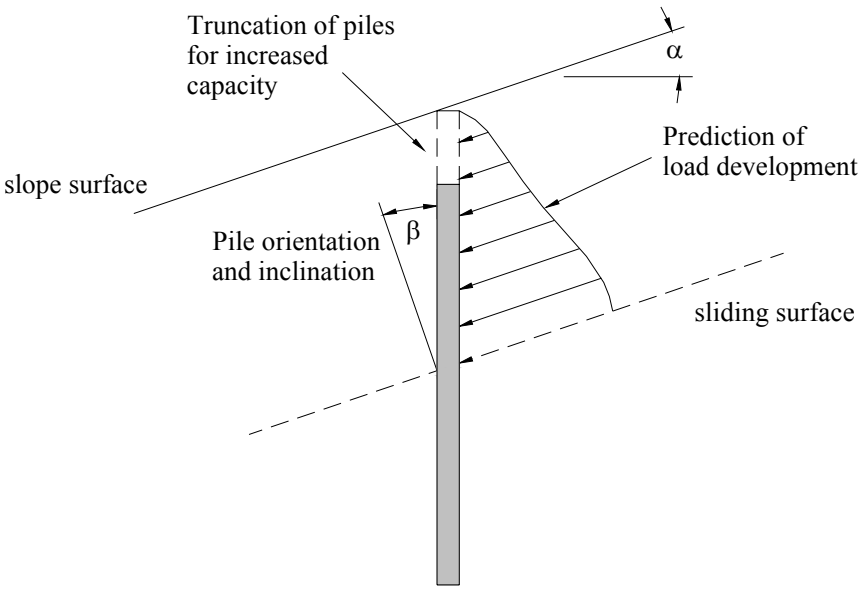

(b)

Figure 2. Issues of pile-stabilized slopes

Review of Design Methods for Slope Stabilization with Piles

Application of Laterally Loaded Piles to Slope Stabilization

Piles installed in failing slopes arrest or slow the rate of slope movement. Pile elements offer passive resistance to downslope soil movement by transferring the loads developed along the pile to stable soil below the failure surface. The soil load transfer to piles depends principally on the magnitude and rate of slope movement, because the pressures developed between piles and soil observe the load-displacement (i.e. stress-strain) relationship of the engineering materials. In fact, the installation of passive piles does not guarantee an end to slope movement, but rather unstable soil continues to slide until sufficient resisting forces are developed along the pile to discontinue the movement. Alternatively, piles installed in a marginally stable slope to increase the factor of safety against sliding are potentially unloaded, where the shear strength of soil along possible failure surfaces is sufficient to oppose triggering causal factors of slope movement (i.e. soil shear strength carries load of soil mass). The loads developed on passive piles due to downslope soil movement are therefore limited by the resisting force required to arrest slope movement or the pressure that causes yielding of the pile and/or surrounding soil.

General Design Approach for Pile Stabilization

Current approaches for stabilizing slopes with pile elements (e.g. Ito and Matsui 1979, Viggiani 1981, Poulos 1995, Hassiotis et al . 1997, Loehr 2003) involve three general design stages, as follows:

1. Evaluating the global stability of the unreinforced slope and calculating the shear force needed to increase the safety factor for the slope to the target value;
2. Evaluating the shear resistance that each pile can provide to resist sliding; and
3. Selecting the type and number of piles to achieve the resistance corresponding to the target factor of safety.

Design methodologies do not necessarily address these stages in the order presented, as each slope remediation project may present specific limitations to the design. Due to construction constraints, for example, the pile size and reinforcement arrangement may be pre-determined. Also, newer design methods may attempt to evaluate global slope stability and pile stability concurrently.

Lateral Resistance of Piles

The influence of pile elements on the global stability of a slope can be evaluated with the conventional definition of limit equilibrium factor of safety. The direct resistance of a pile element, F_R, increases the factor of safety over that of an unreinforced slope.

The factor of safety for a reinforced slope is determined with the following equation:

$$FS = \frac{\Sigma F_R + \Delta F_R}{\Sigma F_D} \tag{1}$$

where ΔF_R = limit resistance of piles,
ΣF_R = resisting forces of slope, and
ΣF_D = driving forces of slope

The design and analysis of pile-stabilized slopes is readily supplemented by existing limit equilibrium methods for evaluating slope stability. Research efforts, therefore, focus on the determination shear resistance provided by the piles.

Slope stabilization with pile elements concerns passive piles, which are those subjected to lateral loads induced by horizontal movements of soil. The analysis and design of passive piles for slope reinforcement may be more complicated than the analysis and design of active piles. The lateral loading condition of passive piles depends on slope movements, which consequently depend on the presence of the pile elements. Current design methodologies estimate these lateral load distributions based on standard soil properties and design the pile elements as active piles. The methods are problematic, because the designs consider only strength limit states of the piles and slope soils. The methods neglect the interdependence of slope movement and the pile loading condition. No indication is provided for the slope movement required to mobilize the calculated resistance for the new factor of safety. Failure to account for slope movement in the design of reinforced slopes constitutes a significant limitation of pile stabilization.

Design methods for pile-stabilized slopes consistently assume that sliding soil moves sufficiently to mobilize the ultimate soil pressure (Reese and Wang 2000). The ultimate soil pressure (i.e. design load) is therefore applied to the pile directly or as an equivalent loading condition. The assumption aids in the structural design of proposed piles and nearly ensures pile stability for reliably-determined ultimate soil pressures. But the prediction of ultimate soil pressure is complicated, and Ito et al. (1981) advises that an accurate estimation of the lateral resistance is essential for stability analyses. An overestimation of ultimate soil pressure results in a conservative pile stability and an unconservative slope stability. Alternatively, an underestimation of ultimate soil pressure results in a conservative slope stability and an unconservative pile stability.

Ultimate soil pressures are most easily and most reliably obtained from p-y relationships. By definition, the ultimate soil pressure is the limiting soil resistance. Unfortunately, p-y curves necessitate prohibitively-expensive pile load tests. Based on failure mechanisms of soil (e.g. plasticity, viscous flow, wedge), investigators have established approximations for ultimate soil pressure in terms of standard soil properties and stress conditions.

Alternative Design Approaches

More sophisticated procedures for designing pile stabilization may include numerical methods and use of finite or boundary element analyses. The accuracy of such solutions depends on the characterization of the interaction between pile and adjacent soil elements. Particularly good representations of the soil-pile interaction yield realistic solutions. Poulos suggests that the most satisfactory method for predicting the stabilizing force provided by the piles is to incorporate an analysis that simulates the movement of a sliding soil mass. The analysis of pile behavior under such boundary conditions is further described by Poulos (1973, 1995) and in Chapter 5 of this report.

Evaluation of Slope Stabilization Using Recycled Plastic Pins

The University of Missouri-Columbia recently developed a slope remediation alternative that uses recycled plastic pins. Recycled plastic pins consist of nearly 40 percent sawdust and are fabricated with post-size dimensions. The research program engaged a comprehensive materials testing program focusing on tension, compression, shear, and flexural strengths of the recycled plastic. Subsequent investigations evaluated interface friction and bending creep of the pins. Recycled plastic pins were ultimately characterized as "weak" reinforcement elements, as opposed to "strong" reinforcement elements such as steel pipes (Loehr et al. 2000). The pins were regarded as adequate, nonetheless, because soil strength often controls the slope remediation.

The design methodology of slope stabilization using recycled plastic pins involves finding the limit lateral resistance of individual reinforcing members. The procedure considers the following limit states (Loehr and Bowders 2003):

- failure of soil around or between reinforcing members – referred to as the limit soil resistance,
- structural failure of reinforcing members in shear or bending due to load application from the soil mass – referred to as the limit member resistance, and
- failure of soil due to insufficient anchorage length – referred to as the limit anchorage resistance.

The determination of each limit state is discussed in the ensuing sections.

The research program acknowledged the potential of slope stabilization with slender pile elements and, as a result, also established the feasibility of soil displacement grouted micropiles as a slope remediation alternative. The analysis and design procedure for SDGM stabilization draws upon the succeeding concepts of recycled plastic pin stabilization. While the stabilizing mechanisms and failure modes are common to both slender pile types, the design must demonstrate the unique behavior of soil reinforced by soil displacement grouted micropiles.

Limit Soil Resistance

The proposed design method employs the model for ultimate soil pressure originally proposed by Ito and Matsui (1975). The ultimate soil pressure of the model increases linearly with depth. The design method assumes that the ultimate soil pressure is mobilized along the entire length of pile subject to lateral soil movement, and the limit soil pressure is integrated from the ground surface to potential sliding depths. The integration, with units of force, is called the limit soil resistance, F_R. The limit soil resistance increases as the depth to the sliding surface increases, because the length over which the ultimate soil pressure is integrated increases. The integration of ultimate soil pressure and the limit soil resistance curve is shown in Figure 3 (a) and (b), respectively.

Limit Anchorage Resistance

Incorporation of limit anchorage resistance ensures that pile elements do not induce passive failure of the soil below the sliding surface. For potential sliding depths, the limit soil pressure is integrated from the depth of the sliding surface to the bottom of the pile. The limit anchorage resistance decreases as the depth to the sliding surface increases (for a given pile length), because the length over which the ultimate soil pressure is integrated decreases. Piles that extend only to the failure surface, for example, clearly offer no resistance to slope movement. The integration of ultimate soil pressure and the limit anchorage resistance curve is shown in Figure 4 (a) and (b), respectively.

Limit Member Resistance

The development of a limit member resistance curve to account for the structural capacity of pile elements uses the ultimate soil pressure and a reduction factor, where the application of the ultimate soil pressure may lead to bending moments or shear forces that exceed the capacity of the reinforcing member (Loehr and Bowders 2003). The reduction factor, α, is the factor by which the ultimate soil pressure is applied to the pile element that just causes the pile to fail in either bending or shear (see Figure 5). The maximum moment (or maximum shear) developed by the factored soil pressure distribution equals the moment capacity (or shear capacity) of the pile section, observing that the limit member resistance represents the maximum load that is carried by the pile.

The limit member resistance curve is developed similarly to the limit soil resistance curve, where the former uses the factored soil pressure distribution along the pile and the latter uses the unfactored soil pressure distribution along the pile. The factored ultimate soil pressure distribution is integrated from the ground surface to the potential sliding depth, such that the length over which the factored soil pressure is integrated increases with sliding depth. The limit member resistance decreases with sliding depth, however, because α decreases with sliding depth. The reduction factor, which is inversely proportional to the maximum moment developed in the pile, decreases with sliding depth; because the moment arm of an equivalent loading condition increases. As the moment arm increases, the calculated maximum moment increases. For this reason, at intermediate sliding depths where α is less than 1.0, member resistance controls the reinforcement capacity. The establishment of the reduction factor and

use of the factor to modify the soil pressure distribution is illustrated in Figure 5. The limit member resistance curve is provided in Figure 6.

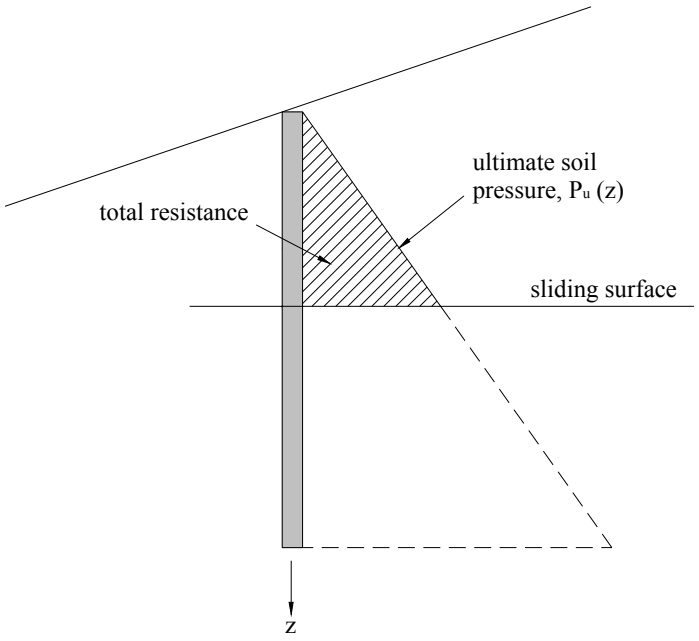

(a) Integration for limiting soil pressure

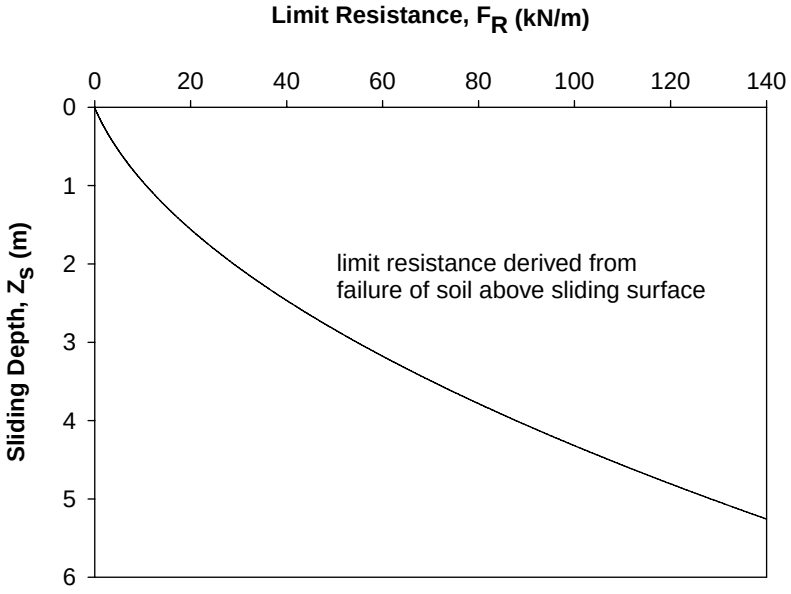

(b) Limit soil resistance curve

Figure 3. Limit soil resistance (Loehr and Bowders 2003)

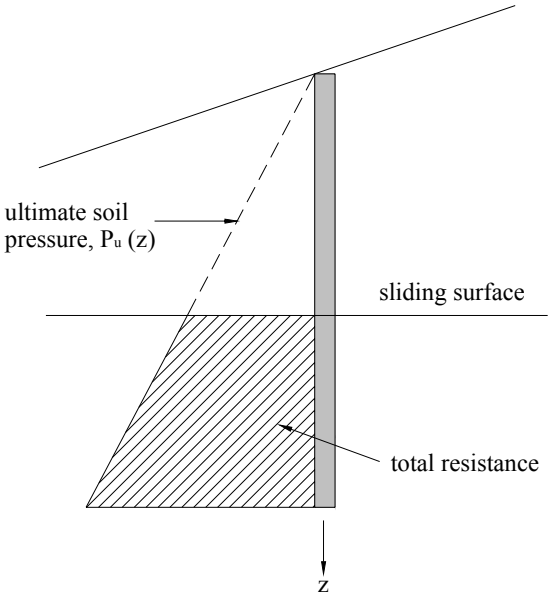

(a) Integration for limiting anchorage resistance

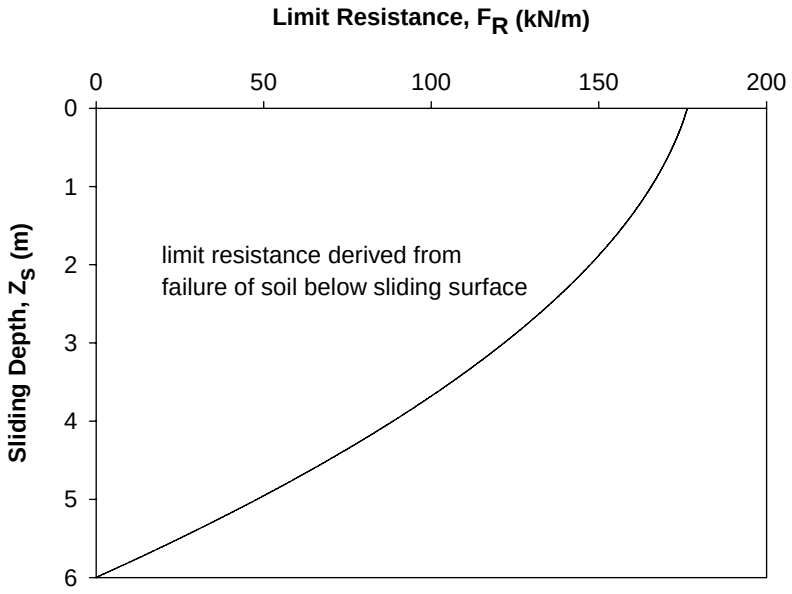

(b) Limit anchorage resistance curve

Figure 4. Limit anchorage resistance (Loehr and Bowders 2003)

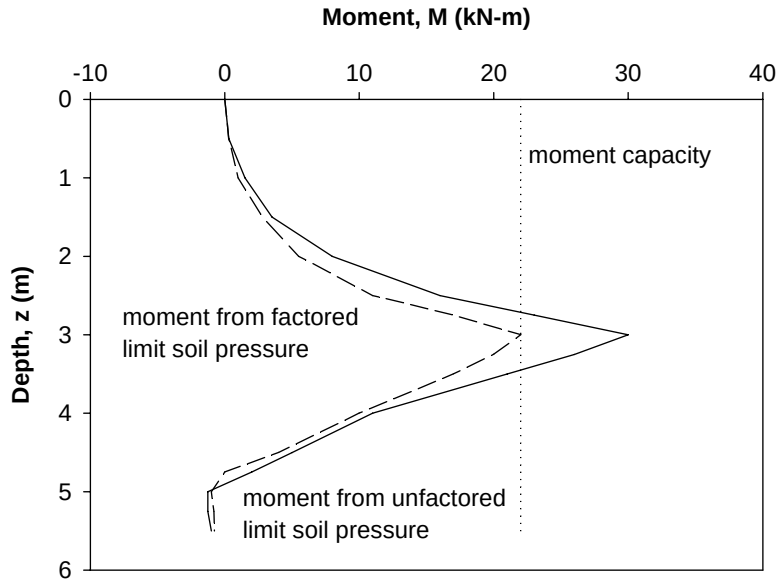

(a)

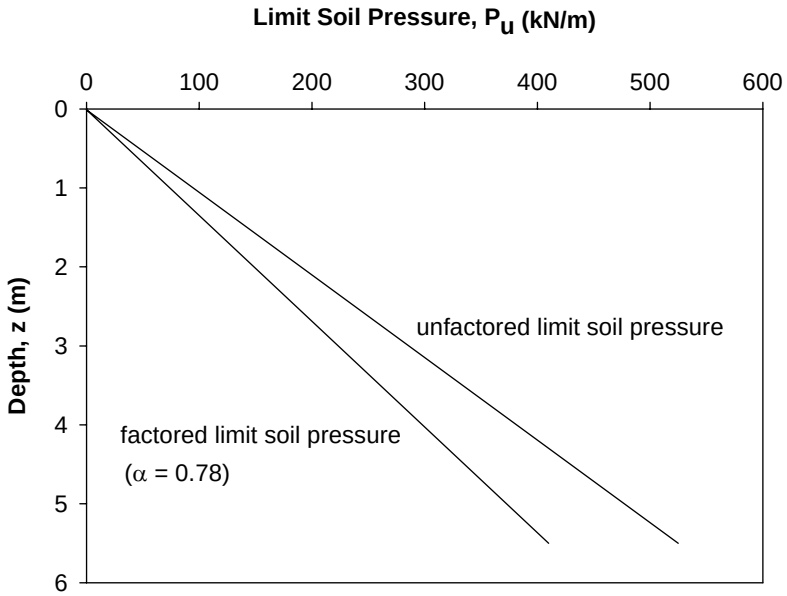

(b)

Figure 5. Factored pressure distributions (Loehr and Bowders 2003)

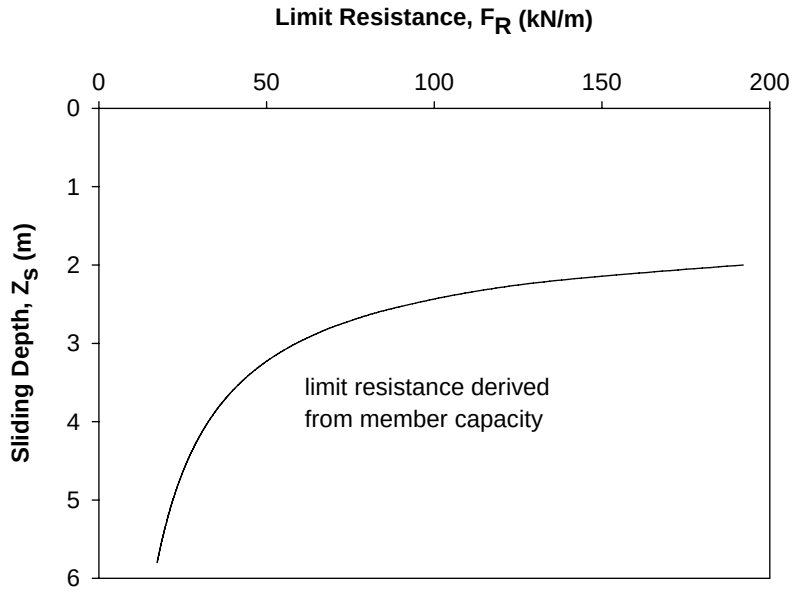

Figure 6. Limit member resistance curve (Loehr and Bowders 2003)

Composite Limit Resistance Curve

For each limit state (e.g. soil resistance, anchorage resistance, and member resistance), a factored or unfactored limit soil pressure is determined and appropriately integrated to find the respective limit resistance for a given sliding depth. The limit resistance of the system is the least of the three limit states considered. Figure 7 shows typical distributions of limit resistance and a composite limit lateral resistance.

A complete assessment of the use of recycled plastic pins for slope stabilization is premature given that the most recent test section was stabilized in 2003. Five test sites were instrumented with slope inclinometers and pore pressure sensors. Additionally, the reinforcing members of several sites were instrumented to monitor the loads and deflections of the members. It is the understanding of the author that investigators from the University of Missouri-Columbia are participating in an ongoing effort to monitor the stability of the reinforced slopes to provide evidence of the effectiveness of the stabilization scheme.

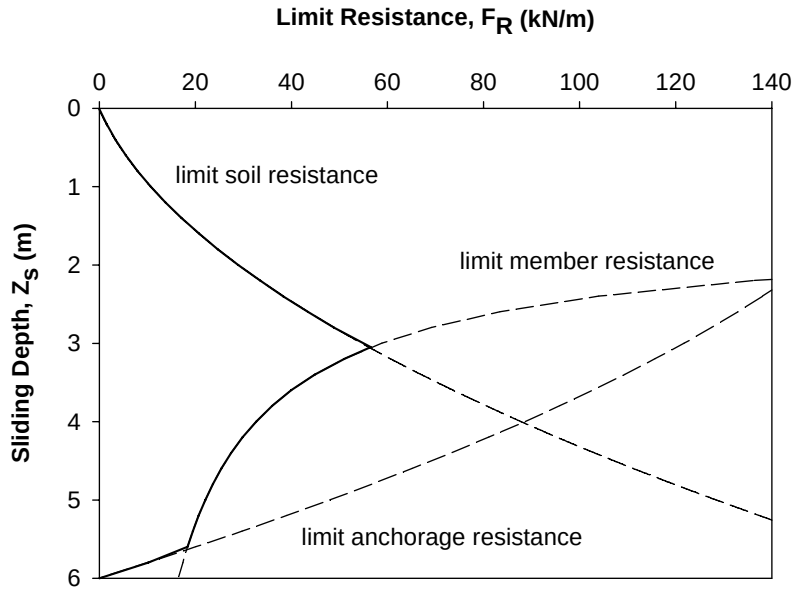

(a) Determination of reduction factor, α

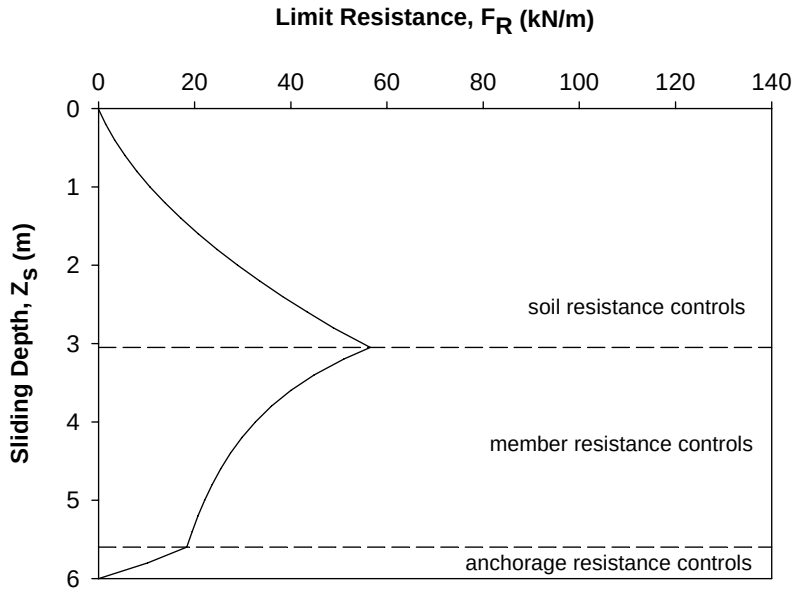

(b) Factored limit soil pressure

Figure 7. Limit resistance distributions for recycled plastic pins (Loehr 2003)

Case Histories of Slope Stabilization with Small-Diameter Piles

Compaction Grout Columns at Attleboro, Massachusetts

Compaction grout columns closely resemble auger-cast piles except that compaction grout columns laterally displace the soil, whereas auger-cast piles generate spoil material that requires disposal. Low slump grout with approximate 28-day compressive strength of 20.7 MPa is pumped into the ground under high pressure (2.1 to 3.4 MPa) to form a relatively cylindrical grout column (Benedict et al. 2001). Irregularities in the columns are normal and expected. The columns accept vertical and lateral loads, such that the method is commonly used for densification of foundation soils, raising and leveling of structures and foundation elements, and mitigation of liquefaction potential. The use of compaction grout columns for slope stabilization is effectively demonstrated by a case study, where compaction grout columns were employed to provide adequate stability and acceptable settlement behavior for an Amtrak track extension. The use of compaction grout columns for track support was initially documented by Benedict et al. (2001).

In order to meet the sight distance requirements of high-speed electrified passenger rail service, a track extension was to be constructed along a wetland underlain by organic soils. The two concerns related to the thick peat layer were global stability and the potential for excessive settlement. Geotechnical analyses suggested that significant consolidation and secondary settlements of the peat layer would be accompanied by future track maintenance issues. Also, a global stability analysis indicated a factor of safety of approximately unity against slope failure. Several ground improvement alternatives were considered. However, due to overhead clearance limitations and the need to address stability and settlement issues concurrently, compaction grout columns were used for the project. Therefore the objective was to design the compaction grout columns as structural members to transfer the train and ballast loads through the thick peat layer to the dense sand stratum.

The design of column sections was based on slope stability, where the stability of the embankment was the controlling design aspect. Due to the large shear forces expected in the compaction grout columns, reinforcement was provided with No. 8 steel rebar. Steel reinforcement was more economical than using high strength grouts or installing additional compaction grout columns. Furthermore, using higher strength grout potentially exposed the compaction grout columns to undetected deficiencies in installation and, consequently, required more rigorous quality control practices.

A pre-blended grout mixture design was developed and included Type II cement, fly ash, sand, and bentonite. Slump and compression tests verified the adequacy of the mixture design, such that following a trial column installation, construction commenced on the embankment. A total of 289 compaction grout columns were installed at equilateral spacing of 1.8 m. As well as checking slope stability and settlement, engineers observed that by transferring the loads from the trains to the sand stratum axially, the reduction of driving forces correspondingly reduced the potential for slope stability failure.

Bored Piles at London, England

Davies et al . (2003) documented the pile stabilization and slope monitoring of a landslide on the M25 Highway in England.

The wettest winter in English history resulted in a slope failure on the M25 Highway around London. The failure extended 80 m upslope from the highway and threatened 198 m of the slope along the transportation corridor. The slope was marginally stable and responded rapidly to rainfall events. Months after the initial failure, rainfall triggered additional movements. The investigation, design, construction, and monitoring programs were fast tracked to stabilize the slope before the next wet season.

The Flint Hall Farm Cutting was constructed between 1976 and 1979. Site investigation indicated that the failure surface was within a stiff to very stiff gray fissured clay (Gault), with overlying Head deposits mantling the upper portion of the slope. The engineering properties of the soils are provided in Table 2.

Table 2. Engineering properties of M25 slope failure soils

	Shear Strength		Typical Properties		
Soil Type	**ϕ' (deg)**	**c' (kPa)**	**c_u (kPa)**	**PI**	**w/c**
Head	14	0.0	50.0	—*	40
Gault	24	1.0	100.1	45	35
Residual Gault	14	0.0	50.0	—*	—*

Notes:
* Data not available

The governing transportation agency specified a stabilization design life of 60 years. The design was therefore unable to employ drainage alternatives as the sole means for preventing further slope movement due to likely blockage of the drainage structures with time. Moreover, the counterforts installed during construction of the slope failed to prevent the landslide. Rather, a structural solution of pinning the sliding soil to the underlying Gault clay with piles was adopted.

The design of piles for stabilizing the slope began by establishing the location of piles on the slope and the pile lengths. Piles were installed one third of the way up the failure and extended 16 m into the ground. The pre-establishment of these variables reduced the number of permutations for the pile design. Pile spacing was then selected to maximize soil arching between the piles and minimize the flow of soil between piles. Piles with 1-m diameters, spaced at 2.5 m offered the aforementioned benefits over alternative pile size and spacing configurations.

The structural design of piles concluded the stabilization design. The design incorporated the method proposed by Viggiani (1981). The method ensures pile stability by adjusting proposed pile sizes and capacities until the controlling failure mechanism of the stabilization

is failure of the soil around the piles. The failure mode offers a non-brittle failure mechanism, which is preferable over the brittle failure mechanism of the development of a plastic hinge in a pile section. Ultimately, 74 piles were installed to stabilize the slope. Post-construction monitoring indicated that despite heavy winter rainfall events sufficient to remobilize failure, the slope was effectively stabilized.

Type "A" In-Situ Earth Reinforcement Technique Walls

Type "A" In-Situ Earth Reinforcement Technique (INSERT) Walls control the movement of unstable slopes by providing passive resistance mobilized in a pattern of vertical and near vertical reinforcing elements installed through a slope failure surface (Pearlman and Withiam 1992). The pile elements are generally connected at the slope surface with a reinforced pile cap, which provides added stiffness for relatively shallow failure planes. Pile diameters range in size from 13 to 23 cm, and the pile elements may be reinforced with centered steel rebar or steel pipes (see Figure 8). Pile elements installed with pipe reinforcement have significantly more capacity than pile elements installed with a centralized reinforcing bar. The slope stabilization applications of Type "A" INSERT walls are illustrated in Figure 8.

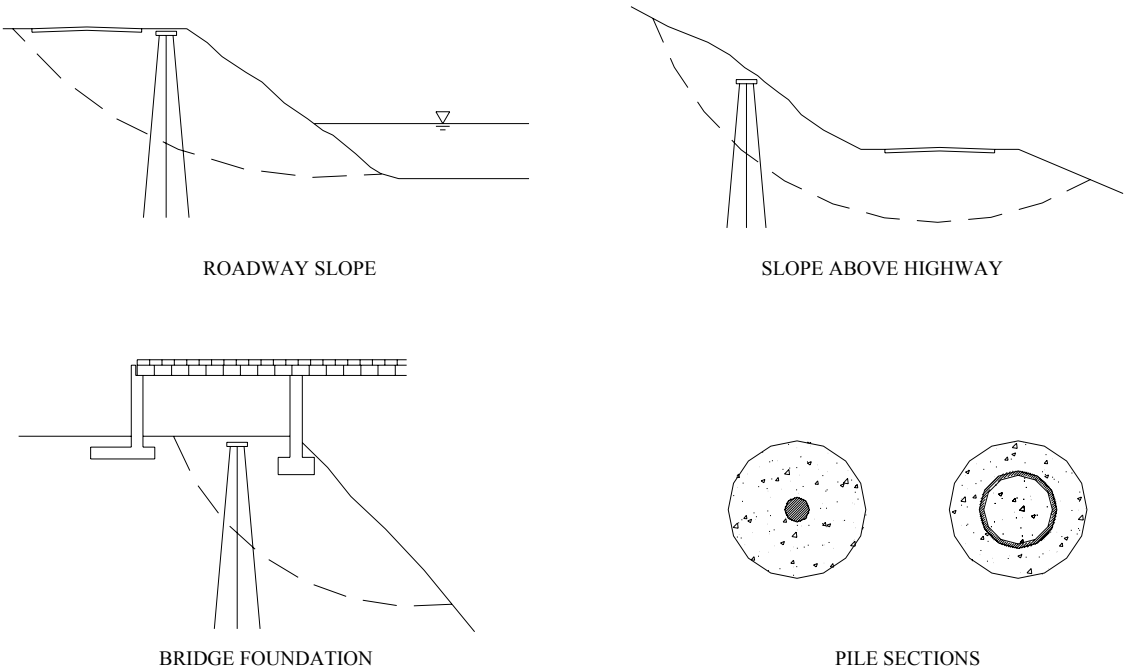

Figure 8. Typical configurations and applications of Type "A" INSERT walls (Pearlman and Withiam 1992)

The procedure for designing Type "A" INSERT walls considers structural failure of the piles and plastic failure of slope soil. The procedure uses a method proposed by Fukuoka (1977) for evaluating the bending moments developed in piles oriented perpendicular to a failure plane. Plastic failure of soil around the piles is analyzed using the method proposed by Ito

and Matsui (1975). The surface area to cross-sectional area ratio of slender pile elements is large, such that small-diameter piles are efficient at mobilizing skin friction (Pearlman and Withiam 1992). The piles generally have higher axial capacity than lateral capacity; and, for this reason, pile elements of Type "A" INSERT walls are battered. The design methodology, however, does not quantitatively indicate the effect pile inclination on the stability of the reinforced slope.

Type "A" In-Situ Earth Reinforcement Technique Wall at Big South Fork River, Kentucky

The use of Type "A" INSERT walls to stabilize a slope in Kentucky is documented by Pearlman and Withiam (1992). The U.S. Army Corps of Engineers observed a moving slope downhill from a bridge abutment and above a land pier supporting an historic railroad bridge. Continued slope movement threatened the stability of the structure.

The slope soil conditions, determined from soil exploration, consisted of medium stiff to stiff silty clay with shale bedrock ($\phi = 19°$, $c = 0$, $\gamma = 19.7$ kN/m^3). The wall design (resembling the "bridge foundation" application of Figure 8 consisted of 14-cm diameter piles, reinforced with No. 11 and 14 rebar. The pile density required to achieve stability was calculated at 2.5 piles per lineal meter, in which piles were oriented from 19° to minus 5° with vertical. Following pile construction, a reinforced cap beam of dimensions 10.7 m x 1.5 m x 0.9 m (L x W x T) was constructed to provide stiffness to the pile wall. Slope monitoring during construction and following construction indicated that lateral displacements were less than 2.5 cm.

Root-Pile Wall at Monessen, Pennsylvania

During construction of a four-lane highway, several slope failures occurred and involved the earth slope, water lines, and a city street above the slope. The slope soil strata varied from hard massive sandstone to red shale with minor limestone interbeds. The overburden fill consisted primarily of silty clays and clayey silts. Based on back analyses, the most-probable values for cohesion and internal friction angle were 4.8 kPa and 17°, respectively. A root pile wall was constructed to correct the slope failure, because the alternative required the least amount of disturbance and the minimum time for construction (Dash and Jovino 1980).

Design of the root-pile wall structure involved: (1) selection of the location; (2) selection of the size; (3) selection of the pile arrangement, including spacing, inclination, length, and size of individual piles; (4) checking the loads and stresses on the individual piles; and (5) checking the probable movements of the structure. At the time of the project, the method was mostly derived from experience and was patented by the Fondedile Corporation.

Construction of the root-pile wall began with the pile cap. Vertical and inclined holes were then drilled through the cap into the slope. The drilled holes were cleaned with air pressure, and No. 9 reinforcing steel rods were then placed in the holes. Grout (1 bag of cement, 22.7 L of water, and 0.071 m^3 of sand) was poured into the hole without external pressure. The structure consisted of 458 12-cm diameter, cast-in-place concrete piles. The root-pile

wall provided a positive solution to the slope instability problem, evidenced by horizontal and vertical movements of the cap-beam which were monitored with time. Prior to installation, movements at the south end were approximately 45 cm. The cap-beam moment ceased, however, after the installation of the root piles. Moreover, the method was rapid, requiring only eight weeks of actual construction time.

RESEARCH TESTING METHODS

Introduction

The current research program aims to develop a rapid, cost effective, and simple remediation system that can be implemented into slope stabilization practices for relatively shallow slope failure (< 5 m) conditions. The non-proprietary remediation technology consists of drilled, composite pile elements (cementitous grout with centered steel reinforcing bar), and the experimental testing establishes the grouted micropiles as a feasible remediation alternative.

The ensuing sections summarize the conception, preparation, and performance of experimental tests for characterizing load transfer of piles subject to lateral soil movement.

Development of Testing Program

Overview of Small-Diameter Grouted Micropiles

Micropiles can be classified as displacement or replacement piles. Displacement piles are generally driven or vibrated into the ground, whereas replacement piles are placed in predrilled boreholes. Grouted micropiles, however, exhibit the characteristics of both pile types. A column of soil is laterally displaced with a reverse pitch auger, and concrete is subsequently placed in the borehole. The feature contributes to the stabilizing mechanisms of the remediation method, because the locally compacted soil offers increased shear strength at the failure surface and increased soil resistance along the entire length of the installed pile. The stabilizing mechanisms of grouted micropiles are reflected in the installation process of the pile elements. The anticipated installation method is illustrated in Figure 9.

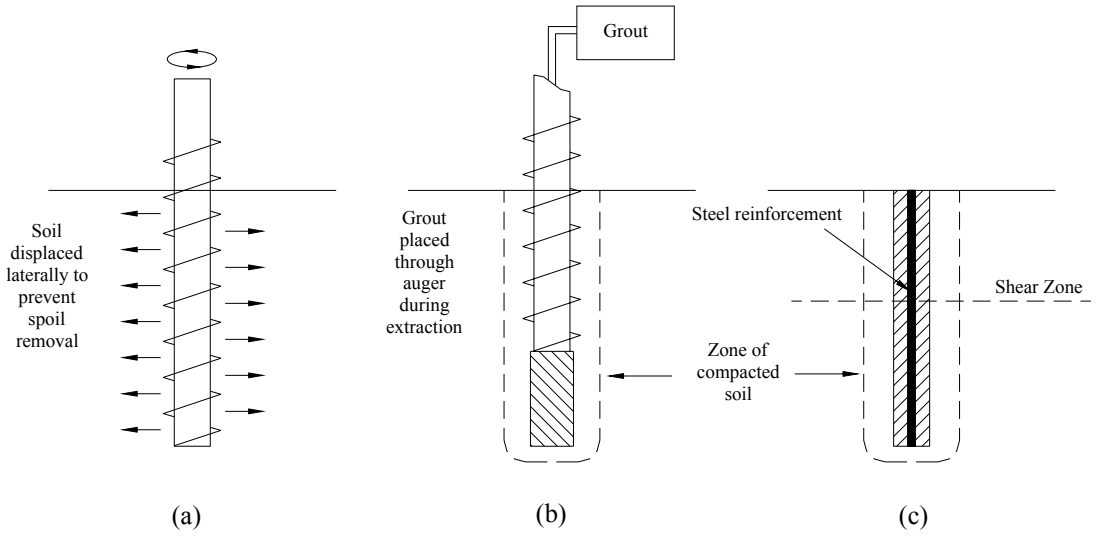

Figure 9. Construction sequence of grouted micropiles

The auger prepares the borehole for placement of concrete, and the matrix soil is forced laterally outward or vertically downward. The local soils densify, and soil-pile system experiences increased strength. Upon reaching the desired pile depth, concrete is placed through the hollow-stem auger concurrent with the removal of the auger. The unreinforced, grouted pile is subsequently reinforced with steel rebar or a steel pipe to improve the structural capacity of the pile element. A steel-reinforced, grouted micropile surrounded by a zone of dense soil remains at the end of construction.

The grouted micropile system is being developed as a simple remediation technology. The research group, at inception of the research project, speculated that the method would be used by state and county highway construction and maintenance crews to repair nuisance slope failures and stabilize unstable slopes. Beyond being easily constructed, however, grouted micropiles offer benefits related to the stabilizing mechanisms of the remediation system. The remediation system employs a larger number of small-diameter micropiles, as opposed to fewer large-diameter drilled piers. The system offers redundancy, such that the failure of one micropile is less critical than the failure of one drilled pier. Moreover, the likely failure mode of grouted micropiles is preferable over the failure modes of other remediation methods, in that the slope structure deforms in smaller increments and offers evidence of movement prior to catastrophic failure. The deformations are ideally observed with the slope monitoring and maintenance programs; and, when necessary, additional piles may be installed to prevent further slope movement or increase the factor of safety for global stability to accommodate increased performance requirements of the slope (i.e. building of structures adjacent to slope).

Development of Test Plan

The testing program for evaluating the feasibility of using grouted micropiles as a slope reinforcement alternative involved laboratory and field testing. The laboratory testing program was completed to satisfy the research objective of measuring material properties of soil and pile elements. The field testing program was completed to satisfy the research objective of interpreting loads induced by lateral soil movement. Laboratory tests and field tests were performed with several common Iowa soils (e.g. loess, glacial till, and weathered shale).

The laboratory testing program consisted of determining properties of soil and concrete samples. The following laboratory tests sufficiently characterized soil and potential concrete mixtures:

- soil classification tests, including grain size distribution and Atterberg limits
- soil compaction characteristics
- unconfined compression tests
- direct shear tests for effective soil shear strength parameters, c and ϕ
- consolidated-undrained triaxial compression tests for empirical development of p-y curves

- compression tests on concrete samples (mixtures of Portland cement, sand, fly ash, chemical admixtures, water, and air) for the determination of elastic modulus, ultimate compressive strength, and rate of strength development

The field testing program consisted of measuring the shear strength of soil reinforced with pile elements. The pile load tests were performed in a manner similar to large-scale direct shear tests. The direct shear boxes, constructed large enough to minimize the influence of box boundaries, contained compacted soil with known properties and piles that extended through the box into existing ground. The shear boxes were pushed laterally to impose uniform lateral translation of soil, modeling the movement of a unit cell of a sliding soil mass. The interface of the shear box and the at-grade elevation resembled the failure surface of a slope failure, and the soil below grade resembled the stable soil of a slope in which piles are installed to provide passive resistance to movement. Instrumentation of the direct shear boxes (displacement gauges and load cell) was installed to measure the load-displacement response of the reinforced soil. Instrumentation of the pile reinforcement (strain gauges) indirectly indicated the loads induced on the piles due to lateral soil movement and the pile response to the loads. Figure 10 shows the large-scale direct shear test set-up.

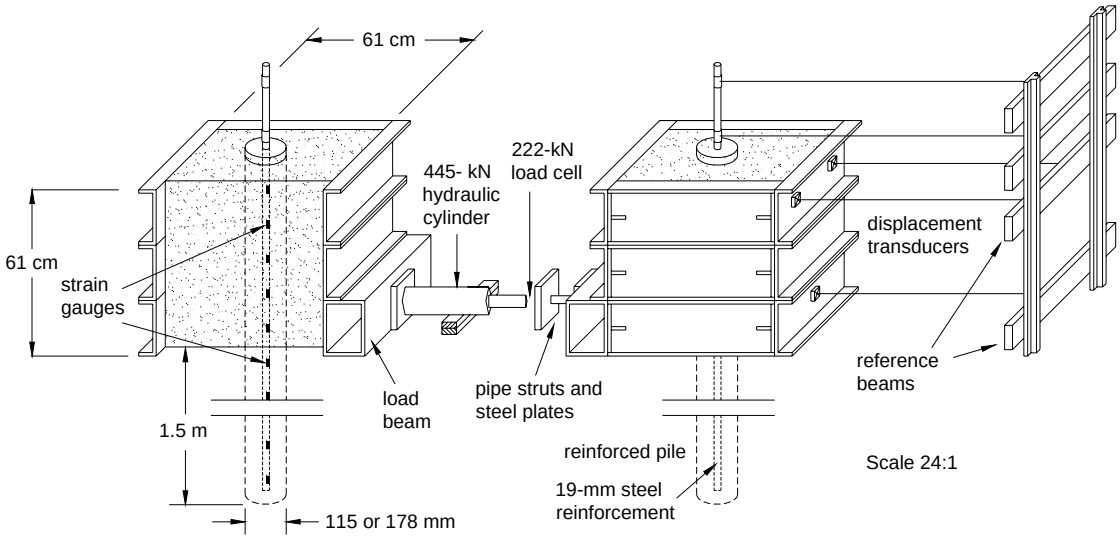

Figure 10. Large-scale direct shear test set-up

Preliminary analyses of proposed pile diameters and steel reinforcement were performed to determine critical pile lengths and demarcate rigid piles from flexible piles. Figure 11 illustrates the relationship between pile head deflection and pile length, where a uniformly distributed load was applied to the uppermost two feet of each pile. Pile lengths greater than 1.8 meters (L/D = 12-14) resulted in flexible pile behavior, evidenced by stabilization of pile head deflection. Based on this data, each pile extended 1.5 meters into existing ground, resulting in total pile lengths of 2.1 meters.

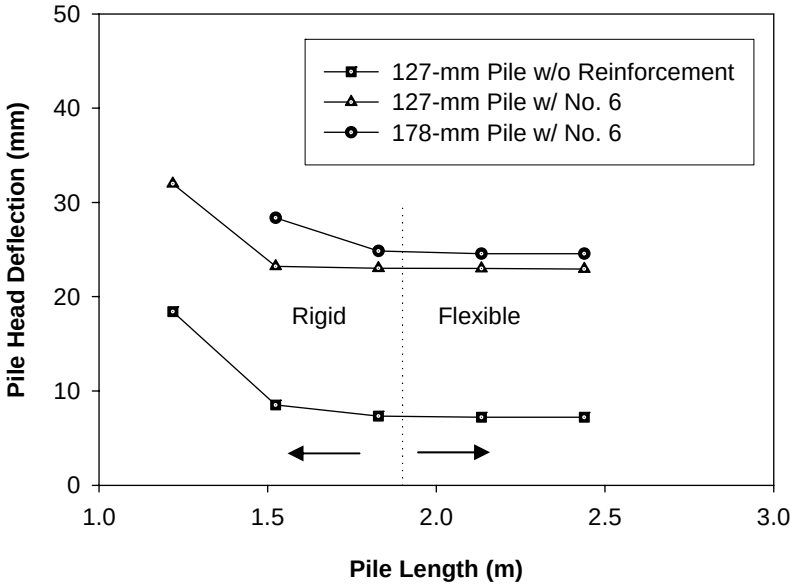

Figure 11. Pile head deflection vs. length for determination of critical pile length

The research testing plan is diagrammed in Figure 12 to show the tests that were performed on soil, pile materials, and reinforced soil. The figure summarizes how each test aids the desired analyses of piles subject to lateral soil movement.

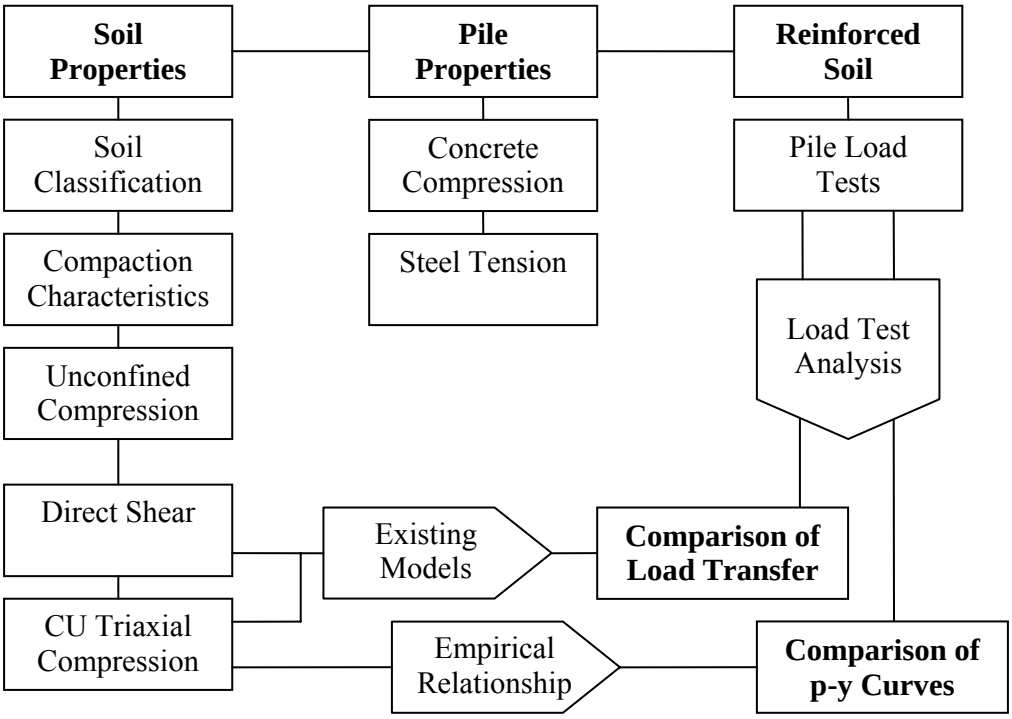

Figure 12. Research testing plan

Test Location, Personnel, and Duration

The research testing program was completed at Iowa State University. Laboratory tests were performed at the Gerald Olson Soil Mechanics Laboratory, and pile load tests were conducted at the Spangler Geotechnical Experimentation Site (SGES) located in Ames, Iowa. Foundation research investigations have previously been performed at the SGES. The site soil conditions, inclusive of p-y curves developed from full-scale pile load tests, have been documented (Hong, 2003). The soil profile and p-y curves of the uppermost soil layers are provided in Appendix A. Engineering properties of the non-stratified glacial till are provided in Table 3.

Table 3. SGES Engineering Properties

Soil Parameter	Range of Values
Density	1920 to 2160 kg/m^3
Cohesion	20 to 210 kPa
Friction Angle	19 to 31 degrees
OCR	1.5 to 4
LL, PI	30 - 40% and 10 - 20%
Soil Classification	CL
Permeability	10^{-4} to 10^{-5} cm/s
Modulus	5,000 to 17,000 kPa

Laboratory testing was conducted from October of 2003 through May of 2004, concurrent with the review of literature and preliminary analyses. The field investigation was conducted during the summer of 2004. Pile load tests were prepared and performed in May and June, respectively.

Soil Acquisition

For the research, the state of Iowa was divided into three upland regions of different topography and surface geology. Soils from the regions (e.g. glacial till, loess, and weathered shale) were collected for use in the testing program. The soils were characterized with laboratory testing and used in pile load tests. Employment of the same soils in laboratory and field testing was necessary for pile load test data interpretation and analysis.

The north central portion of the state is comprised of glacial till from the Des Moines Lobe Glaciation. Glacial till was obtained in Ames, Iowa.

The western portions of the state, which are adjacent to the Missouri River floodplain, have deep loess soils that form very steep hillslopes and narrow drainage divides. The western Iowa loess is often referred to as friable loess. Figure 13 illustrates the loess deposits with a photograph of the Loess Hills. Loess used in testing was obtained from a cut section in the Loess Hills of western Iowa. The loess source, which is in Turin, Iowa, is shown in Figure 14.

Weathered shale was obtained from a slope failure near Luther, Iowa. The weathered shale source, shown in Figure 15, is located on Highway E57 next to the Des Moines River.

Figure 13. Loess hills of western Iowa

(a)

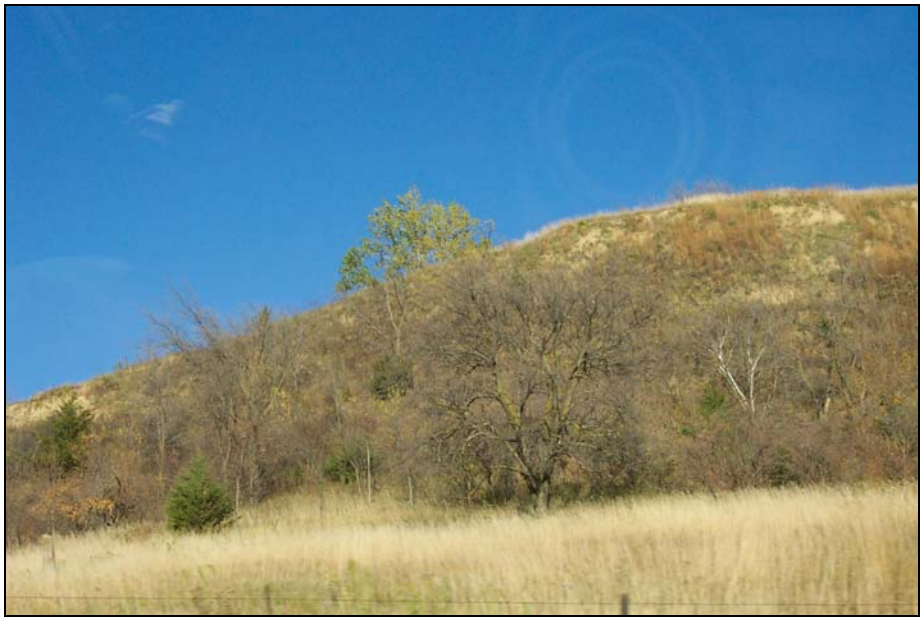

(b)

Figure 14. Loess source (Turin, Iowa)

(a)

(b)

Figure 15. Weathered shale source (Luther, Iowa)

Laboratory Testing Program

Soil Classification

Gradation analysis and Atterberg limit tests were performed on each soil sample according to ASTM D 2487 [Test Method for Classification of Soils for Engineering Purposes] and ASTM D 4318 [Standard Test Method for Liquid Limit, Plastic Limit, and Plasticity Index of Soils] (ASTM 2000), respectively. The Atterberg limits for each soil are provided in Table 4. Gradation analyses of the soils are provided in Table 5 and Figure 16.

Table 4. Atterberg limits

Soil Type	LL	PL	PI
Loess	29	23	6
Glacial Till	24	15	9
Weathered Shale	35	24	11

Table 5. Gradation analysis

Soil Type	Gravel (> 2.00 mm)	Sand (> 0.075 mm)	Silt (> 0.002 mm)	Clay (< 0.002 mm)
Loess	0.0	2.9	90.9	6.2
Glacial Till	1.4	46.3	37.7	14.6
Weathered Shale	0.0	9.1	51.7	39.2

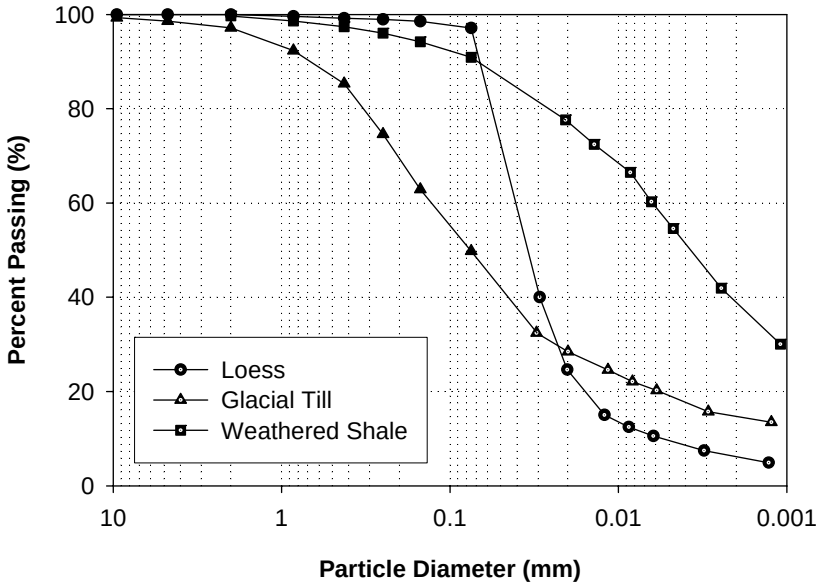

Figure 16. Grain size distribution curve

Each soil was classified according to the Unified Soil Classification System (USCS), the AASHTO classification system, and the United States Department of Agriculture (USDA) textural classification system. Soil classifications are provided in Table 6.

Table 6. Soil classifications

	USCS		AASHTO		USDA
Soil Type	**Group Symbol**	**Group Name**	**Classification**	**GI***	**Textural Classification**
Loess	ML	Silt	A-4	(6)	Silt loam
Glacial Till	CL	Sandy lean clay	A-4	(2)	Sandy loam
Weathered Shale	CL	Lean clay	A-6	(11)	Silty clay loam

Notes:
* Group Index = $0.01\ (F_{200} - 35)\ [0.2 + 0.005\ (LL - 40)] + 0.01\ (F_{200} - 15)\ (PI - 10)$

Moisture and Density Properties

The specific gravity was determined for each soil type. The tests were performed according to ASTM C 128 [Specific Gravity and Absorption of Fine Aggregate] (ASTM 2002). Specific gravities are provided in Table 7.

Table 7. Specific gravities

Soil Type	**G_s**
Loess	2.72
Glacial Till	2.66
Weathered Shale	2.69

The compaction moisture-density relationship was developed with the standard Proctor test, performed according to ASTM D 698, Method A [Standard Test Method for Determining the Moisture-Density Relations of Soils and Soil-Aggregate Mixtures] (ASTM 2000). The maximum dry unit weights and optimum moisture contents are provided in Table 8, and the moisture-density relationships are shown in Figure 17.

Table 8. Maximum dry unit weights and optimum moisture contents

Soil Type	**w_{opt} (%)**	**$\gamma_{d\ max}$ (kN/m^3)**
Loess	18	15.55
Glacial Till	14	17.75
Weathered Shale	18	16.65

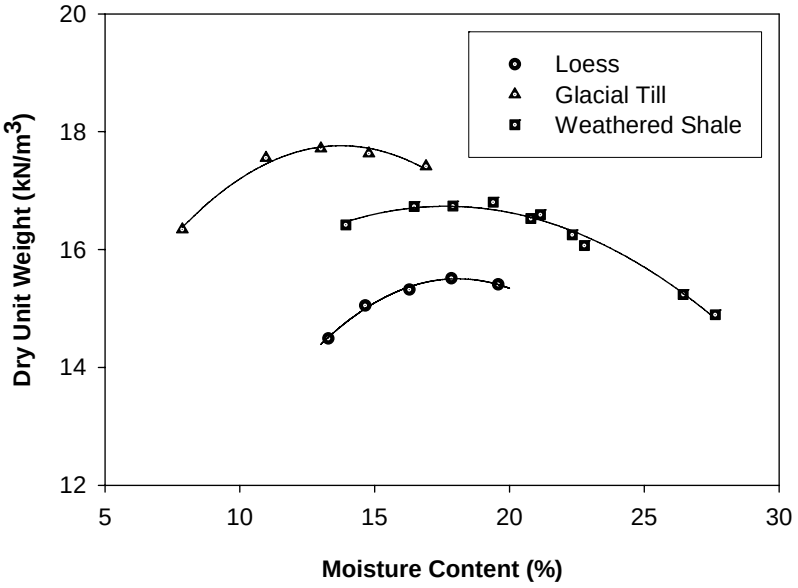

Figure 17. Graph of dry unit weight vs. moisture content

Upon acquisition of soil samples, moisture contents were determined for the in-situ moisture of the soil. The natural moisture contents, provided in Table 9, were used as the conditions for subsequent test preparation.

Table 9. Natural moisture contents

Soil Type	$w_{natural}$ (%)
Loess	8.6
Glacial Till	11.8
Weathered Shale	21.8

Direct Shear Test

Direct shear tests were performed on each sample to determine effective cohesion, c, and effective internal friction angle, ϕ. Samples were compacted, saturated under load, and then sheared at a sufficiently-slow rate to avoid build-up of excess pore water pressures. The loess and glacial till samples were sheared at 1.27 mm per minute, and the less-permeable weathered shale samples were sheared at 0.025 mm per minute. The effective shear strength parameters are provided in Table 10, and the failure envelopes are shown in Figure 18.

Table 10. Effective shear strength parameters from direct shear tests

			Compaction	
Soil Type	**ϕ (deg)**	**c (kPa)**	**γ_d (kN/m^3)**	**w (%)**
Loess	28	25	14.9	14
Glacial Till	31	31	17.8	12
Weathered Shale	21	24	16.3	22

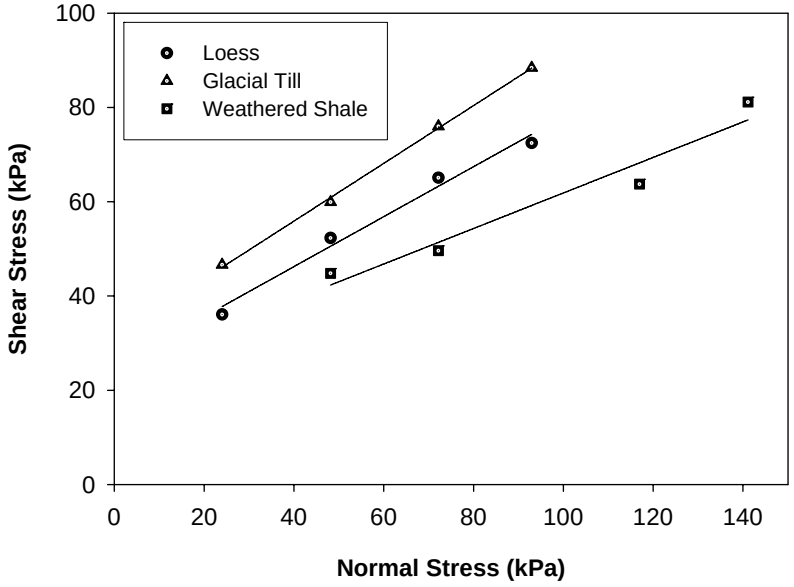

Figure 18. Direct shear test failure envelopes

Unconfined Compression Test

The unconfined compression test is a unique case of the triaxial test. In this instance, the confining pressure, σ_3, equals zero. The soil sample experiences considerable deformation as an axial load is applied. The unconfined compression strength, q_u, is commonly used as an indicator for the consistency of saturated clays (Das 1999). Additionally, the unconfined compression strength indicates the value of the undrained shear strength, s_u. Equation (19) defines the relationship between undrained shear strength and unconfined compression strength. The equation is valid for clays, which routinely assume the undrained friction angle, ϕ, equals zero for the design of foundations.

$$s_u = \frac{q_u}{2} \tag{2}$$

where s_u is the undrained shear strength and q_u is the unconfined compression strength. Average unconfined compressive strengths are provided in Table 11.

Table 11. Unconfined compression strength

	Unconfined Strength (kPa)		Compaction		
Soil Type	**Average**	**Std Dev**	**γ_d (kN/m^3)**	**w (%)**	**n**
Loess	19.3	6.6	15.6	31	3
Glacial Till	105.5	9.8	20.0	17	5
Weathered Shale	8.0	—*	16.0	23	1

Notes:
* Data not available
n = number of tests

Typical stress-strain relationships for unconfined compression tests in loess, glacial till, and weathered shale are provided in Figures 19 through 21.

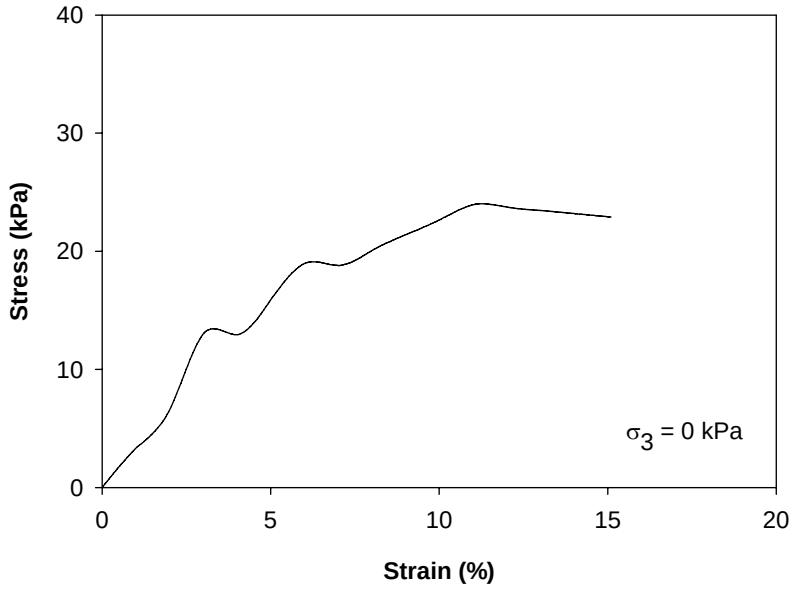

Figure 19. Unconfined compression test stress-strain relationship for loess

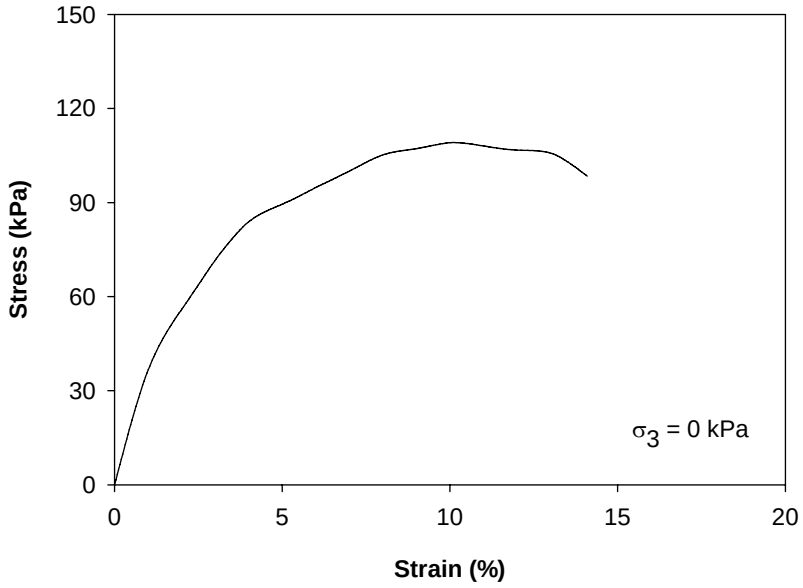

Figure 20. Unconfined compression test stress-strain relationship for glacial till

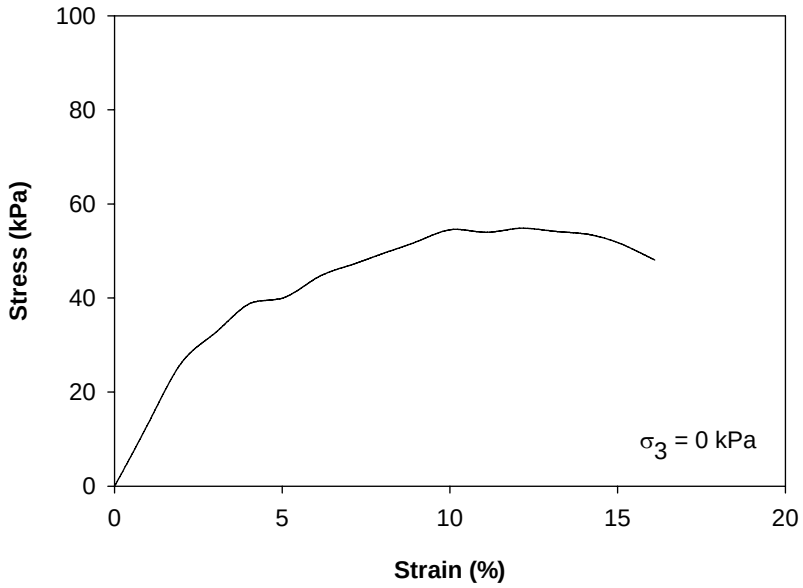

Figure 21. Unconfined compression test stress-strain relationship for weathered shale

Consolidated-Undrained (CU) Triaxial Test

Consolidated-undrained (CU) triaxial tests were performed on a single specimen for each soil type. Each of the three test specimens (one specimen per soil type) was saturated and subsequently consolidated at 34.5 kPa. The specimen was loaded and the stress-strain behavior was recorded by a data acquisition system. Following the loading, the specimen was consolidated at 103.5 kPa. The specimen was reloaded and allowed to strain significantly more than at the lower confining pressure. Confining pressures of 34.5 and 103.5 kPa were selected to develop boundary p-y curves from which intermediate load-displacement curves could be used for the analysis. The stress-strain relationships for triaxial compression tests in loess, glacial till, and weathered shale are provided in Figures 22 through 24.

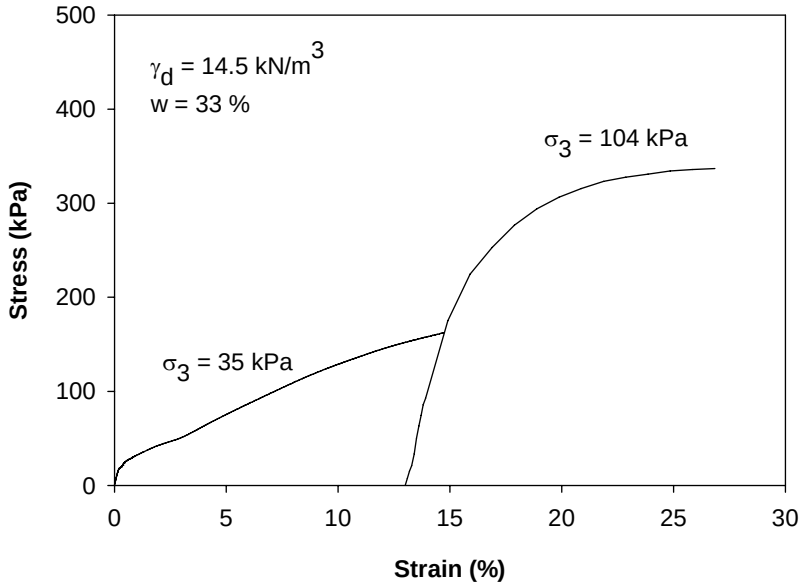

Figure 22. CU triaxial test stress-strain relationship for loess

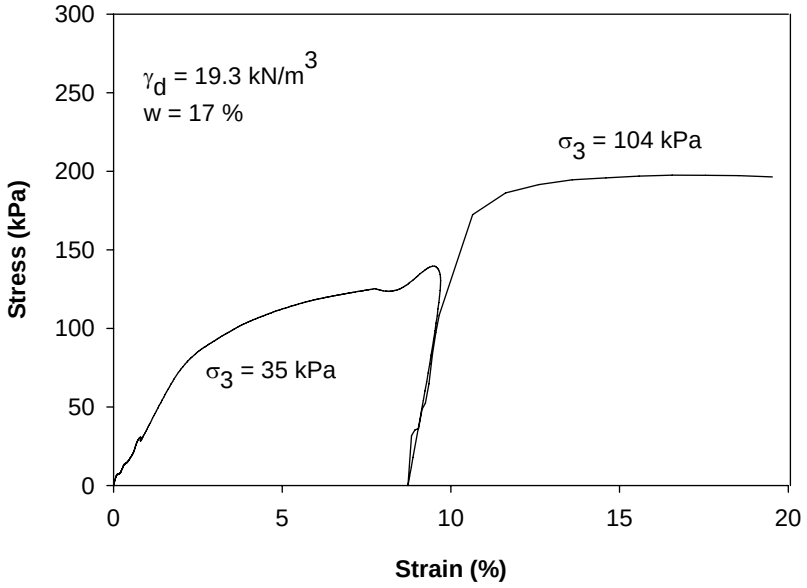

Figure 23. CU triaxial test stress-strain relationship for glacial till

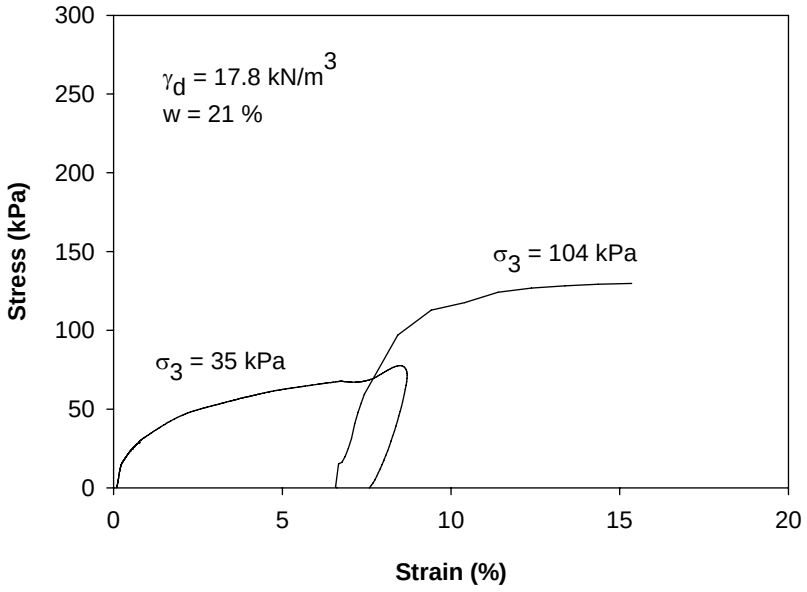

Figure 24. CU triaxial test stress-strain relationship for weathered shale

The load-displacement behavior of the triaxial tests, including the behavior of the unconfined compression tests, was used in developing p-y curves for pile load test analyses. The ultimate soil pressure (p_u) and strain at 50 percent of maximum load (ε_{50}) define the shape of p-y curves developed from triaxial compression tests. The p-y curves were developed from an equation of the following form (Reese and Wang 2000):

$$\frac{p}{p_u} = 0.5 \left(\frac{y}{y_{50}}\right)^n \tag{3}$$

where p_u = ultimate soil resistance (force/length)

y_{50} = deflection at one - half the ultimate soil resistance (length)

$n = \frac{1}{3}$ for soft clay, proposed by Matlock (1970)

$n = \frac{1}{4}$ for stiff clay, proposed by Reese and Welch (1975)

The ultimate soil resistance, p_u, is the smaller value given by the following equations (Reese and Wang 2000):

$$p_u = [3 + \frac{\gamma'}{c_u} + \frac{J}{b} x]\, c_u\, b \tag{4}$$

$$p_u = 9\, c_u\, b \tag{5}$$

where γ' = aveage effective unit weight from ground to p - y curve

x = depth to p - y curve

c_u = undrained shear strength

b = pile diameter

J = empirical coefficient (0.25 for soft clay, 0.5 for medium and stiff clay)

The y_{50} is determined with the following equation:

$$y_{50} = 2.5\, \varepsilon_{50}\, b \tag{6}$$

Based on strengths from unconfined compression tests, the loess was characterized as soft clay. The glacial till and weathered shale was characterized as stiff clay. Figures 25 through 28 show the p-y curves developed from CU triaxial tests. The p-y curves of Figure 28, those

used for the load test analysis, correspond to strengths measured with no confining stress (σ_3 = 0 kPa). The undrained shear strength was assumed to equal one-half of the unconfined compressive strength.

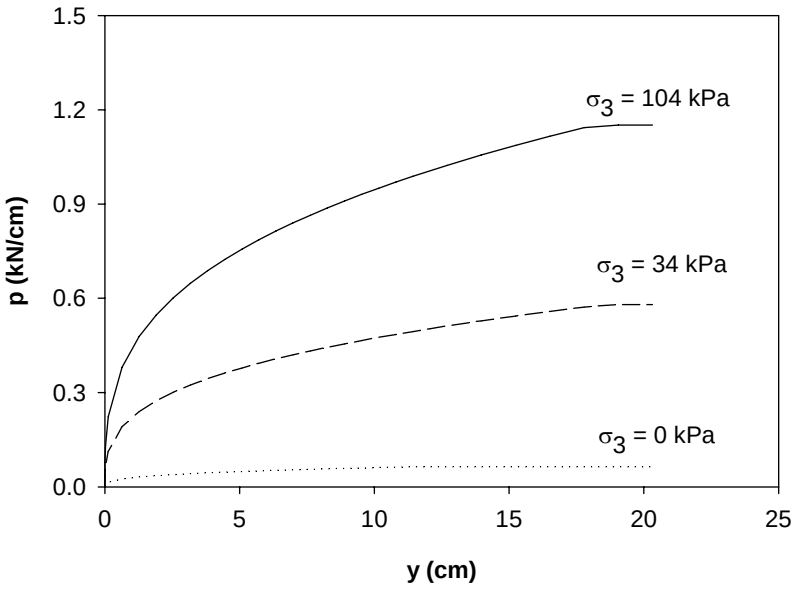

Figure 25. Load-displacement (p-y) curves for loess

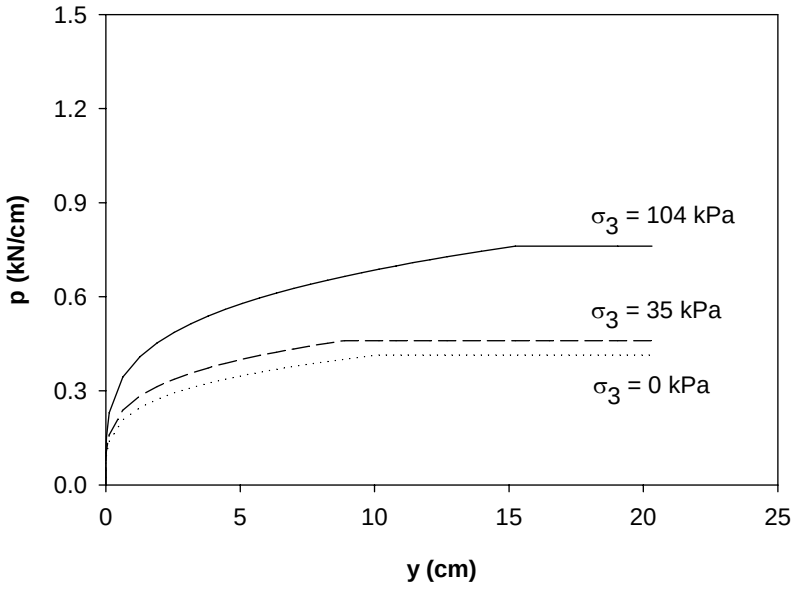

Figure 26. Load-displacement (p-y) curves for glacial till

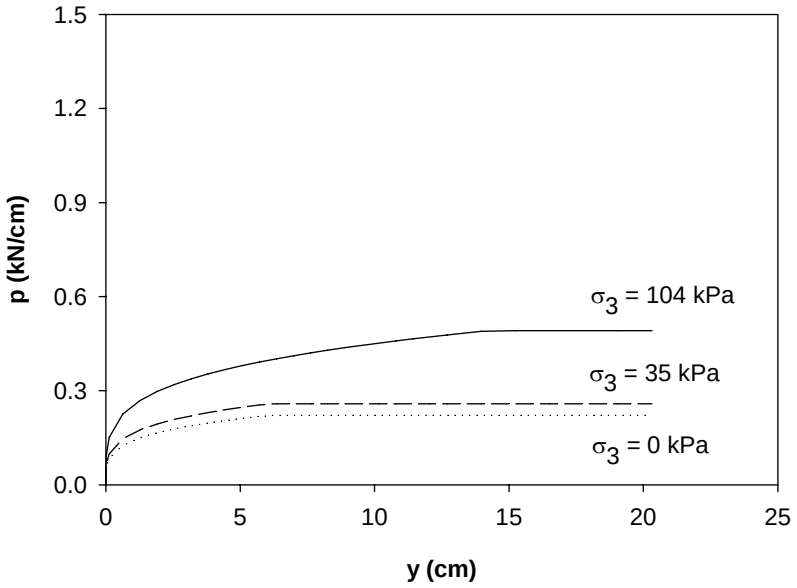

Figure 27. Load-displacement (p-y) curves for weathered shale

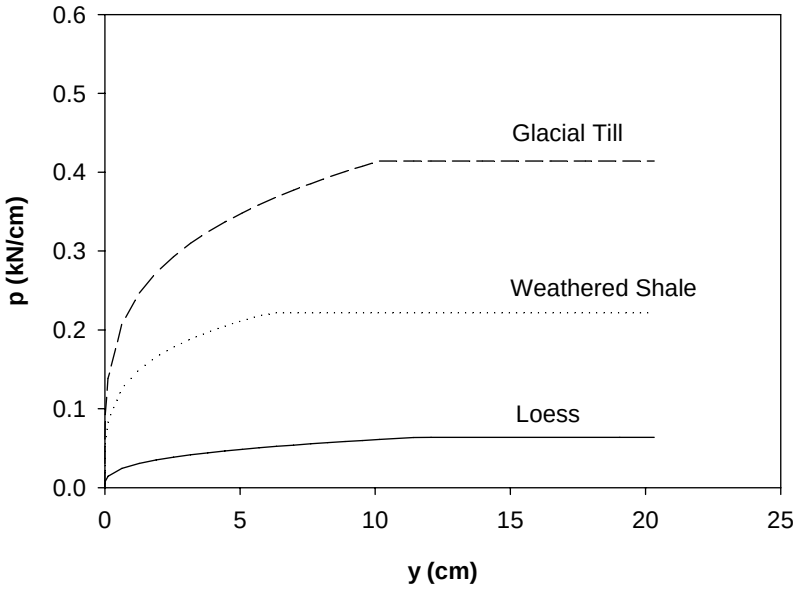

Figure 28. Load-displacement (p-y) curves for analysis

Concrete Mixture Design

The proposed micropiles employed small diameters (100 to 200 mm), and the workability of a potential concrete mixture design was of critical importance to the construction and subsequent performance of the piles under the loading conditions of slope reinforcement. Several high-slump concrete mixtures for use in soil displacement grouted micropiles were evaluated. Based principally on self-compacting concrete (SCC) and controlled low-strength material (CLSM), a new mixture design was tested and recommended for use in the pile load tests. The proposed mixture design satisfied the preliminary performance criteria established at the onset of the research project, in that the concrete mixture was highly fluid and achieved sufficiently high compressive strength (> 27.6 MPa).

The selection of a concrete mixture design for use in pile load tests evolved from published mixture designs for CLSM (CTRE 2003) and SCC (Schlagbaum 2002) of residential and structural applications. The SCC and CLSM mixture designs were developed and subjected to preliminary tests. Freshly mixed concrete was tested for workability, and hardened concrete was tested for compressive strength. A concrete mixture for soil displacement grouted micropiles was then developed to approximately exhibit the flow properties of CLSM and the mechanical performance properties of SCC. Mixture proportions and performance properties of each concrete mixture are provided in Table 12.

Table 12. Preliminary mixture proportions and test results

Category	Criteria	SCC [a]	CLSM [b]	Selected Mixture
Constituent	Cement (lb/cy)	600	100	600
	Fly ash (lb/cy)	n/a	400	125
	Fine aggregate (lb/cy)	1340	2600	2700
	Coarse aggregate (lb/cy)	1700	n/a	n/a
	w/cm	0.55	1.12	0.65
Admixtures	HRWR [c] (fl oz/cwt)	8	n/a	8
	VMA [d] (fl oz/cwt)	2	n/a	2
Performance	21-day strength (MPa)	54.35	2.68	30.34
	Slump (cm)	17.8	27.9	27.4

[a] Schlagbaum (2002)
[b] Center for Transportation Research and Education (2003)
[c] High range water reducer
[d] Viscosity modifying admixture

Concrete sand was obtained from Hallet Materials in Ames, Iowa. Gradation of the sand is shown in Figure 29.

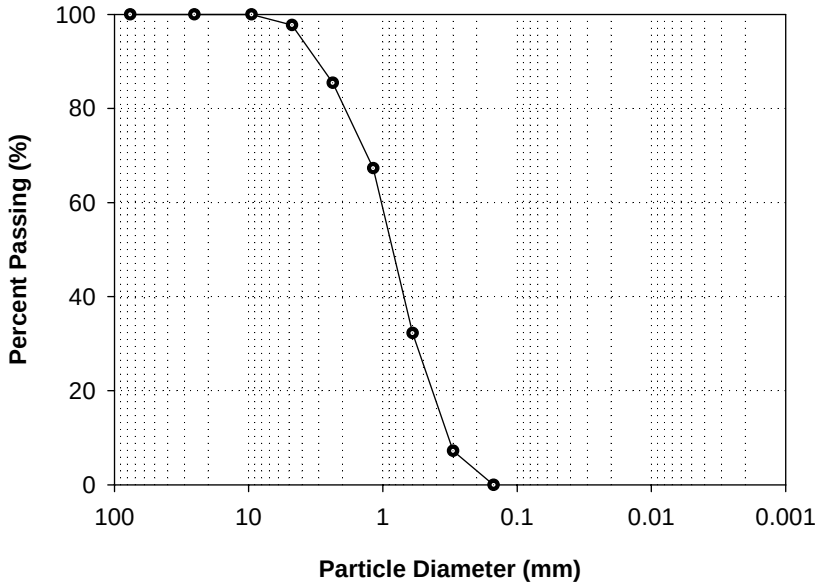

Figure 29. Concrete sand gradation

The compressive strength development of each flowable concrete mixture design is provided in Table 13 and Figure 30.

Table 13. Compressive strength development for concrete mixtures

Days	CLSM	SCC	SDGM
0	—*	—*	—*
7	1.71	35.38	20.10
14	2.28	47.51	28.74
21	2.68	54.35	30.34
28	—*	—*	30.85

Notes:
Strengths in units of MPa
* Data not available

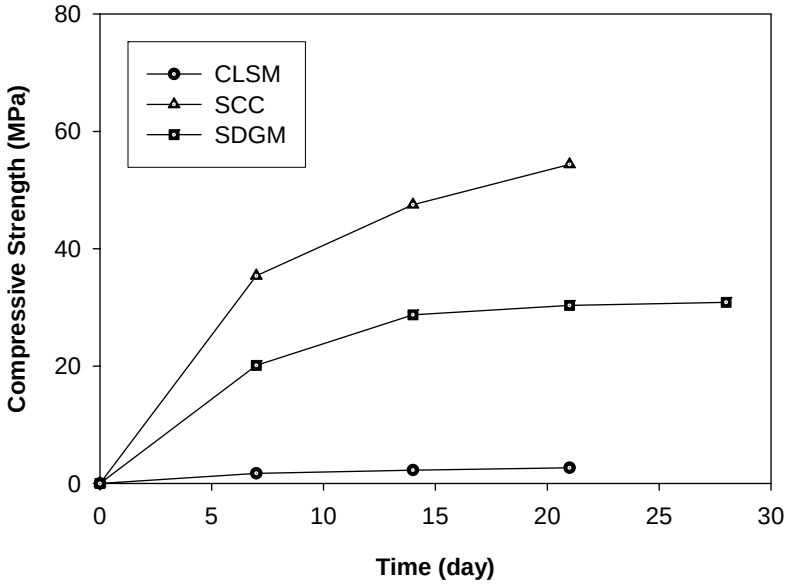

Figure 30. Strength development of concrete mixtures

Sufficient testing has not yet been performed to optimize mechanical and flow properties of the mixture design with respect to cost effectiveness. This evaluation is complicated by issues of composite materials, constructability, and costs associated with quality control/assurance practices. The development of more advanced concrete/grout mixtures is beyond the scope of the current research project.

Field Testing Program

Load Test Plan

The pile load test plan evaluated soil type, pile size, and the effect of pile grouping as each parameter relates to the performance of the slope reinforcement system. Each reinforcement parameter influences the response of piles subject to lateral soil movement. The influence of the parameters on pile behavior is evidenced by the dependence of p-y curves on the parameters.

The pile load test plan, provided in Table 14, included seven load tests of 14 different pile configurations. Direct shear boxes were loaded against each other, where each test involved the simultaneous loading of two boxes. The full-scale tests were conducted to evaluate the performance of 115-mm and 178-mm piles, each reinforced with a centered No. 19 steel rebar.

Table 14. Pile load test plan

Test Number	Box Numbers	Soil Types	Pile Sizes*
1	1	Loess	No Pile
	2	Weathered Shale	No Pile
2	3	Glacial Till	No Pile
	4	Loess	114-mm Pile
3	5	Glacial Till	112-mm Pile
	6	Weathered Shale	117-mm Pile
4	7	Weathered Shale	114-mm Pile **
	8	Loess	183-mm Pile
5	9	Glacial Till	178-mm Pile
	10	Weathered Shale	(2) 113-mm Piles
6	11	Loess	(2) 114-mm Piles
	12	Weathered Shale	173-mm Pile
7	13	Glacial Till	(2) 113-mm Piles
	14	Glacial Till	(2) 115-mm Piles

Notes:
All piles with No. 19 rebar
* Measured after pile exhumation
** No pile reinforcement

Site Preparation and Load Test Set-Up

Pile load tests were conducted at the Spangler Geotechnical Experimentation Site in Ames, Iowa. The site was covered by vegetation that required removal prior to testing. Figure 31 shows the clearing of site vegetation with a skid loader. Frequent and heavy rainfall events resulted in difficult working conditions on the flat, bare site. The field testing site was ultimately covered with gravel to facilitate wet-weather access. The presence of gravel, however, had no influence on the test performance and obtained test results.

Pile load tests were laid out prior to excavating control soil pads and compacting soil in shear box forms. The initial test layout ensured that sufficient spacing was available for the necessary load frame and loading system (e.g. load cells, hydraulic cylinders). The use of string lines helped in keeping shear box forms aligned with loading counterparts. Figure 32 shows the initial test layout.

Control soil pads were excavated at each shear box location. The control pads, excavated with plan dimensions of 75 cm and to depths of 30 cm, ensured that all potential failure surfaces during load testing were contained within the soil of known shear strength parameters (i.e. loess, glacial till, weathered shale). A failure surface located at the interface of the existing site soil and the soil of the shear box would likely complicate the evaluation of the load-displacement behavior of laterally-pushed shear boxes. The soil pads served as a means for control to facilitate more reliable load test analyses. Figure 33 shows the manually-excavated control soil pads.

Soil was compacted in the control soil pads and shear box forms with hand tampers. The compaction of soil occurred at approximately natural moisture for each soil type, and the compaction effort was uncontrolled. Soil sampling that followed pile load tests, however, indicated that relatively uniform density was achieved during the preparation of the load tests. The results of the soil sampling investigation (i.e. moisture and density, dynamic cone penetrometer, unconfined compression, and Ko stepped blade) are described in Chapter 4. Figures 34 and 35 show the compaction of soil in control soil pads and shear box forms, respectively.

Figure 36 shows completed shear box forms containing compacted soil. The forms were elevated approximately 2.5 to 5 centimeters, such that failure surfaces potentially exhibit some thickness.

Piles were installed through the shear box forms approximately 1.5 meters into the glacial soils of the experimentation site. Boreholes were prepared with the Iowa State University Mobile B57 drill rig, used principally for relatively shallow soil sampling and site investigation. Figure 37 shows the preparation of boreholes. Smaller-diameter piles were prepared with a 114-mm-diameter auger. Larger-diameter piles were prepared using a hollow-stem auger with a 178-mm outside diameter. Exhumation of piles following the performance of pile load tests indicated that actual/measured pile diameters were of approximately the same dimension as auger diameters.

The developed concrete mixture was prepared at the testing site and, upon completion of individual boreholes, bottom-fed into the cavity using a PVC casing. Estimated concrete slump ranged from 20 cm to 24 cm, making vibration of the material unnecessary, as planned. Although bottom-feeding the concrete mixture through PVC casing prevented segregation and ensured pile integrity and uniformity, the concrete mixture was principally bottom-fed to avoid placement of concrete through a variable water table. Figure 38 shows the placement of concrete through the casing. The strength of concrete was verified by performing compression tests on 76-mm-diameter test cylinders. The cylinders from each batch (one batch per pile) were field cured for two days following pile installation and subsequently stored in a humid room. The cylinders were tested on the same day the pile load test was performed. Compressive strengths at the time of pile load testing (approximately 2-3 weeks) ranged from 26.9 MPa to 34.1 MPa. The average compressive strength was 29.6 MPa with a standard deviation of 2.4 MPa (42 tests). The compressive strengths were used to develop unique moment-curvature graphs for each pile and are provided in Appendix B.

Pile reinforcement (No. 19 rebar for all piles) was incorporated into the grouted boreholes immediately following the satisfactory placement of concrete. The reinforcement was centered in the borehole with spacers and orientated such that strain gauges were facing the tension-side of the piles. Figure 39 shows several shear box forms with compacted soil and steel-reinforced pile elements. The piles remained undisturbed for approximately two weeks following installation so that the concrete mixture developed adequate strength for loading.

(a)

(b)

Figure 31. Clearing of site vegetation at SGES

Figure 32. Test layout

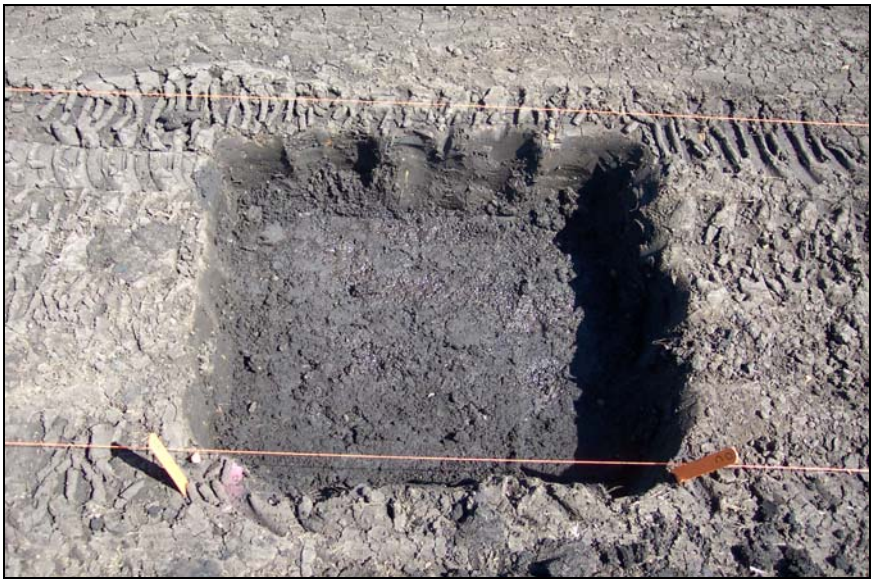

(a)

(b)

Figure 33. Excavation of control soil pads

(a)

(b)

Figure 34. Compaction of soil control soil pads

(a)

(b)

Figure 35. Compaction of soil shear box forms

Figure 36. Prepared shear box forms

(a)

(b)

Figure 37. Preparation of borehole

(a) (b)

Figure 38. Placement of concrete through PVC casing

(a)

(b)

Figure 39. Reinforced soil in shear box forms

Load Test Performance

Large-scale direct shear tests were conducted on the composite system of soil and slender pile elements. The research group measured the load-displacement behavior of shear boxes, the load-displacement behavior of pile heads, and the strain of pile reinforcement (subsequently converted to bending moment for comparison with predicted moment values). The following paragraphs detail the instrumentation that was used to measure loads and deflections, the equipment that was used to apply horizontal loads to the shear boxes, and the data acquisition system.

The displacement of each shear box was measured with three displacement gauges. Two gauges were mounted to the top of the box (left and right), and one gauge was mounted to the bottom of the box (middle). Use of three gauges to measure displacement provided the data set with redundancy and offered evidence of rotation (about vertical axis) and tilt (about horizontal axis) of the box with continued loading. The instrumentation was mounted on wood reference beams, which were attached to fence posts driven into existing ground outside the zone of influence of the test system. The arrangement for measuring displacements is shown in Figure 40.

Displacement gauges were additionally mounted to the section of reinforcement extending above the pile head. The distance between the two gauges was measured, such that the difference in displacement was used to calculate the pile head slope (i.e. rotation) at a given load. The pile head slopes were used to adjust the lower of the displacement gauges for more accurate pile head displacements (i.e. pile head displacement at the soil surface). The use of displacement gauges to measure pile head displacement and slope is shown in Figure 41.

Strain of the pile reinforcement was measured concurrent with load and displacement measurements. Strain gauges were installed on the reinforcement at pre-determined elevations, based on moment profiles from preliminary analyses. A total of ten strain gauges were used to define the strain and moment profiles of piles during loading. The employed strain gauges were type FLA-3-11, gauge factor 2.13, manufactured by Tokyo Sokki Kenkyujo Co., Ltd. Each gauge level consisted of a single gauge on the tension-side of the reinforcement. The installation of strain gauges is shown in Figure 42.

The loading system of the large-scale direct shear tests included a load frame (pipe struts and steel plates); a pump-controlled, 12-in-stroke hydraulic cylinder; and a load cell. The capacity of the loading system, controlled by the load cell, was 50 kips. The loading system was placed between the shear boxes of a given test, and equivalent loads were simultaneously applied to each shear box by pressurizing the ram cylinder. The loading system is shown in Figure 43.

The electronic deflection measuring devices, the load cell, and strain gauges produce a voltage signal that was monitored through an analog-to-digital data acquisition system. The instrumentation was connected to individual terminal channels of the acquisition hardware, and the system software was programmed to record a measurement reading at 3-second intervals. The data acquisition system, mounted inside a cargo van for protection against

inclement weather and transportation of the system around the site, is shown in Figure 44.

Figure 40. Displacement gauge locations on shear boxes

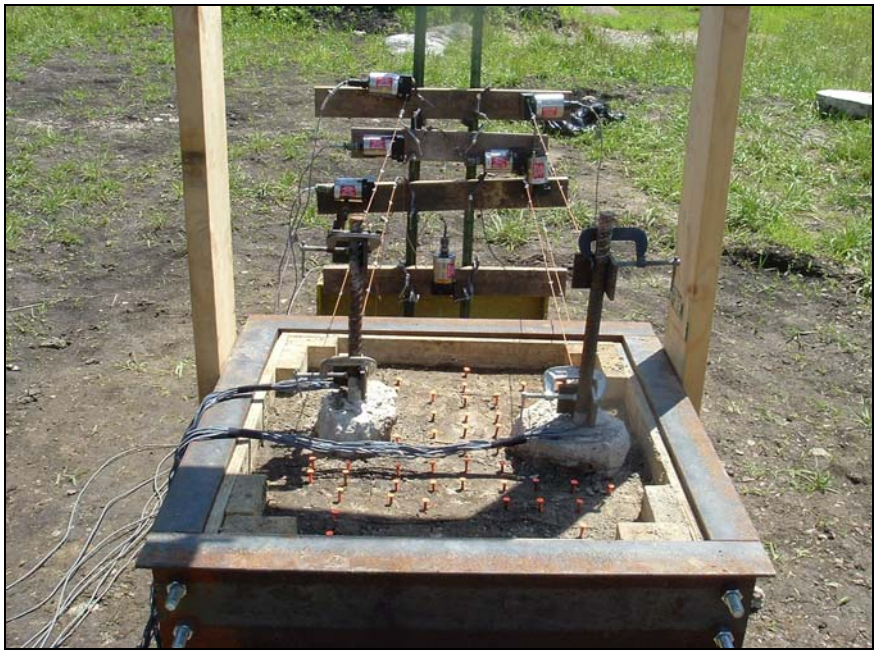

Figure 41. Displacement gauge locations on piles

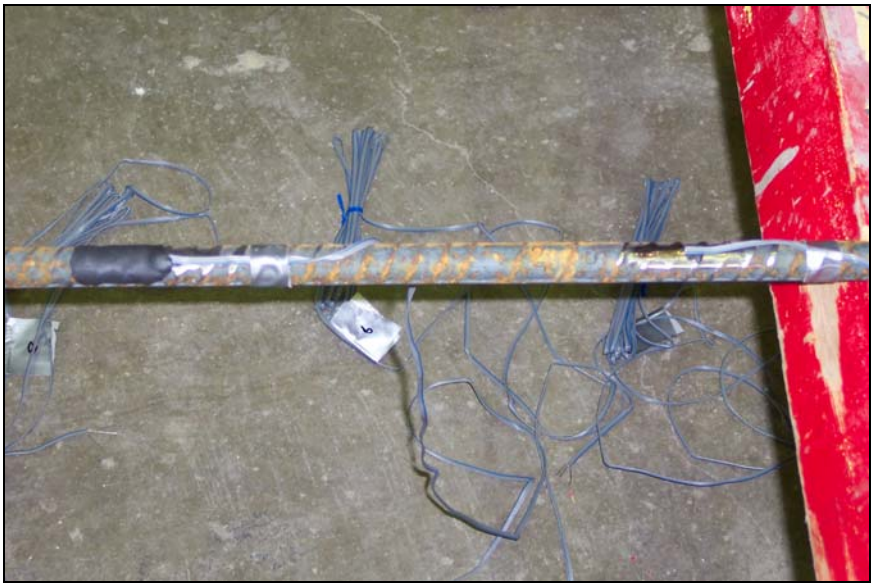

(a)

(b)

Figure 42. Displacement gauge locations on piles

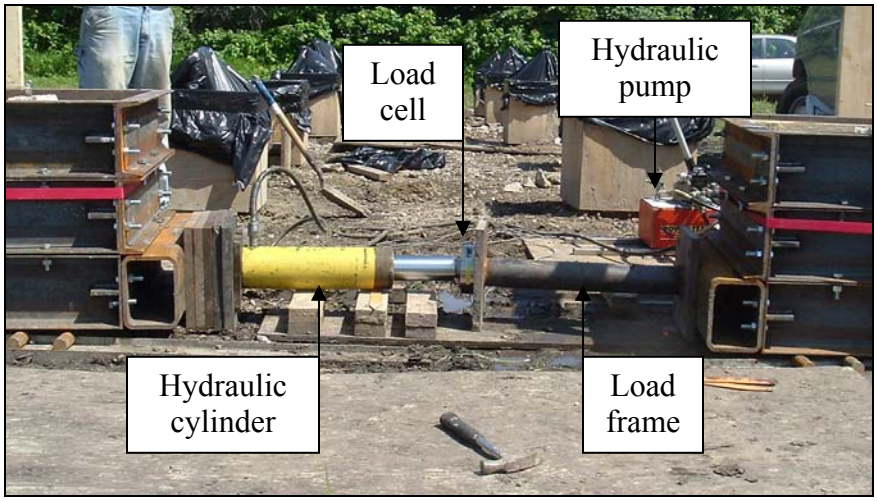

Figure 43. Pile load test loading system

Figure 44. Data acquisition system

Pile load tests were performed by monitoring shear box displacements and controlling the load applied to each shear box. Load increments of approximately 1 kN were applied to the system, and the displacements of each shear box were monitored at the relatively constant load. The next load increment was applied when the rate of displacement for each box became small. The research group believed that the loading process most accurately offered drained soil behavior, as opposed to undrained soil behavior, because excess pore pressure are more likely to dissipate at slower shearing rates. The test performance method resulted in loading times between 90 and 180 minutes. After a pile load test was completed, the shear boxes and loading system were disassembled and moved to the next test location.

The load-displacement data of Appendix C shows unload-reload cycles. As the shear boxes

were pushed laterally, the loading system (e.g. hydraulic cylinder, load cell, load frame) became overextended and increasingly unstable. The applied load of the system was released and, upon adjustment of the loading system, reapplied.

Data Interpretation (Strain-Curvature-Moment Relationship)

As the evaluation of pile response is generally completed by examining the deflection, shear, and moment of a pile, the analysis of test data required an understanding of the relationship between steel strain and bending moment. Data interpretation (i.e. conversion of strain to moment) was achieved by performing moment-curvature analyses for the pile sections, with input parameters being cross-sectional configuration (e.g. diameters, reinforcement arrangement) and material properties (e.g. strength, modulus). For the full range of loading, from an unloaded condition to section failure, the relationship examines member ductility, development of plastic hinges, and redistribution of elastic moments that occur in reinforced concrete sections (Nilson 1997). The analysis additionally provides the strain distribution through pile sections, such that the strain of pile reinforcement is directly related to bending moment. The relationship between pile flexural stiffness (EI) and bending moment is shown in Figure 45 to indicate the stages of pile behavior for the range of possible loading conditions.

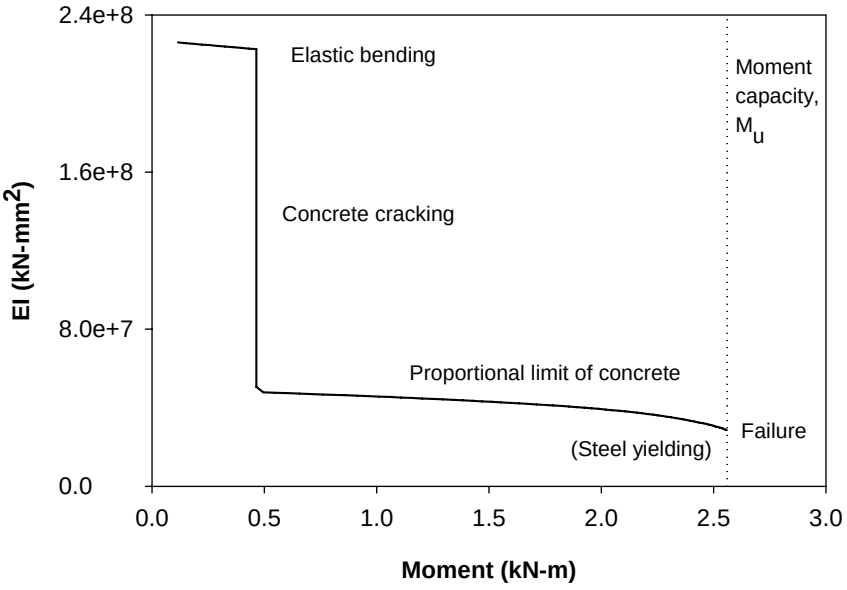

Figure 45. Pile stiffness-moment relationship

Strain profiles for uncracked and cracked pile sections are shown in Figure 46 to illustrate the relationship between the neutral axis position, curvature, and strain. Given curvature and "maximum" strain, the gauge strain (i.e. strain at tension side of reinforcement) is obtained with the following equation:

$$\varepsilon_{gage} = \varepsilon_{max} - \psi \left(\frac{d_p}{2} \pm \frac{d_b}{2}\right) \tag{7}$$

where ε_{gage} = gauge strain

ε_{max} = strain at top of section, as illustrated

ψ = curvature

d_p = pile diameter

d_b = reinforcement diameter

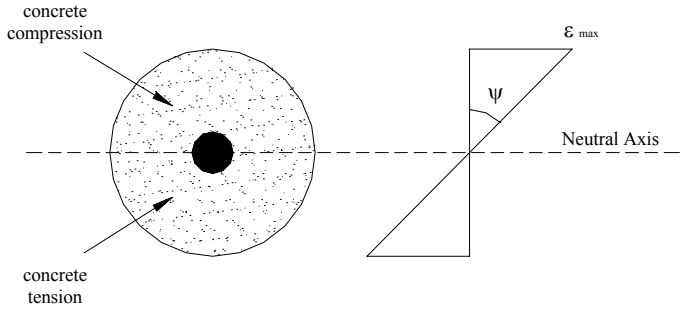

(a)

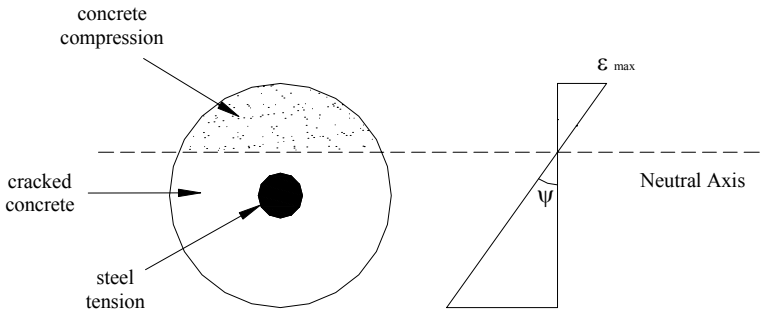

(b)

Figure 46. Pile sections with strain profiles

Equation (7) facilitates the conversion of "maximum" strain and curvature, obtained from LPILE analyses, to gauge strain. Stiffness and gauge strain vs. moment is graphed in Figure 47 and is the means by which gauge strain is converted to moment for subsequent comparison with predicted pile response by LPILE. Graphs of pile stiffness and gauge strain vs. moment for specified pile sections and material properties are provided in Appendix B.

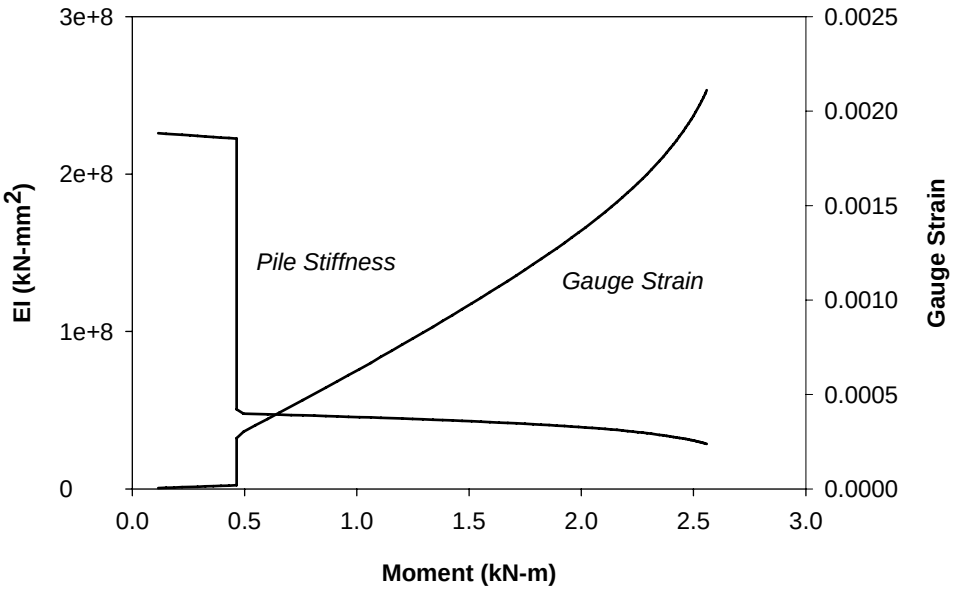

Figure 47. Stiffness and gauge strain vs. moment

The conversion of measured strain values to bending moments is demonstrated in Table 15 and Figure 48. The strains of Table 16 are those measured in Pile 14 B upon application of 15.57 kN to the test shear box, and the moments are observed in the moment profiles of Figure 101.

Table 15. Conversion of measured strain to bending moment (Pile 14 B)

	15.57 kN	
Depth (cm)	**μS ***	**M** (kN-m)**
13	4	0.108
25	37	0.463
38	114	0.463
51	115	0.463
64	410	0.675
76	1388	1.989
102	1814	2.292
152	6	0.137
178	0	0.008
203	-4	-0.095

Notes:
* μS is measured
** M is obtained from curves
M_{crack} = 0.463 kN-m
M_u = 2.357 kN-m

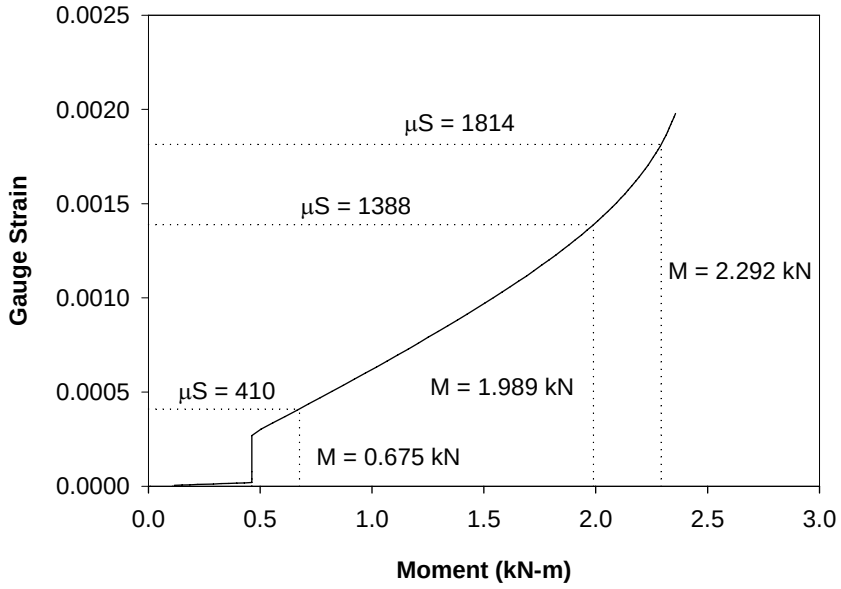

Figure 48. Conversion of measure strain to bending moment (Pile 14 B)

The implications of the moment-curvature relationship include structural behavior of the piles subject to a range of loading conditions and the design of piles for lateral loading. The proposed design methodology, presented in Chapter 6, involves the design of piles that experience bending moment forces that exceed the moment required to crack the concrete on the tension side of the pile section. Further loading mobilizes tension in the steel reinforcement and additional compression in the concrete. Load is distributed to the steel and the concrete until the concrete fails in compression (i.e. concrete crushing), at which point the section moment capacity is achieved. The load is then carried solely by reinforcing steel, and the reinforcement likely yields soon thereafter.

The design moment capacity (i.e. moment for which piles are subjected) of piles is a basic SDGM stabilization design input, and the design is highly dependent on the structural behavior of pile elements. The design of pile sections that remain uncracked is uneconomical and unnecessary. Rather, more efficient designs accept that concrete cracks under tension loads and target moment development in piles between concrete cracking and mobilization of moment capacity. The prediction of structural behavior of piles is reliable, such that the actual moment capacity of the pile and a factor of safety equal to 1.2 was used for the design moment capacity (i.e. $M_{all} = M_u / 1.2$) and calculation of the stabilizing force of the pile.

LOAD TEST RESULTS

Introduction

This chapter provides the results from load tests on piles subject to lateral soil movement. The material of the chapter facilitates the load test analysis and supports the discussion of results and design methodology of the ensuing chapters.

Shear Box Load-Displacement Relationship

The measured load-displacement relationships of the shear boxes, provided in Figures 49 through 52, indicate the contribution of the pile to the shear strength of the system. The difference between the reinforced soil load and the unreinforced soil load, for a given soil type and lateral displacement, is the load carried by the pile. The total load applied to the piles can be used for estimating the load distributions along the piles with increasing lateral translation of soil.

Figure 49 provides the load-displacement (i.e. stress-strain) behavior of unreinforced soil. Loess, as evidenced by low dry density (14 kN/m^3), exhibited low strength compared to glacial till and weathered shale. Glacial till provided intermediate strength and initial modulus values. Weathered shale exhibited a stiff response to initial shearing and gave the highest peak strength of the three soils. Upon further shearing, weathered shale exhibited strain softening behavior and approached a residual strength comparable to the glacial till.

The 115-mm-diameter piles offered considerable resistance to lateral soil movement. The installation of the small-diameter, isolated piles resulted in peak loads ranging from 215 to 325 percent of the loads for unreinforced soil. The use of 178-mm-diameter piles offered additional resistance with peak loads ranging from 325 to 390 percent of the loads for unreinforced soil.

The installation and loading of grouped piles offered some quantitative evidence of soil arching and increased capacity due to group effects. Peak loads of grouped piles were matched against peak loads of isolated piles, and the use of grouped piles offered 19 to 105 percent increase in reinforcement capacity. Percent increases of approximately 100 percent indicate a potential influence due to group effects. The low peak loads are attributed to failure to fully mobilize the pile moment capacities of grouped piles installed in glacial till and weathered shale, as supported by the moment data. For tests with grouped piles, the loading system was particularly unstable. Moment capacities were not achieved, because the tests were terminated prematurely.

Table 16 provides the peak loads of each test and a comparison of the loads with other tests of the same soil type. The presented improvement factors are ratios of peak loads for reinforced and unreinforced tests and tests of one and two piles.

Table 16. Peak loads and improvement factors

Box	Diameter (mm)	Soil Type	Peak Load (kN)	Improvement Factors	
				Reinforced / Unreinforced	2 Piles / 1 Pile
1	—	L	1.65	—	—
2	—	S	5.47	—	—
3	—	T	4.04	—	—
4*	114	L	5.34	3.24	—
5*	112	T	10.45	2.59	—
6*	117	S	11.70	2.14	—
7*	115	S	6.01	1.10	—
8*	183	L	6.41	3.88	—
9*	178	T	14.10	3.49	—
10**	113	S	13.96	2.55	1.19
11**	114	L	10.94	6.63	2.05
12*	173	S	17.79	3.25	—
13**	113	T	16.01	3.96	1.53
14**	115	T	16.28	4.03	1.56

Notes:
— not applicable
* single pile
** multiple piles
L = loess
T = glacial till
S = weathered shale

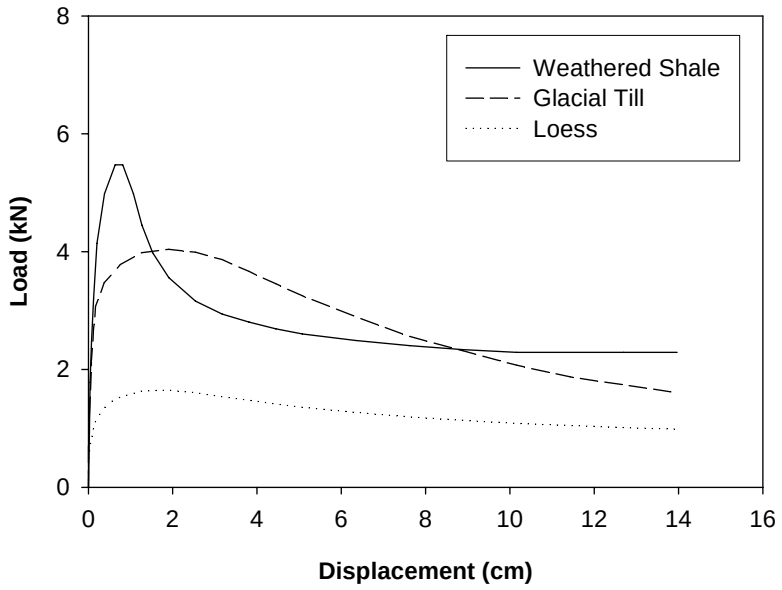

Figure 49. Load vs. displacement for unreinforced soil

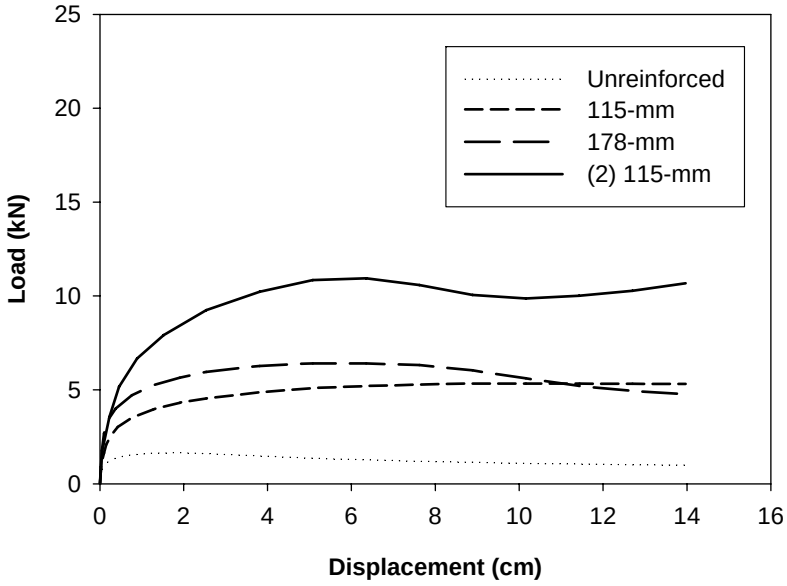

Figure 50. Load vs. displacement for loess

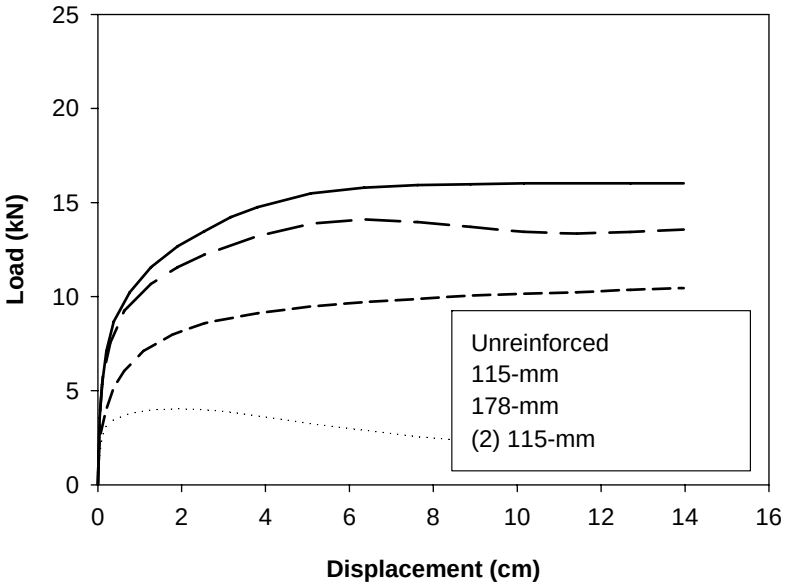

Figure 51. Load vs. displacement for glacial till

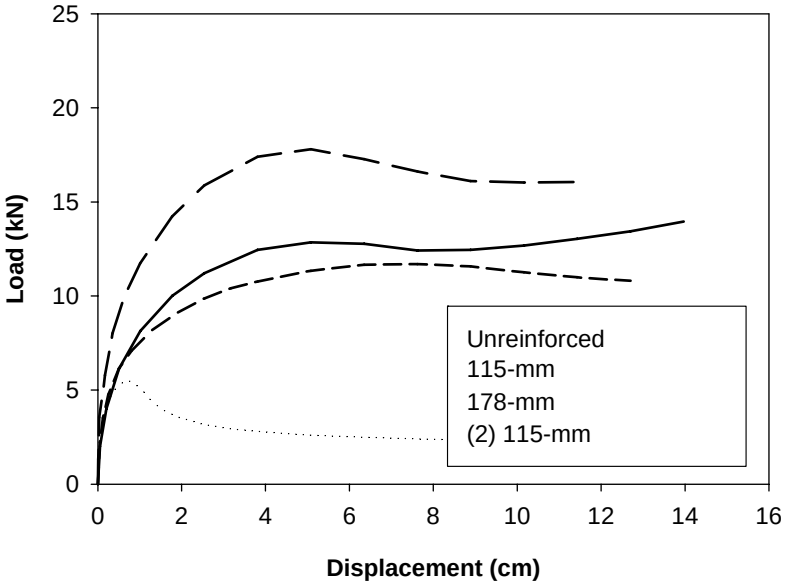

Figure 52. Load vs. displacement for weathered shale

Pile Head Load-Displacement Relationship

The measured pile head load-deflection relationships are provided in Appendix E. The loads refer to the load applied to the shear box, and the pile head deflection is the displacement measured with the lower-most transducer attached to the pile (i.e. Δx_2 in Figure 53). The pile head deflections of Figures E 1 through E 10 are uncorrected for deflection at the soil surface. Nevertheless, the figures illustrate the pile head load-displacement relationship, where the original data exhibited some scatter and was represented with smoothed curves. Moreover, the lower-most transducers were attached to the piles close to the soil surface, and piles experienced relatively small pile head rotations at pre-peak loads. Consequently, the corrected pile head deflections do not differ considerably from those presented. Based on pile head slope, corrected pile head deflections are adjusted for the pile deflection at the soil surface and used in the analyses of laterally load piles. The calculation of pile head slope and corrected pile head deflection are performed with the following equations:

$$\text{P.H. Slope} = \frac{\Delta x_1 - \Delta x_2}{L} \tag{8}$$

$$\text{P.H. Deflection (corrected)} = \Delta x_2 - \frac{L'}{L}\left(\Delta x_1 - \Delta x_2\right) \tag{9}$$

Pile head load-deflection relationships show the nonlinear pile head load-displacement relationship. The load-displacement curves generally follow those of reinforced soil, as previously presented. The pile head deflections of tests with grouped piles are illustrated with a single plot. Within the range of data scatter, the two piles experienced similar pile head deflections. A single curve adequately represents the pile head behavior of both piles.

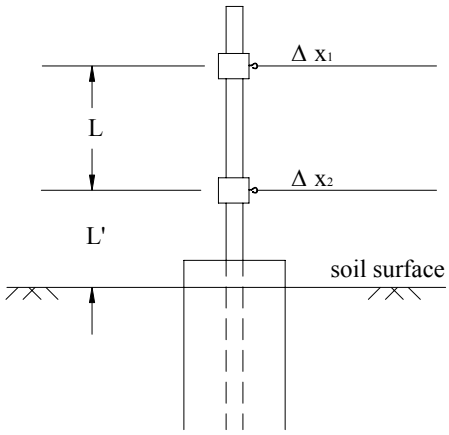

Figure 53. Measurement and correction for pile head deflection

Relative Displacement of Shear Box and Pile

The relative displacement of shear boxes and pile heads are provided in this section to support the observed pile behavior during the performance of the load tests. During loading, a gap formed in front (i.e. load-side) of the pile at the soil surface. Figures relating gap width (corrected pile head δ – shear box δ) and load, in addition to displaying the test data, indicate the behavioral stages of piles subject to lateral soil movement. Figure 54 illustrates the behavioral stages, as follows:

- Stage 1 – mobilization of soil shear stresses and elastic bending of pile,
- Stage 2 – mobilization of pile flexural stiffness, and
- Stage 3 – incipient failure due to mobilization of pile moment capacity

Stage 1 is characterized by relatively linear behavior of the soil and the intact pile element. The stress development at the soil-pile interface is insufficient to cause yielding of soil or cracking of the pile, such that a gap of negligible width forms. Stage 2 commences with the development of a bending moment in the pile element that causes the tension-carrying concrete to crack. The pile stiffness immediately drops, and the pile element becomes more flexible. Further loading of the pile causes more rapid pile rotation and pile head deflection. Coincidentally, the gap formation occurs more rapidly. Stage 3 commences with the mobilization of the pile moment capacity. Gap formation which occurs during Stage 3 occurs under constant load. The failed pile element is incapable of carrying additional load. Gaps of significant width (approximately 10 mm) form with the mobilization of pile moment capacity.

The gap width, when plotted against shear box displacement, takes on a bilinear relationship and provides an alternative approach for supporting the behavioral stages of piles subject to lateral soil movement. Interestingly, the data follows Slope I (see Figure 55) for shear box displacements corresponding to pre-peak loads (Stages 1 and 2). Upon mobilization of the pile moment capacity, however, the data follows Slope II for shear box displacements corresponding to the peak load (Stage 3). In each case of the bilinear rate of gap formation, Slope II is greater than Slope I. The difference in slopes indicates that the gap forms more quickly following mobilization of the pile moment capacity during Stage 3 loading.

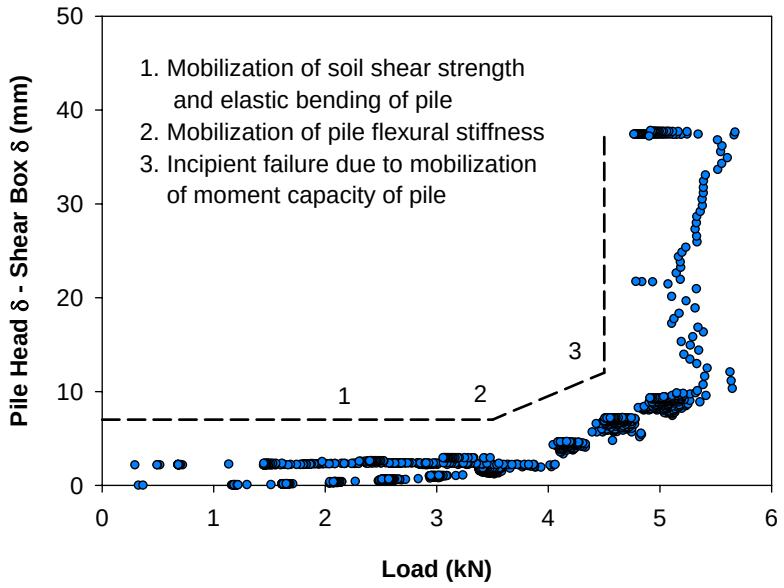

Figure 54. Behavioral stages of piles subject to lateral soil movement (Pile 4)

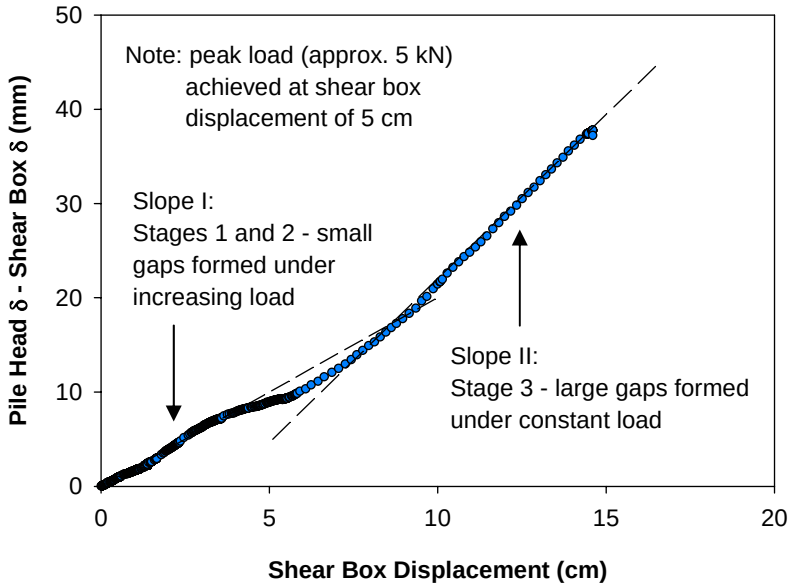

Figure 55. Bilinear rate of gap formation with behavior stages of loading (Pile 4)

Figures 56 through 75 provide the relationship between gap width, load, and shear box displacement for each of the pile load tests. Table 17 provides the loads and slopes of the behavioral stages of loading.

Table 17. Loads and slopes of behavioral stages of loading

	Load (kN)			Slope (mm/mm)	
Pile	**Stage 2**	**Stage 3**	**Peak****	**Slope I**	**Slope II**
4	3.8	5.3	5.34	0.18	0.36
5	6.3	10.0	10.45	0.12	*—
6	7.8	10.9	11.70	0.10	0.16
8	5.3	6.3	6.41	0.05	0.11
9	10.0	13.9	14.10	0.12	*—
10	9.7	12.8	13.96	0.12 / 0.21	*—
11	8.0	10.6	10.94	0.11	0.34
12	13.8	16.9	17.79	0.10	*—
13	10.9	15.9	16.01	0.13 / 0.16	*—
14	12.5	16.3	16.28	0.11	*—

Notes:
** peak loads from Table 16
*— bilinear rate of gap formation not apparent

Gap formation occurs, because the deflection of the pile head, due to rotation of the pile, exceeds the displacement of the surface soil. Pile head deflection exceeded soil movement, even at early stages of the test (see Figures 56 through 75). Poulos (1995) recognized that pile head movement which exceeds soil movement is associated with the "intermediate mode", defined by mobilization of soil strength along the pile in both the moving and stable soil. The development of a gap is fundamentally important, because the load distributions along the piles are directly affected by the exposed–and therefore, unloaded–length of pile. The length of pile in which deflection exceeded shear box displacement was more accurately subject to passive soil pressures in the direction opposite that of soil movement.

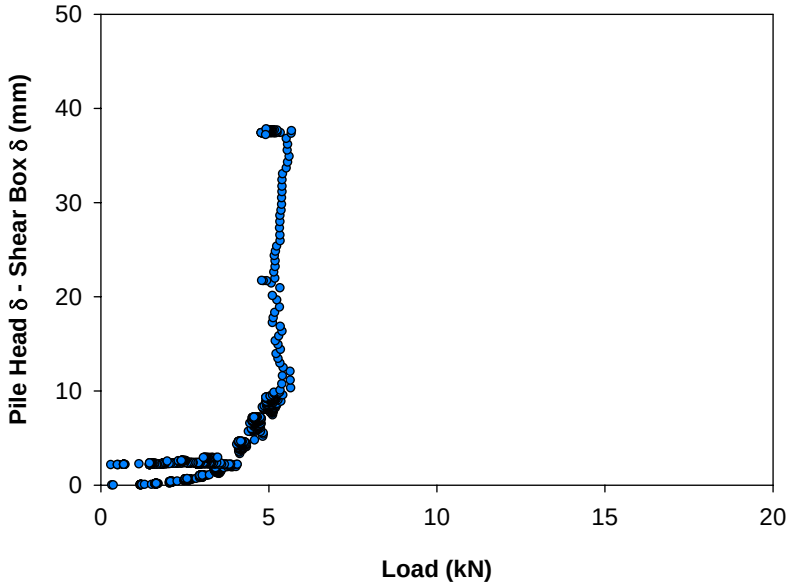

Figure 56. Relative displacement for loess (Pile 4)

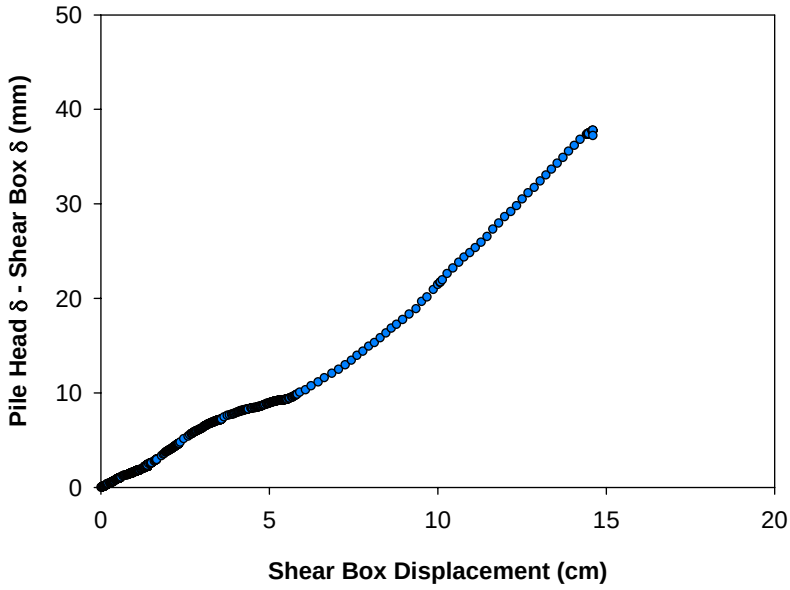

Figure 57. Relative displacement for loess (Pile 4)

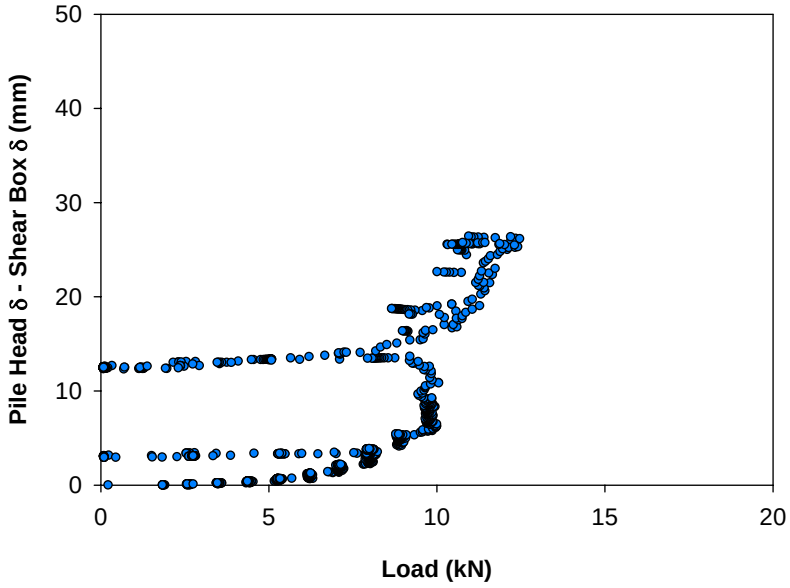

Figure 58. Relative displacement for glacial till (Pile 5)

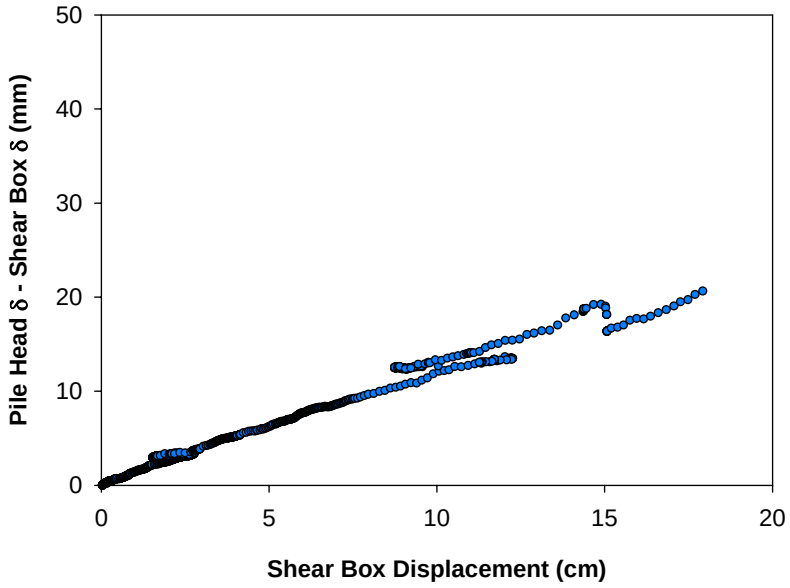

Figure 59. Relative displacement for glacial till (Pile 5)

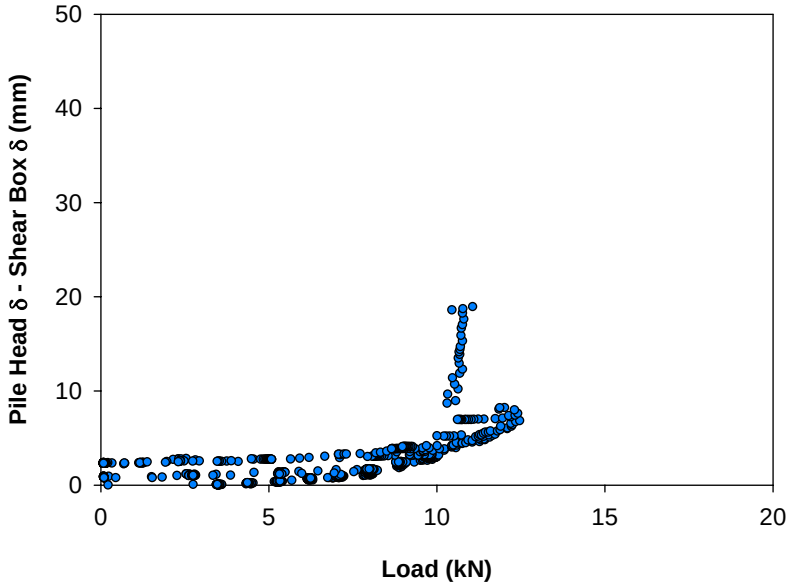

Figure 60. Relative displacement for weathered shale (Pile 6)

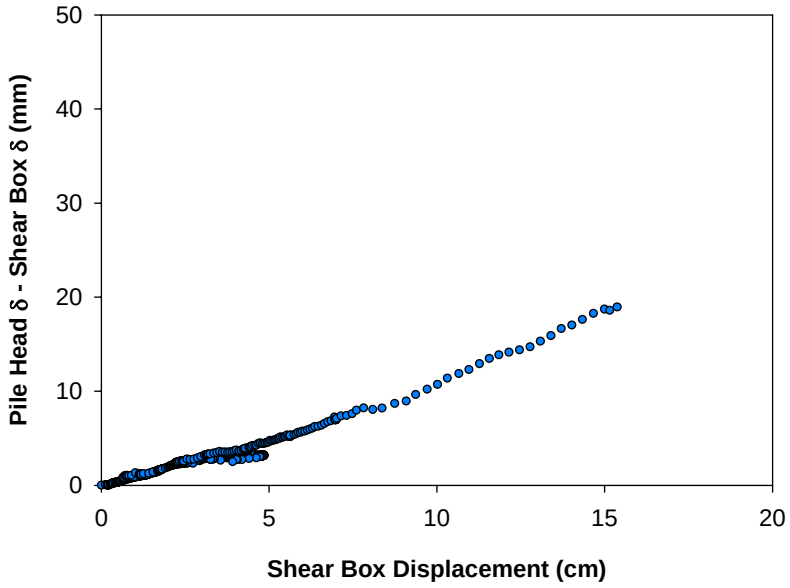

Figure 61. Relative displacement for weathered shale (Pile 6)

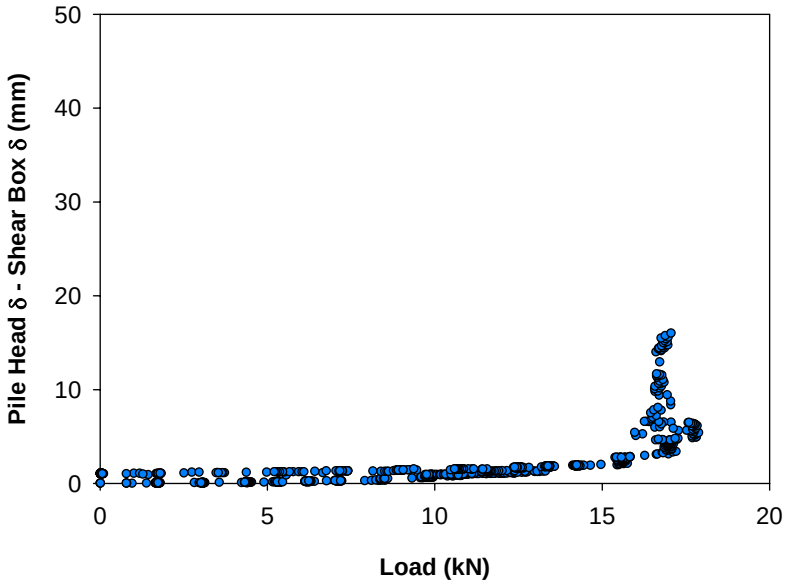

Figure 62. Relative displacement for loess (Pile 8)

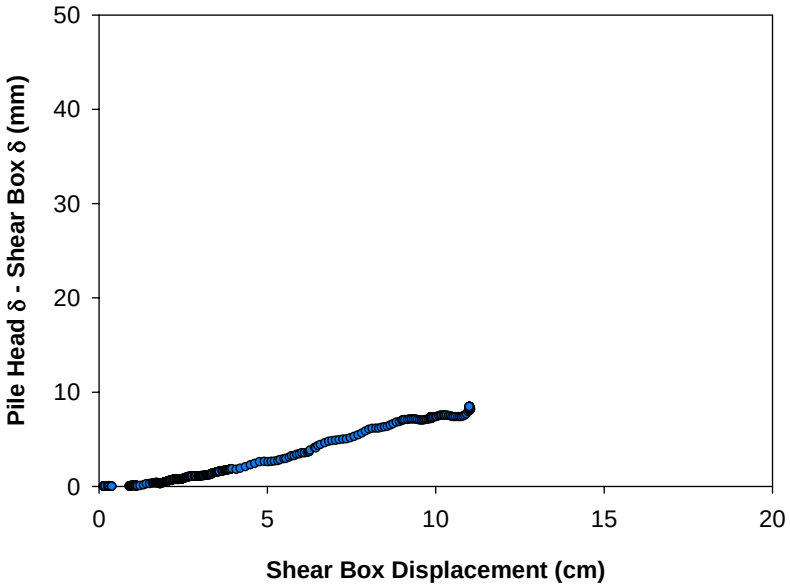

Figure 63. Relative displacement for loess (Pile 8)

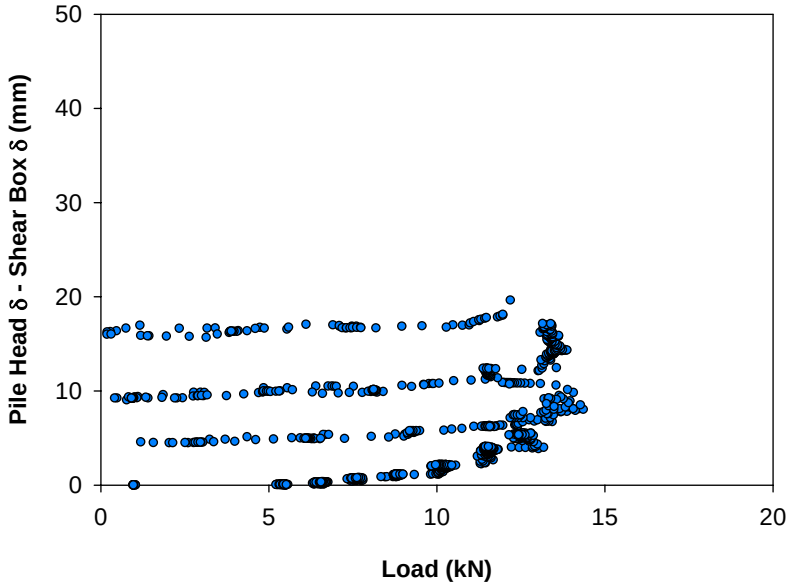

Figure 64. Relative displacement for glacial till (Pile 9)

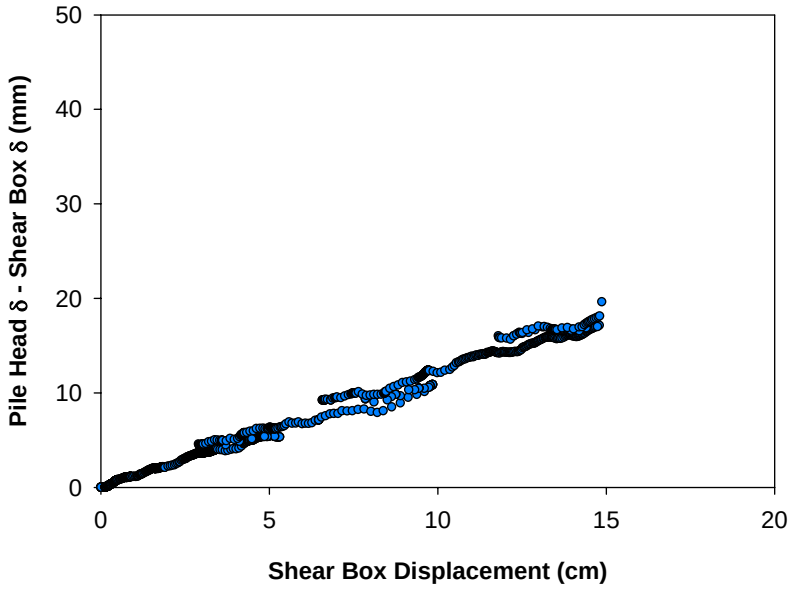

Figure 65. Relative displacement for glacial till (Pile 9)

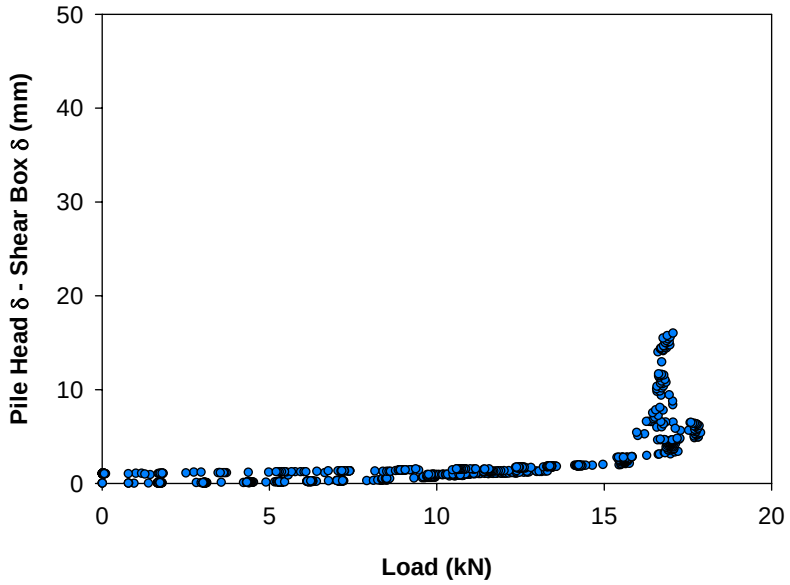

Figure 66. Relative displacement for weathered shale (Pile 12)

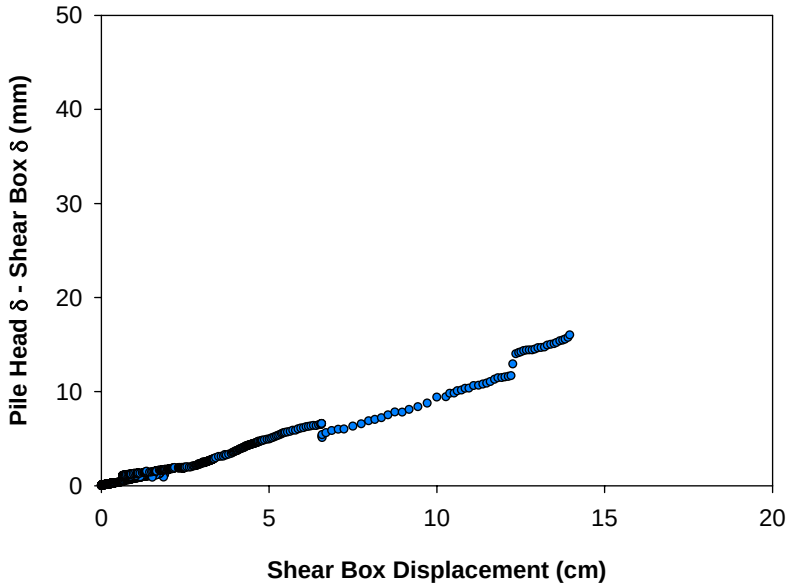

Figure 67. Relative displacement for weathered shale (Pile 12)

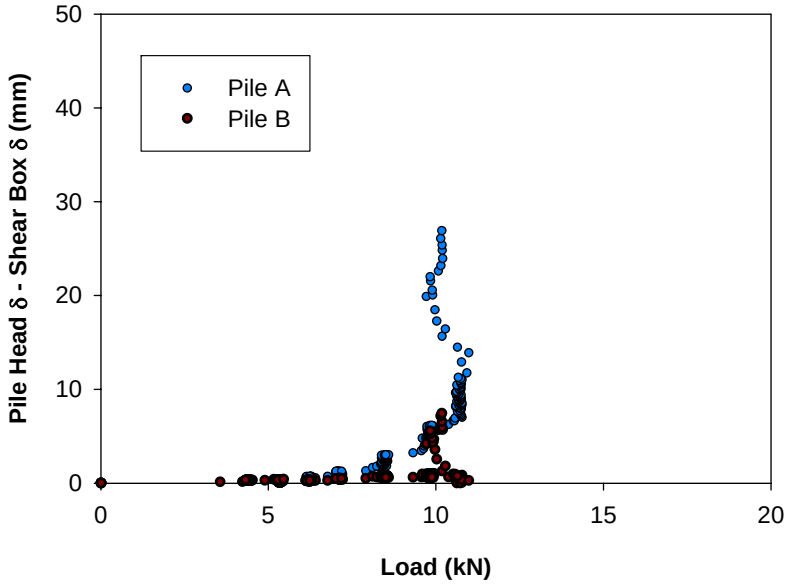

Figure 68. Relative displacement for loess (Piles 11 A and B)

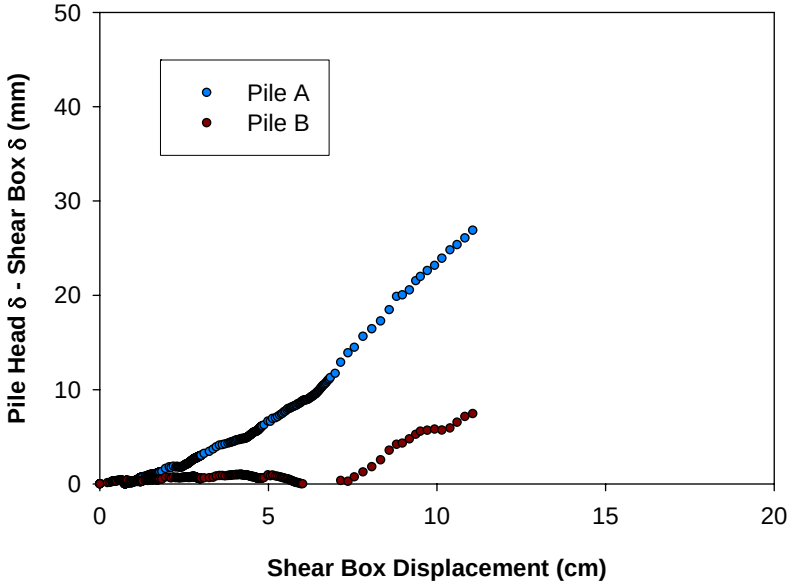

Figure 69. Relative displacement for loess (Piles 11 A and B)

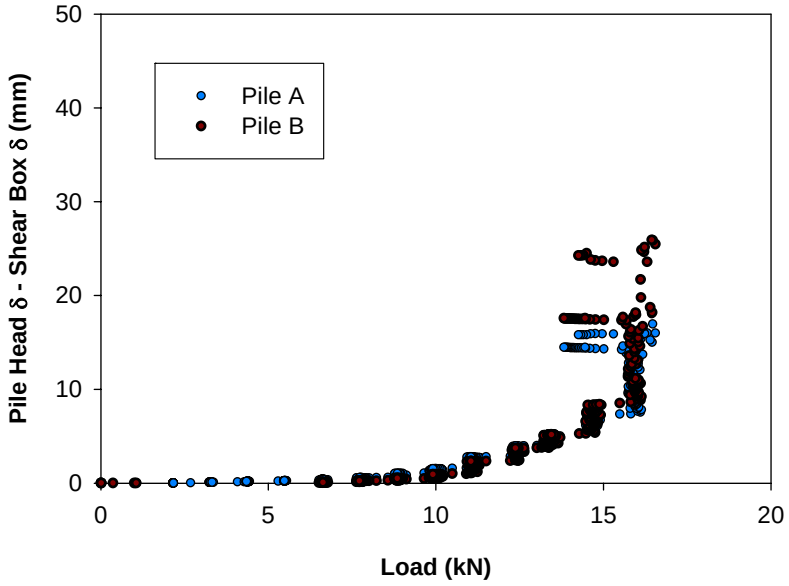

Figure 70. Relative displacement for glacial till (Piles 13 A and B)

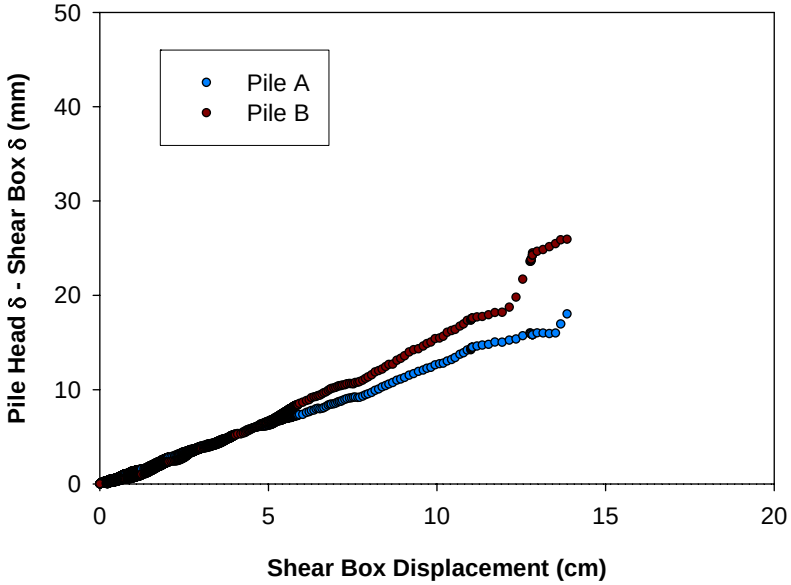

Figure 71. Relative displacement for glacial till (Piles 13 A and B)

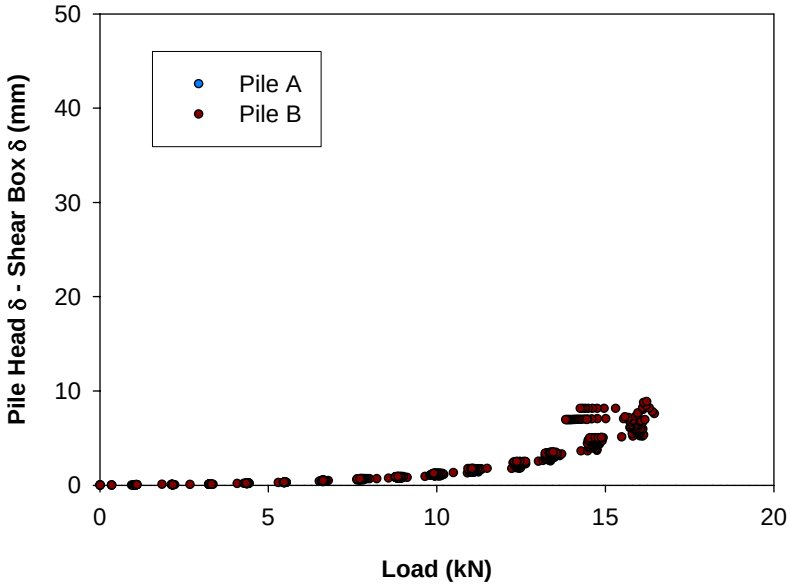

Figure 72. Relative displacement for glacial till (Piles 14 A and B)

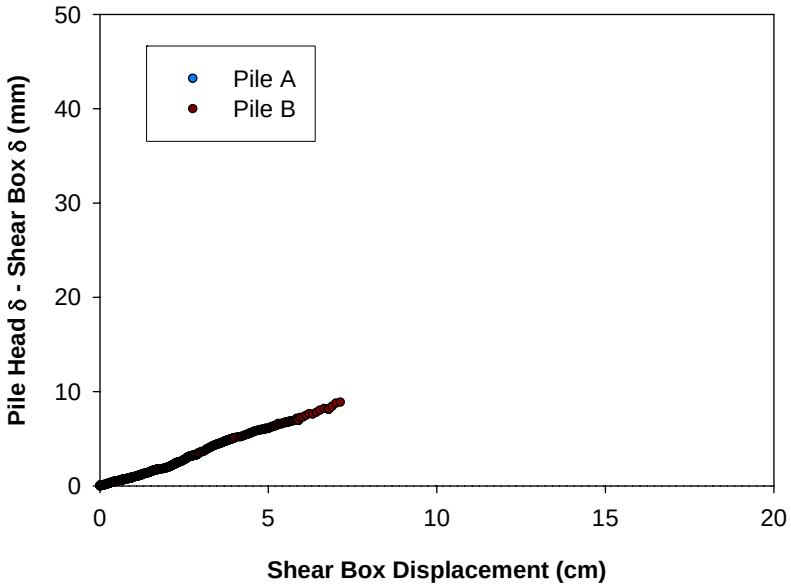

Figure 73. Relative displacement for glacial till (Piles 14 A and B)

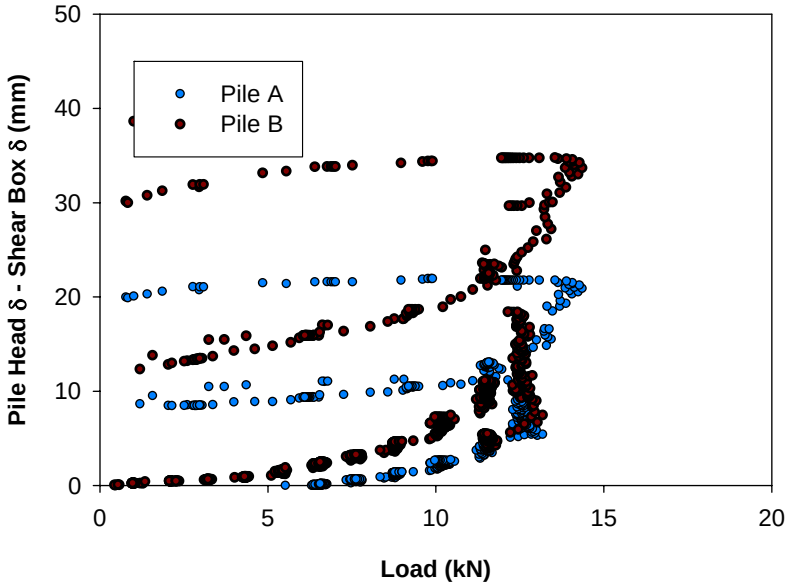

Figure 74. Relative displacement for weathered shale (Piles 10 A and B)

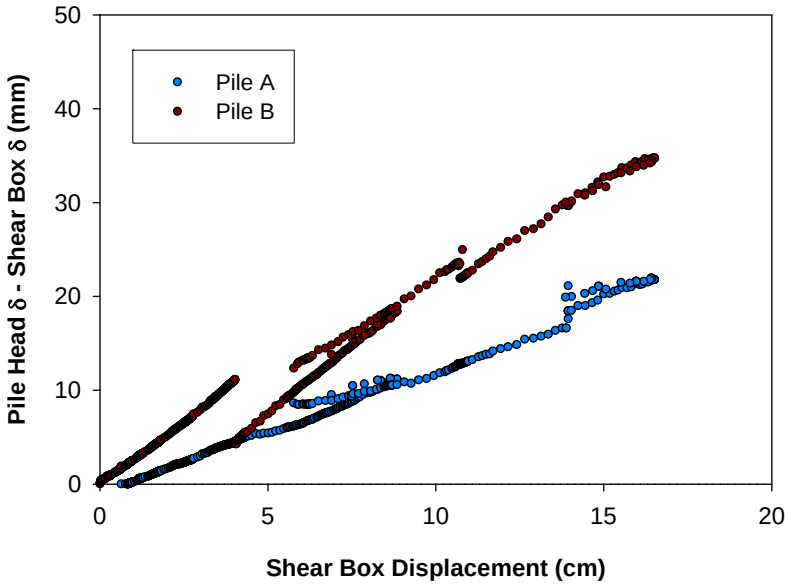

Figure 75. Relative displacement for weathered shale (Piles 10 A and B)

Photogrammetry

Cameras were mounted above the piles of each load test to document the observed behavior of pile heads and surface soil at different stages during pile loading. The pictures, provided in Figures 79 through 88, show the data used to indicate the behavioral stages of piles subject to lateral soil movement and illustrate the gap formation between the pile head and surface soil. The pictures also indicate soil stress build-up around the piles. Radial cracking observed in front of isolated piles warrants a brief discussion on the relationship between radial and tangential stress, and the discussion is extended to include soil arching phenomena as occurs during loading of grouped piles.

Relationship Between Radial and Tangential Stress

The major principal stress of soil at the upslope soil-pile interface, applied in the radial direction of the pile and referred to as radial stress, increases during uniform lateral translation of soil. Cavity expansion theory suggests that an expanding cylinder in soil offers an elastic response mechanism of the soil, whereby the radial stress increases (Handy and White unpublished). The radial stress increase, directly related to the loading condition of the pile, is accompanied by a decrease in tangential stress of the same magnitude for a given radial distance from the cylinder. The tangential stress becomes negative after the radial stress exceeds twice the in-situ lateral stress. As soil is capable of withstanding negligible tension (i.e. not to exceed apparent cohesion, if applicable), tension cracks appear in the radial direction about the cavity. The series of tension cracks are also referred to as radial cracks. Figure 76 illustrates the relationship between radial and tangential stresses with Mohr's circle depiction of the change stress state with loading. Figure 77 shows the radial and tangential stresses of an isolated pile subject to lateral soil movement.

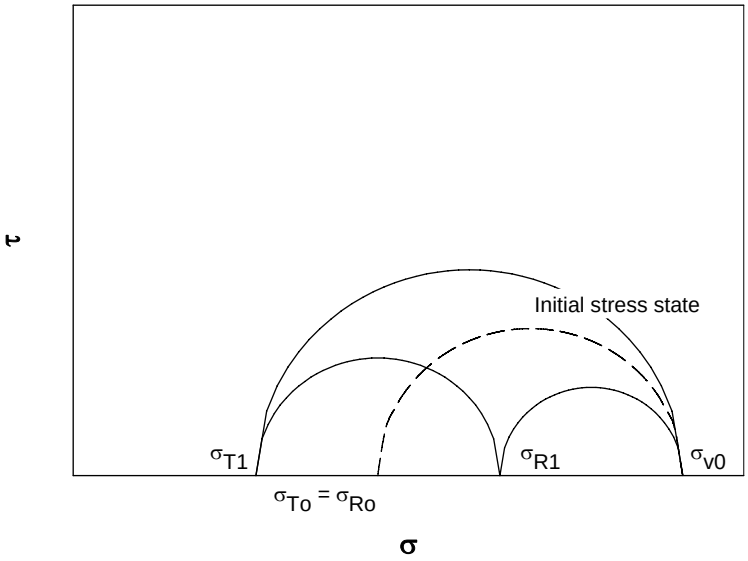

Figure 76. Mohr's circle depiction of stress state change with loading

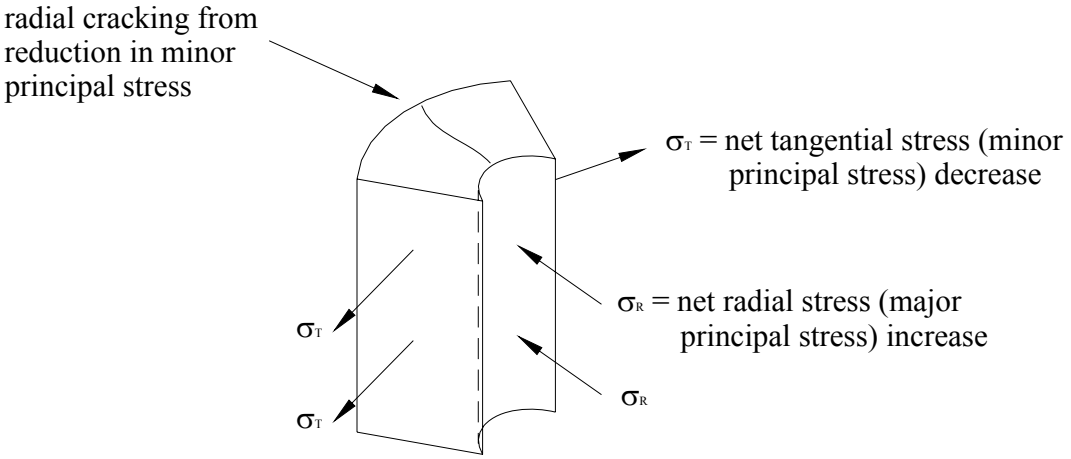

(a)

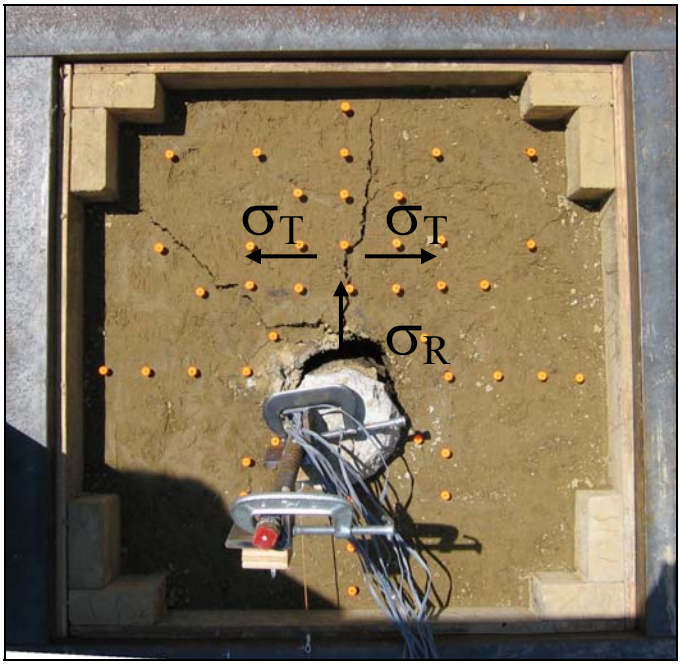

(b)

Figure 77. Radial and tangential stresses of single piles subject to soil movement

Grouped Piles Subject to Lateral Soil Movement and Soil Arching

Soil arching is the transfer of stresses from yielding soil to adjacent, non-yielding soil. The phenomenon is observed in the application of pile stabilization, where an arch occurs between stiff pile elements installed in a row. The influence of soil arching on pile stabilization generally benefits the stability of reinforced slopes. Unfortunately, research investigators and design engineers do not fully understand the conditions necessary for soil arching to occur or the quantitative effects of soil arching on the capacity of slope reinforcement.

Soil arching was observed during the pile load tests of grouped piles subject to lateral soil movement. The phenomenon was evidenced by an arch that developed between adjacent piles of the tests. The formation of the arch is described in terms of radial and tangential stresses of soil. As for isolated piles subject to lateral soil movement, radial stresses develop in front of grouped piles. The difference between isolated piles and grouped piles subject to lateral soil movement is that the directions of the major principal stresses from grouped piles do not extend radially from the pile centers, but rather form an arch. The arch is the path of the major principal stress, and the direction perpendicular to the arch is direction in which the minor principal stress acts. The major principal stress increase is still accompanied by a decrease in the minor principal stress, and the reduced minor principal stresses that occur during loading result in tension cracks in the direction parallel to the major principal stress. The arch formation is illustrated in Figure 78.

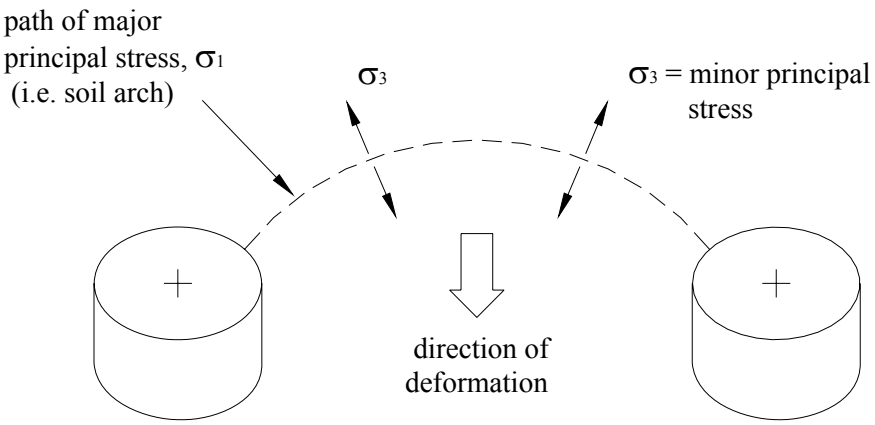

(a)

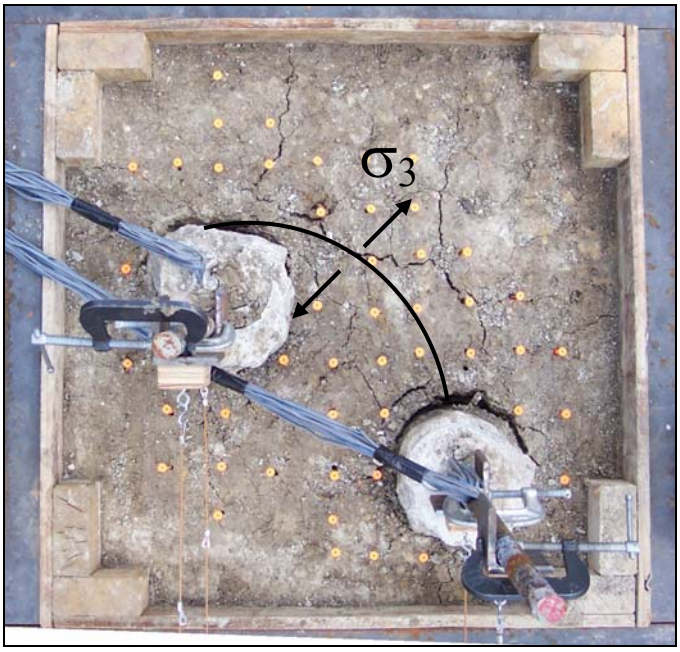

(b)

Figure 78. Radial and tangential stresses of multiple piles subject to soil movement

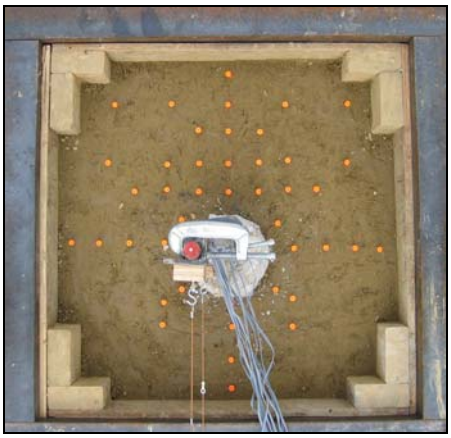

(a) 0 cm

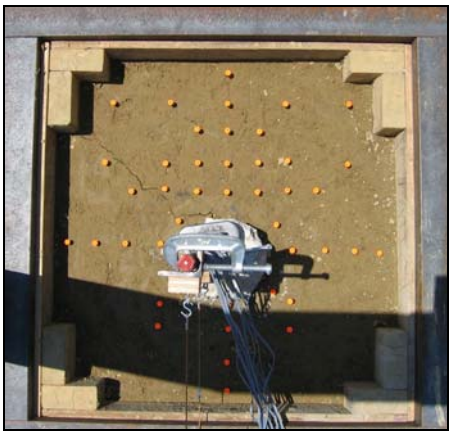

(b) 0 cm

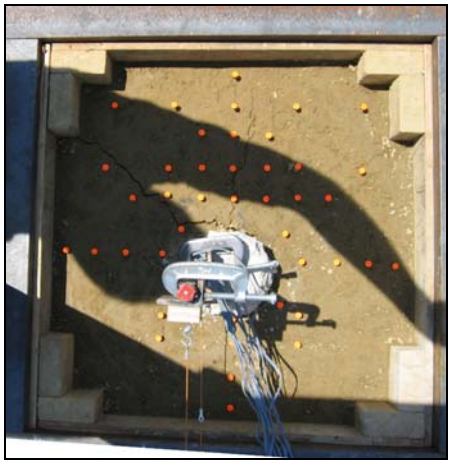

(c) 5 cm

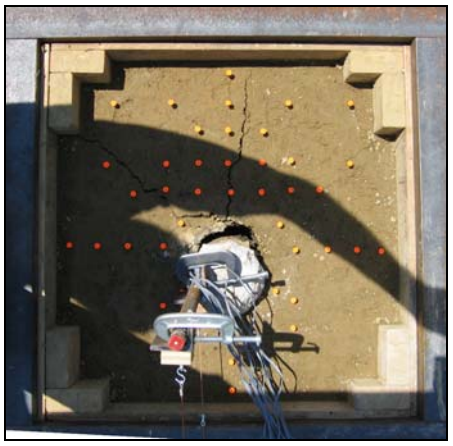

(d) 13 cm

(e) 15 cm

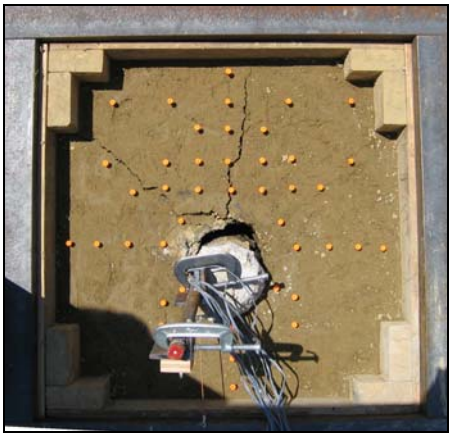

(f) 16 cm

Figure 79. Box 4 photogrammetry pictures (127-mm Pile in loess)

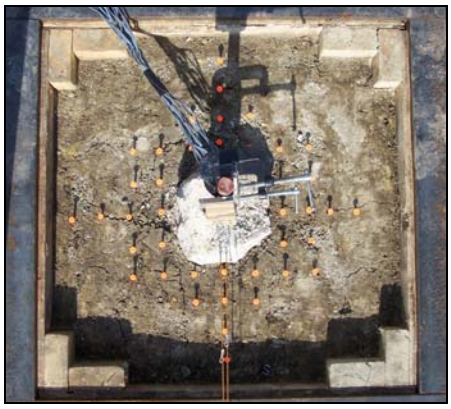

(a) 0 cm

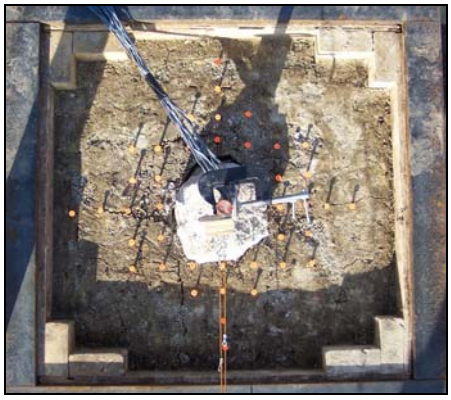

(b) 2 cm

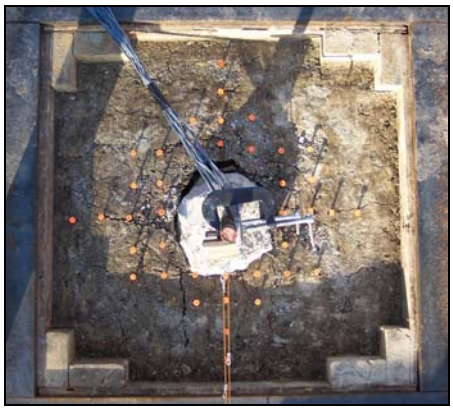

(c) 6 cm

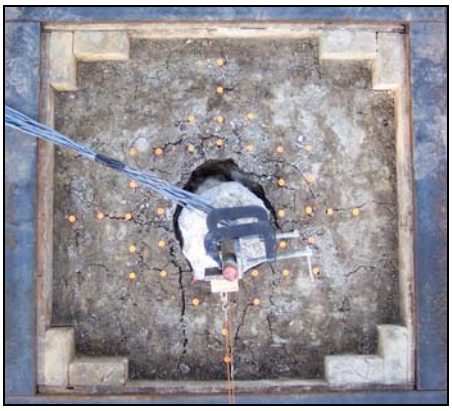

(d) 13 cm

(e) 21 cm

Figure 80. Box 5 photogrammetry pictures (127-mm Pile in glacial till)

(a) 0 cm

(b) 3 cm

(c) ~ 4 cm

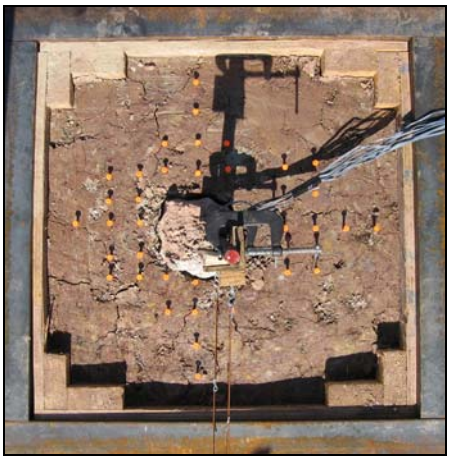

(d) ~ 10 cm

Figure 81. Box 6 photogrammetry pictures (127-mm Pile in weathered shale)

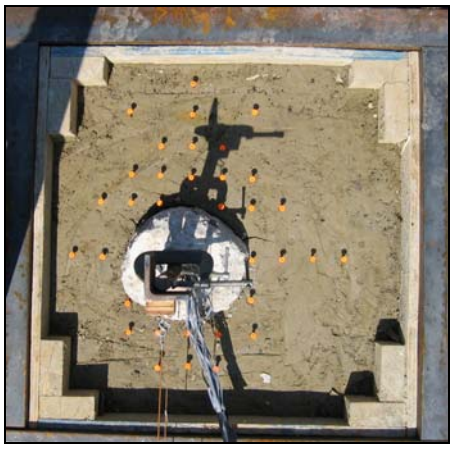

(a) 0 cm

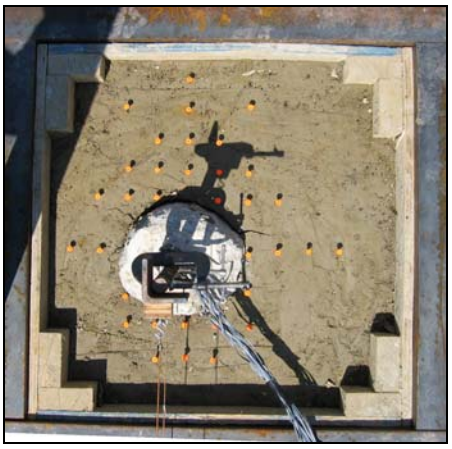

(b) 1 cm

(c) 3 cm

Figure 82. Box 8 photogrammetry pictures (178-mm Pile in loess)

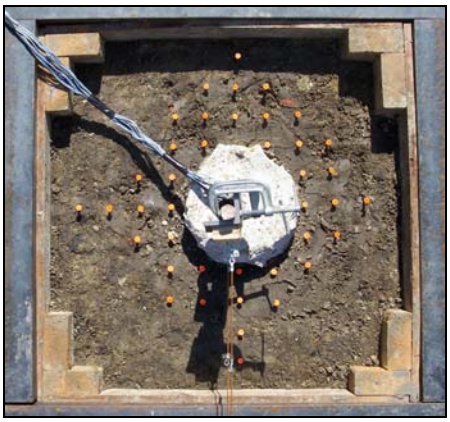

(a) 0 cm

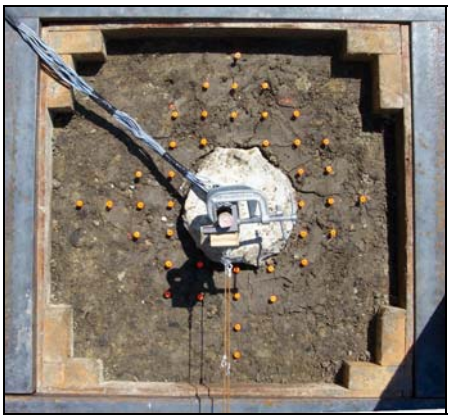

(b) 4 cm

(c) 7 cm

(d) 8 cm

(e) 11 cm

(f) 17 cm

Figure 83. Box 9 photogrammetry pictures (178-mm Pile in glacial till)

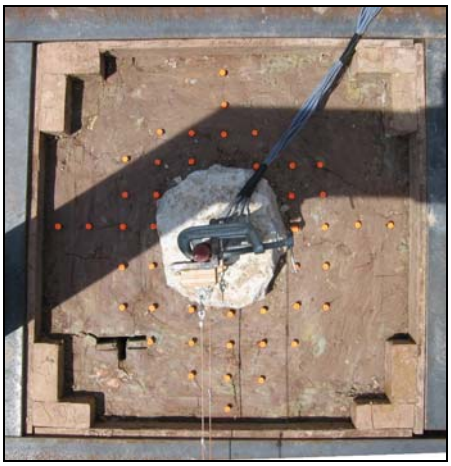

(a) 0 cm

(b) 14 cm

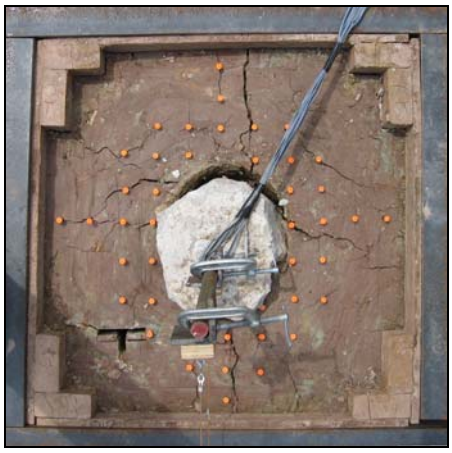

(c) 19 cm

(d) 20 cm

Figure 84. Box 12 photogrammetry pictures (178-mm Pile in weathered shale)

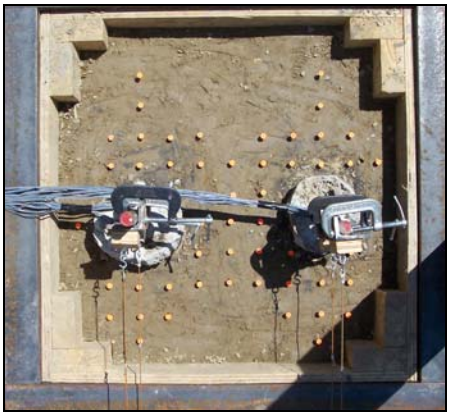

(a) 0 cm

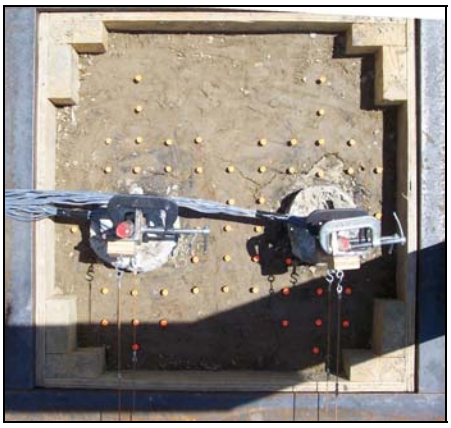

(b) 2 cm

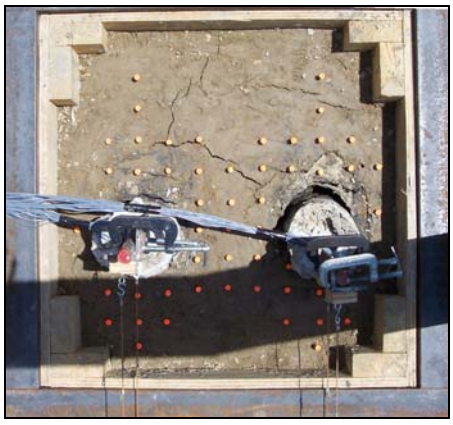

(c) 11 cm

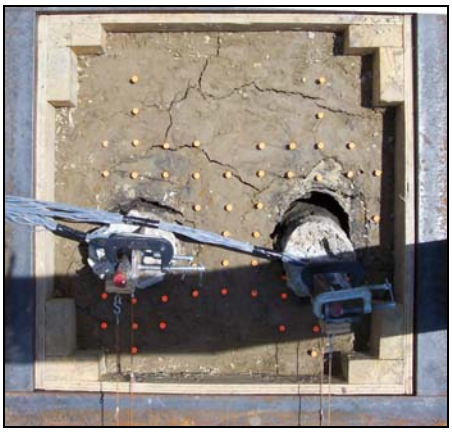

(d) 15 cm

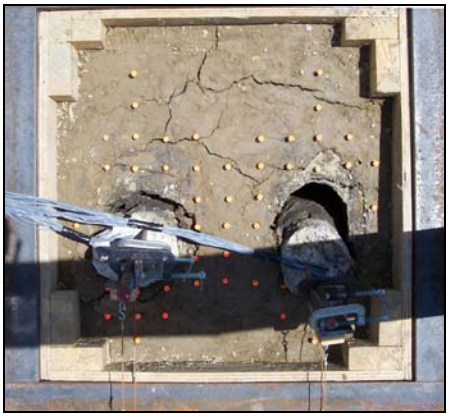

(e) 23 cm

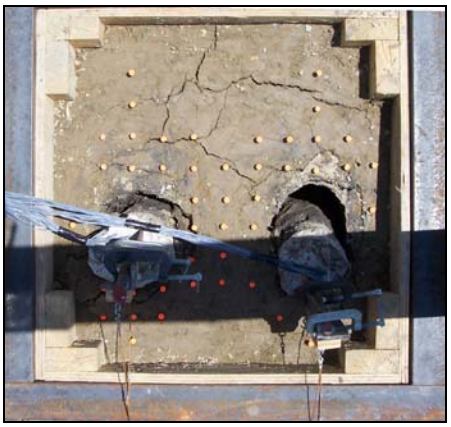

(f) 25 cm

Figure 85. Box 11 photogrammetry pictures [(2) 127-mm Piles in loess]

(a) 0 cm

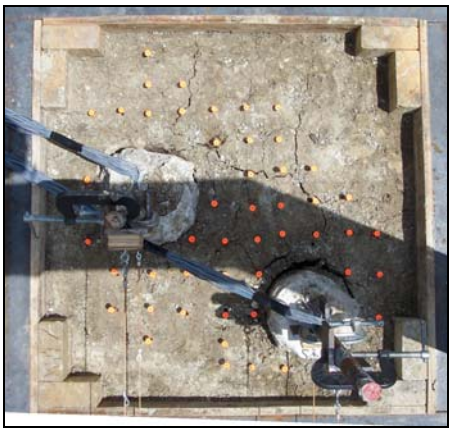

(b) 10 cm

(c) 14 cm

Figure 86. Box 13 photogrammetry pictures [(2) 127-mm Piles in glacial till]

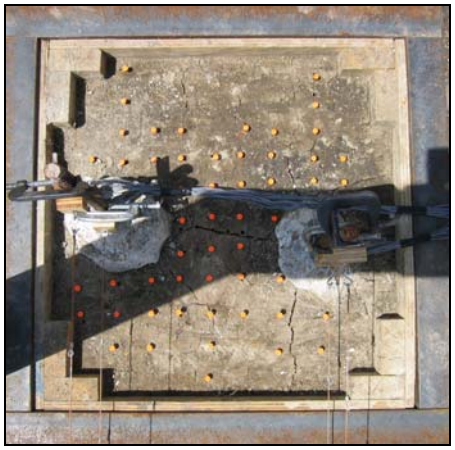

(a) 0 cm

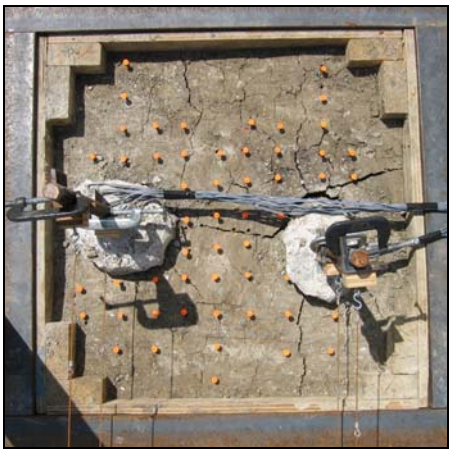

(b) 8 cm

(c) 10 cm

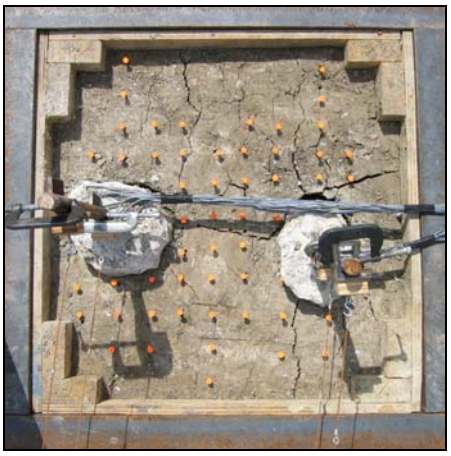

(d) ~ 13 cm

Figure 87. Box 14 photogrammetry pictures [(2) 127-mm Piles in glacial till]

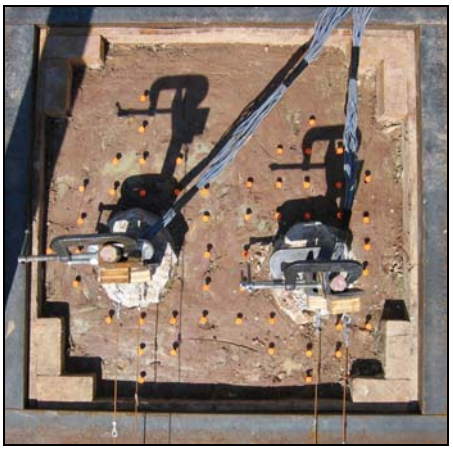

(a) 0 cm

(b) 8 cm

(c) 15 cm

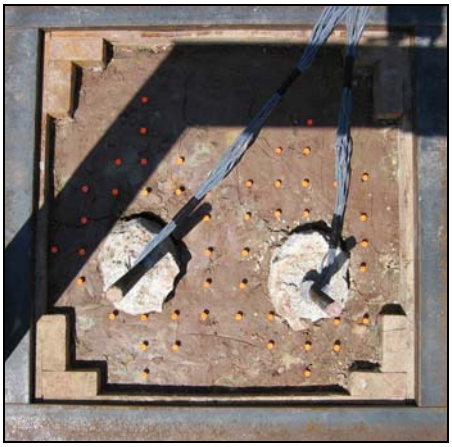

(d) End

Figure 88. Box 10 photogrammetry pictures [(2) 127-mm Piles in weathered shale]

Shear Box Rotation and Tilt

Shear box rotation about the vertical axis and shear box tilt about the horizontal axis (see Figures 89 and 90) are provided in Appendix F. The figures are presented solely to document a possible cause of poor correlation between measured and predicted pile behaviors. A tilted box, for example, potentially subjects the pile element to a component of axial load, altering the pile performance. Ultimately, shear box rotation or tilt was not used to explain pile load test behavior.

Table 18 provides the maximum values of shear box rotation and tilt per test.

Table 18. Maximum shear box rotation and tilt

Test	Rotation	Tilt
4	2.3	0.6
5	1.2	3.5
6	1.8	3.1
8	1.8	0.0
9	0.9	1.6
10	0.9	4.6
11	0.4	0.3
12	1.0	1.2
13	0.7	2.6
14	4.5	3.2

Notes:
All units in degrees

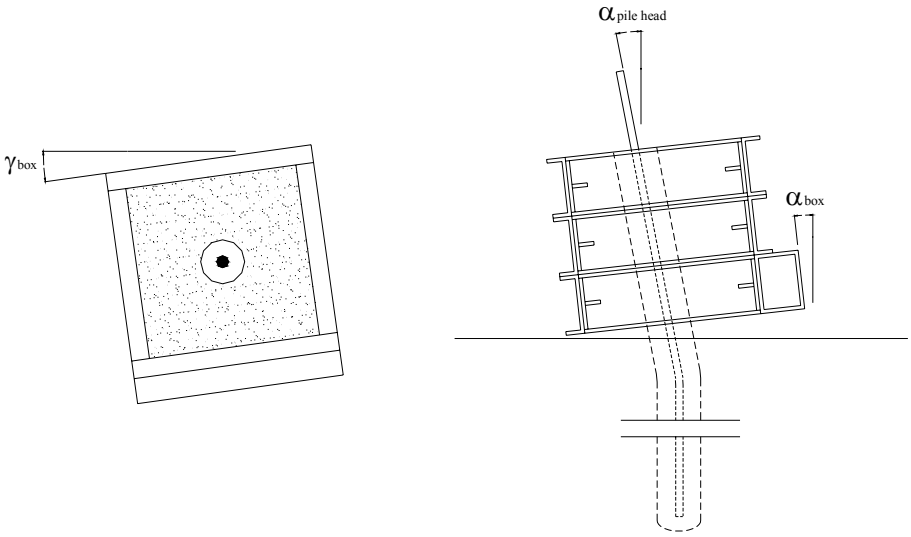

(a) plan view (rotation) (b) elevation view (tilt)

Figure 89. Shear box rotation and tilt

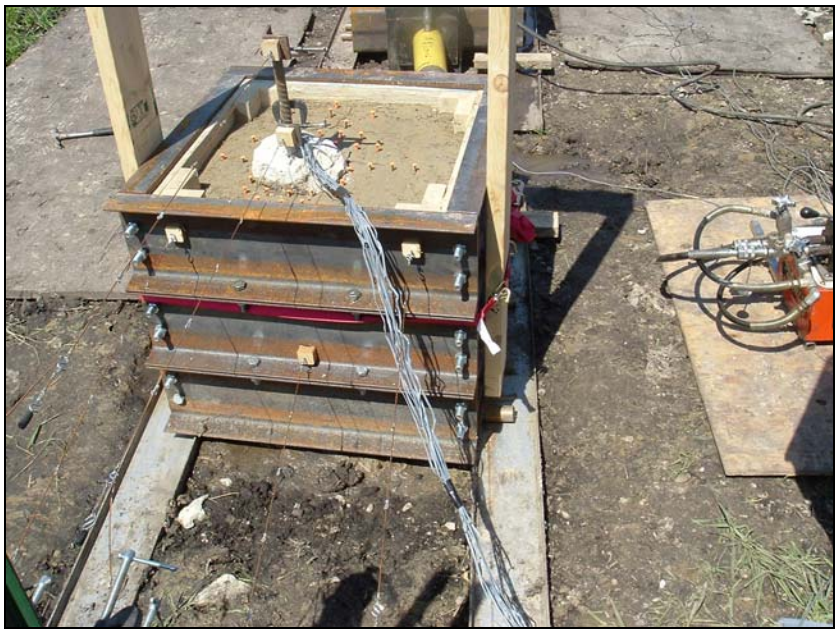

(a) rotation (Box 8)

(b) tilt (Box 5)

Figure 90. Shear box rotation and tilt

Pile Bending Moment Distributions

The *strain* of steel reinforcement was measured along the entire length of piles during the pile load tests. Strain profiles for each pile are provided in Appendix G. Strain measurements were converted to bending moments by performing moment-curvature analyses, as documented in Chapter 3. Bending moment profiles for the piles are provided in Figures 91 through 103. The depths of the y-axis are taken from the pile head (at the soil surface), and the loads provided in the legends of each figure represent the load applied to the shear box when the strain of pile reinforcement was measured.

The bending moments provide influential evidence that piles failed due to mobilization of the moment capacity and support our interpretation of the behavioral stages of piles subject to lateral soil movement. The maximum bending moments for most isolated piles approximately equaled the section moment capacities. Approximately one third of the grouped piles mobilized the full moment capacity. The tests performed on grouped piles were terminated earlier than tests on isolated piles, which may explain the lower measured strains.

The location at which the maximum bending moment developed is additionally important for evaluating the performance of laterally loaded piles. Maximum bending moments generally develop approximately 3 to 4 pile diameters from the load application. Maximum measured strain developed at approximately 4 pile diameters below the load application. The use of additional strain gauges near the maximum moment location would facilitate a more accurate maximum moment depth. Nevertheless, the piles performed in accordance with generally accepted behavior.

The maximum bending moments and depths to the maximum moments are provided in Table 19. Additionally, the table provides the depths of plastic hinge development in terms of pile diameters below the shear surface.

Table 19. Maximum moment and depth of plastic hinge development

Pile	M_{max} (kN-m)	Depth (mm)*	Depth (Pile Diameters)**
4	2.60	965	3.34
5	2.24	1016	3.86
6	2.70	1016	3.69
8	2.13	1498	4.99
9	5.26	1067	2.71
10 A	2.44	965	3.34
10 B	1.86	787	1.81
11 A	2.12	813	2.01
11 B	2.60	1067	4.23
12	7.34	1524	5.43
13 A	0.75	1016	3.86
13 B	0.86	1016	3.79
14 B	2.29	1067	4.13

Notes:
* from pile head (soil surface)
** from shear surface

The negative strains measured in the length of pile subject to lateral soil movement, as seen in Figures 93 through 96, remain unexplained. Predicted bending moments associated with negative moment development due to pile rotation into the soil behind the piles are of significantly less magnitude than the moments corresponding to the strain mobilized in the reinforcement. Furthermore, despite the apparent mobilization of the cracking moment, cracking along the uppermost length of the piles was not observed during pile exhumation. The principal concern of the research group is that the strain follows a seemingly systematic pattern, in that the strains increase with increasing load and that the pattern occurs at multiple strain gauge levels. The issue is clearly more complicated than attributing the readings to poor strain gauge performance.

Negative strains were also measured near the tips of Piles 8 and 9 (Figures 94 and 95, respectively). The development of negative bending moments at these elevations is not unusual, but the conversion from measured strain to moment values is slightly erroneous. The negative bending moments result in compression strains, where the neutral axis position is located at the center of the rebar. Upon cracking of the pile and shifting of the neutral axis position, however, tension is mobilized in the pile reinforcement. Tension strains are acquired, and the moment profiles experience a sign reversal at the particular gauge elevation. After a pile cracks, the employed moment-curvature analysis, from which strains are converted to moment, is valid only for the initial loading direction.

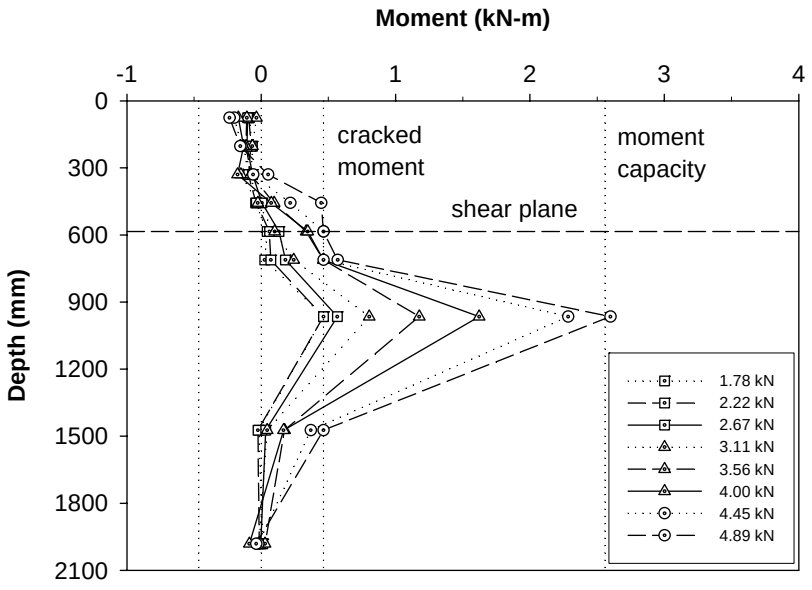

Figure 91. Bending moment profiles for reinforced loess (Pile 4)

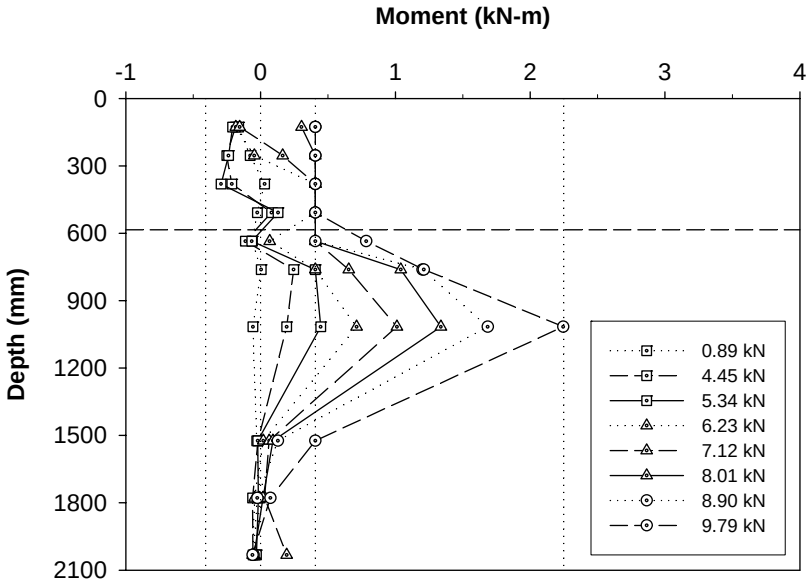

Figure 92. Bending moment profiles for reinforced glacial till (Pile 5)

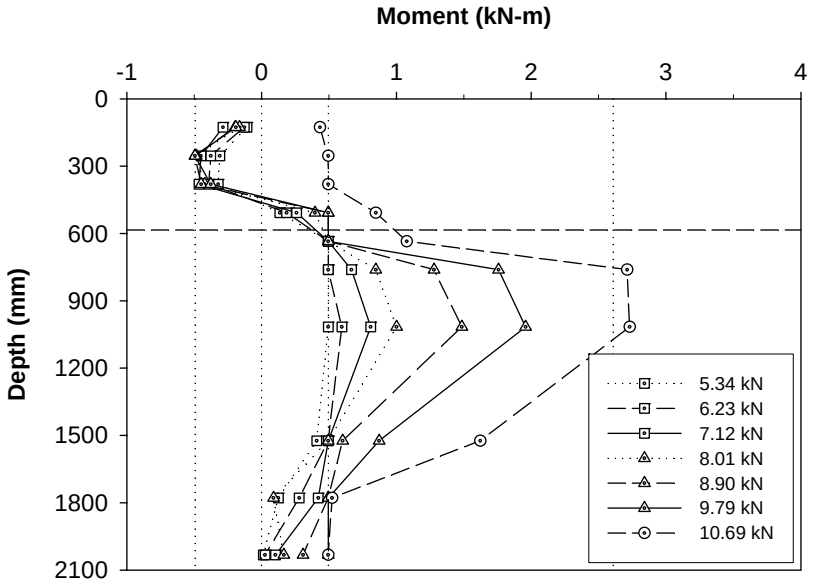

Figure 93. Bending moment profiles for reinforced weathered shale (Pile 6)

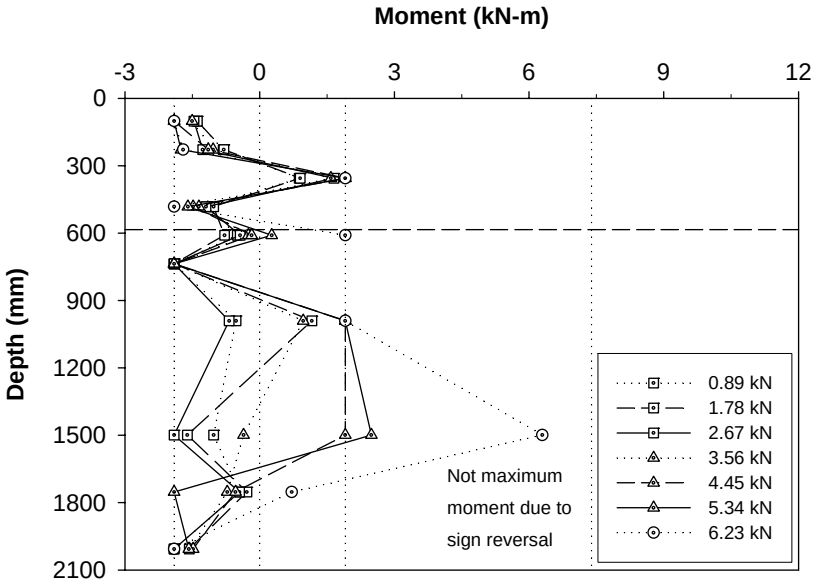

Figure 94. Bending moment profiles for reinforced loess (Pile 8)

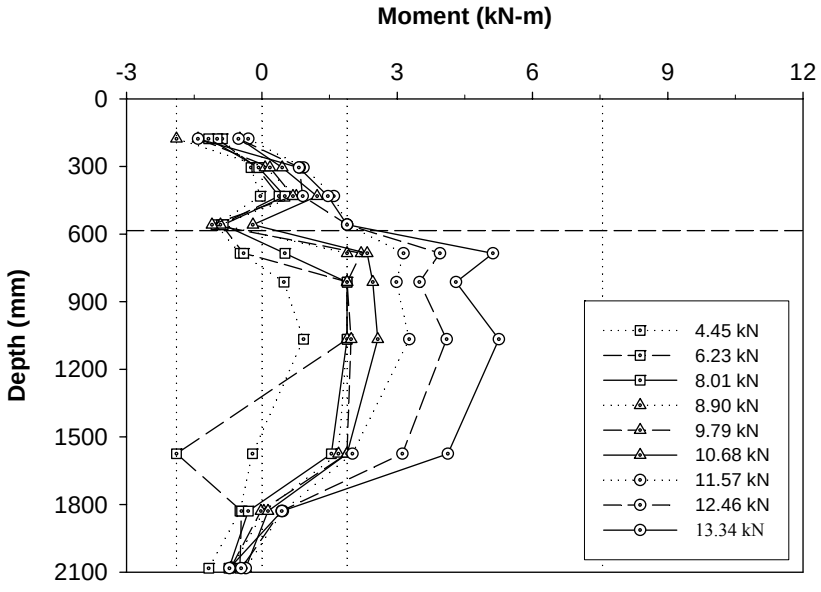

Figure 95. Bending moment profiles for reinforced glacial till (Pile 9)

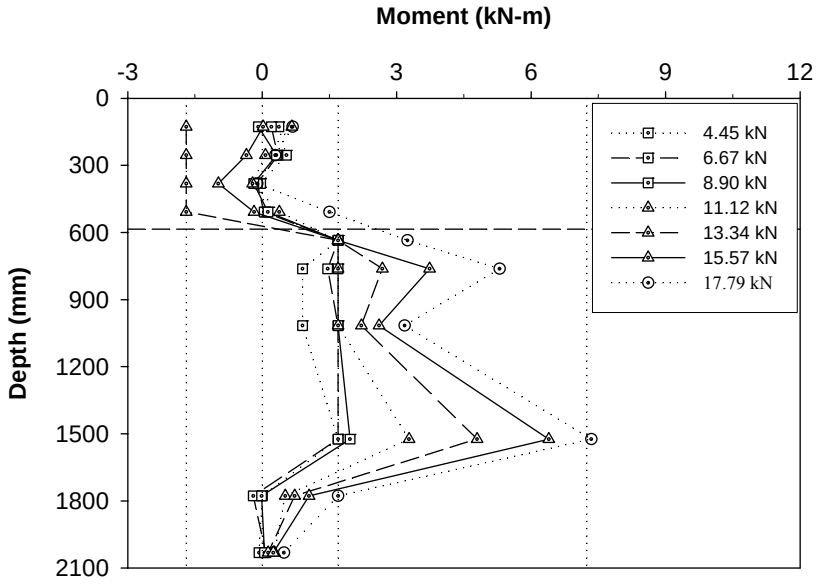

Figure 96. Bending moment profiles for reinforced weathered shale (Pile 12)

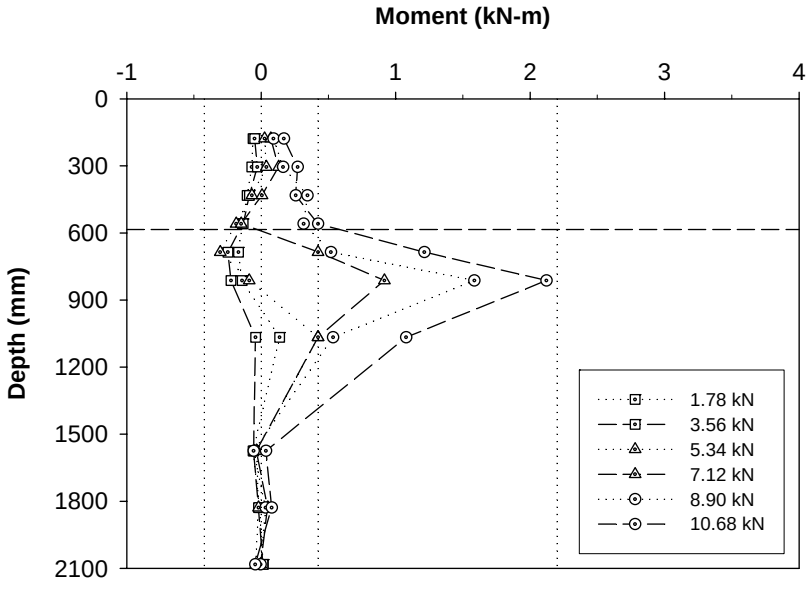

Figure 97. Bending moment profiles for reinforced loess (Pile 11 A)

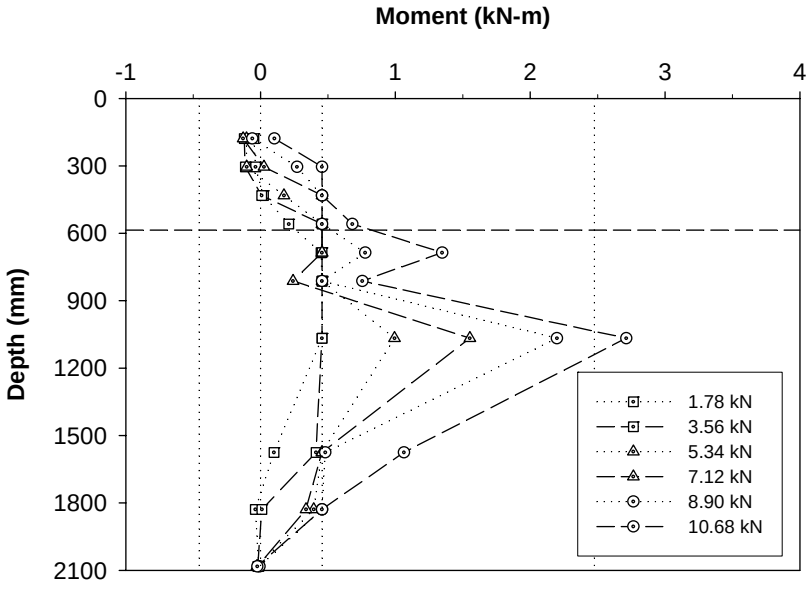

Figure 98. Bending moment profiles for reinforced loess (Pile 11 B)

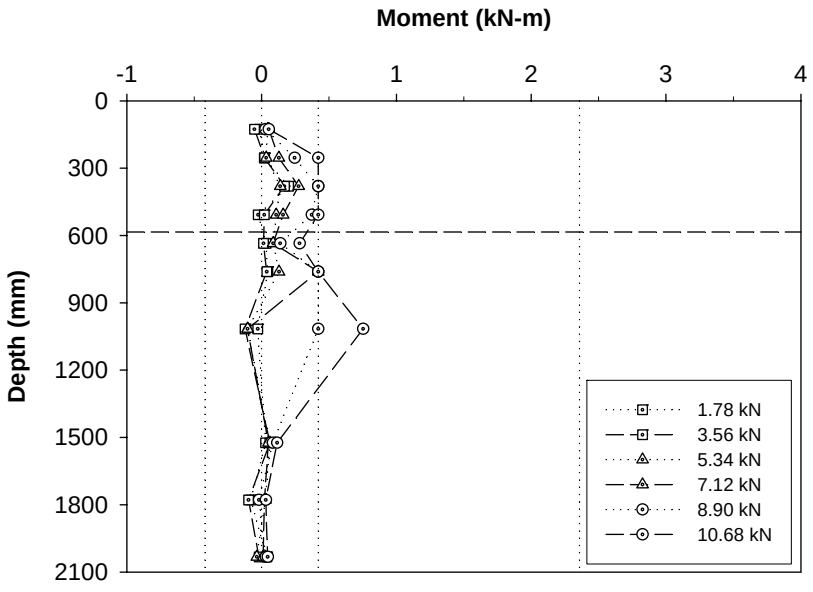

Figure 99. Bending moment profiles for reinforced glacial till (Pile 13 A)

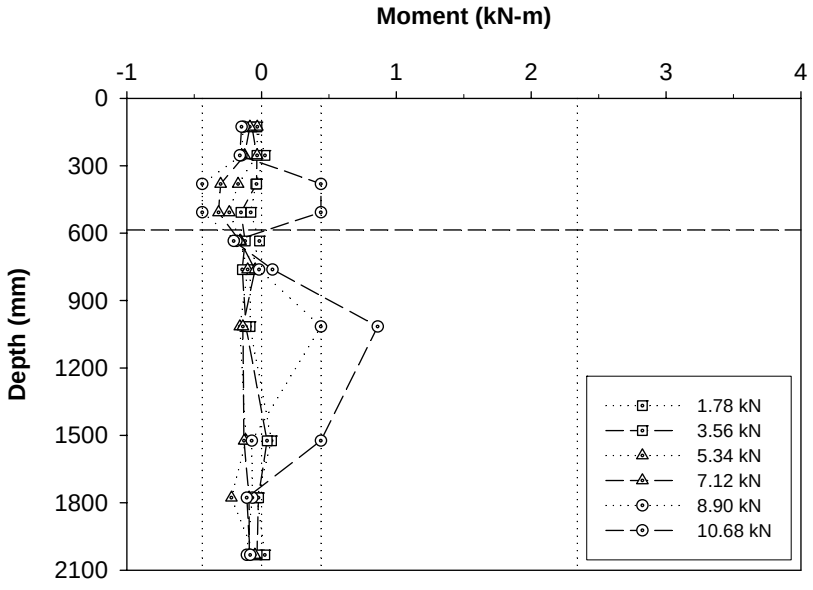

Figure 100. Bending moment profiles for reinforced glacial till (Pile 13 B)

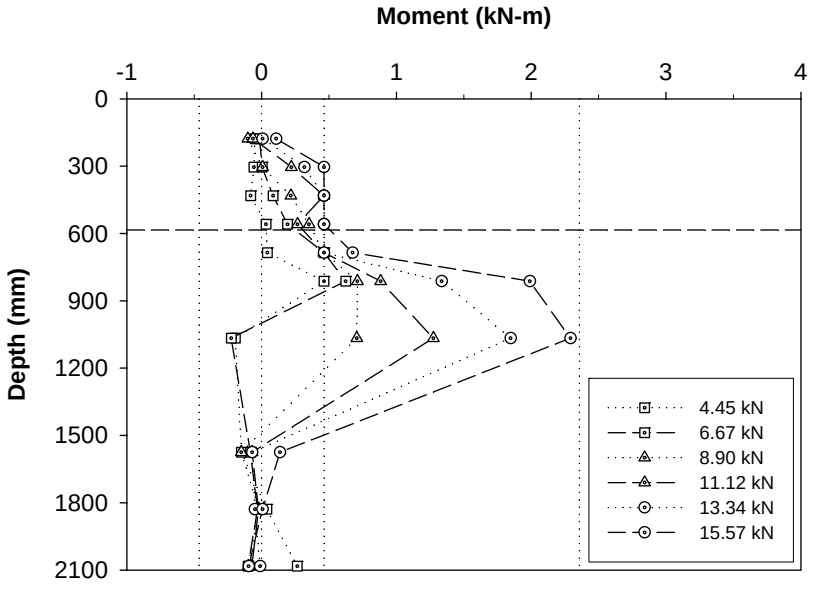

Figure 101. Bending moment profiles for reinforced glacial till (Pile 14 B)

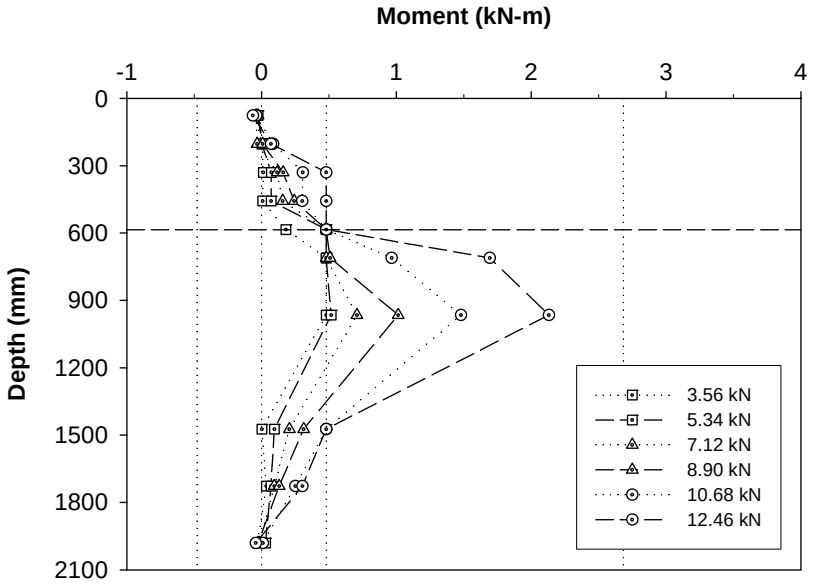

Figure 102. Bending moment profiles for reinforced weathered shale (Pile 10 A)

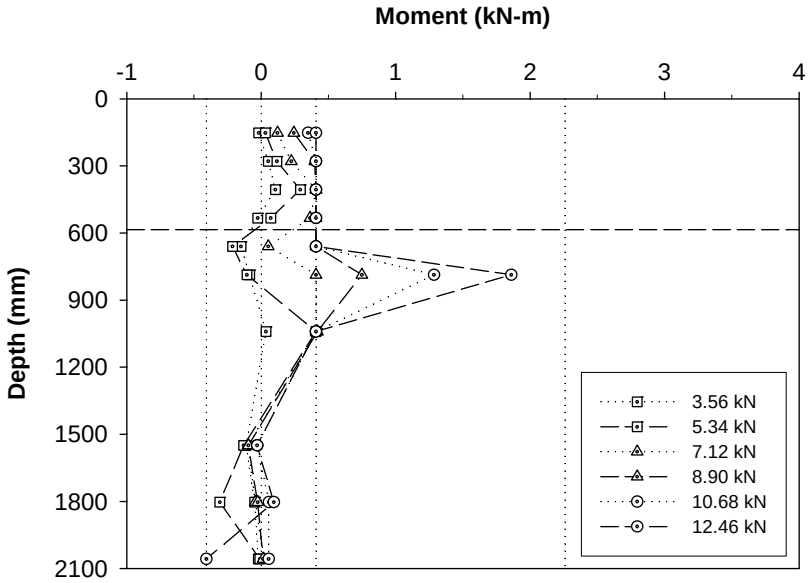

Figure 103. Bending moment profiles for reinforced weathered shale (Pile 10 B)

Soil Sampling

The compacted soil from select boxes was sampled after the performance of pile load tests. Sampling with Shelby tubes and in-situ testing devices – namely, Dynamic Cone Penetrometer and K_o Stepped Blade – helped to characterize the soil conditions before and after loading of piles. Specifically, soil sampling evaluated moisture and density, strength profiles, and lateral earth pressure profiles.

Moisture and Density

Shelby tube samples were taken from select boxes, and ranges for unit weight and moisture contents are presented in Table 20.

Table 20. Measured unit weight and moisture content

Soil Type	γ_d (kN/m^3)	w (%)	n	$\gamma_{d,max}$ (kN/m^3)	w_{opt} (%)
Loess	13.8 – 14.8	25 - 35	5	15.6	18
Glacial Till	18.5 – 19.2	14 - 18	6	17.8	14
Weathered Shale	16.5 – 18.2	18 - 23	2	16.7	18

Notes:
n = number of samples

Dynamic Cone Penetrometer (DCP)

The dynamic cone penetrometer (DCP) is an instrument used principally for pavement evaluation and construction control. The data obtained in the field is most commonly used to develop pavement structural numbers, CBR, and elastic moduli values (ASTM 2003). The research group, for this project, used the dynamic cone penetrometer to evaluate the uniformity of soil within the soil boxes. Uniform CBR profiles suggest uniform density, whereas variable CBR profiles suggest variable density attributed to non-uniform compaction effort. The CBR values were developed from equations presented in ASTM D 6951-03 [Use of the Dynamic Cone Penetrometer in Shallow Pavement Applications] (ASTM 2002), as follows:

$$\mathrm{CBR} = \frac{292}{\mathrm{DCP}^{1.12}}, \text{ for loess} \tag{10}$$

$$\mathrm{CBR} = \frac{1}{(0.017019 \cdot \mathrm{DCP})^2}, \text{ for glacial till and weathered shale} \tag{11}$$

Table 21 provides average DCP Index and CBR values for each soil type. The values are averages through the profile of the shear box soil and the soil of the control pads. Figures 104 through 106 show the CBR profiles for compacted loess, glacial till, and weathered shale.

Table 21. Profile (915 mm) average DCP index and CBR values

Soil Type	Test	Average DCP (mm/blow)	Average CBR
Loess	1	163	1.8
	4	198	1.0
	8	165	1.3
	11	150	1.2
Glacial Till	3	84	2.1
	5	74	2.5
	9	62	3.8
	14	74	3.0
Weathered Shale	2	71	2.6
	6	55	3.4
	12	59	3.3
	10	90	2.1

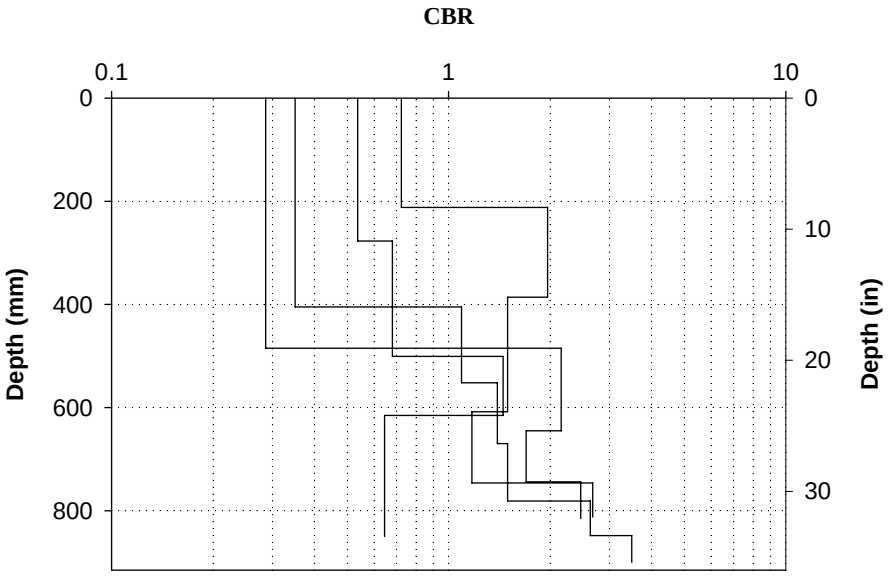

Figure 104. DCP results in loess

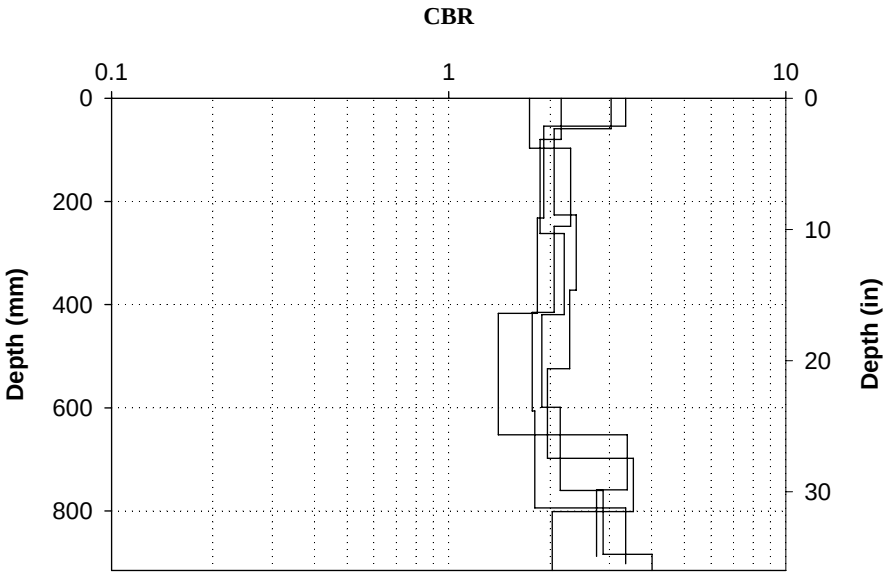

Figure 105. DCP results in glacial till

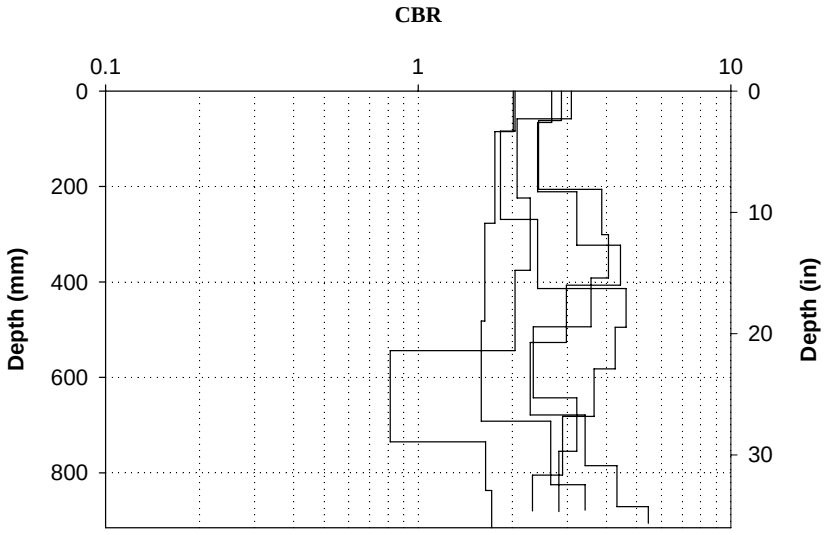

Figure 106. DCP results in weathered shale

K_o Stepped Blade

The Ko Stepped Blade was developed at Iowa State University to measure the in-situ lateral stress condition of soil. Soil pressures corresponding to known levels of disturbance are measured with pneumatic cells designed using a pressure-balance principle (Mings 1987). The relationship between soil disturbance and measured stress is subsequently used to extrapolate a pre-insertion (undisturbed) soil stress. The extrapolation principle is diagrammed in Figure 107.

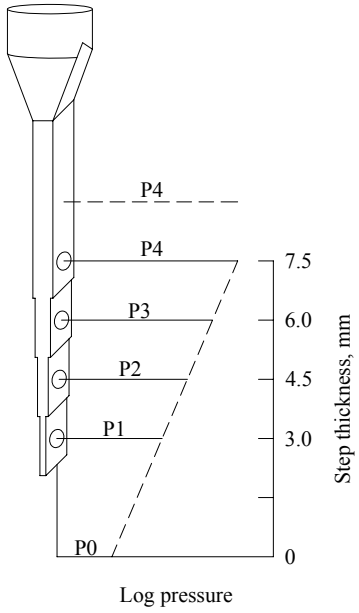

Figure 107. Extrapolation principle of K_o stepped blade (Mings 1987)

The K_o stepped blade device is shown in Figure 108, and the K_o stepped blade test performance is shown in Figure 109. The K_o stepped blade test was performed in weathered shale, on four sides of a 178 mm pile.

Figure 108. K_o stepped blade console

Figure 109. K_o stepped blade test performance

The K_o stepped blade test was incorporated into the soil sampling plan to support the observed soil behavior around piles subject to lateral soil movement. The research group observed the formation of a gap at the soil surface at the front (i.e. load side) of the pile. The gap was a consequence of pile head rotation away from the load. Associated with the gaps are unloaded lengths of pile in the direction of shear box movement and low lateral soil pressures in front of the pile. Conversely, the research group observed bulging of soil behind the pile. Associated with the bulging soil are loaded lengths of pile in the direction opposing shear box movement and high lateral soil pressure behind the pile. At greater depths, the lateral soil pressure in front of the pile exceeds the lateral soil pressure behind the pile, confirming that the net load is applied to piles in the direction of lateral soil movement. Figures 110 and 111 show the formation of a gap and soil bulging observed during testing.

Figure 110. Gap in front of pile (115-mm Pile in glacial till)

Figure 111. Soil bulging behind pile (115-mm Pile in glacial till)

Figures 112 through 115 show the extrapolation of lateral soil pressure at four locations within the weathered shale reinforced with a 178-mm pile. Figures 116 and 117 show the lateral stress profiles of the box. Figure 116 supports the previously discussed behavior of soil in front and behind the pile. The lateral stress in front of the pile is low at the top of the box and high at the bottom of the box, whereas the lateral stress behind the pile is high at the top of the box and low at the bottom of the box. The lateral stress on each side of the pile, as shown in Figure 117, is relatively constant with depth.

The magnitudes of lateral stress from the K_o Stepped Blade test, at first glance, appear high. The cohesion of weathered shale was responsible these test results. The Rankine passive earth pressure was evaluated for the soil condition, as follows (Das 1999):

$$\sigma_p = \sigma_v \, K_p + 2\,c\,\sqrt{K_p} \qquad (12)$$

where, $\gamma = 17.5\ \text{kN/m}^3$

$c = 27.6$ kPa, from unconfined test

$K_p = 2.2$ for $\phi = 22^o$

The Rankine passive earth pressure is shown on the lateral stress profiles of Figures 116 and 117. Despite the slightly-high lateral stress values from the tests, the qualitative information of the figures is valuable for understanding the system behavior.

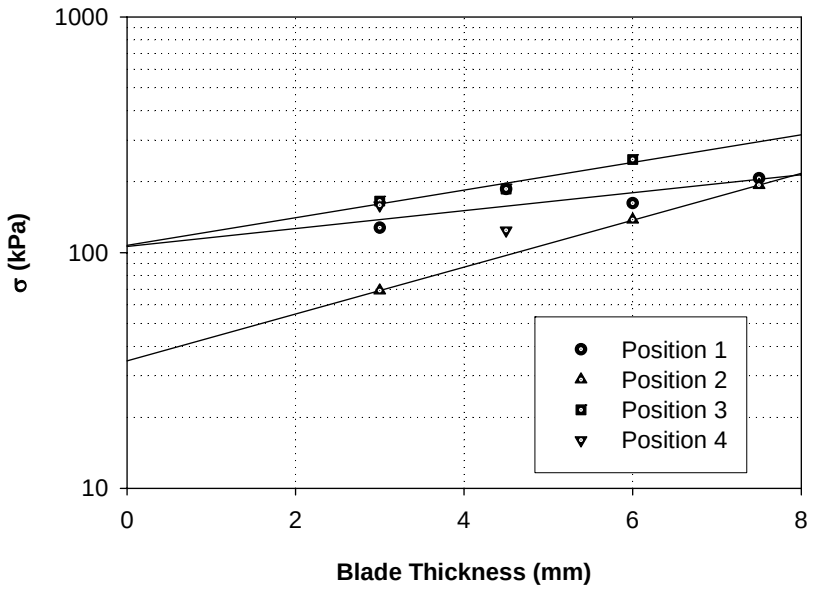

Figure 112. K_o stepped blade results (behind pile)

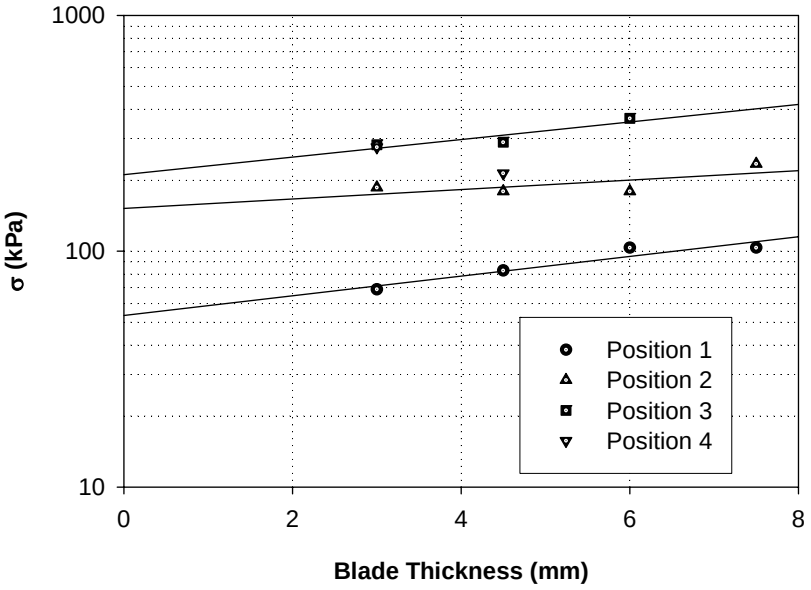

Figure 113. K_o stepped blade results (front of pile)

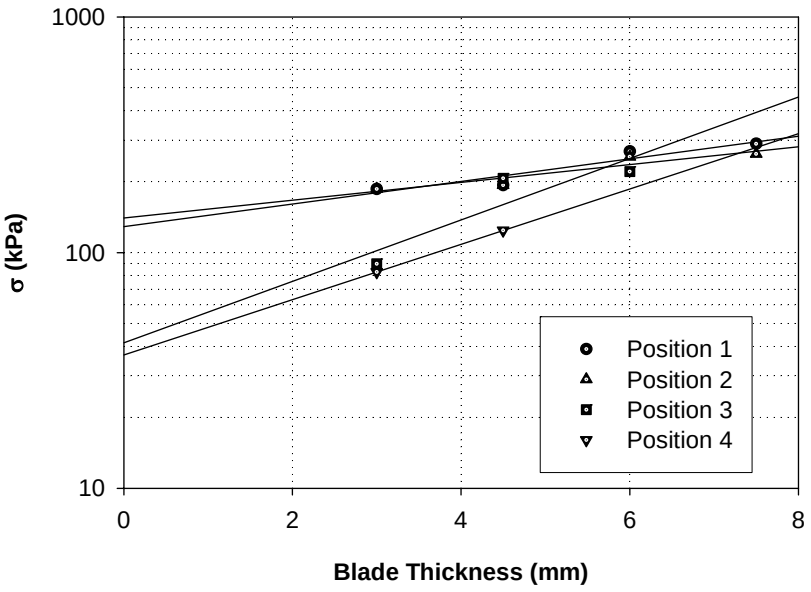

Figure 114. K_o stepped blade results (left side of pile)

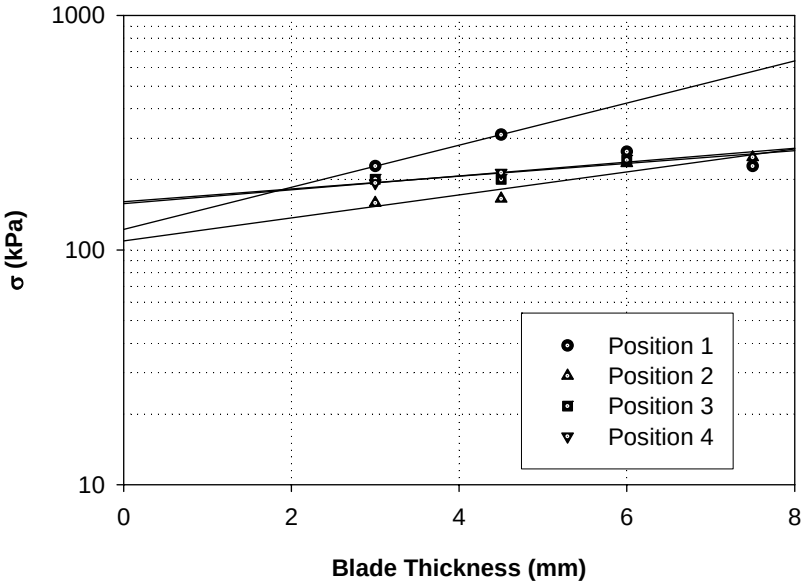

Figure 115. K_o stepped blade results (right side of pile)

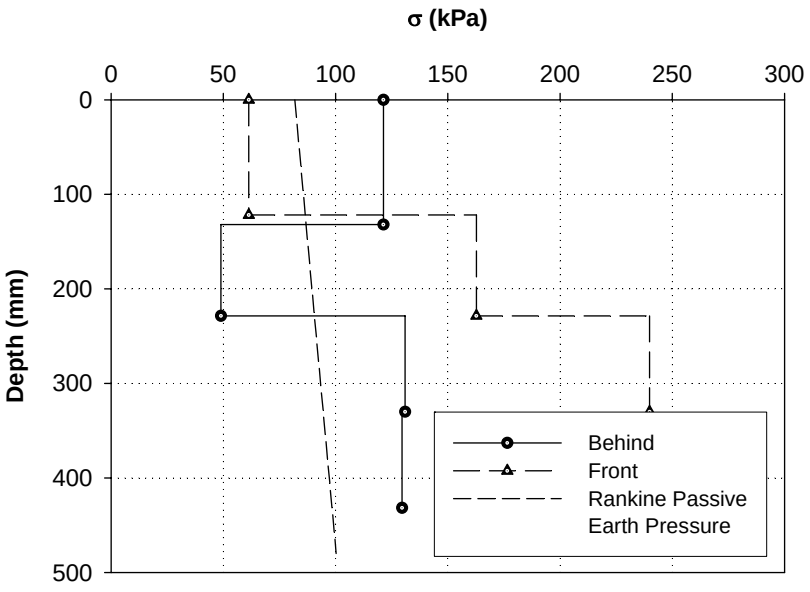

Figure 116. Lateral earth pressure profiles (behind and front of pile)

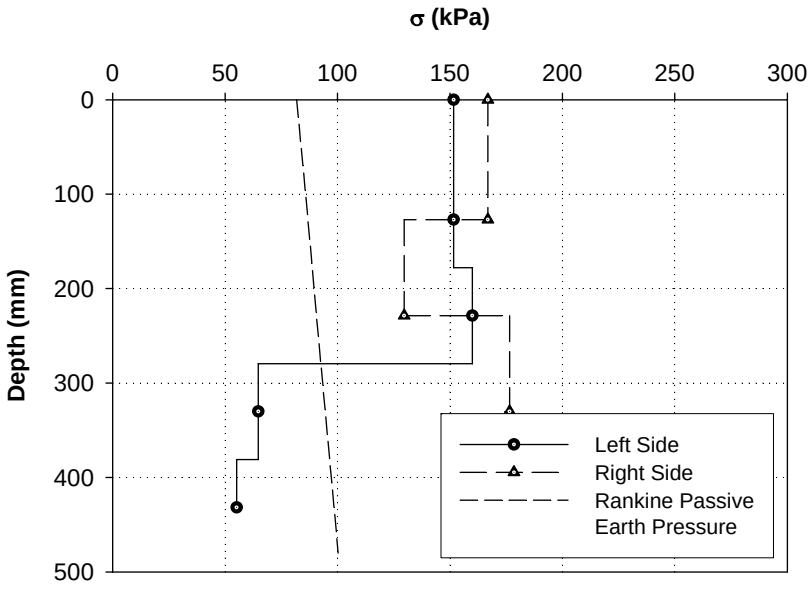

Figure 117. Lateral earth pressure profiles (sides of pile)

Exhumation of Piles

The piles of each load test were exhumed to examine pile condition after failure, pile uniformity, and pile diameter. The exhumation of piles offered physical evidence of the failure of piles due to mobilization of the pile moment capacity. Figure 118 shows a representative pile failure. Moreover, the figure shows that the depth at which the maximum moment developed is approximately four pile diameters below the shear surface. The failure depth agrees with depths of maximum measured strain and, therefore, supports the load test results.

Figures 119 through 121 show that the installed piles were quite cylindrical. Irregularities of pile diameter with depth were of small magnitude, and circular pile sections for the load test analyses were employed with minimal consequence. The load test analysis required accurate pile dimensions for the development of unique moment-curvature relationships (see Appendix B). Upon exhumation of the piles, the piles were cleaned and the diameters were measured at several locations along the pile length. The measured pile diameters are provided in Table 22.

(a) Exhumation of piles with excavator

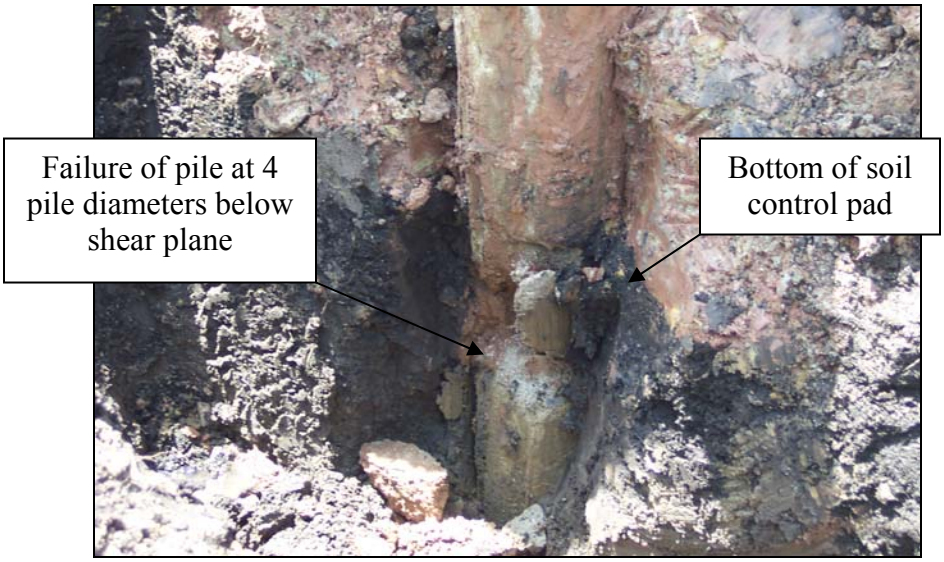

(b) Location of maximum moment and pile failure

Figure 118. Exhumation of piles

Figure 119. Exhumed 127-mm pile (Pile 5)

Figure 120. Exhumed 178-mm pile (Pile 9)

Figure 121. Exhumed 127-mm piles (Pile 14 A and 14 B)

Table 22. Measured diameters of exhumed piles

Pile	Diameter (mm)
4	114
5	112
6	117
7	114
8	183
9	178
10 A	114
10 B	112
11 A	114
11 B	114
12	173
13 A	112
13 B	114
14 A	114
14 B	117

LOAD TEST ANALYSIS AND DISCUSSION OF RESULTS

Introduction

This chapter details the analysis of experimental pile load tests. The results of the previous chapter facilitate the analysis and its objectives.

Load Test Analysis

The principal objectives of the load test analysis and characterization of load transfer of piles subject to lateral soil movement are to: (1) describe the finite difference lateral response analysis method proposed by Reese and Wang (2000), (2) evaluate the analysis method by comparing predicted pile behavior with measured results, and (3) verify the predicted structural performance of pile elements under the loading conditions of slope reinforcement. Achievement of the analysis objectives supports an understanding of load transfer mechanisms of the system and the development of the proposed design methodology.

Analysis Approach

The pile-soil reaction and passive pile response depend on the relative displacement between the soil and the piles (Poulos 1973; Byrne *et al* . 1984). Evaluating this relative soil displacement is complicated, because the pile response depends on the soil displacement, which is itself affected by the pile. Displacement-based methods, therefore, incorporate lateral soil displacements into pile response analyses to consider the effect of soil-pile interaction. Solutions for predicting soil-pile response due to soil movement are generally derived from the finite element method (Carter 1982; Springman 1989; Stewart *et al* . 1993) or the finite difference method (Poulos 1973; Byrne *et al* . 1984).

The governing differential equation for the system of piles subject to free-field lateral soil movement closely resembles that for conventional laterally loaded piles with a fixed free field (Byrne *et al* . 1984). The finite difference lateral response analysis method has recently been modified to suit the p-y method of laterally loaded piles by Reese and Wang (2000). In this analysis, the lateral pressure due to pile-soil interaction is obtained from the relative displacement between the pile and soil and the specified p-y relationship. The beam flexure equation, for the case of a pile subject to free-field lateral soil movement, is:

$$EI\frac{d^4y}{dx^4} + Q\frac{d^2y}{dx^2} - p(y - y_s) + w = 0 \qquad (13)$$

with EI equal to the pile flexural stiffness, Q equal to the axial load, p equal to the soil reaction per unit length, y equal to the lateral deflection of the pile, y_s equal to the free-field soil movement, and w equal to an externally-applied load distribution.

The lateral response analysis method proposed in Reese and Wang (2000) was elected for interpreting the experimental test data and characterizing the measured pile behavior. The analysis incorporated the nonlinear subgrade reaction model of soil behavior, and pile behavior

following the moment-curvature relationship of reinforced concrete pile sections. As described in the introduction, the method uses the relative displacement between soil and pile elements and cycles through the beam flexure equation (see Equation 13) in a finite difference form. This analysis employed computer software, namely *LPILE* Plus Version 4.0m (Reese and Wang 2000), to perform finite difference calculations and identify the pile response to the imposition of specified boundary conditions.

The *LPILE* analysis setup and corresponding free-field slope movement assumption is illustrated in Figure 122. Each soil layer was modeled with the p-y curves shown in Figure 123. Structural behavior of piles followed the moment-curvature relationships of reinforced concrete pile sections, as previously discussed. The shear and bending moment at the pile head equaled zero to satisfy pile head fixity conditions. The final input for performing the analysis was the free-field horizontal soil movement. Soil movements corresponded to the uniform lateral translation of the shear boxes imposed during the experimental testing. This soil movement was measured and, therefore, available for input into the analysis.

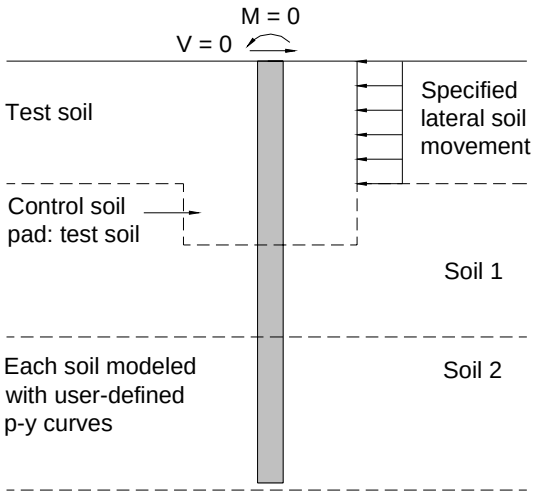

Figure 122. LPILE analysis setup

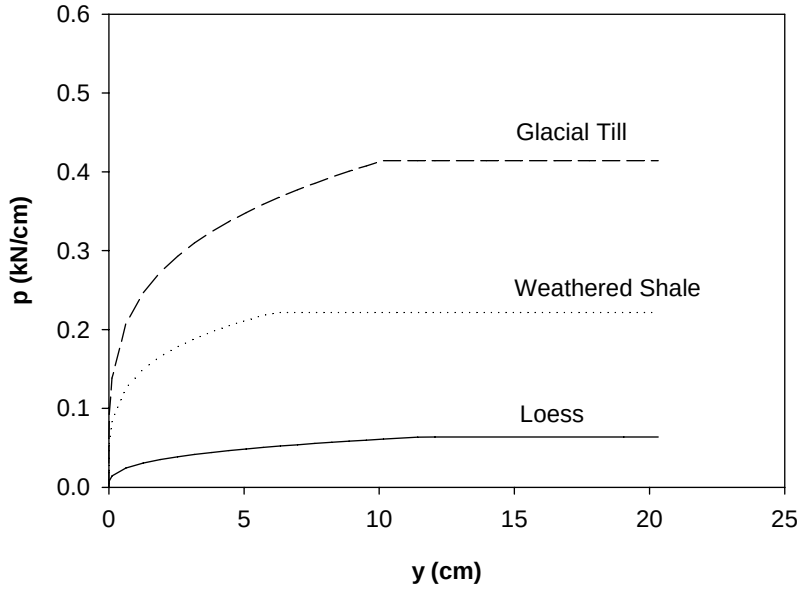

Figure 123. Load-displacement (p-y) curves for analysis

Evaluation of Analysis Method

The objective of the load test analysis was achieved by comparing measured pile behavior with predicted pile behavior estimated from the finite difference method. Correlation of pile head deflection and maximum moment values indicated that the predicted soil reaction matched the loading condition achieved during testing. The correlations of measured and predicted values of pile head deflection and maximum moment were linearized by plotting measured data against predicted data. Ideal correlation, in which measured data equals predicted data, was indicated by a 1:1 line, provided in the figures as a reference.

Correlation of isolated pile behavior is demonstrated in Figures 124 and 125, and pile behavior correlation for group piles is demonstrated in Figures 126 and 127.

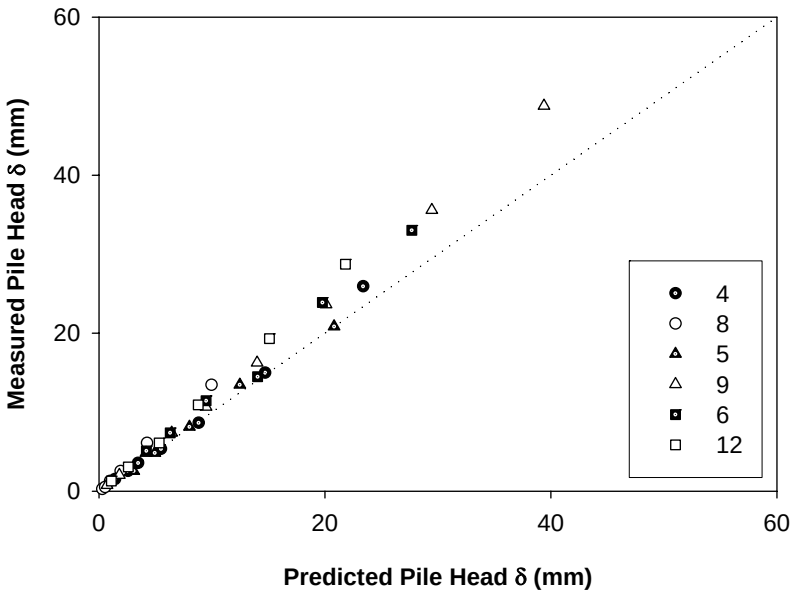

Figure 124. Pile head deflection correlation for isolated piles

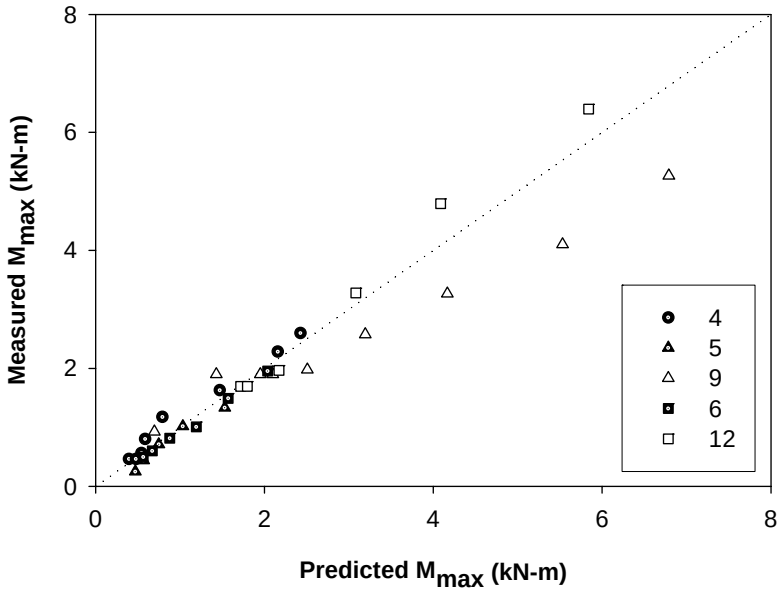

Figure 125. Maximum moment correlation for isolated piles

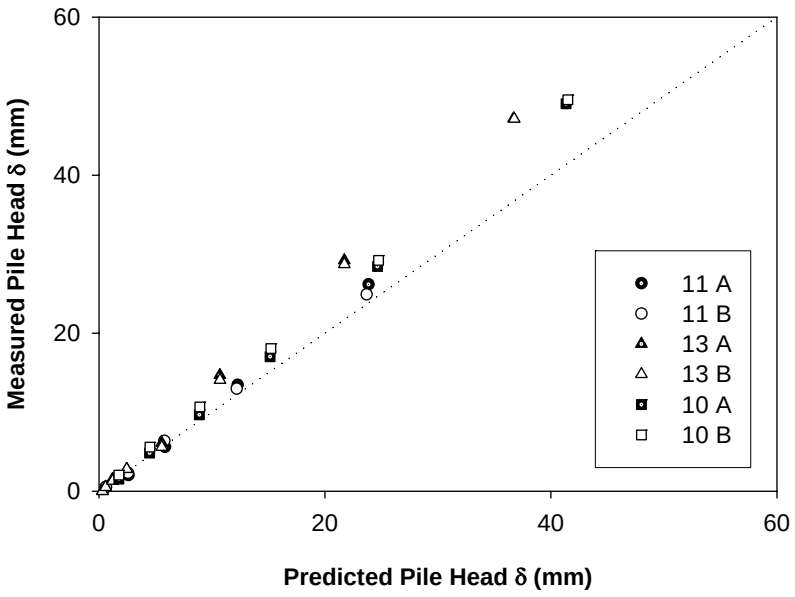

Figure 126. Pile head deflection correlation for grouped piles

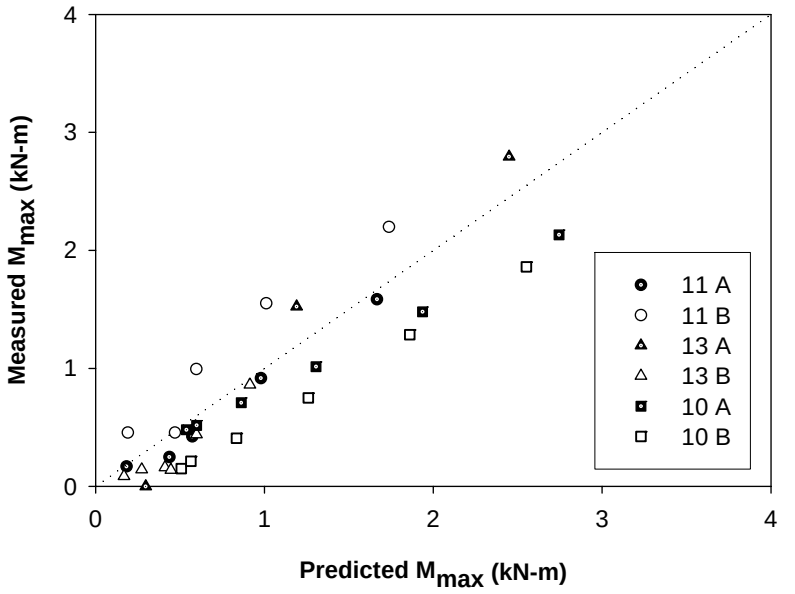

Figure 127. Maximum moment correlation for grouped piles

Correlation and regression predictability are closely related (Ott and Longnecker 2001). The proportionate reduction in error for a regression is the coefficient of determination, which is defined as follows:

$$r^2 = \frac{SS(Total) - SS(Residual)}{SS(Total)} \tag{14}$$

where $SS(Total) = \Sigma_i (y_i - \bar{y}_i)^2$

$SS(Residual) = \Sigma_i (y_i - \hat{y}_i)^2$

y_i = measured value

$\bar{y}_i$ = average of measured values

$\hat{y}_i$ = predicted value

An r^2 value of zero indicates no predictive value and poor correlation, whereas an r^2 value of unity indicates perfect predictability and excellent correlation. Recognizing that the coefficient of determination depends on the number correlation points and the load (stage of loading) at which the pile behavior was compared, the calculated coefficients of determination are provided in Table 23.

Table 23. Coefficients of determination for pile load test analyses

	r^2	
Pile	**Pile Head Deflection**	**Bending Moment**
4	0.988	0.946
5	0.997	0.957
6	0.952	0.984
8	0.900	---
9	0.949	0.494
12	0.915	0.978
11 A	0.990	0.975
11 B	0.996	0.880
13 A	0.911	0.911
13 B	0.918	0.672
14 B	0.980	0.966
10 A	0.966	0.836
10 B	0.958	0.569

Sample bending moment profiles are provided in Figures 128 through 130 to demonstrate that, while measured and predicted maximum moment values may not closely agree at one particular elevation, measured bending moments generally corresponded to those predicted along the entire length of the piles. The two loads at which bending moment profiles are compared (e.g. 1.78 kN and 4.45 kN for Pile 4) were selected to indicate pile behavior correlation during Stage 1 and Stage 2 loading.

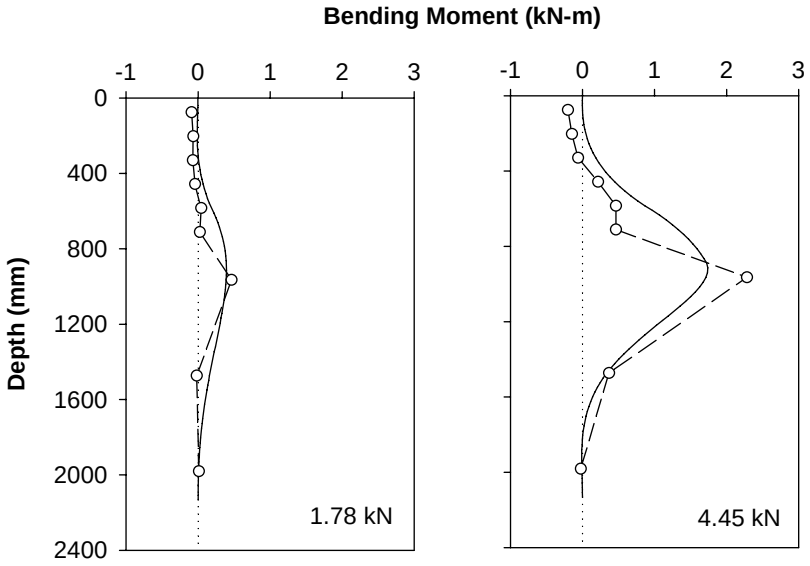

Figure 128. Sample bending moment correlation for isolated pile in loess (Pile 4)

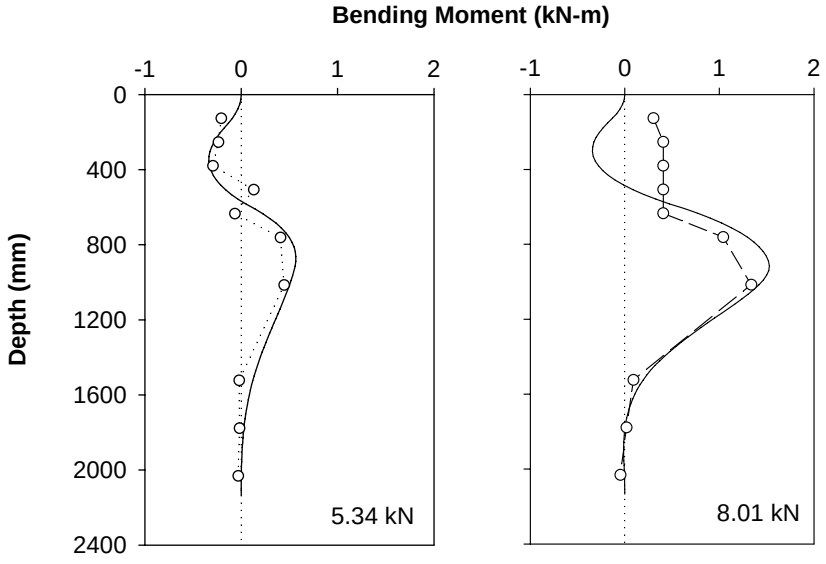

Figure 129. Sample bending moment correlation for isolated pile in glacial till (Pile 5)

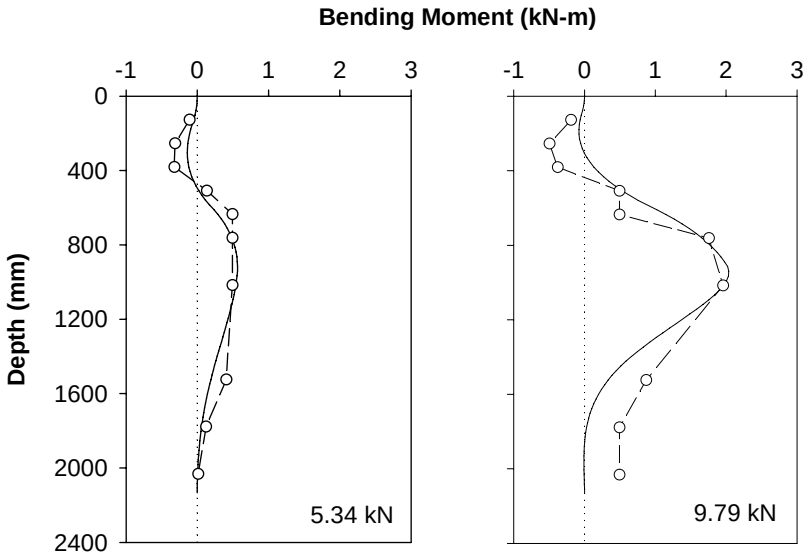

Figure 130. Sample bending moment correlation for isolated pile in weathered shale (Pile 6)

Verification of Predicted Structural Performance of Pile Elements

Figures 131 and 132 were developed to show the maximum moment achieved in the pile during loading. The measured maximum moments corresponding to the maximum applied load on the pile are plotted against the maximum moments predicted with LPILE for the appropriate load application. The plot indicates whether LPILE over-predicts or under-predicts the moment induced in a pile subject to a given loading. Additionally, the graphs show the cracking moment and the moment capacity of the pile section for each test pile. The location of the measured maximum moment on this continuum indicates the level of bending stresses that were achieved during experimental testing and whether the loading of the system mobilized the ultimate soil pressure or the moment capacity of the pile sections.

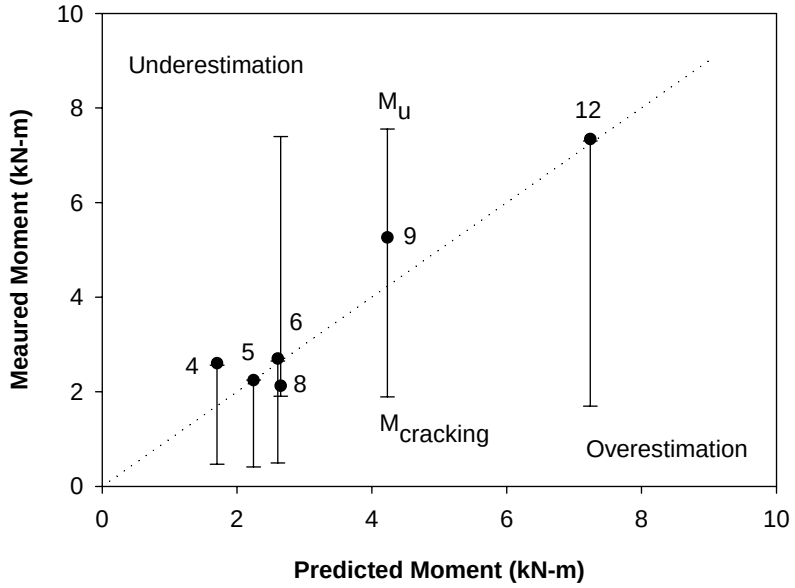

Figure 131. Measured and predicted moments for isolated piles

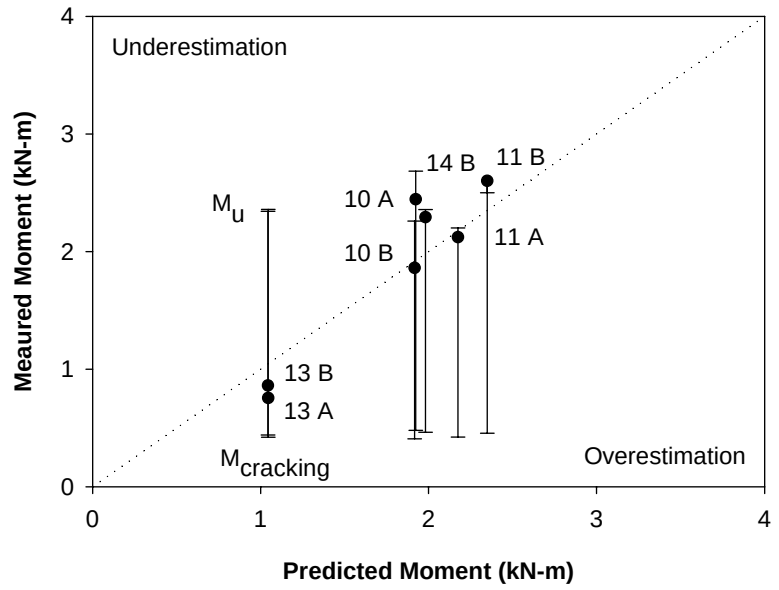

Figure 132. Measured and predicted moments for grouped piles

Discussion of Results

Comparison of Load Distributions with Existing Analytical Models

The principal consequence of failing to mobilize the ultimate soil pressure is the inability to directly deduce the ultimate soil pressure profile with depth. Existing analytical models and the proposed design methodology, however, assume that loads develop along piles as a factored ultimate soil pressure profile (Loehr and Bowders 2003). The research established that the loads which developed along the piles vary approximately linearly with depth, indicating that the ultimate soil pressure likely varies linearly with depth. The research group accepts the dependence of ultimate soil pressure on effective stress and recommends using analytical models which incorporate overburden pressure (e.g. Ito and Matsui 1975, Brinch Hansen 1961) for designing pile stabilization. The results, however, do not document the conclusion that such analytical models are always more appropriate than those models which may incorporate only undrained shear strength.

Extension of Pile Performance Prediction for Design of Alternative Pile Sections

The ability to accurately predict structural performance of pile sections is important for making stabilization with soil displacement grouted micropiles a robust slope remediation alternative. The benefits of designing piles to be weak or strong, depending on the controlling failure mechanism and required capacity of stabilizing piles, include the design of practical slope reinforcement systems and optimization of the designs to satisfy the cost constraints of the slope remediation.

The load test analysis required the validation of the predicted structural performance of the test piles. The analysis objective was achieved, as evidenced by the close correlation between measured maximum moments in failed piles (i.e. moment capacity) and the computed moment capacities of LPILE. Measured pile head deflections and bending behavior, which is highly dependent on pile flexural stiffness (changing with continued loading), was also well predicted with LPILE. As a result, LPILE is used to reliably analyze and design pile sections with alternative material properties and reinforcement arrangements.

SLOPE REINFORCEMENT DESIGN METHODOLOGY

Introduction

The proposed design method offers a rational approach to slope stabilization with grouted micropiles. The design methodology incorporates the following elements:

- Limit equilibrium analyses of unstable, unreinforced slopes
- Reinforcing effect of small-diameter pile elements, including structural capacity of the pile sections and the effect of the pile elements on the global stability of the reinforced slope
- Approach for designing pile sections, based on calculated moment capacities
- Recommendations for arrangement of piles on slopes

Overview of Limit State Design Methodology

To provide adequate stability for unstable slopes, inclusive of considering the potential failure of the reinforced slope, the proposed design procedure incorporates limit states. Specifically, the design procedure incorporates strength limit states that address potential failure mechanisms of pile-stabilized slopes. The possible modes of failure for slopes stabilized with pile elements include: (1) mobilization of the ultimate soil pressure and failure of the soil above the sliding surface, (2) passive failure of soil below the sliding surface due to insufficient anchorage, and (3) structural failure of individual pile elements due to bending forces developed in the piles that exceed the capacity of the pile sections. The service limit states associated with the design of other earth and building structures are less important to the stabilization of nuisance slope failures. Small deformations of the slope are generally accepted, provided the slope maintains its primary function.

The presently discussed design procedure does not make the assumption that the stabilized slope moves sufficiently to mobilize the ultimate soil pressure along each pile element. Rather the design procedure assumes that a sufficient number of piles are installed to arrest slope movement before the ultimate soil pressure is allowed to develop. The unique stabilization approach, in which pile stability possibly controls the stabilization design, emphasizes the evaluation of limit states corresponding to the previously mentioned failure modes. The next section, based on the approach for designing recycled plastic pin stabilization (ref. Chapter 2), offers a step-by-step procedure for developing limit resistance curves.

Development of Limit States

Step 1 – Establish Design Input Variables

Step 1.a

Establish in spreadsheet software, to reference for subsequent calculations, the design input variables (see Figure 133).

The necessary soil parameters are:

- Effective cohesion, c'
- Effective internal friction angle, ϕ'
- Unit weight, γ
- Soil modulus, E_s

The necessary parameters related to properties and arrangement of pile elements are:

- Pile diameter, b
- Stiffness, EI
- Moment capacity, M_u
- Center-to-center spacing, D_1

Step 1.b

Calculate the Rankine passive, at-rest, and active lateral earth pressure (LEP) coefficients (K_p, K_o, and K_a, respectively) with Equations (15) through (17). Calculate the clear distance between piles, D_2, with Equation (18).

$$K_p = \tan^2(45 + \frac{\phi}{2}) \text{ for passive LEP,} \quad (15)$$

$$K_o = 1 - \sin\phi \text{ for at-rest LEP, and} \quad (16)$$

$$K_a = \tan^2(45 - \frac{\phi}{2}) \text{ for active LEP,} \quad (17)$$

$$D_2 = D_1 - b \quad (18)$$

Soil Properties	
c (kPa)	10.0
ϕ (deg)	14
γ_t (kN/m^3)	18.8
E_s (kPa)	20700

K_p	1.638
K_o	0.758
K_a	0.610

Pile Properties	
b (mm)	178
EI (kN-m^2)	657.3
M_u (kN-m)	25.90
D_1 (m)	0.91

D_2 (m)	0.73

Figure 133. Calculation of design input variables

Step 2 – Calculate Limit Soil Resistance

Step 2.a

Establish and calculate N_ϕ, J_1, J_2, and J_3 using Equations (19) through (22) (see Figure 134). The variables, each a function of the internal friction angle, are used solely to simplify the later calculation of ultimate soil pressure. For the preliminary calculations, the units of internal friction angle are radians.

$$N_\phi = \tan^2\left(\frac{\pi}{4} + \frac{\phi}{2}\right), \tag{19}$$

$$J_1 = N_\phi^{1/2} \tan\phi + N_\phi - 1, \tag{20}$$

$$J_2 = 2\tan\phi + 2N_\phi^{1/2} + N_\phi^{-1/2}, \text{ and} \tag{21}$$

$$J_3 = N_\phi \tan\phi \tan\left(\frac{\pi}{8} + \frac{\phi}{4}\right), \tag{22}$$

N_ϕ	1.63825
$\tan\phi$	0.24933
$N_\phi \tan\phi$	0.40846
J_1	0.95738
J_2	3.83982
J_3	0.19922

Figure 134. Calculation of simplifying variables

Step 2.b

For depths from the ground surface to the pile tip (6-m-length pile in this case), at approximately 0.2-m intervals, calculate the vertical overburden pressure, σ_v, with Equation (23). The uppermost depth is established at z = 0.001 m. The use of a non-zero value eliminates the "division by zero" error of spreadsheet software. Calculate the ultimate soil pressure, P_u, with

Equation (24) (see Figure 135).

$$\sigma_v = \gamma\, z\,, \tag{23}$$

$$P_u(z) = c\, D_1 \left(\frac{D_1}{D_2}\right)^{J_1} \left[\frac{1}{N_\phi \tan\phi}\left\{e^{\frac{D_1-D_2}{D_2} J_3} - 2\, N_\phi^{1/2} \tan\phi - 1\right\} + \frac{J_2}{J_1}\right] \tag{24}$$

$$- c \left\{D_1 \frac{J_2}{J_1} - 2\, D_2\, N_\phi^{-1/2}\right\} + \frac{\sigma_v}{N_\phi}\left\{D_1 \left(\frac{D_1}{D_2}\right)^{J_1} \cdot e^{\frac{D_1-D_2}{D_2} J_3} - D_2\right\}$$

z = 0.001 m

Depth	Overburden Pressure	Ult Soil Pressure
z (m)	σ_v (kPa)	$P_u(z)$ (kN/m)
0.0	0.19	3.79
0.2	3.76	4.76
0.4	7.52	5.78
0.6	11.28	6.80
0.8	15.04	7.82
1.0	18.80	8.84
1.2	22.56	9.86
1.4	26.32	10.88
1.6	30.08	11.90
1.8	33.84	12.92
2.0	37.60	13.94

Figure 135. Calculation of ultimate soil pressure

Step 2.c

Establish potential sliding depths, Z_s, for which the limit soil resistance, F_S, is calculated. For relative ease of calculation, use sliding depths equal to the depths at which ultimate soil pressures are calculated as follows:

$$Z_s = z \tag{25}$$

Step 2.d

Calculate the limit soil resistance, F_S, by integrating the ultimate soil pressure from the ground surface to each sliding depth. Use the trapezoidal rule of integration, as illustrated with Equation (26). Make certain that $F_S = 0$ at the ground surface.

$$F_S = F_{S,n-1} + \frac{(P_{u,n-1} + P_{u,n})}{2} \cdot (z_n - z_{n-1}) \tag{26}$$

Step 2.e

Divide the calculated limit soil resistance, F_S, by the pile spacing, D_1, to obtain limit soil resistance per unit length of slope, denoted F_S' (see Figure 136).

$$F_S'(\text{kN/m}) = \frac{F_S\ (\text{kN})}{D_1\ (\text{m})} \tag{27}$$

Depth	Overburden Pressure	Ult Soil Pressure	Slide Depths	Limit Soil Resistance	
z (m)	σ_v (kPa)	$P_u(z)$ (kN/m)	Z_s (m)	F_S (kN)	F_S' (kN/m)
0.0	0.19	3.79	0.0	0.00	0.00
0.2	3.76	4.76	0.2	0.81	0.89
0.4	7.52	5.78	0.4	1.87	2.05
0.6	11.28	6.80	0.6	3.13	3.44
0.8	15.04	7.82	0.8	4.59	5.04
1.0	18.80	8.84	1.0	6.26	6.87
1.2	22.56	9.86	1.2	8.13	8.93
1.4	26.32	10.88	1.4	10.20	11.21
1.6	30.08	11.90	1.6	12.48	13.71
1.8	33.84	12.92	1.8	14.96	16.44
2.0	37.60	13.94	2.0	17.65	19.39

Figure 136. Calculation of limit soil resistance

Step 3 – Calculate Limit Anchorage Resistance

Step 3.a

The maximum F_S value is located at the sliding depth equal to the pile length. Identify this value ($F_{S,max}$) for subsequent calculations (see Figure 137). Calculate the limit anchorage resistance, F_A, by subtracting the F_S value, for each sliding depth, from $F_{S,max}$. Calculation of the limit anchorage resistance in this manner is equivalent to integrating the ultimate soil pressure from each sliding depth to the pile tip.

Step 3.b

Divide the calculated limit anchorage resistance, F_A, by the pile spacing, D_1, to obtain limit anchorage resistance per unit length of slope, denoted F_A' (see Figure 137).

$$F_A'(\text{kN/m}) = \frac{F_A\ (\text{kN})}{D_1\ (\text{m})} \tag{28}$$

Slide Depths	Limit Soil Resistance		Limit Anchorage Resistance	
Z_s (m)	F_S (kN)	F_S' (kN/m)	F_A (kN)	F_A' (kN/m)
0.0	0.00	0.00	114.23	125.52
0.2	0.81	0.89	113.41	124.63
0.4	1.87	2.05	112.36	123.47
0.6	3.13	3.44	111.10	122.09
0.8	4.59	5.04		
1.0	6.26	6.87		
1.2	8.13	8.93		
1.4	10.20	11.21	104.03	114.32
1.6	12.48	13.71	101.75	111.81
1.8	14.96	16.44	99.27	109.08
2.0	17.65	19.39	96.58	106.13
2.2	20.54	22.57	93.69	102.95
2.4	23.63	25.97	90.59	99.55
2.6	26.93	29.60	87.30	95.93
	30.44	33.45	83.79	92.08
	34.14	37.52	80.09	88.01
	38.05	41.82	76.17	83.71
3.4	42.17	46.34	72.06	79.19
3.6	46.49	51.08	67.74	74.44
3.8	51.01	56.05	63.22	69.47
4.0	55.74	61.25	58.49	64.28

$F_{S,max} - F_S = F_A$
$F_A = 114.23 - 0.81$ kN

At $Z_s = 6$ m,
$F_S = 114.23$ kN

Figure 137. Calculation of limit anchorage resistance

Step 4 – Calculate Limit Member Resistance

Step 4.a

Calculate the polynomial constants in Equation (29), f_1 and f_2, using Equations (30) and (31). Also calculate the characteristic length, β, with Equation (32), based on relative stiffness of the soil and the pile (see Figure 138).

$$P_u = f_1 + f_2 z \tag{29}$$

$$f_1 = c D_1 \left(\frac{D_1}{D_2}\right)^{J_1} \left[\frac{1}{N_\phi \tan\phi}\left\{e^{\frac{D_1-D_2}{D_2}J_3} - 2 N_\phi^{1/2} \tan\phi - 1\right\} + \frac{J_2}{J_1}\right] \tag{30}$$

$$- c \left\{D_1 \frac{J_2}{J_1} - 2 D_2 N_\phi^{-1/2}\right\}$$

$$f_2 = \frac{\gamma}{N_\phi}\left\{D_1 \left(\frac{D_1}{D_2}\right)^{J_1} \cdot e^{\frac{D_1-D_2}{D_2}J_3} - D_2\right\} \tag{31}$$

$$\beta = \sqrt[4]{\frac{E_s}{4\,E_p I_p}} \tag{32}$$

f_1 (kN/m)	10.69
f_2 (kN/m^2)	5.10
β (m^{-1})	1.68

Figure 138. Calculation of polynomial constants and characteristic length

Step 4.b

For each potential sliding depth, calculate the maximum moment developed along the pile with Equation (36). This step requires preliminary calculation of A, B, and z2 with Equations (33) through (35).

$$A = \frac{Z_s}{12E_p I_p \beta^3}\{3(2+\beta Z_s)f_1 - Z_s(3+2\beta Z_s)f_2\} \tag{33}$$

$$B = \frac{-(Z_s)^2}{12E_p I_p \beta^2}(3f_1 - 2Z_s f_2) \tag{34}$$

$$z_2 = \frac{1}{\beta}\tan^{-1}\frac{A+B}{A-B} \tag{35}$$

$$M_{max} = -2E_p I_p \beta^2 e^{-\beta z_2}(A\sin\beta z_2 - B\cos\beta z_2) \tag{36}$$

Step 4.c

Calculate the reduction factor, α, by which the ultimate soil pressure is increased or, more commonly, decreased. The reduction factor is given by Equation (37) and varies with the depth to the sliding surface, Z_S.

$$\alpha = \frac{M_u}{M_{max}} \tag{37}$$

Step 4.d

Calculate the limit member resistance, F_M, for each potential sliding depth, by multiplying the reduction factor, α, and the limit soil resistance, F_S (see Equation (38)).

$$F_M = \alpha F_S \tag{38}$$

Step 4.e

Divide the calculated limit member resistance, F_M, by the pile spacing, D_1, to obtain limit member resistance per unit length of slope, denoted F_M' (see Equation (39)).

$$F_M'(\text{kN/m}) = \frac{F_M\ (\text{kN})}{D_1\ (\text{m})} \tag{39}$$

					Limit Member Resistance	
A (m)	B (m)	z_2 (m)	M_{max} (kN-m)	α	F_M (kN)	F_M' (kN/m)
0.000	0.000	0.464	0.021	1241.26	0.00	0.00
0.000	0.000	0.385	0.530	48.84	39.69	43.62
0.0		0.326	1.288	20.10	37.54	41.26
0.0		0.283	2.236	11.58	36.20	39.78
0.002	-0.001	0.251	3.319	7.80	35.81	39.35
0.002	-0.001	0.227			36.24	39.82
0.003	-0.001	0.209			37.46	41.16
0.003	-0.002	0.195			39.49	43.40
0.004	-0.002	0.185	7.606	3.41	42.49	46.70
0.004	-0.002	0.178	8.290	3.12	46.74	51.37
0.004	-0.002	0.174	8.664	2.99	52.75	57.97
0.004	-0.002	0.174	8.651	2.99	61.49	67.57
0.004	-0.002	0.180	8.175	3.17	74.87	82.28
0.003	-0.002	0.193	7.166	3.61	97.34	106.97
0.003	-0.001	0.224	5.568	4.65	141.58	155.58

At Z_S = 0.2 m,
F_S = 0.81 kN

$F_M = \alpha\ F_S$
F_M = 48.84 x 0.81 kN

Figure 139. Calculation of limit member resistance

Step 5 – Plot Composite Limit Resistance Curve

The composite limit resistance, used for designing slope reinforcement, is the minimum of the limit resistances for the three respective failure modes (i.e. F_R = minimum(F_S, F_A, F_M)) (see Figure 140). Plot the composite limit resistance as a function of sliding depth, Z_s (see Figure 141).

$F_R = \min(F_S, F_A, F_M)$

Composite Limit Resistance	
F_R (kN)	F_R' (kN/m)
0.00	0.00
0.81	0.89
1.87	2.05
3.13	3.44
4.59	5.04
6.26	6.87
8.13	8.93

Figure 140. Calculation of composite limit resistance

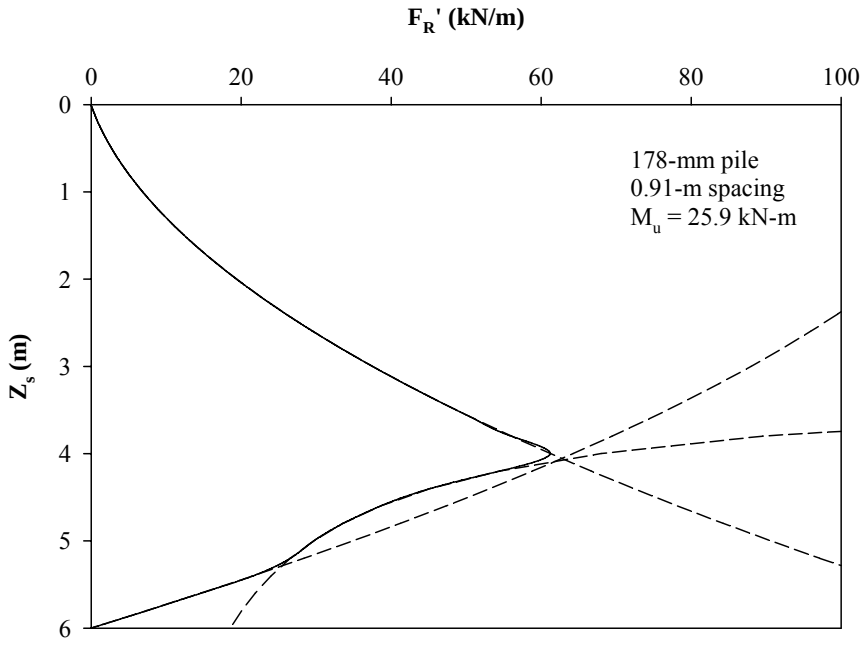

Figure 141. Composite limit resistance curves

Design Procedures

The design protocol, detailed in the ensuing sections, proceeds with the following steps:

1. Global stability analysis for unreinforced slope
2. Calculation of required stabilizing force
3. Development of composite limit resistance curves
4. Calculation of required number of rows and piles
5. Global and local stability analyses for reinforced slope
6. Material cost analysis

Step 1 – Perform the Global Stability Analysis for Unreinforced Slope

The performance of slope stability analyses for the unreinforced slope is necessary to evaluate the condition of the slope. A detailed analysis, performed in conjunction with a slope investigation, aids in establishing the cause of instability and effective remediation alternatives. Site investigations that encounter high groundwater tables, for example, may suggest that reduced effective stresses are responsible for slope instability. The influence of the groundwater table elevation on the stability of a slope is easily verified by performing multiple stability analyses. Subsurface drainage may be considered to be a primary remediation alternative when groundwater causes slope instability. Subsurface drainage fails to improve the stability of slopes, however, when groundwater has little effect on the unstable slope. Rather, the performed analyses may suggest that slope geometry and/or weak slope soils are responsible for slope instability. In this case, slope reinforcement and use of piles for slope stabilization may be considered to be a potential remediation alternative.

Perform the stability analysis of the unreinforced slope to indicate the required capacity of slope reinforcement. In addition to the factor of safety, document the forces driving and resisting slope movement and the depths to the failure surface along the slope profile. The stability analysis may involve the documentation of multiple failure surfaces, where the failure surface of the unreinforced slope does not necessarily match the failure surface of the reinforced slope.

Step 2 – Calculate the Required Stabilizing Force

The stability of an unreinforced slope and global stability specifications control the required capacity of slope reinforcement. Use the total resisting and driving forces (ΣF_R and ΣF_D, respectively) from the stability analysis and the target factor of safety to calculate the required stabilizing force, ΔF_R (see Equation (40)).

$$\Delta F_R = FS \cdot \Sigma F_D - \Sigma F_R \text{ , per unit length of slope} \qquad (40)$$

where, ΔF_R = total stabilizing force,

ΣF_R = total resisting force (unreinforced slope),

ΣF_D = total driving force (unreinforced slope), and

FS = factor of safety

The achievement of ΔFR with the installation of piles necessarily satisfies the established stability requirements for the slope.

Step 3 – Develop Composite Limit Resistance Curves

Develop the limit resistance curves for soil displacement grouted micropiles, as presented earlier in this chapter. Table 24 provides the moment capacities and stiffness values of several steel-reinforced pile sections, determined from a pile section analysis with LPILE. The table values

are inputs for developing composite limit resistance curves. Design charts (i.e. prepared composite limit resistance curves for select soil parameters and pile sections) are provided in Appendix D for the convenient design of pile size, spacing, and reinforcement.

Table 24. Properties of SDGM sections

		M_u (kN-m)		EI (kN-m^2)	
b (mm)	**Reinforcement**	**Unfactored**	**Factored**	**Uncracked**	**Cracked**
102	(1) No. 19	1.634	1.362	129	28
127	(1) No. 19	3.015	2.512	316	60
127	(1) No. 25	3.238	2.699	316	77
127	102-mm Pipe*	13.375	11.146	316	n/a
178	(1) No. 19	7.189	5.991	1210	161
178	(1) No. 25	8.144	6.787	1210	224
178	(1) No. 32	8.688	7.240	1210	276
178	(4) No. 19	15.598	12.998	1380	488
178	152-mm Pipe*	31.554	26.295	1380	n/a
203	(1) No. 25	11.667	9.723	2070	316
203	(1) No. 32	12.536	10.446	2070	402
203	(4) No. 25	31.840	26.533	2580	1090

Notes:
Concrete strengths are 27.6 MPa
Steel yield strengths are 413.7 MPa
Factored moment capacity uses FS = 1.2
* Pipe thicknesses are 3 mm

Step 4 – Calculate the Required Number of Rows and Piles

Step 4.a

The sliding depths along the slope width are variable, and the use of a single F_R' value for all pile rows oversimplifies the calculation of the required number of rows. Rather, the accurate estimation of the total stabilizing force, ΔF_R, requires the determination of unique stabilizing forces, F_R', obtained from the composite limit resistance curve for sliding depths at each pile row location. The process of identifying limit resistances at each pile row location facilitates the effective and reliable design of pile stabilization. The pile row locations are generally established to maximize F_R'. When the limit soil resistance controls the design, for example, pile rows may be installed on the slope at a location where the sliding depth is largest, ensuring that the limit member resistance does not control the reinforcement stability and stabilization design.

Calculate the required number of pile rows with Equation (41), based on the required stabilizing force of the reinforcement, ΔF_R, and the limit resistances for individual rows of piles, F_R'.

$$n = \frac{\Delta F_R}{F_R'} \tag{41}$$

where n = number of required pile rows

The number of pile rows is conservatively rounded (e.g. n = 2.4 → 3 pile rows required), and a new factor of safety is later calculated based on the achieved ΔF_R.

Step 4.b

Calculate the required number of piles with the number of required pile rows, the pile spacing, and the length of slope needing stabilization (see Equation (42)).

$$\text{Number of Piles} = \frac{\text{Slope length}}{D_l} \cdot n \tag{42}$$

Step 5 – Perform Global and Local Stability Analyses for Reinforced Slope

Step 5.a

Calculate the factor of safety for the reinforced slope with Equation (43), based on the achieved ΔF_R. The computed factor of safety is likely greater than the target factor of safety, because the design methodology conservatively rounds the required number of pile rows.

$$FS = \frac{\Sigma F_R + \Delta F_R}{\Sigma F_D} \tag{43}$$

Step 5.b

Ensure the local stability of the reinforced slope. Identify potential failure surfaces that exist above or below stabilizing piles (see Figure 142), and verify that the factors of safety corresponding to the failure surfaces exceed the stability requirements.

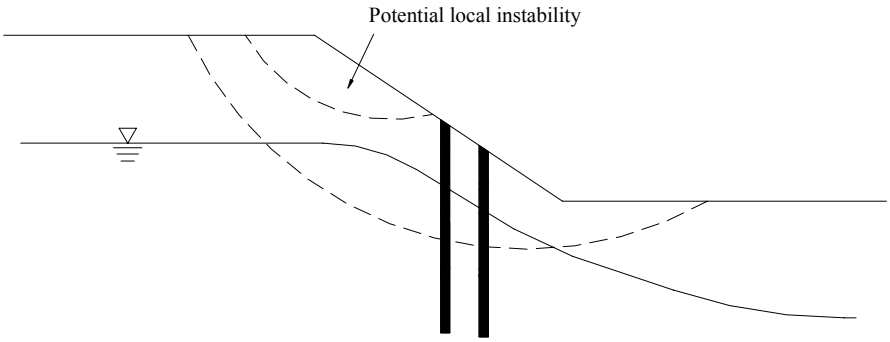

Figure 142. Local instability of reinforced slope

The recommended layout of soil displacement grouted micropiles employs equilateral spacing, such that the stabilization system achieves maximum benefit from soil arching. Equilateral spacing of SDGM reinforcement is illustrated in Figure 143.

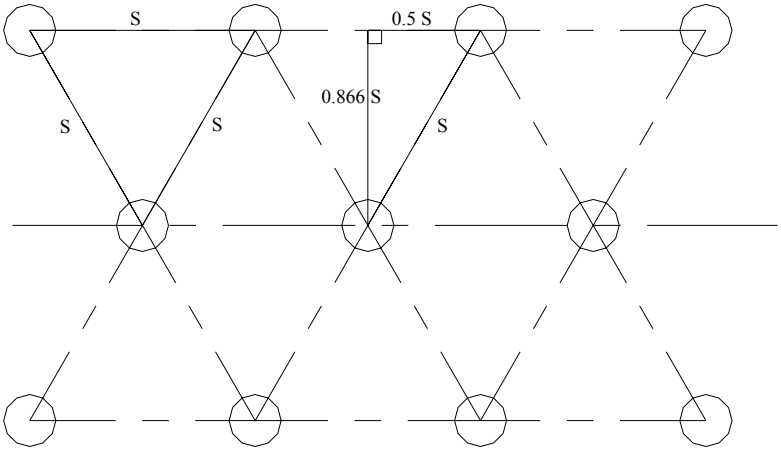

Figure 143. Equilateral spacing of SDGM reinforcement

Step 6 – Perform Material Cost Analysis

Evaluate the cost effectiveness of the design option by performing a material cost analysis. Establish and apply unit prices to the calculated material quantities for the number of piles required to stabilize the unstable slope. A general equation for the material cost of pile stabilization is provided in Equation (44).

$$\text{Cost} = \text{Unit Price} \cdot \frac{\text{Quantity}}{\text{Piles}} \cdot \text{Piles} \tag{44}$$

Sample Design

The sample design demonstrates the stabilization potential of small-diameter pile elements and the effectiveness of the proposed stabilization approach. The demonstration also compares the remediation method with conventional remediation practices of local transportation agencies to show that pile stabilization is recurrently more appropriate than excavation (i.e. benching and/or slope flattening) and construction of drainage structures.

Slope Description

Low shear strength parameters associated with weathered shale result in slope instability throughout Iowa. Remediation of the slope failures is uniquely challenging, because conventional remediation practices may fail to address the cause of instability. Conventional remediation practices target drainage as a general cause of instability, as opposed to low shear strength of slope soil. Slope reinforcement and, more specifically, pile stabilization is likely more effective in preventing continued slope movements in weak soil.

The emblematic slope used to demonstrate the proposed design methodology stands with a maximum height of 6 meters and slope of 3.5:1 (21-m width). The slope geometry is typical of slopes along transportation corridors in Iowa. The slope consists of weathered shale, and residual shear strength parameters for the material were obtained by conducting ring shear tests on weathered shale samples from a project site in Ottumwa, Iowa. The groundwater table was adjusted to provide a factor of safety equal to unity. The location of the groundwater table is sufficiently low to support pile stabilization as the appropriate remediation alternative over the construction of drainage structures.

Step 1 – Global Stability Analysis for Unreinforced Slope

Global stability analyses were performed with SLOPE/W, a slope stability software program, to evaluate the stability of the unreinforced slope. The anticipated failure surface is provided in Figure 144. The forces resisting and driving slope movement, along with corresponding factors of safety, for several limit equilibrium methods are provided in Table 25.

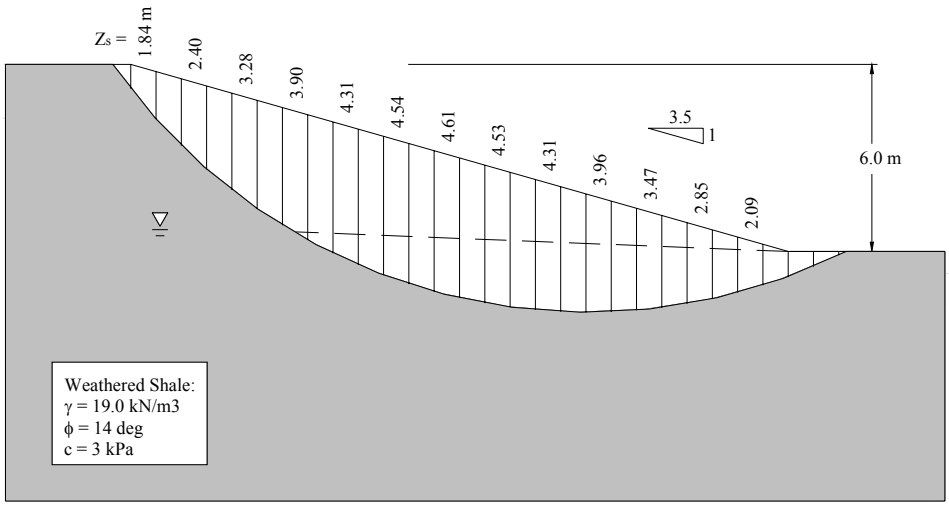

Figure 144. Potential failure surface

Table 25. Stability parameters for unreinforced slope

(kN/m)	Ordinary Method	Bishop's Simplified	Janbu's Method
ΣF_R*	6755	7348	340.2
ΣF_D*	6549	6549	328.6
FS	1.03	1.12	1.03

Notes:
* Moments for Ordinary and Bishop's methods

Step 2 – Calculation of Required Stabilizing Force

The total required stabilizing force, ΔF_R, is determined with the forces of Table 25 and a factor of safety equal to 1.3.

$$\Delta F_R = FS \cdot \Sigma F_D - \Sigma F_R$$

$$\Delta F_R = 1.3 \cdot 328.6\,\text{kN/m} - 340.17\,\text{kN/m}$$

$$\Delta F_R = 87.1\,\text{kN/m}$$

Step 3 – Development of Composite Limit Resistance Curves

The composite limit resistance curves indicate that member resistance controls the design, such that a second design option employs steel pipe reinforcement. The two stabilization design options of different steel reinforcement are developed herein. The composite limit resistance curves are provided in Figures 145 and 146.

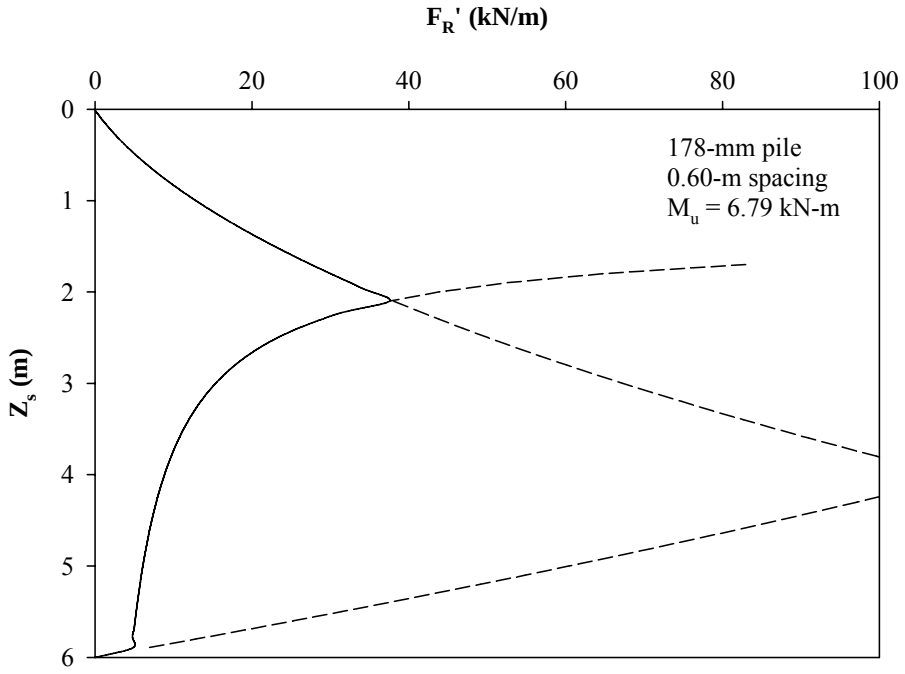

Figure 145. Limit resistance curves for 178-mm pile with centered No. 25

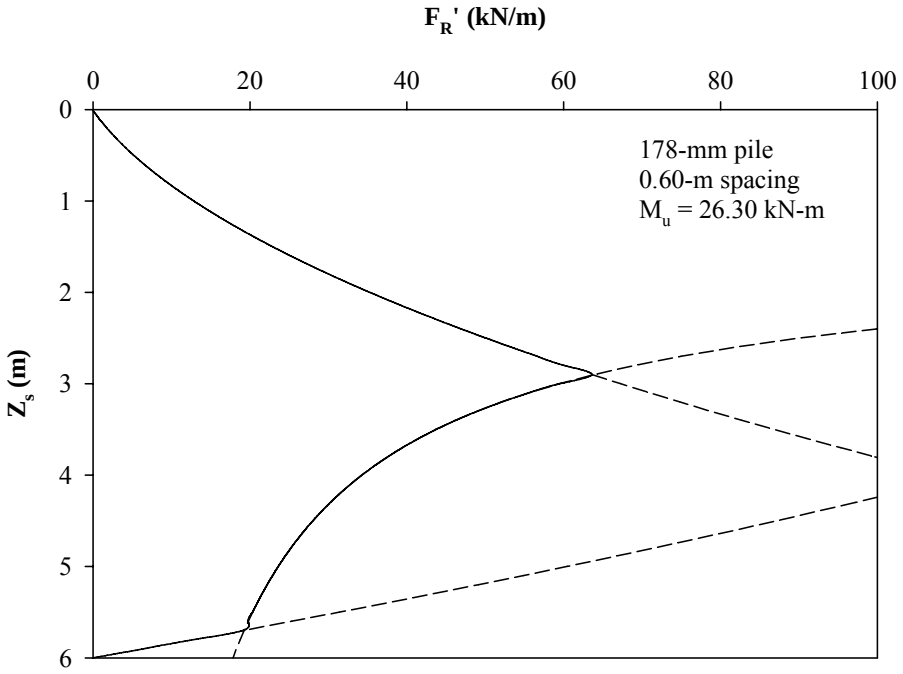

Figure 146. Limit resistance curves for 178-mm pile with 152-mm steel pipe

Step 4 – Calculate the Required Number of Rows and Piles

Step 4.a

Table 26. Stabilizing forces along sliding depths of slope profile

Z_S (m)	178-mm Pile (1) No. 25	178-mm Pile 152-mm Pipe
2.09	37.57	—
2.85	17.84	60.10
3.47	11.30	43.74
3.96	8.85	—
4.31	7.81	—
ΔF_R	83.37	103.84
n	5	2

Notes:
Units of kN/m
Z_S values from Figure 227
n = number of required rows
ΔF_R = sum of stabilizing forces for each row

Step 4.b

The required number of piles was calculated for a 91-m (300-ft) slope length.

$$\text{Number of Piles} = \frac{\text{Slope length}}{D_1} \cdot n$$

$$\text{Number of Piles} = \frac{91\,\text{m}}{0.60\,\text{m}} \cdot 5 = 758 \text{ piles for centered No. 25 reinforcement}$$

$$\text{Number of Piles} = \frac{91\,\text{m}}{0.60\,\text{m}} \cdot 2 = 303 \text{ piles for 152 - mm pipe reinforcement}$$

Step 5 – Global and Local Stability Analyses for Reinforced Slope

Step 5.a

$$FS = \frac{\Sigma F_R + \Delta F_R}{\Sigma F_D}$$

$$FS = \frac{340.2 + 83.4}{328.6} = 1.29 \text{ for centered No. 25 reinforcement}$$

$$FS = \frac{340.2 + 103.8}{328.6} = 1.35 \text{ for 152 - mm pipe reinforcement}$$

Step 5.b

Local stability is ensured by performing a stability analysis in which potential failure surfaces are limited to a particular location. The rows of piles are simply modeled by high strength soil, such that a failure surface generated by slope stability software will not pass through the piles. The likely failure surface for local instability, shown in Figure 147, corresponds to a factor of safety of 1.35.

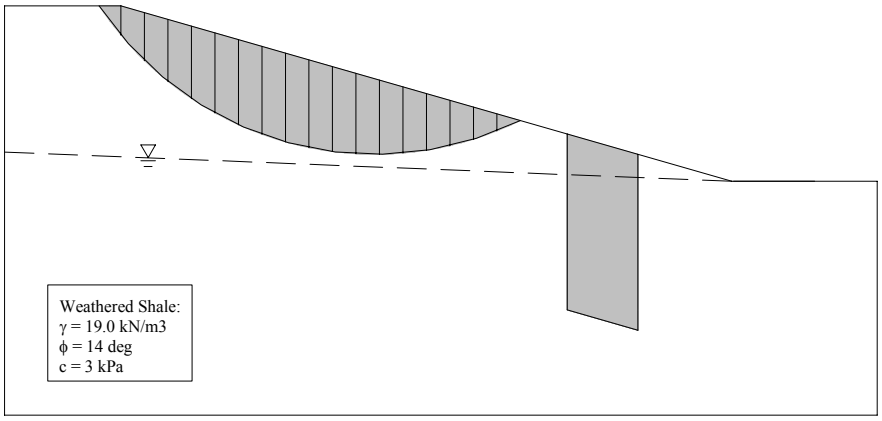

Figure 147. Failure surface for local instability

Step 6 – Material Cost Analysis

The unit costs and total material costs are developed in Table 27.

Table 27. Material cost analysis

	178-mm Pile	178-mm Pile

	(1) No. 25	152-mm Pipe
No. Piles (per 91-m slope)	758	303
Concrete volume (m^3)	113.7	45.5
Concrete cost ($)	8,900	3,500
Steel cost ($)	19,000	45,500
Material cost (per 91-m slope)	27,900	49,000
Material cost (per m^2)	14.00	24.60
Notes:		
Unit costs: \$78 / m^3 concrete, \$25 / No. 25, \$150 / 152-mm pipe		

SUMMARY AND CONCLUSIONS

Introduction

It is apparent, from examples in literature and from pile load tests performed at the Iowa State University Spangler Geotechnical Experimentation Site, that small-diameter pile elements provide effective passive resistance to lateral soil movement. Traditional procedures for designing pile stabilization involve the design of large-diameter, heavily-reinforced pile sections, such that the bending moment induced by the application of the ultimate soil pressure does not exceed the moment capacity of the proposed section. An alternative stabilization approach, presented in the thesis, employs small-diameter pile elements. The thesis outlines a rational design procedure for slope reinforcement with grouted micropiles and discusses the benefits associated with implementing the unconventional remediation method into slope stabilization practices.

Successes of Research

The program of work accomplished in the research study includes the performance of a comprehensive literature review on the state of knowledge of slope stability and slope stabilization, the preparation and performance of 14 full-scale pile load tests, the analysis of load test results, and the documentation of a design methodology for implementing the technology into current practices of slope stabilization.

The load transfer of piles subject to lateral soil movement associated with unstable slopes has been the focus of international analytical and experimental studies. The results of this research project, however, represent a significant contribution to the ongoing evaluation of pile stabilization. The experimental testing plan, executed in a controlled environment, involved testing full-scale pile elements subject to uniform lateral translation of soil and incorporated three critical parameters of pile stabilization (e.g. soil type, pile size, pile spacing).

Conclusions

The main conclusions developed from the research study are summarized as follows:

Review of literature

- Prediction of lateral soil movement profiles is difficult, and alternative design and analysis methods of pile stabilization incorporate a limit state methodology.
- Ultimate soil pressures are most easily and most reliably obtained from p-y relationships, but p-y curves necessitate prohibitively-expensive pile load tests.
- Other researchers have established approximations for ultimate soil pressure in terms of standard soil properties and stress conditions.
- Recent investigations have established the feasibility of stabilizing relatively shallow slope failures with slender pile elements.

Laboratory Investigation

- Load-displacement (p-y) curves are empirically developed from unconfined and consolidated-undrained (CU) triaxial compression test results.

Field Investigation

- Slender pile elements are effectively installed with simple construction equipment (i.e. small drill rig and concrete mixer) and minimal labor.
- Displacement and strain gauges indicate the load-displacement behavior of reinforced soil and also the loads induced on piles due to lateral soil movement, respectively.
- The 115-mm-diameter piles offered considerable resistance to lateral soil movement. The 178-mm-diameter piles offered additional resistance, beyond that achieved with smaller pile elements.
- Installation and loading of multiple piles offered some evidence of soil arching and increased capacity due to group effects.
- Gap formation occurred at the front of piles, and the relative displacement of shear boxes and pile heads indicated behavioral stages of pile loading.
- Section moment capacities were mobilized in most pile elements, and the failure of the pile elements was supported by observation of cracked piles upon exhumation.

Analytical Investigation

- The pile-soil reaction depends on the relative displacement between the soil and pile elements and also the specified p-y relationship.
- The finite difference lateral response analysis method (Reese and Wang 2000) for laterally loaded piles is suitable for evaluating the response of grouted micropiles subject to lateral soil movement, as evidenced by correlations of pile head deflection and maximum moment.
- Ultimate soil pressures were not mobilized during the performance of pile load tests. The pressures, however, are presumably proportional to the loads induced on piles subject to lateral translation of soil and therefore vary approximately linearly with depth.
- Structural performance of pile elements under the loading conditions of slope reinforcement is effectively predicted with LPILE software.

Design and Feasibility Investigation

- Design of pile stabilization with grouted micropiles is performed with relative ease.
- The proposed design methodology is robust, in that the method is readily adaptable to achieve reinforcement requirements for a wide range of slope failure conditions. Piles are potentially designed to be strong or weak, depending on the project-specific requirements and the preferences of the design engineer.
- Designs of pile stabilization with grouted micropiles are cost-effective with regards to material costs. The pile elements are installed with traditional engineering materials (i.e. concrete, steel), and the installation does not require specialized equipment.

RECOMMENDATIONS

Immediate Impact

The research study established the feasibility of slope stabilization with small-diameter pile elements, and the research group recommends that pilot studies of slope reinforcement with grouted micropiles be performed to more fully understand and verify the load transfer mechanisms of the stabilization system.

Long-Term Impact

Current practices of slope remediation often fail to address the cause of slope instability. Construction of drainage structures, for example, is ineffective in stabilizing a slope with a low groundwater table and low shear strength parameter values. As a result, select slope failures are repaired on multiple occasions. As evidence of the efficiency and cost-effectiveness of stabilization of nuisance slope failures with grouted micropiles is accumulated, local transportation agencies will more readily employ the remediation alternative. Employment of the technology is important, because the technology is often more appropriate for stabilizing shallow slope failures.

Future Investigation Needs

The recommendations for future research include the monitoring of pilot studies of slope reinforcement with grouted micropiles, supplementary experimental studies, and advanced numerical studies, as follows:

Slope Stabilization and Monitoring Studies

- Develop site-specific stabilization designs based in-situ soil tests (e.g. borehole shear test, Ko stepped blade test) and pile load tests.
- Monitor slope movement and load transfer of the stabilization system with inclinometers, piezometers, daily rainfall records, strain measurements, and survey markers.

Experimental Studies

- Directly measure load-displacement (p-y) relationships of soil, and correlate p-y curves with standard soil properties. Develop ultimate soil pressure (pu) envelopes with respect to overburden and/or confining stress for given soil and pile properties.
- Perform pile load tests on battered and truncated piles to investigate the influence of orientation on the stabilization potential of slender pile elements. This experimental study is the next most important task for improving remediation with grouted micropiles.

Numerical Studies

- Perform 3-D finite element analyses of experimental testing of this research study. The analyses serve as calibration for constitutive models of engineering materials and boundary conditions of slope reinforcement.
- Perform 3-D finite element analyses of slope reinforcement to investigate the complicating issues of slope stabilization, as follows:
    - Numerical investigations (3-D FEA) indicate the influence of interactions between adjacent piles, namely soil arching.
    - The imposition of displacement compatibility between piles and adjacent soil results in stress concentrations of which current analytical models fail to consider.

REFERENCES

Abramson, L. W., Lee, T. S., Sharma, S. and Boyce, G. M. 2002. *Slope Stability and Stabilization Methods*. 2nd ed. New York: John Wiley & Sons, Inc.

Anderson, W. I. 1998. *Iowa's Geological Past: Three Billion Years of Change*. Iowa City: University of Iowa Press.

ASTM C128. 2002. Specific gravity and absorption of fine aggregate. American Standard Testing Methods.

ASTM D698, Method A. 2000. Standard test method for moisture-density relations of soils and soil-aggregate mixtures. American Standard Testing Methods.

ASTM D2487. 2000. Standard test method for classification of soils for engineering purposes. American Standard Testing Methods.

ASTM D4318. 2000. Standard test method for liquid limit, plastic limit, and plasticity index of soils. American Standard Testing Methods.

ASTM D6951, 2003. Standard test method for use of the dynamic cone penetrometer in shallow pavement applications. American Standard Testing Methods.

Barrett, R. K., Ruckman, A. C., Myles, B. and Steward, J. 2002. Launched soil nails stabilize embankments. *http://www.soilnaillauncher.com* (accessed 12 May 2004).

Benedict, C., Haider, T. and Byle, M. 2001. Compaction grout columns for track support. *Foundations and Ground Improvement* 113:74-88.

Bransby, M. F. and Springman, S. 1999. Selection of load-transfer function for passive lateral loading of pile groups. *Computational Geotechnics* 24.3: 155-184.

Broms, B. B. 1964a. Lateral resistance of piles in cohesionless soils. *Journal of the Soil Mechanics and Foundation Division* 90.SM3: 123-156.

Broms, B. B. 1964b. Lateral resistance of piles in cohesive soils. *Journal of the Soil Mechanics and Foundation Division* 90.SM2: 27-63.

Coduto, D. P. 2001. *Geotechnical Engineering: Principles and Practices*, 2nd ed. New York: Pearson Education,

COM624 1993. Laterally loaded pile analysis program for the microcomputer. *FHWA-SA-91-048*. Computer program documentation. S. T. Wang and L. C. Reese.

Crozier, M. J. 1986. Landslides - causes, consequences and environment. London: Croom Helm. 252.

CTRE. 2003. Flowable mortar helps prevent settling of bridge approaches. *Technology News* June.

Das, B. M. 1999. *Principles of Foundation Engineering*, 4th ed. Boston: PWS Publishing Co

Davidson, D. T. 1960. Geologic and engineering properties of pleistocene materials in Iowa. *Iowa Highway Research Board Bulletin* 20.

Davies, J. P., Loveridge, F. A., Patterson, D. and Carder, D. 2003. Stabilization of a landslide on the M25 highway London's main artery. *http://www.hatch.ca/Infrastructure/* (accessed 18 July 2004).

Elias, V. and Juran, I. 1991. Soil nailing for stabilization of highway slopes and excavations. *Report FHWA-RD-89-198*.

Elias, V., Christopher, B. R. and Berg, R. R. 2001. Mechanically stabilized earth walls and reinforced soil slopes design and construction guidelines. *Report FHWA-NHI-00-043*.

FLAC 2004. *FLAC/Slope User's Guide*, 2nd ed.. Minneapolis: Itasca Consulting Group Inc.

Forrester, K. 2001. *Subsurface Drainage for Slope Stabilization*. New York: ASCE Press.

Fox, N. S. and Cowell, M. J. 1998. *Geopier Foundation and Soil Reinforcement Manual*.

Scottsdale: Geopier Foundation Company Inc..
Fukuoka, M. 1977. The effects of horizontal loads on piles due to landslides. *Proceedings, 9th International Conference on Soil Mechanics and Foundation Engineering*. Tokyo. 27-42.
Handy, R. L. and White, D. J. (unpublished). Stress zones near displacement piers: radial cracking and wedging.
Hansen, B. 1961. The ultimate resistance of rigid piles against transversal forces. *Bulletin 12*. Copenhagen: Danish Geotechnical Institute,.
Holtz, R. D., Christopher, B. R., and Berg, R. R. 1997. *Geosynthetic Engineering*. Richmond, VA: BiTech Publishers Ltd.
Hong, L. 2003. Laterally loaded intermediate cast-in-drilled-hole (CIDH) concrete piers: evaluation of scale and base shear effects. Master's thesis submitted to the Department of Civil, Construction and Environmental Engineering. Ames, IA: Iowa State University
Ito, T. and Matsui, T. 1975. Methods to estimate lateral force acting on stabilizing piles. *Soils and Foundations* 15.4: 43-59.
Ito, T., Matsui, T. and Hong, P. W. 1981. Design method for stabilizing piles against landslide – one row of piles. *Soils and Foundations* 21.1: 21-37.
Loehr, J. E., Bowders, J. J. and Salim, H. 2000. Slope stabilization using recycled plastic pins-constructability. *Final Report Missouri DOT RDT 00-007*.
Loehr, J. E. and Bowders, J. J. 2003. Slope stabilization using recycled plastic pins-assessment in varied site conditions. *Final Report Missouri DOT RDT 03-016*.
Lohnes, R. A., Kjartanson, B. H., and Barnes, A. 2001. Regional approach to landslide interpretation and repair. *Final Report Iowa DOT Project TR-430*.
Mings, C.L. 1987. Ko stepped blade tests in alluvial clay. Master's thesis submitted to the Department of Civil, Construction and Environmental Engineering. Ames, IA: Iowa State University.
Mitchell, J. K. 1993. *Fundamentals of Soil Behavior.* 2nd ed.. New York: John Wiley & Sons Inc.
Nilson, A. H. 1997. *Design of Concrete Structures*. 12th ed.. New York: McGraw Hill Companies Inc.
Ott, R. L. and Longnecker, M. 2001. *Statistical Methods and Data Analysis* 5th ed. Pacific Grove, CA: Duxbury Press.
Pan, J. L., Goh, A. T. C., Wong, K. S. and Teh, C. I. 2002. Ultimate soil pressures for piles subjected to lateral soil movements. *Journal of Geotechnical and Geoenvironmental Engineering* June: 530-535.
Pearlman, S. L. and Withiam, J. L. 1992. Slope stabilization using in situ earth reinforcements. *Presented at ASCE Conference*, Berkeley.
Polster, D. F. 2003. Soil bioengineering for slope stabilization and site restoration. *Mining and the Environment III* May: 25-28.
Popescu, M. 1994. A suggested method for reporting landslide causes. *Bulletin IAEG* 50: 71-74.
Poulos, H. G. and Davis, E. H. 1980. *Pile Foundation Analysis and Design*. New York: John Wiley & Sons Inc.
Poulos, H. G. 1995. Design of reinforcing piles to increase slope stability. *Canadian Geotechnical Journal* 37:890-897.
Reese, L. C., William, R. C. and Koop, F. D. 1974. Analysis of laterally loaded piles in sand. *Proceedings, 6th Offshore Technology Conference* 2:473-483.

Reese, L. C. and Allen, J. D. 1977. *Drilled shaft design and construction guidelines manual*, *volume II*. U.S. Department of Transportation Offices of Research and Development Implementation Division HDV-22.

Reese, L. C. and Wang, S. T. 2000. *LPILE Plus 4.0 Technical Manual*. Ensoft, Inc.

Robertson, P. K. and Campanella, R. G. 1983. Interpretation of the cone penetrometer test. *Canadian Geotechnical Journal*. 20.4: 718-745.

Robertson, P. K., Campanella, R. G., Brown, P. T., Grof, I. and Hughes, J. M. 1985. Design of axially and laterally loaded piles using in situ tests: a case history. *Canadian Geotechnical Journal* 22.4: 518-527.

Robertson, P. K., Davies, M. P. and Campanella, R. G. 1987. Design of laterally loaded driven piles using the flat dilatometer. *Geotechnical Testing Journal* 149.89: 30-38.

Rogers, C. D. F. and Glendinning, S. 1997. Stabilization of shallow slope failures with lime piles." *Transportation Research Record* 1589:83-91.

Santi, P. M. 2001. Horizontal wick drains as a cost-effective method to stabilize landslides. *Geotechnical News* 17. 2: 44-46.

Schlagbaum, T. 2002. Economic impact of self-consolidating concrete (SCC) in ready mixed concrete. *First North American Conference on the Design and Use of Self-Consolidating Concrete* November:12-13.

Schlosser and Francois 1991. Recommendations Clouterre. *Report U.S. Department of Transportation, NTIS No. PB94-109980*.

Sotir, R. B. and Gray, D. H. 1996. *Biotechnical and Soil Bioengineering Slope Stabilization: A Practical Guide for Erosion Control.* New York: John Wiley & Sons Inc.

Spiker, E. C.and Gori, P. L. 2003. National landslide hazards mitigation strategy – a framework for loss reduction. *U.S. Geological Survey Circular* 1244:4-13.

Viggiani, C. 1981. Ultimate lateral load on piles used to stabilize landslides. *Proceedings, 10th International Conference on Soil Mechanics and Foundation Engineering* 3:555-560. Stockholm.

Walker, B. and Fell, R. 1987. *Soil Slope Instability and Stabilization*. Rotterdam: A.A.Balkema Publishers.

Wong, D. O., FitzPatrick, B. T. and Wissman, K. J. 2004. Stabilization of retaining walls and embankments using rammed aggregate piers. *Geotechnical Engineering in Transportation Projects* 126.2: 1866-1875.

Wu, T. H. 1995. Evaluation of remedial measures for embankment failures. *Report FHWA/OH-95019.*

APPENDIX A: P-Y CURVES FOR ISU SGES

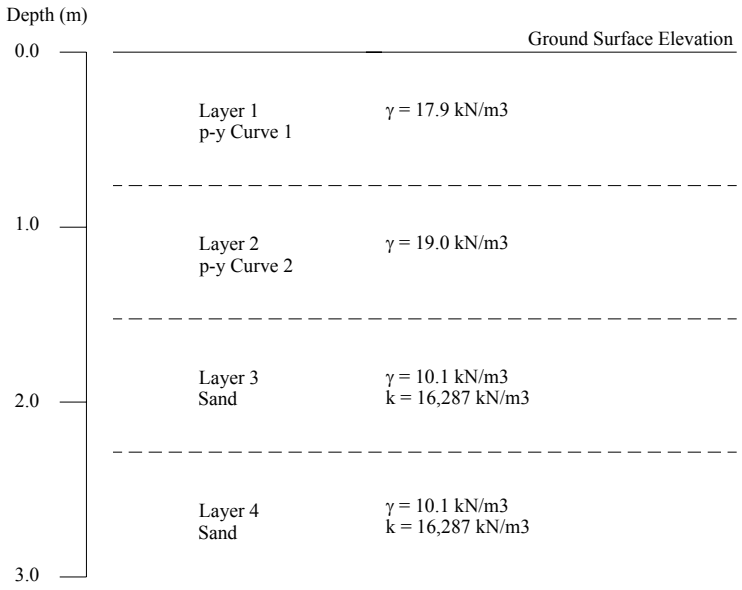

Figure A 1. Iowa State University SGES site soil profile

Table A 1. Iowa State University SGES p-y curves

p-y Curve 1		p-y Curve 2	
y (cm)	**p (kN/m)**	**y (cm)**	**p (kN/m)**
0.0	0.0	0.0	0.0
0.2	35.4	0.3	65.0
0.5	50.6	1.0	125.2
1.0	73.4	2.9	173.7
2.2	96.8	4.7	191.4
3.5	111.2	6.6	201.6
4.7	121.5	8.4	207.9
5.9	128.9	10.3	213.7
7.2	133.5	12.2	217.7
8.4	137.7	14.0	220.8
9.7	140.8	15.9	223.6
10.9	143.1	17.8	225.4
12.2	144.1	19.7	227.1
13.4	145.4	21.5	227.5
14.7	146.4	23.4	227.8
15.3	146.4	25.2	228.4
15.9	146.4	25.9	228.5

APPENDIX B: MOMENT-CURVATURE GRAPHS PER PILE

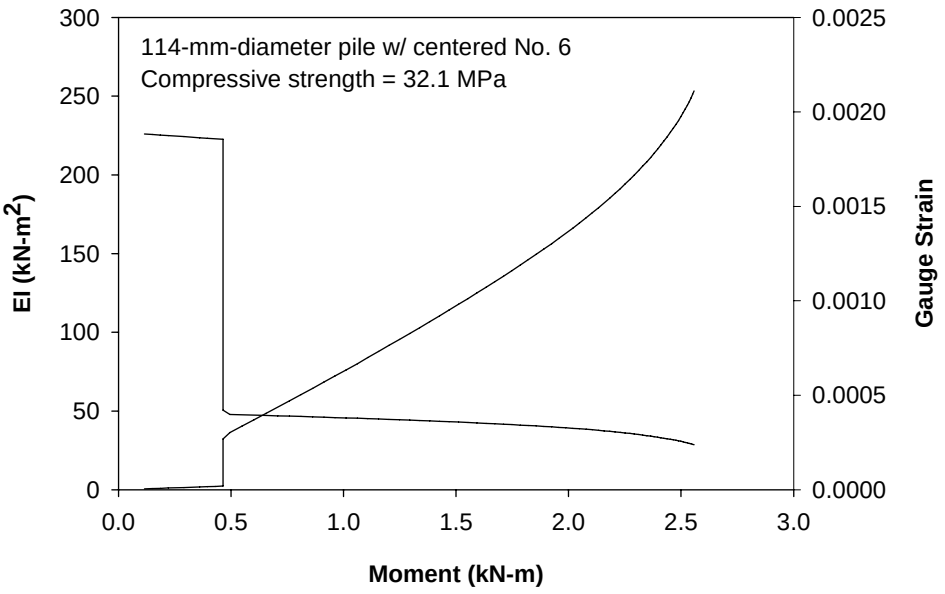

Figure B 1. Flexural stiffness and gauge strain vs. bending moment (Pile 4)

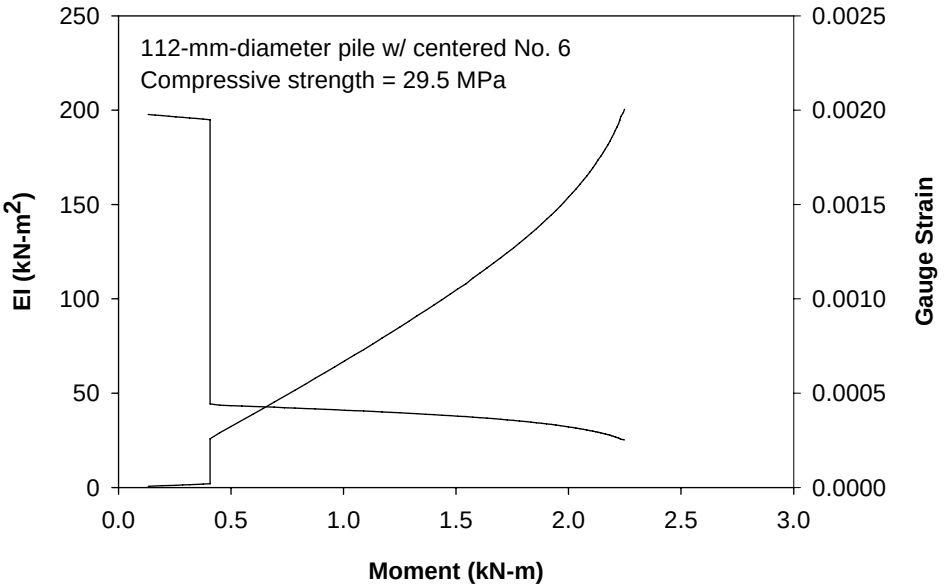

Figure B 2. Flexural stiffness and gauge strain vs. bending moment (Pile 5)

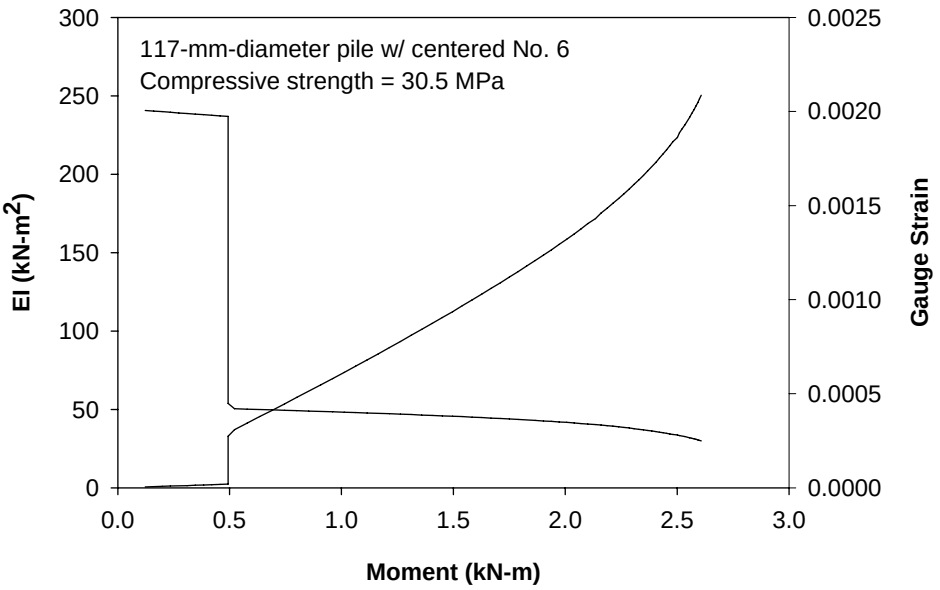

Figure B 3. Flexural stiffness and gauge strain vs. bending moment (Pile 6)

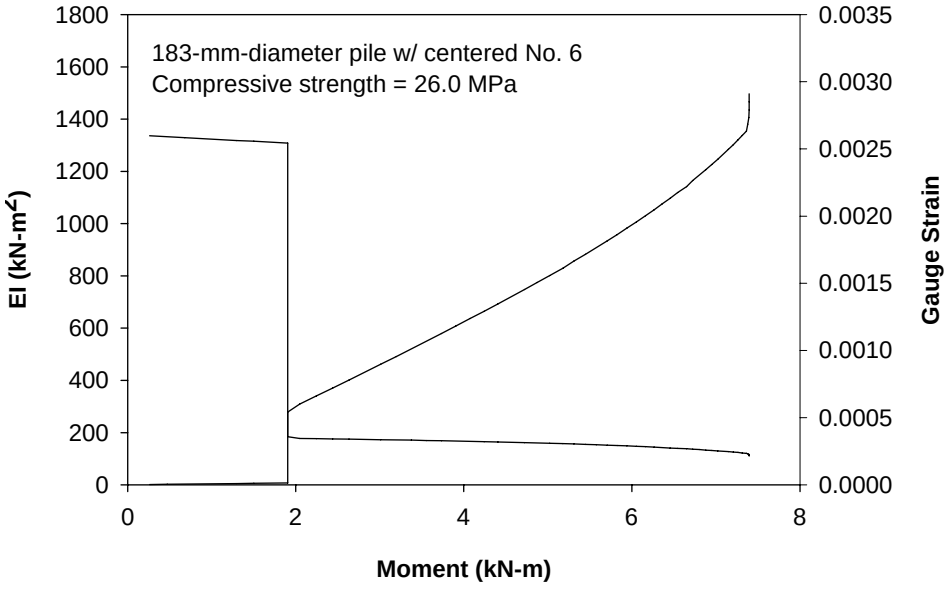

Figure B 4. Flexural stiffness and gauge strain vs. bending moment (Pile 8)

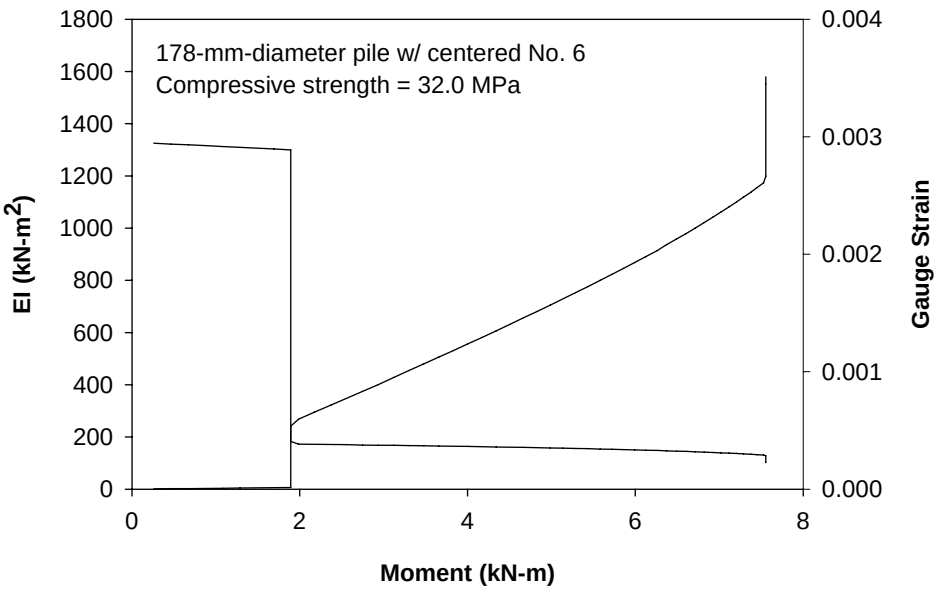

Figure B 5. Flexural stiffness and gauge strain vs. bending moment (Pile 9)

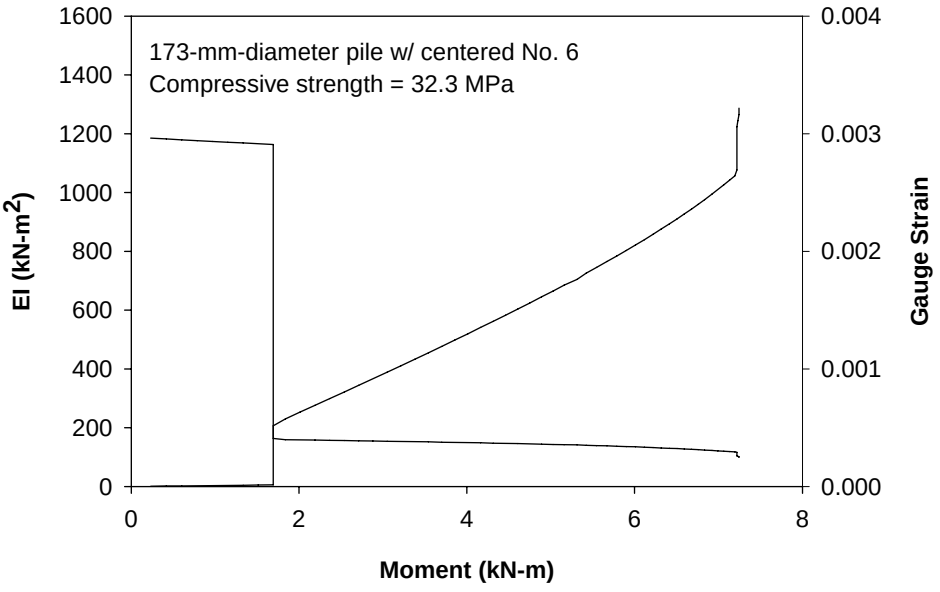

Figure B 6. Flexural stiffness and gauge strain vs. bending moment (Pile 12)

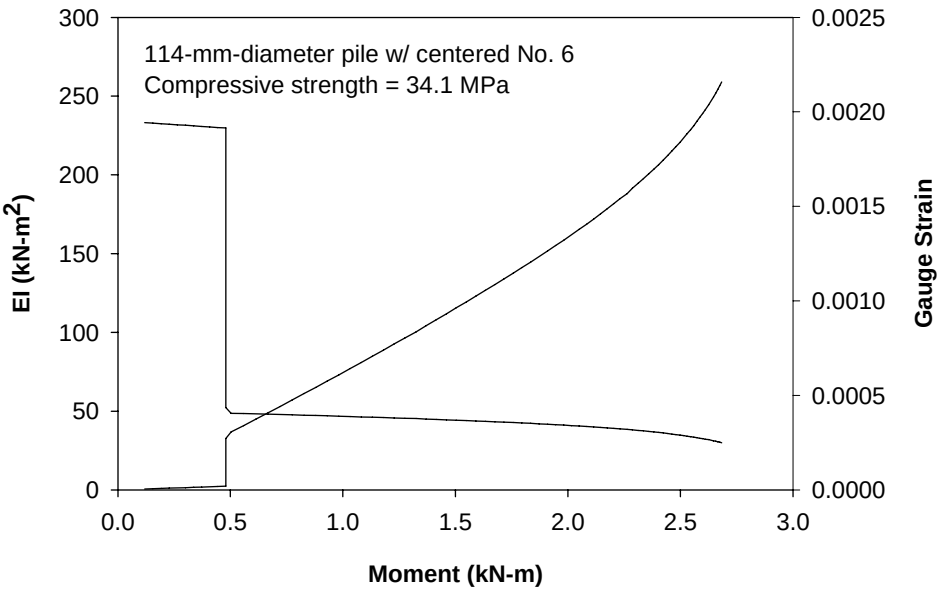

Figure B 7. Flexural stiffness and gauge strain vs. bending moment (Pile 10 A)

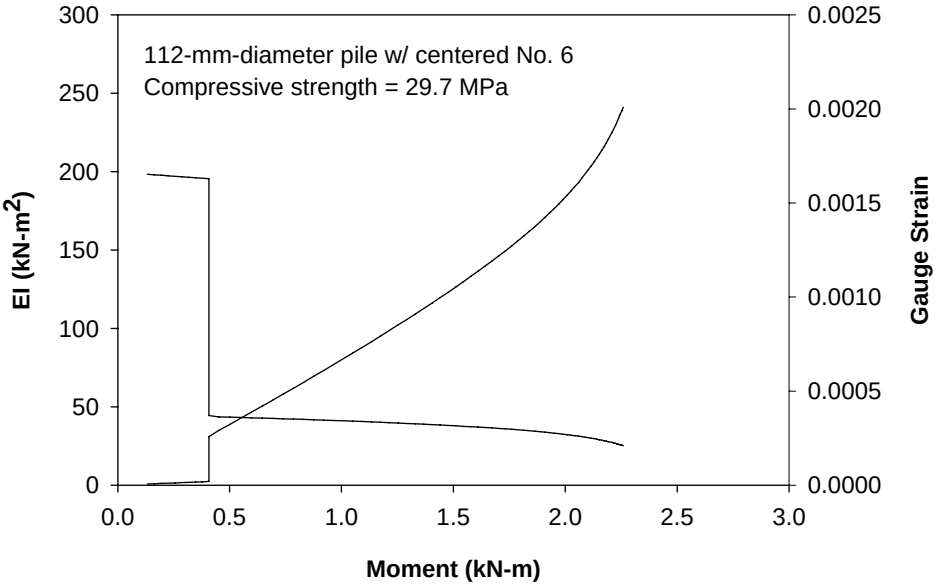

Figure B 8. Flexural stiffness and gauge strain vs. bending moment (Pile 10 B)

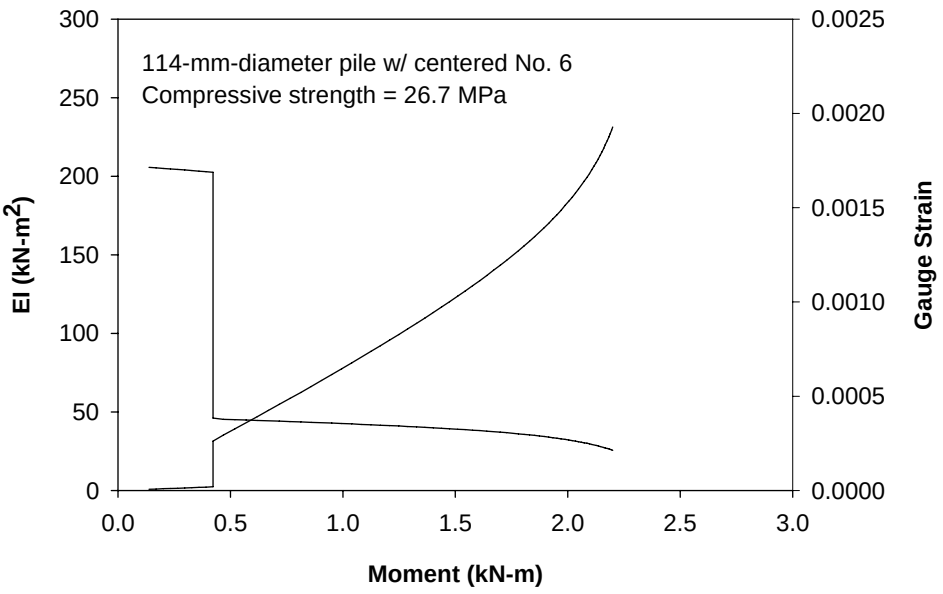

Figure B 9. Flexural stiffness and gauge strain vs. bending moment (Pile 11 A)

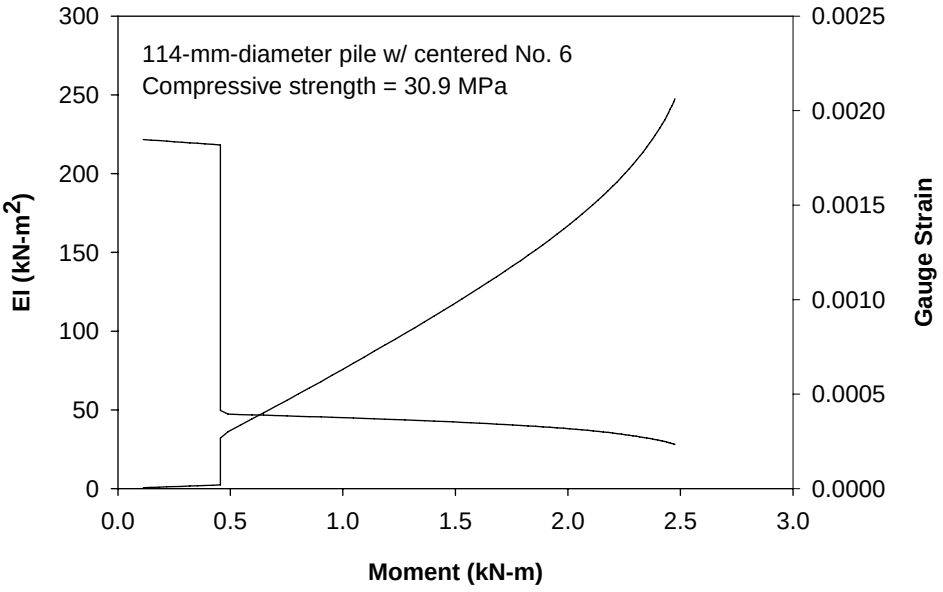

Figure B 10. Flexural stiffness and gauge strain vs. bending moment (Pile 11 B)

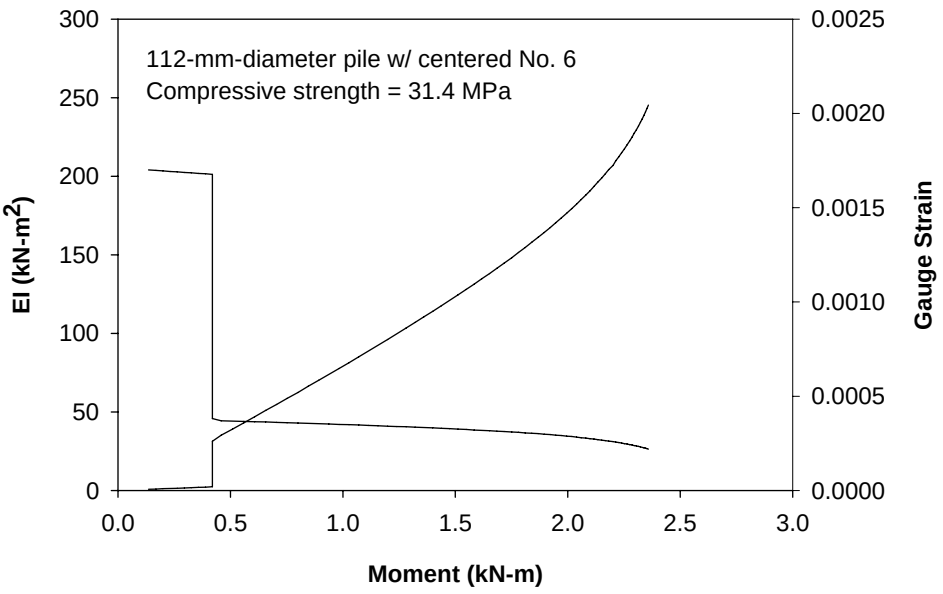

Figure B 11. Flexural stiffness and gauge strain vs. bending moment (Pile 13 A)

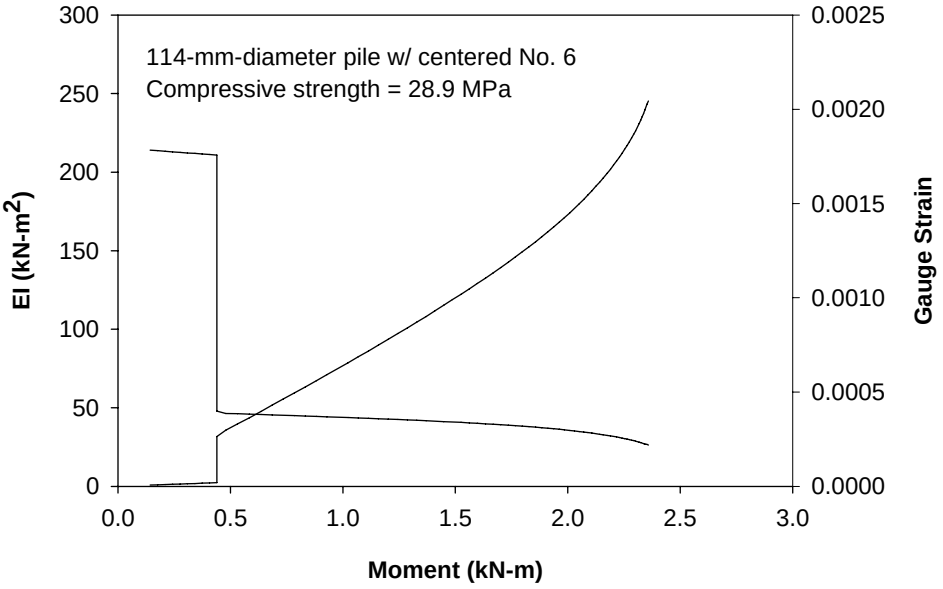

Figure B 12. Flexural stiffness and gauge strain vs. bending moment (Pile 13 B)

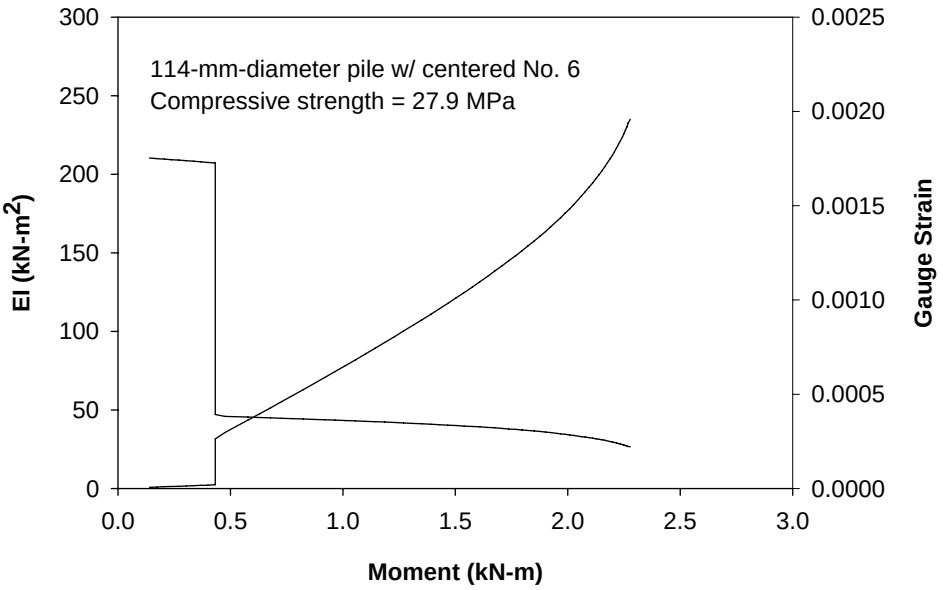

Figure B 13. Flexural stiffness and gauge strain vs. bending moment (Pile 14 A)

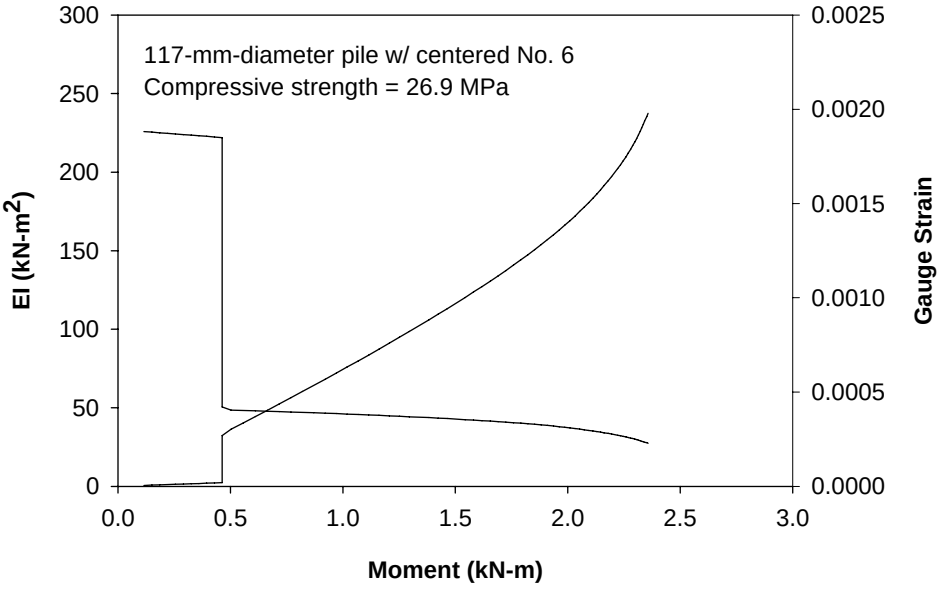

Figure B 14. Flexural stiffness and gauge strain vs. bending moment (Pile 14 B)

APPENDIX C: PILE LOAD TEST DATA

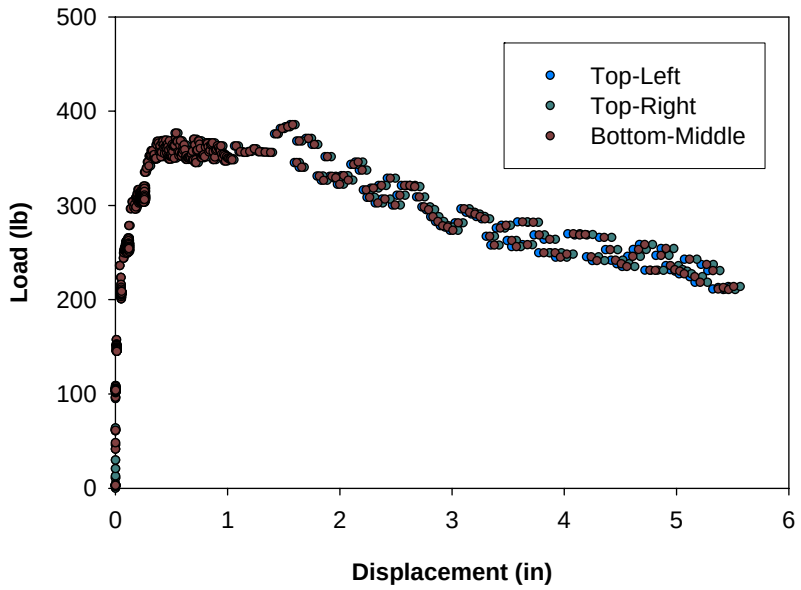

Figure C 1. Load-displacement for unreinforced loess

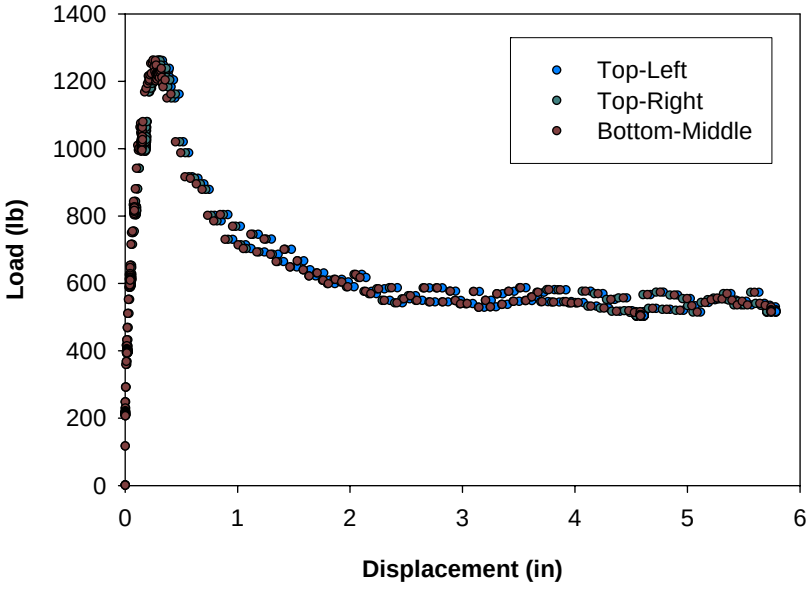

Figure C 2. Load-displacement for unreinforced weathered shale

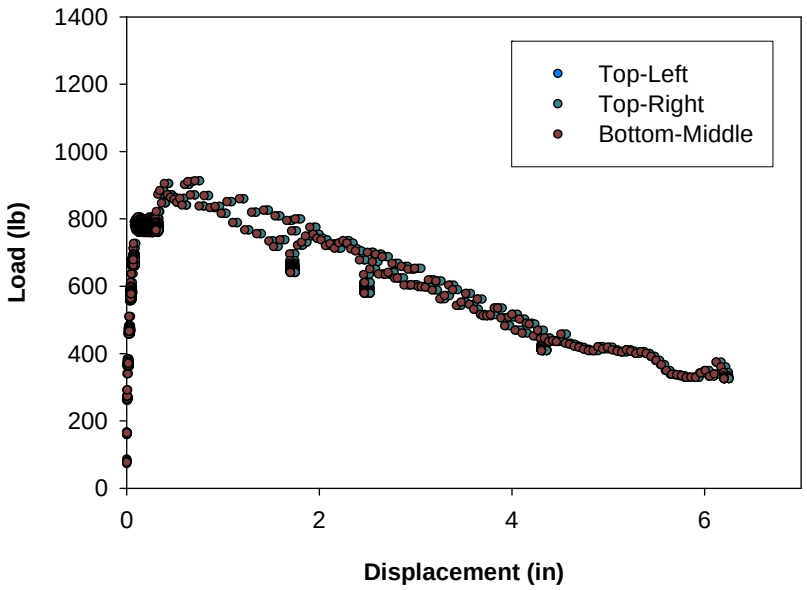

Figure C 3. Load-displacement for unreinforced glacial till

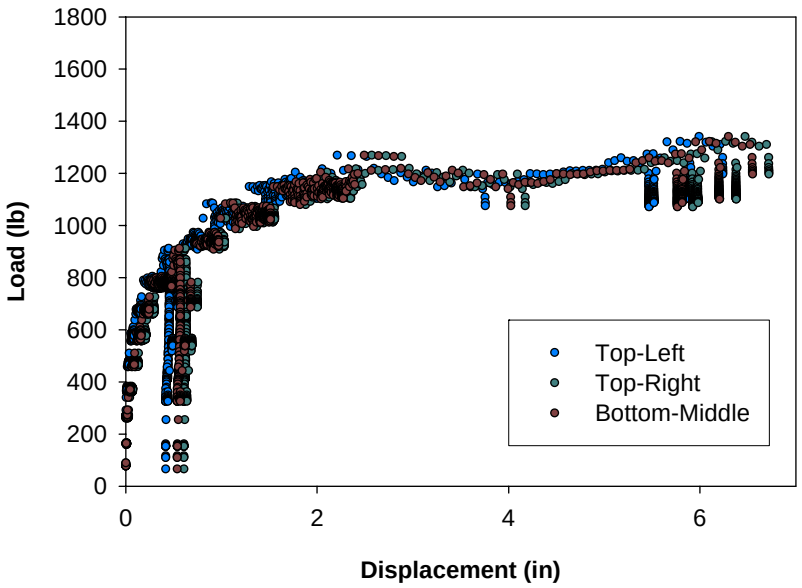

Figure C 4. Load-displacement for loess (Pile 4)

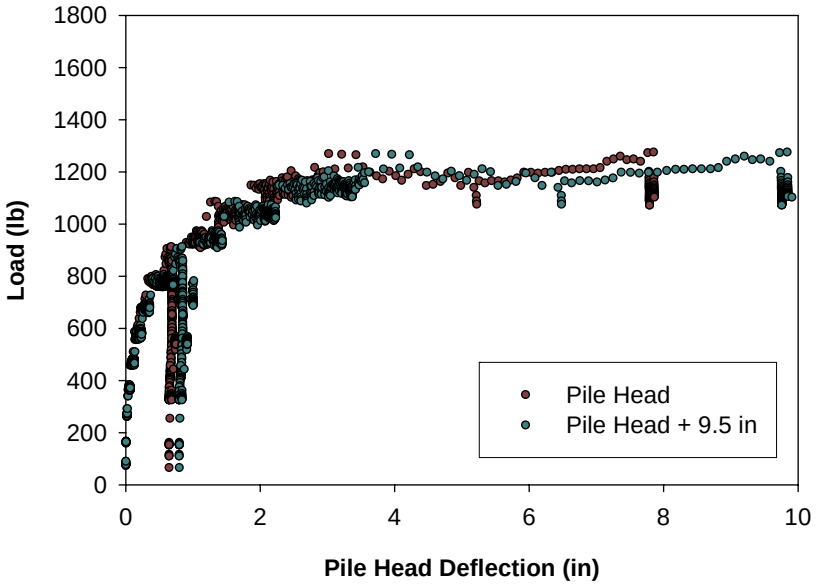

Figure C 5. Pile head deflection for glacial loess (Pile 4)

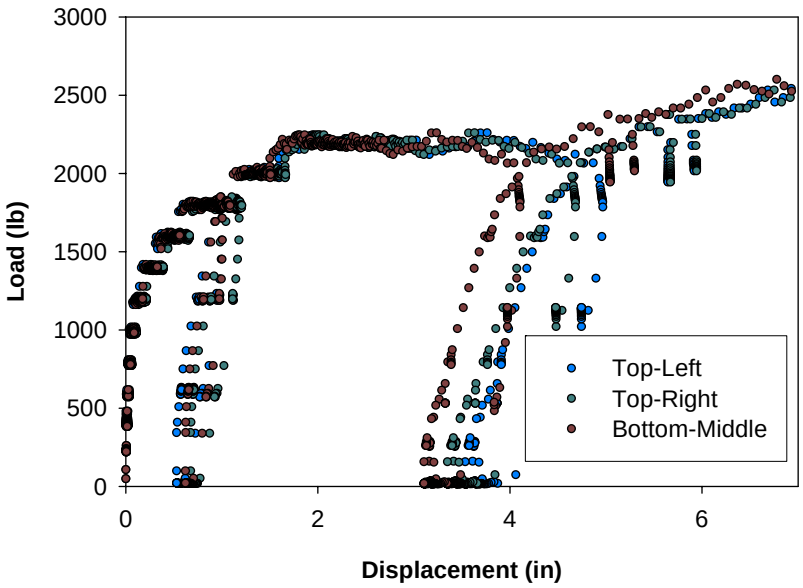

Figure C 6. Load-displacement for glacial till (Pile 5)

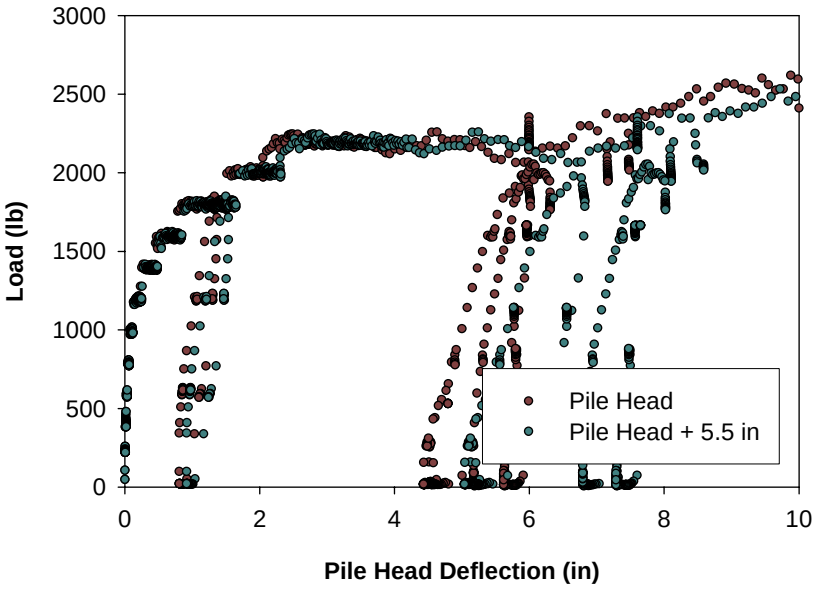

Figure C 7. Pile head deflection for glacial till (Pile 5)

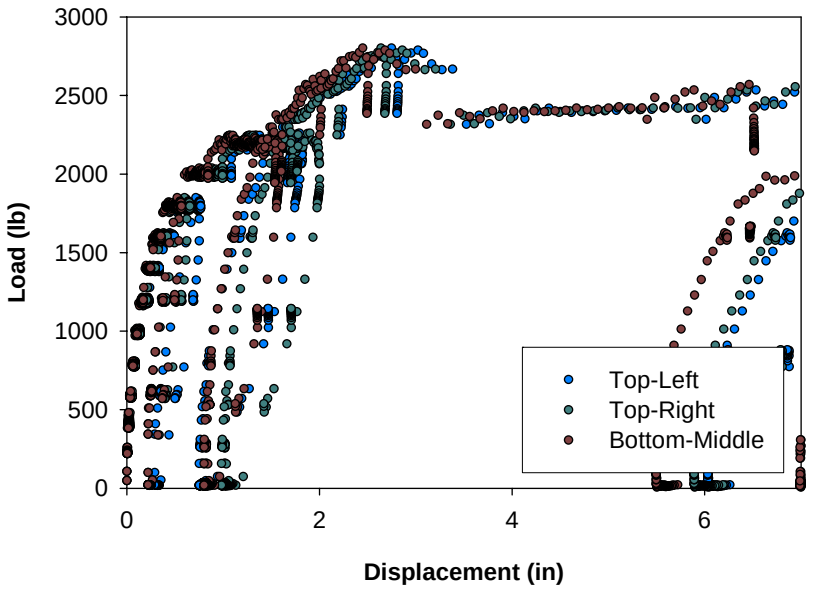

Figure C 8. Load-displacement for weathered shale (Pile 6)

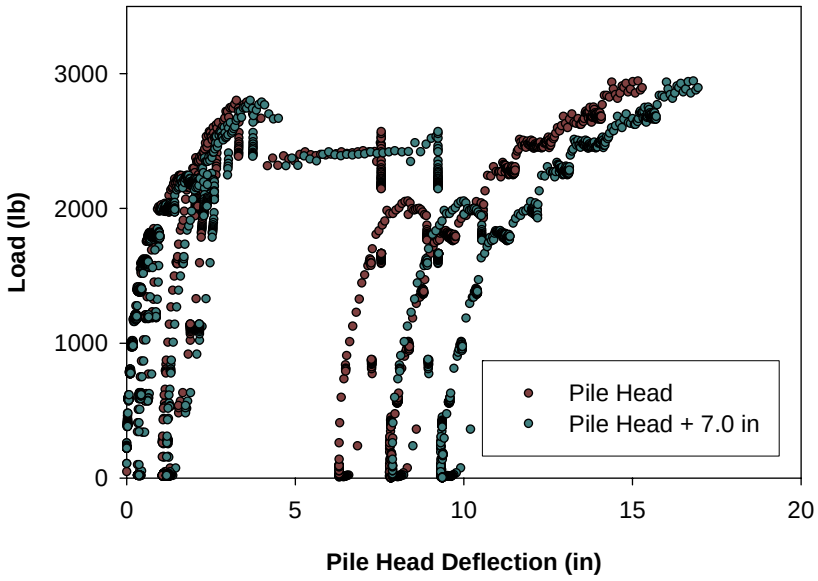

Figure C 9. Pile head deflection for weathered shale (Pile 6)

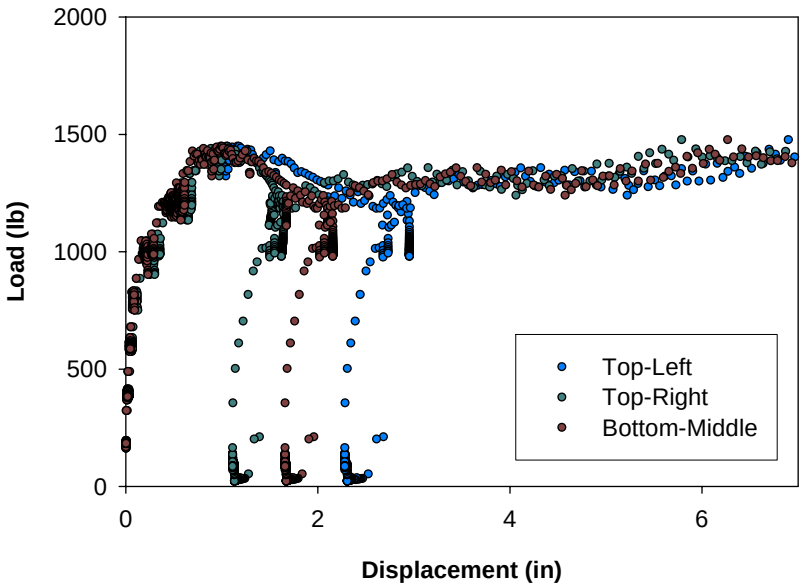

Figure C 10. Load-displacement for weathered shale (Pile 7)

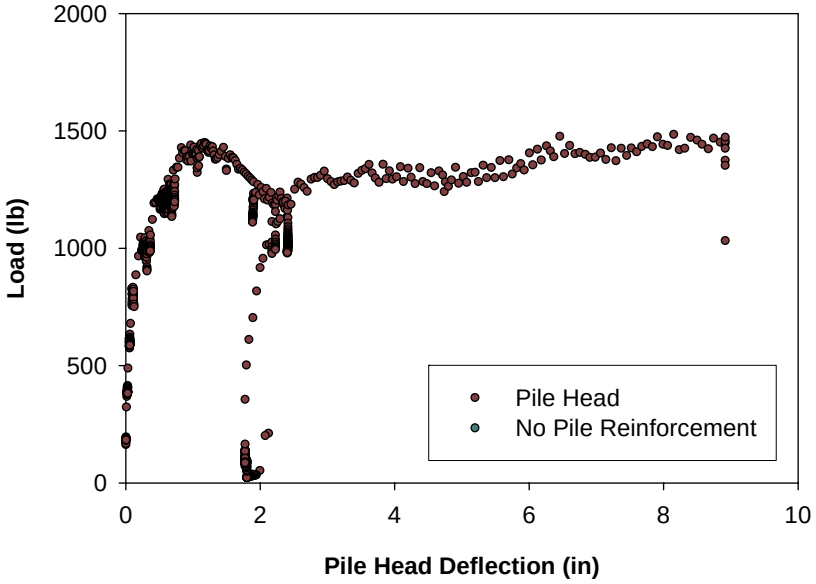

Figure C 11. Pile head deflection for weathered shale (Pile 7)

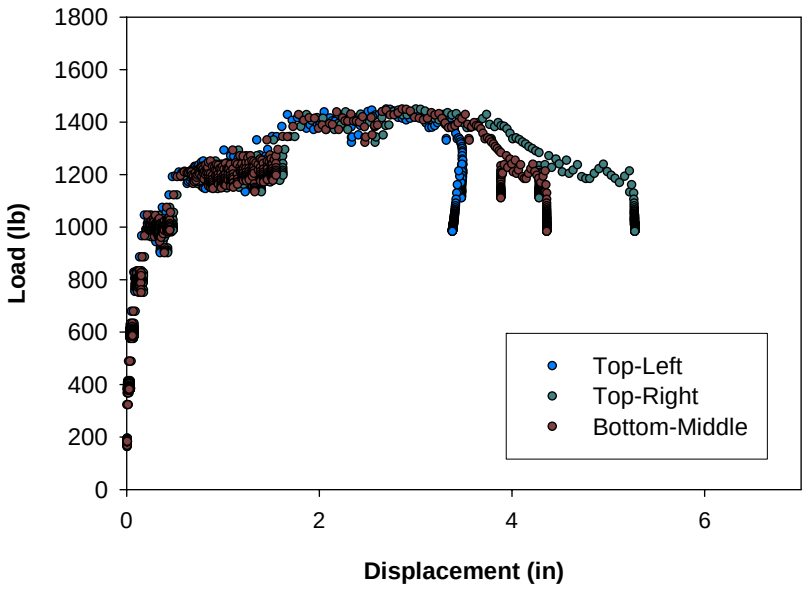

Figure C 12. Load-displacement for loess (Pile 8)

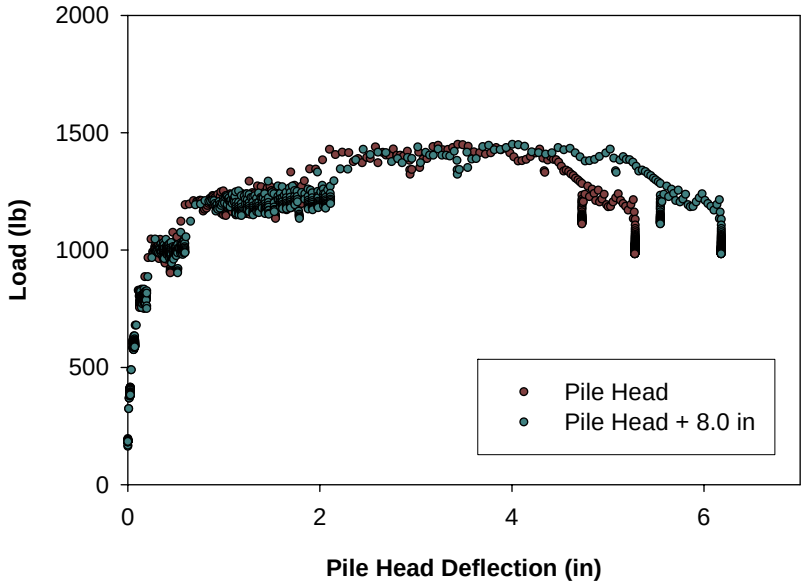

Figure C 13. Pile head deflection for loess (Pile 8)

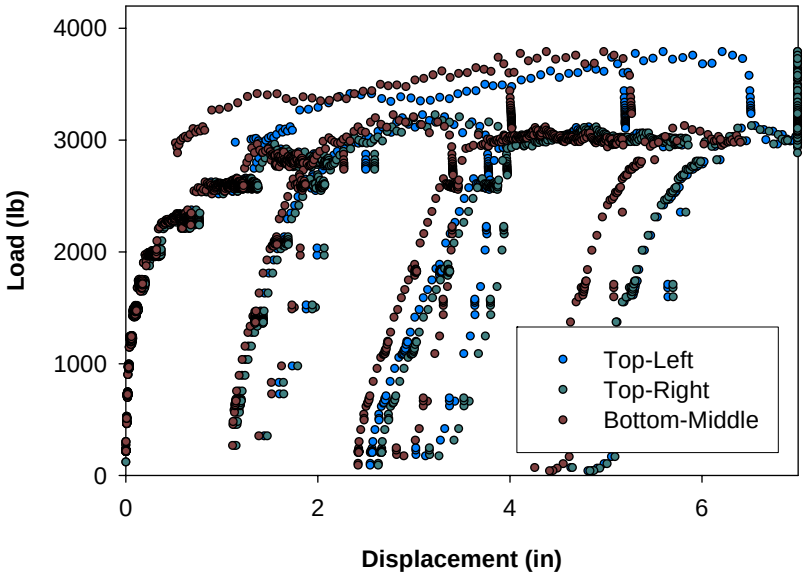

Figure C 14. Pile head deflection for glacial till (Pile 9)

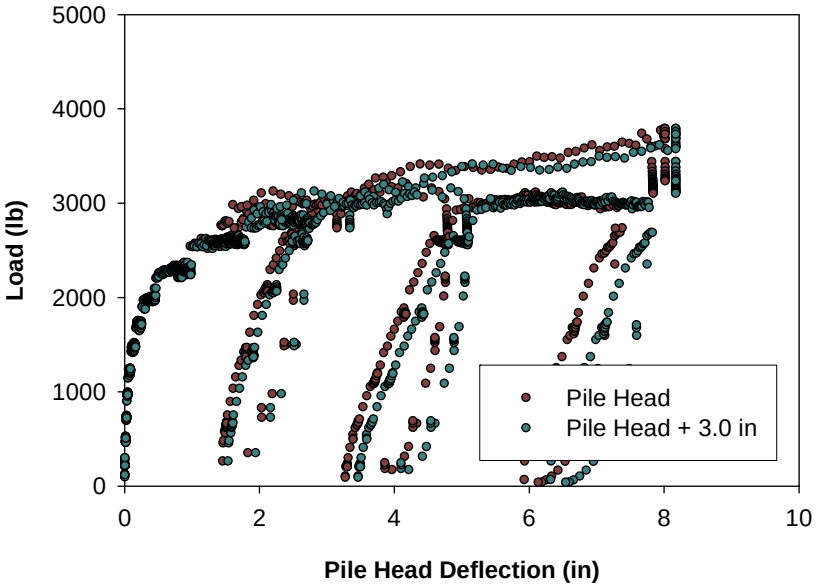

Figure C 15. Pile head deflection for glacial till (Pile 9)

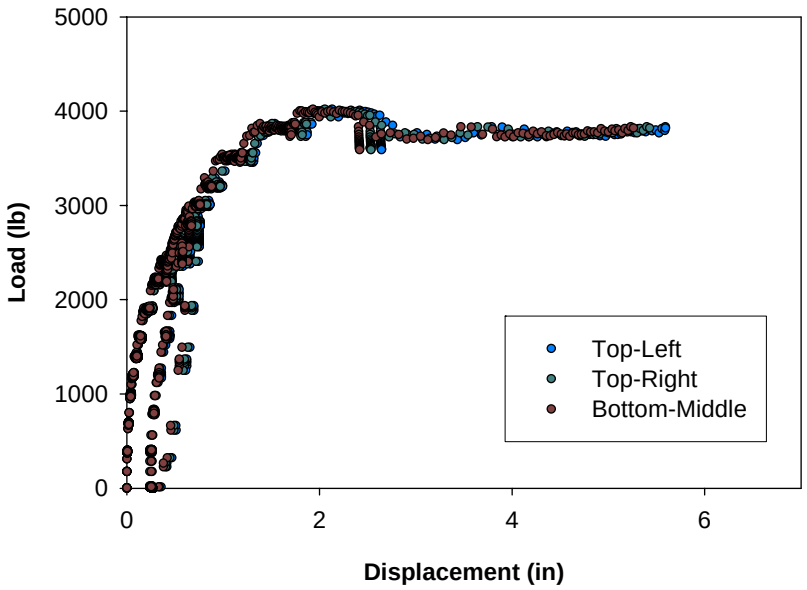

Figure C 16. Load-displacement for weathered shale (Pile 12)

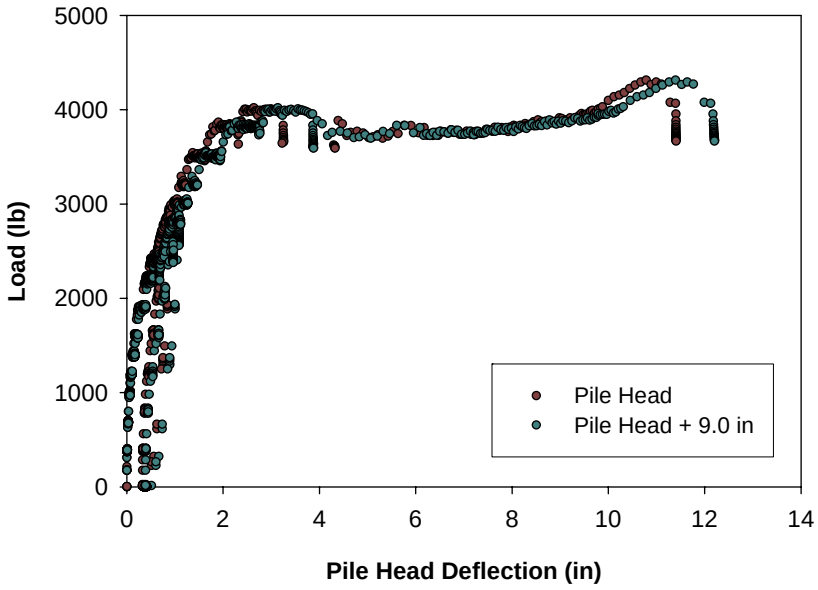

Figure C 17. Pile head deflection for weathered shale (Pile 12)

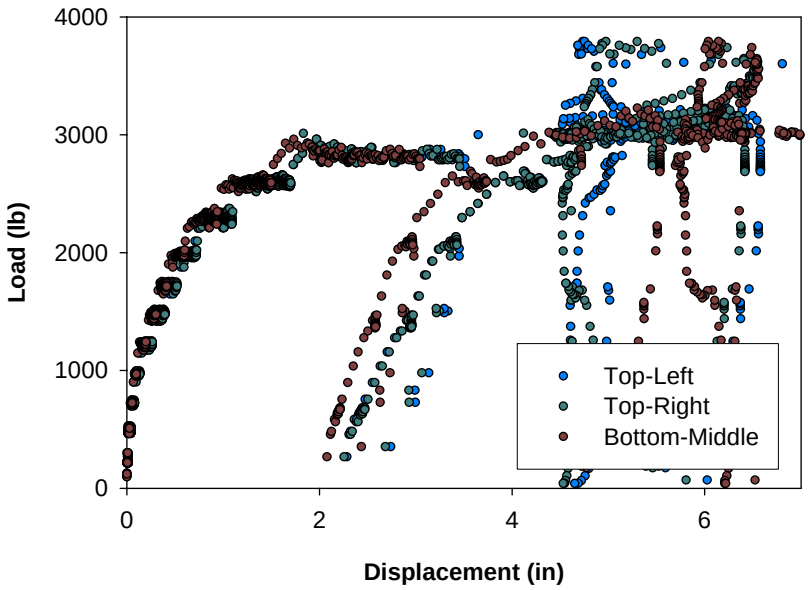

Figure C 18. Load-displacement for weathered shale (Piles 10 A and B)

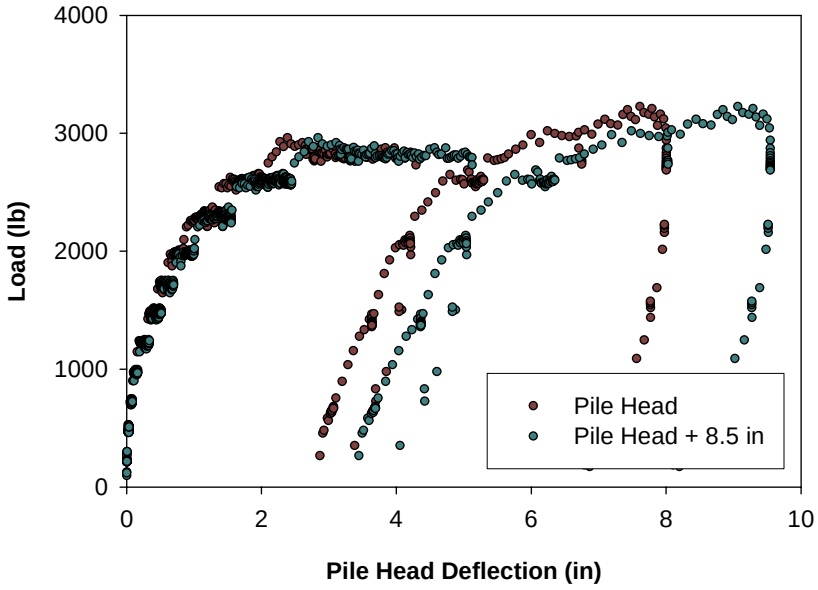

Figure C 19. Pile head deflection for weathered shale (Pile 10 A)

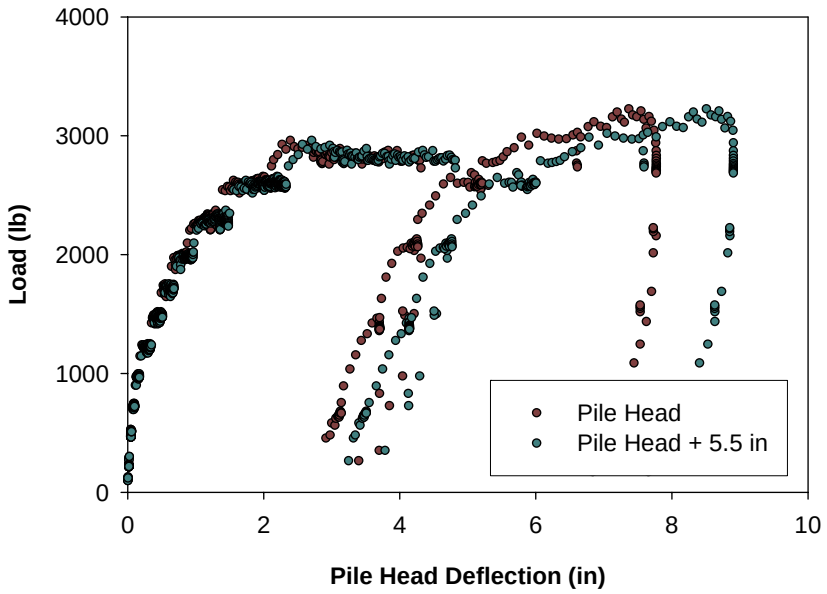

Figure C 20. Pile head deflection for weathered shale (Pile 10 B)

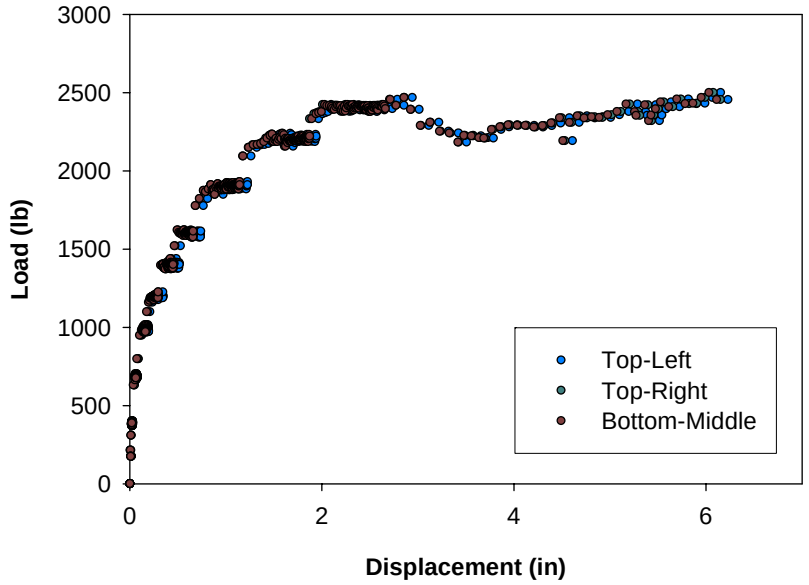

Figure C 21. Load-displacement for loess (Piles 11 A and B)

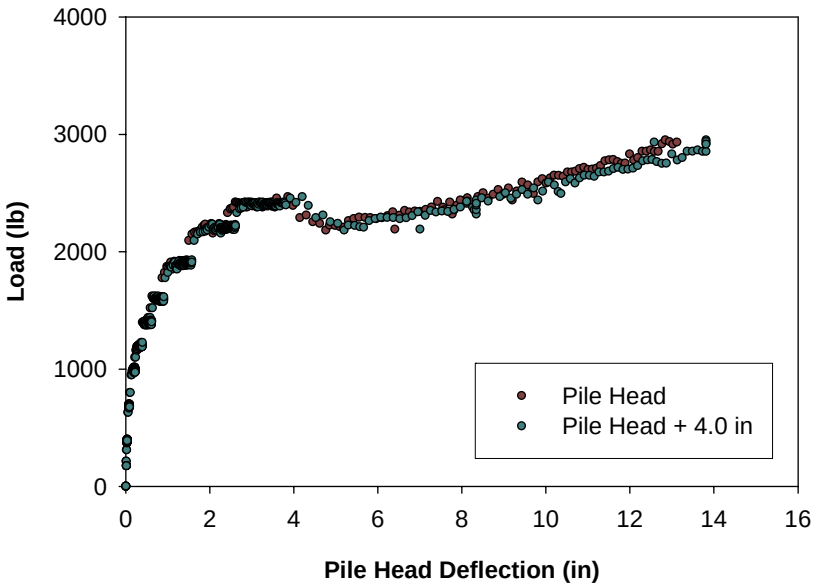

Figure C 22. Pile head deflection for loess (Pile 11 A)

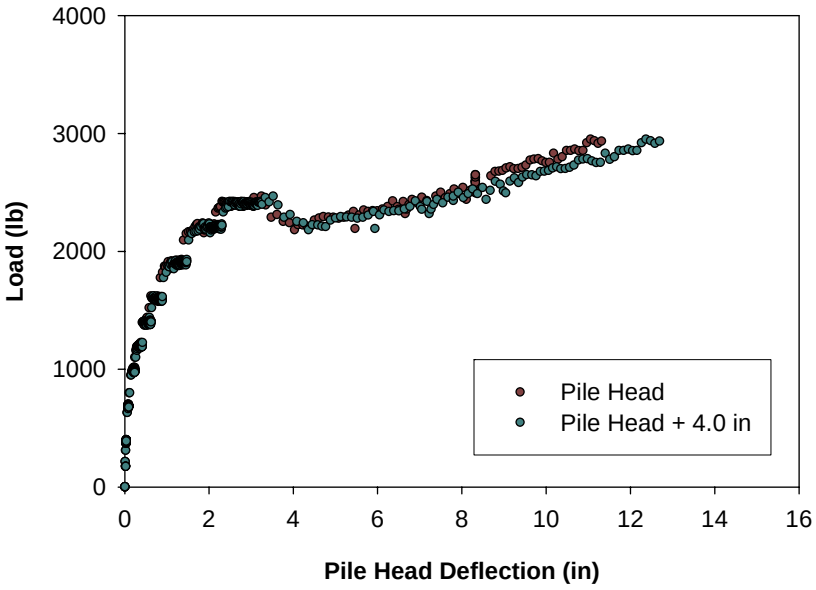

Figure C 23. Pile head deflection for loess (Pile 11 B)

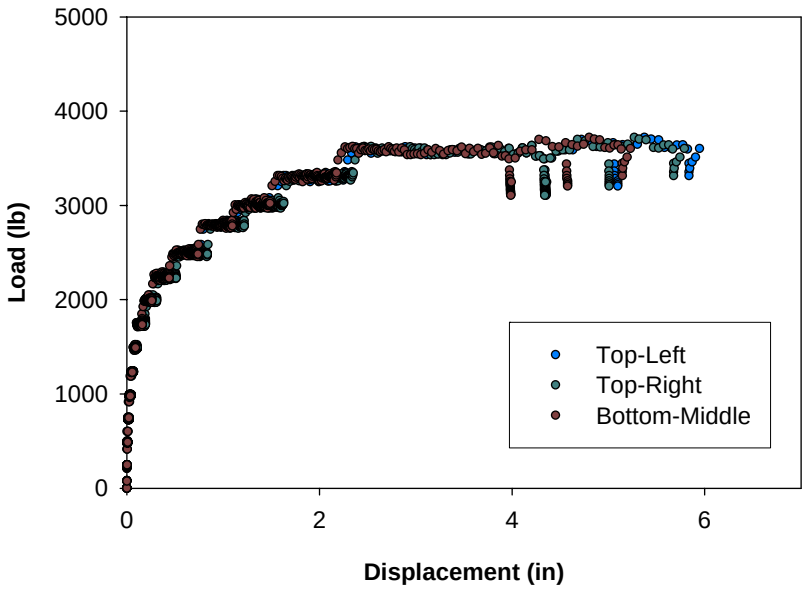

Figure C 24. Load-displacement for glacial till (Piles 13 A and B)

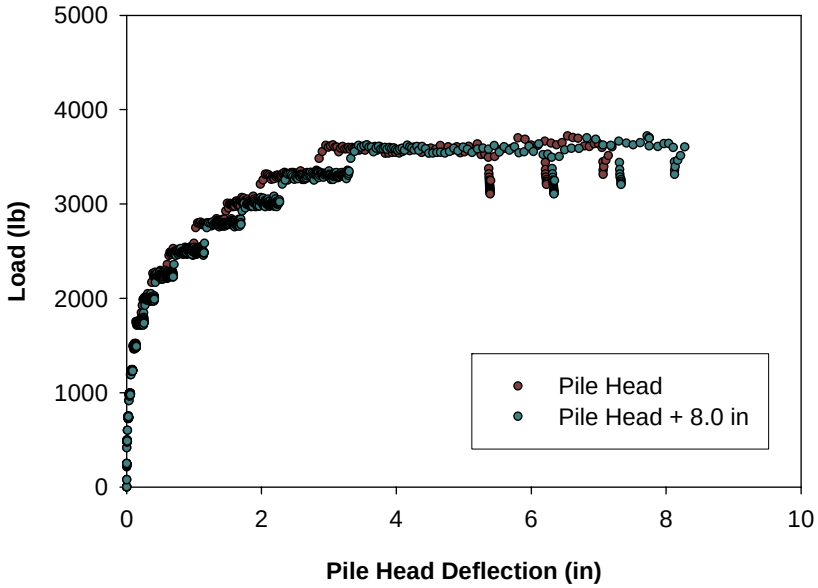

Figure C 25. Pile head deflection for glacial till (Pile 13 A)

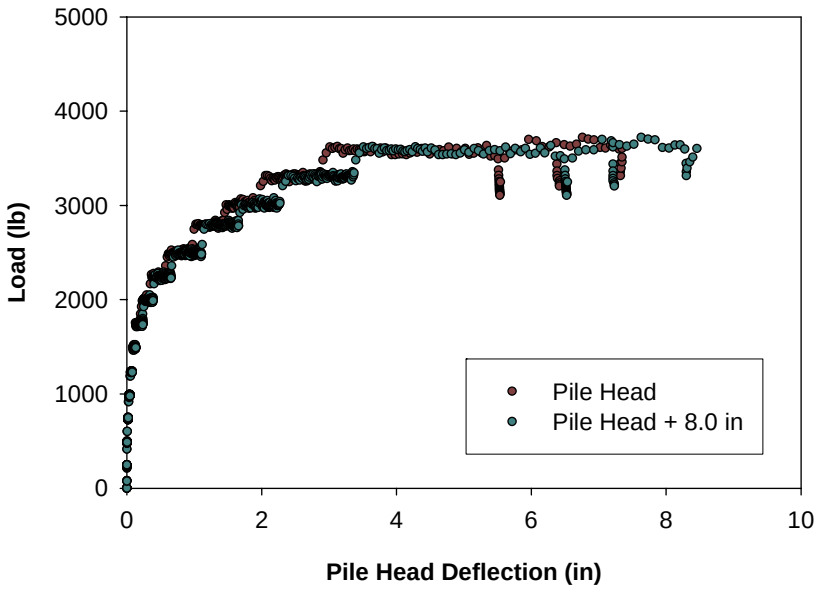

Figure C 26. Pile head deflection for glacial till (Pile 13 B)

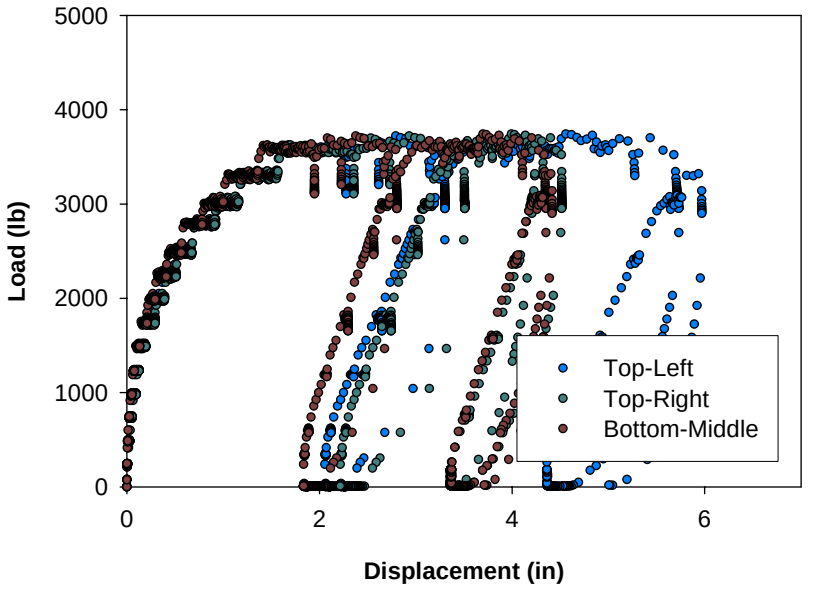

Figure C 27. Load-displacement for glacial till (Piles 14 A and B)

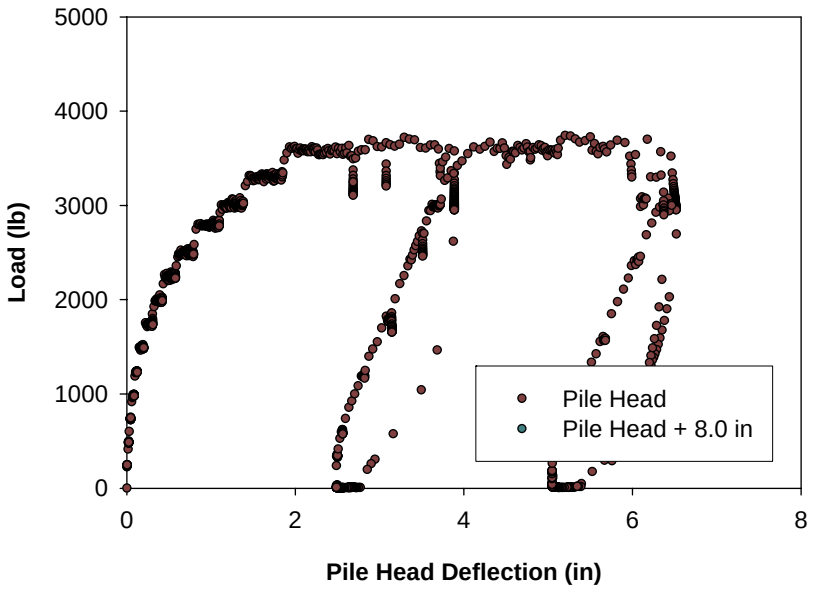

Figure C 28. Pile head deflection for glacial till (Pile 14 A)

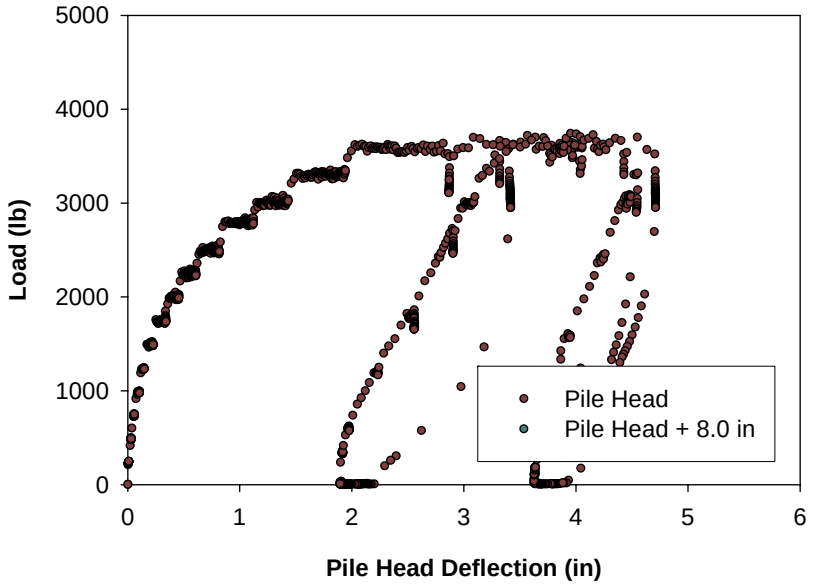

Figure C 29. Pile head deflection for glacial till (Pile 14 B)

APPENDIX D: SHEAR BOX LOAD-DISPLACEMENT RELATIONSHIPS

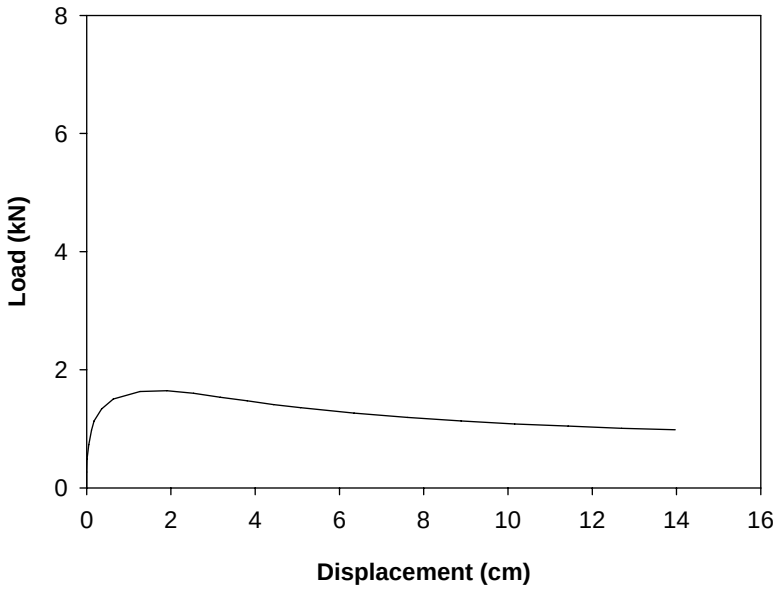

Figure D 1. Load vs. displacement for unreinforced loess

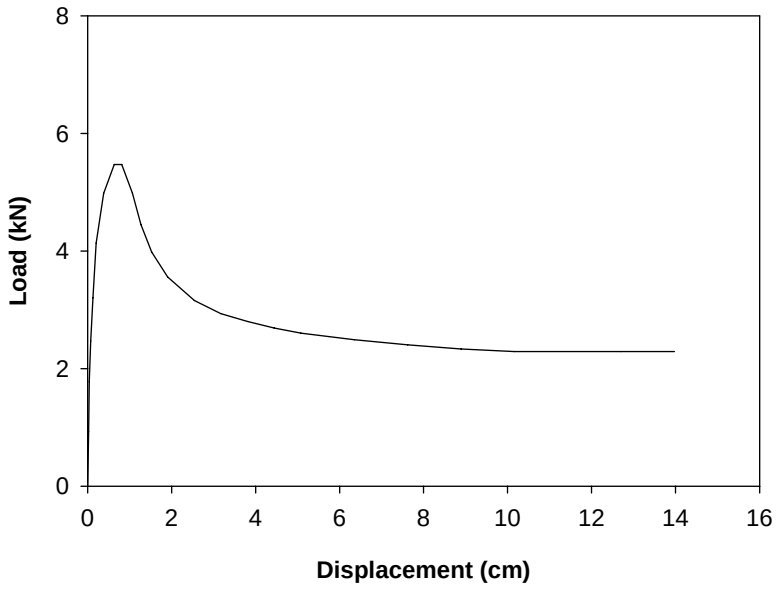

Figure D 2. Load vs. displacement for unreinforced weathered shale

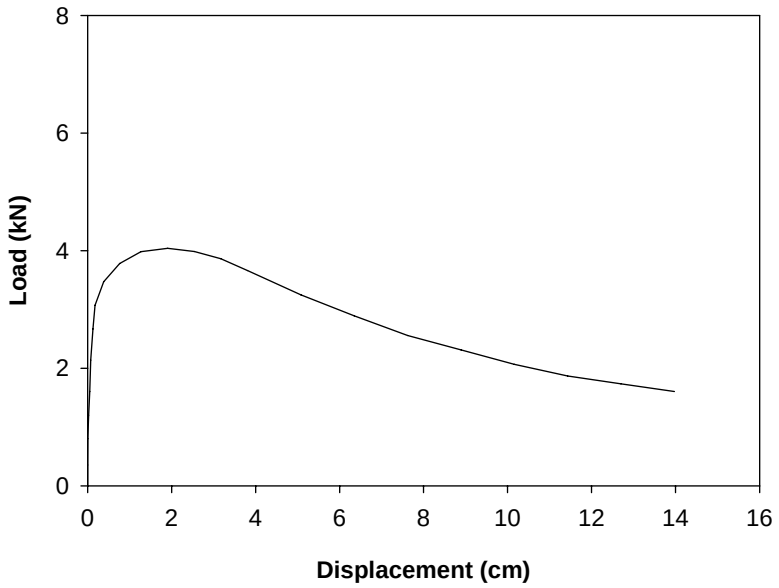

Figure D 3. Load vs. displacement for unreinforced glacial till

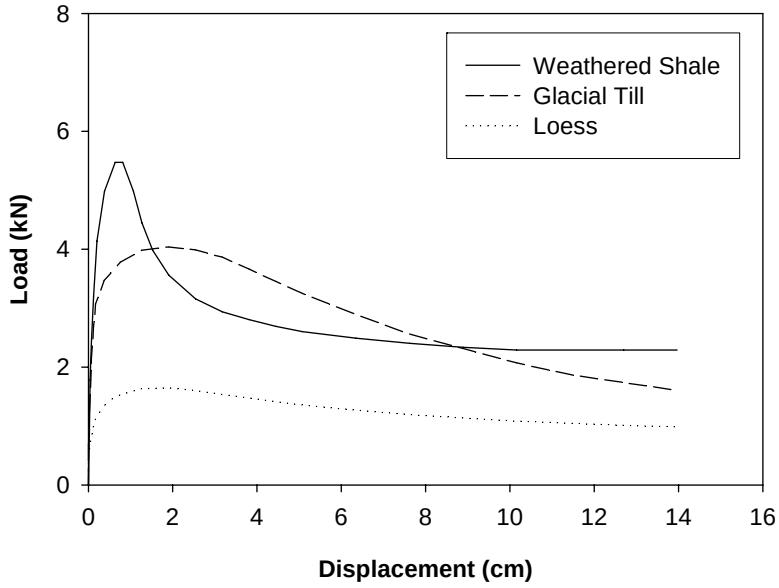

Figure D 4. Load vs. displacement for unreinforced soils

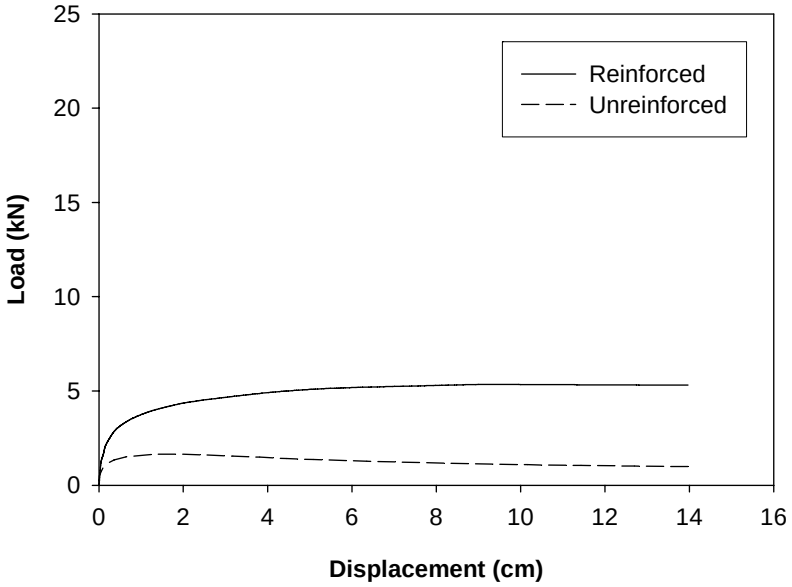

Figure D 5. Load vs. displacement for loess (Pile 4)

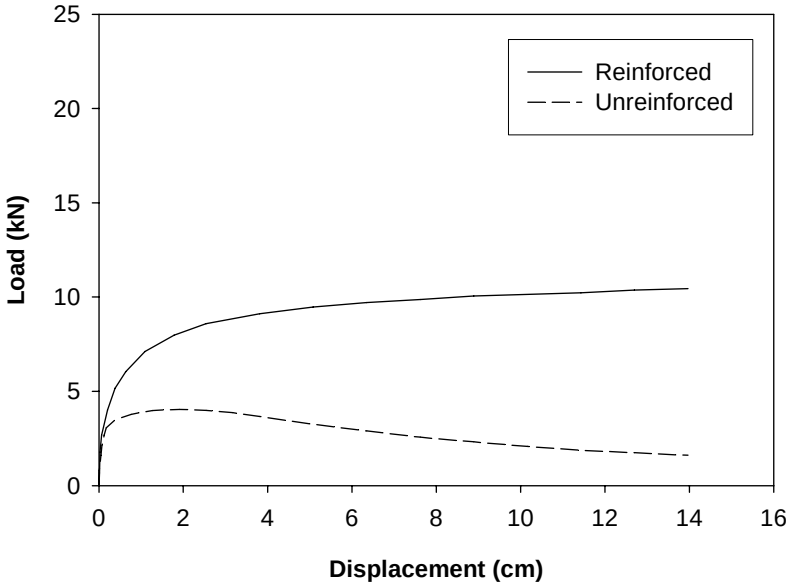

Figure D 6. Load vs. displacement for glacial till (Pile 5)

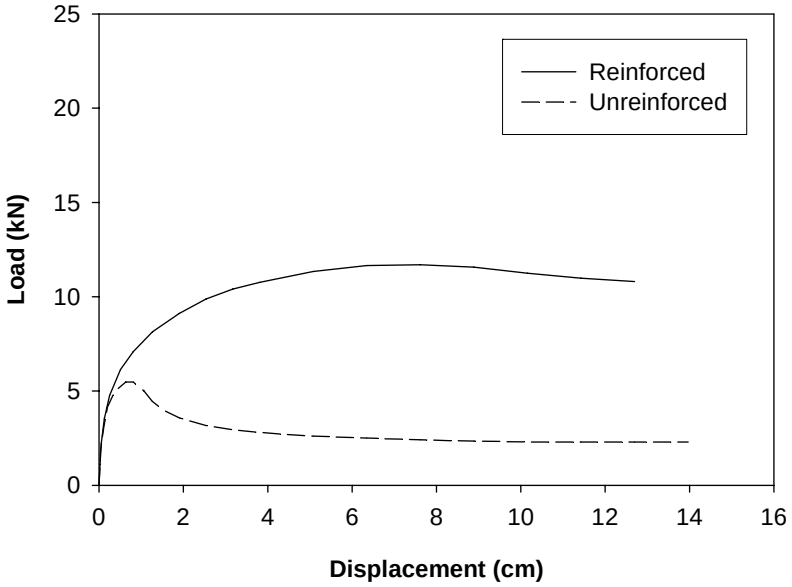

Figure D 7. Load vs. displacement for weathered shale (Pile 6)

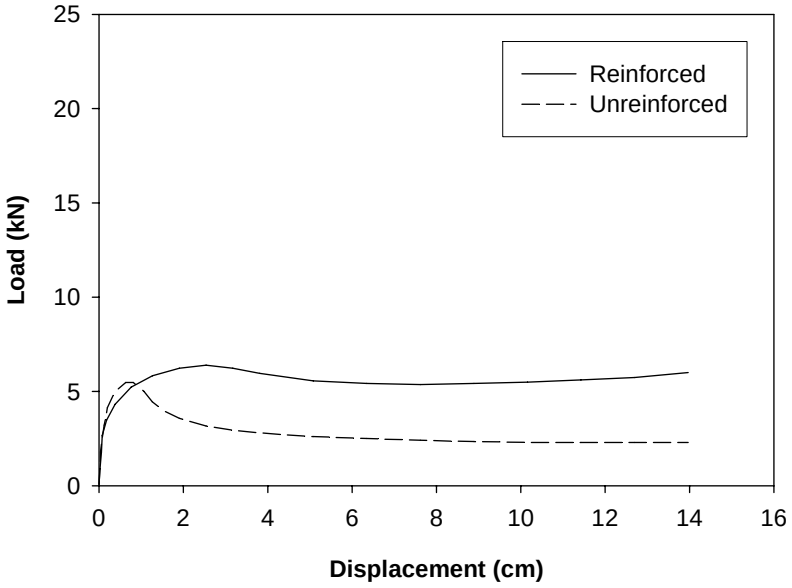

Figure D 8. Load vs. displacement for weathered shale (Pile 7)

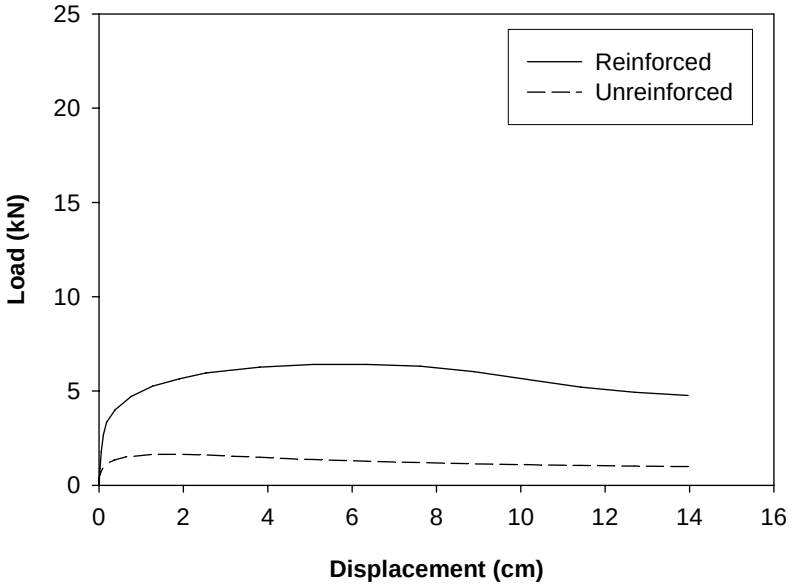

Figure D 9. Load vs. displacement for loess (Pile 8)

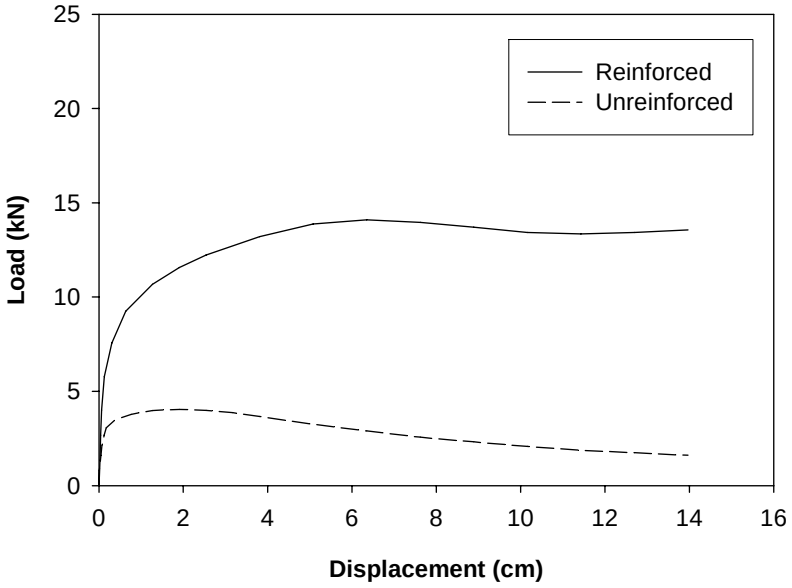

Figure D 10. Load vs. displacement for glacial till (Pile 9)

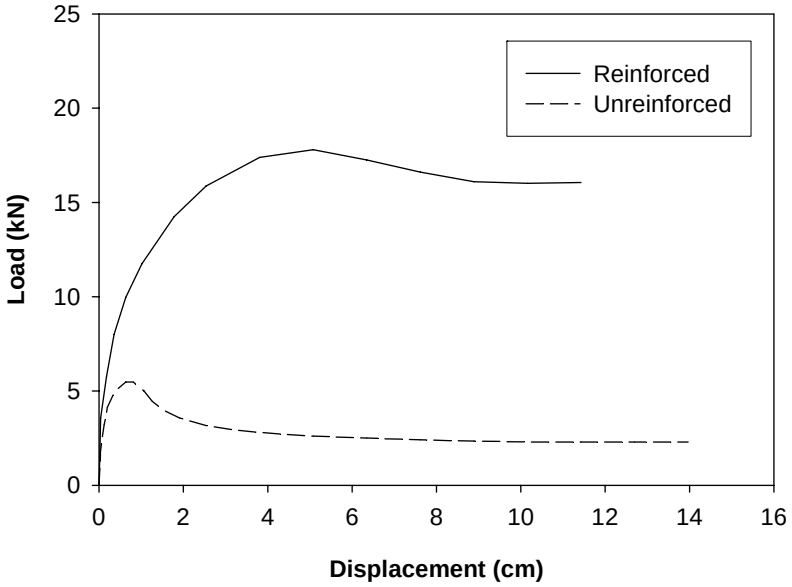

Figure D 11. Load vs. displacement for weathered shale (Pile 12)

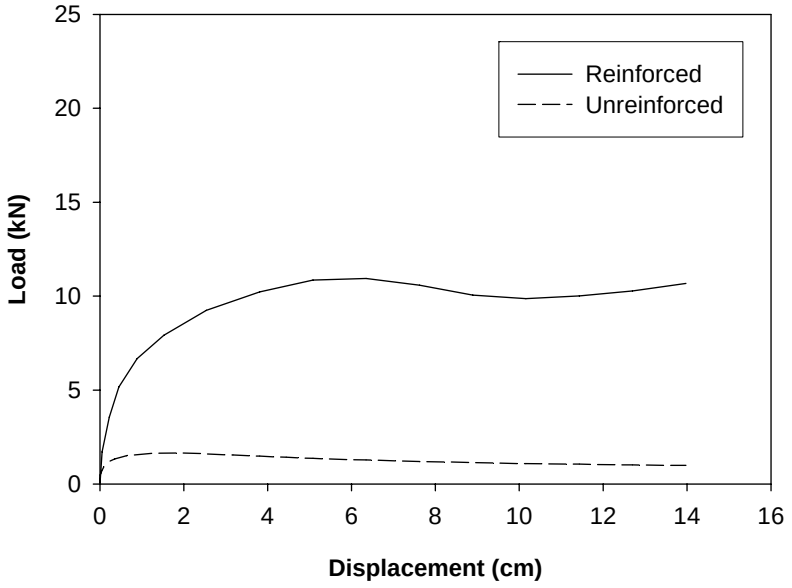

Figure D 12. Load vs. displacement for loess (Piles 11 A and B)

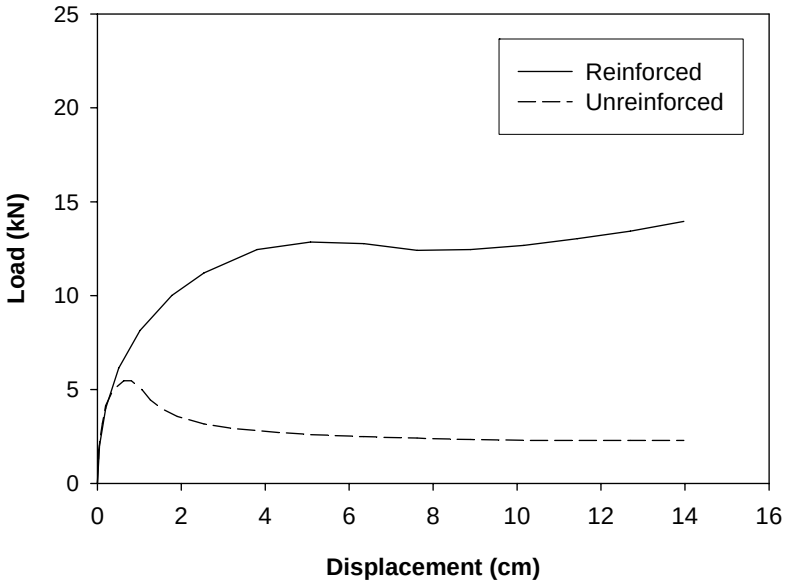

Figure D 13. Load vs. displacement for weathered shale (Piles 10 A and B)

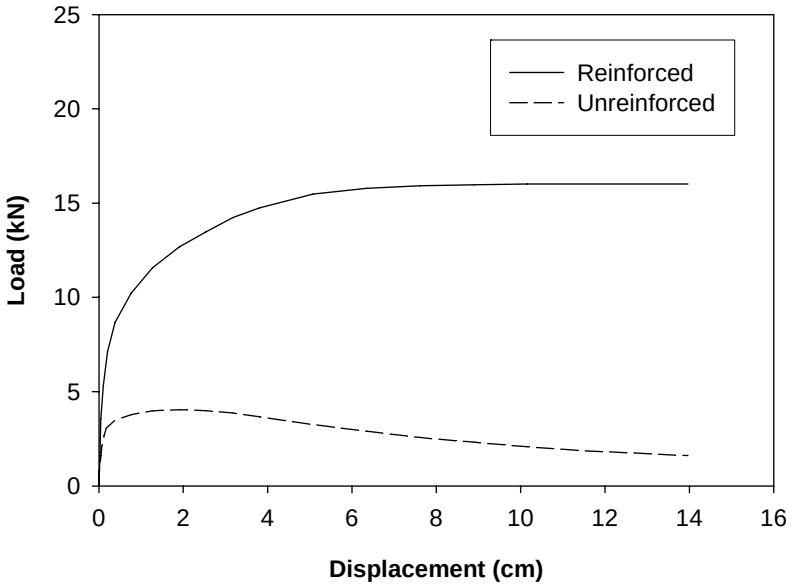

Figure D 14. Load vs. displacement for glacial till (Piles 13 A and B)

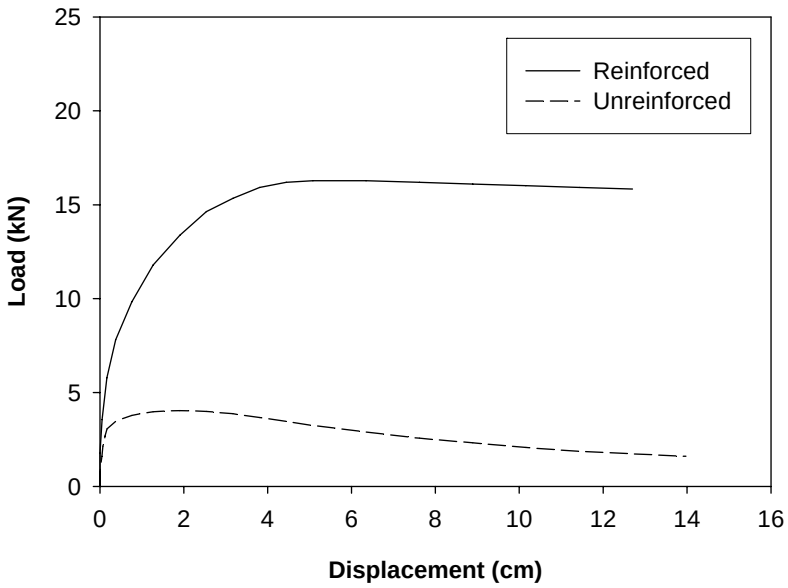

Figure D 15. Load vs. displacement for glacial till (Piles 14 A and B)

APPENDIX E: PILE HEAD LOAD-DISPLACEMENT RELATIONSHIPS

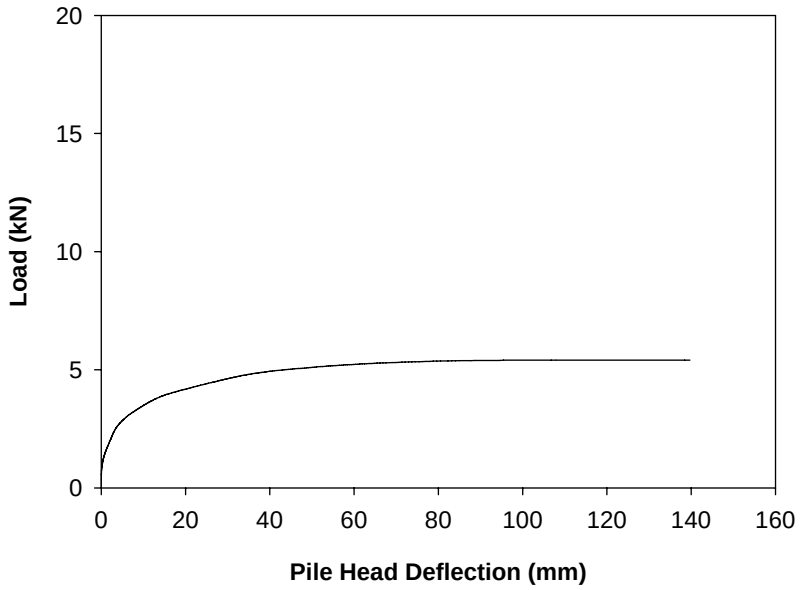

Figure E 1. Pile head load-deflection for loess (Pile 4)

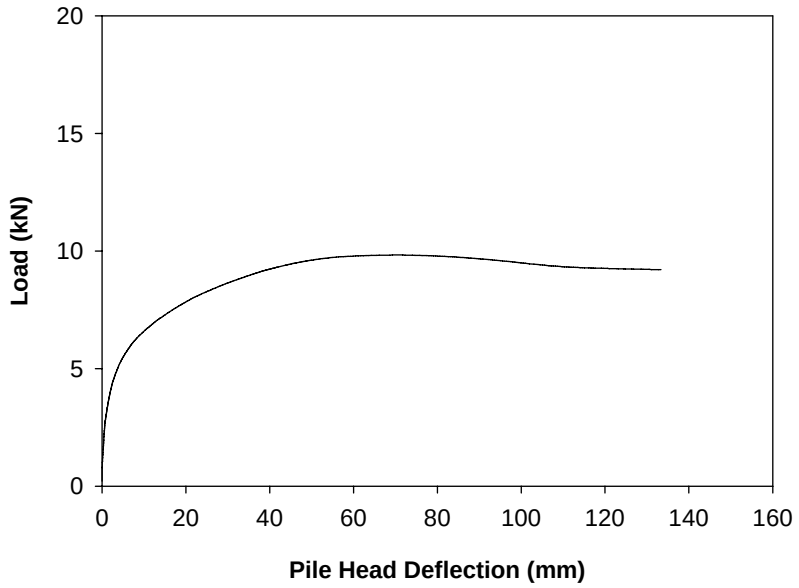

Figure E 2. Pile head load-deflection for glacial till (Pile 5)

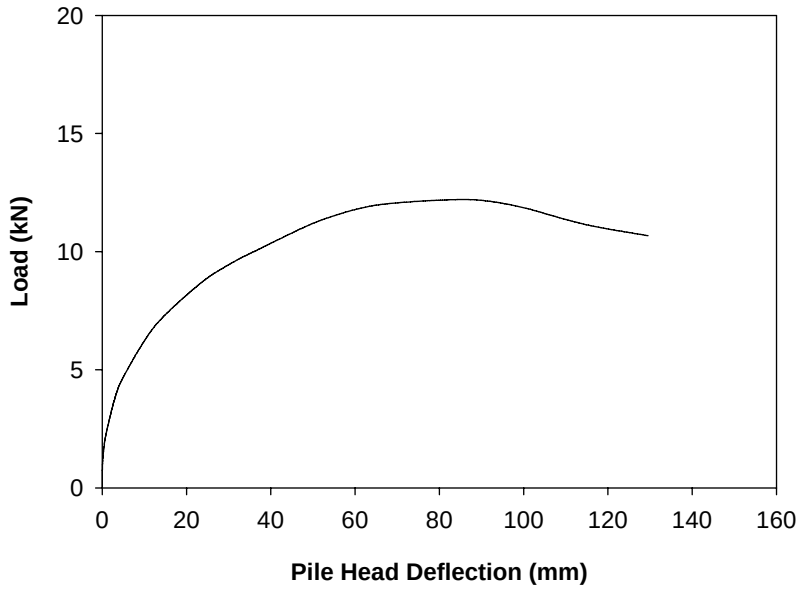

Figure E 3. Pile head load-deflection for weathered shale (Pile 6)

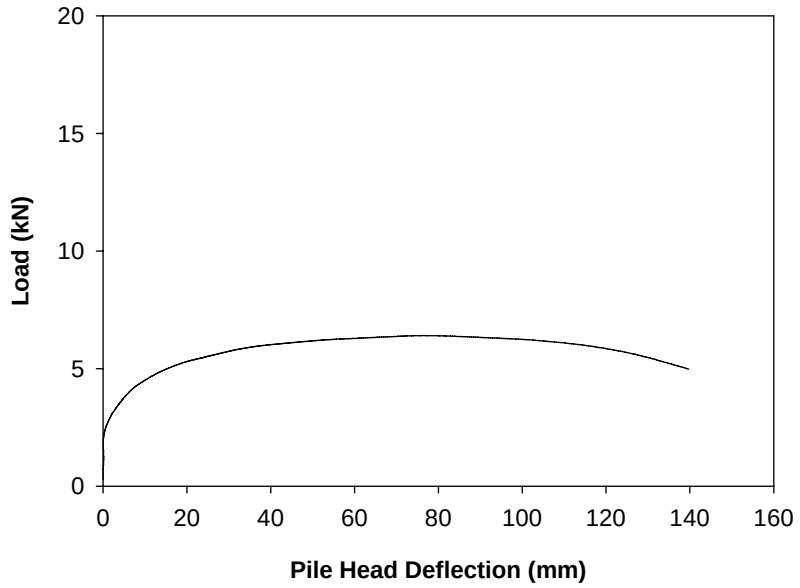

Figure E 4. Pile head load-deflection for loess (Pile 8)

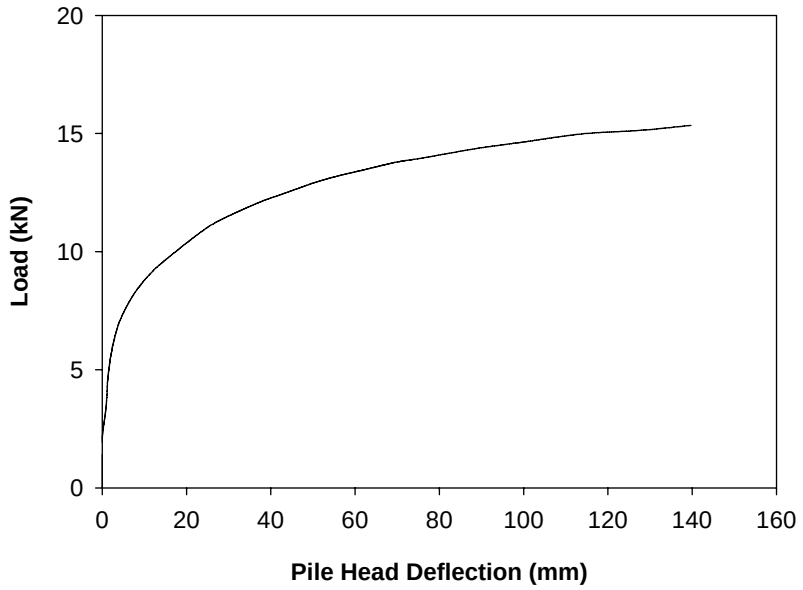

Figure E 5. Pile head load-deflection for glacial till (Pile 9)

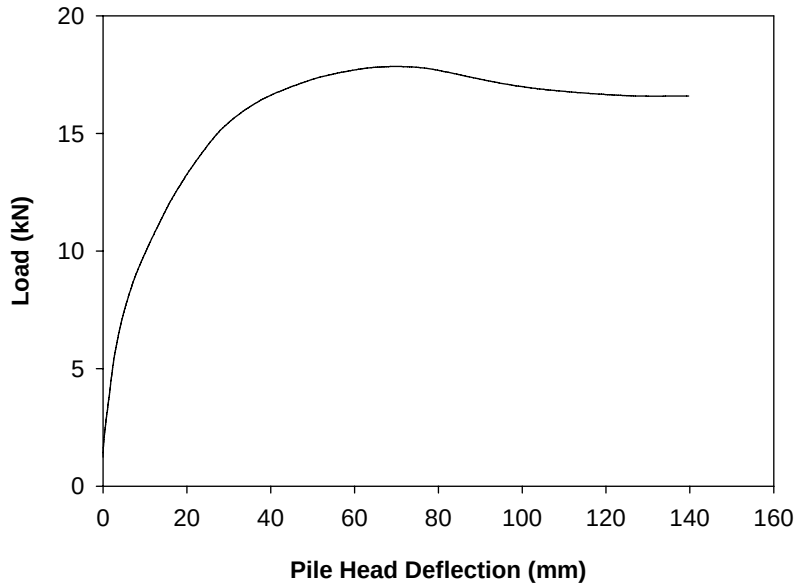

Figure E 6. Pile head load-deflection for weathered shale (Pile 12)

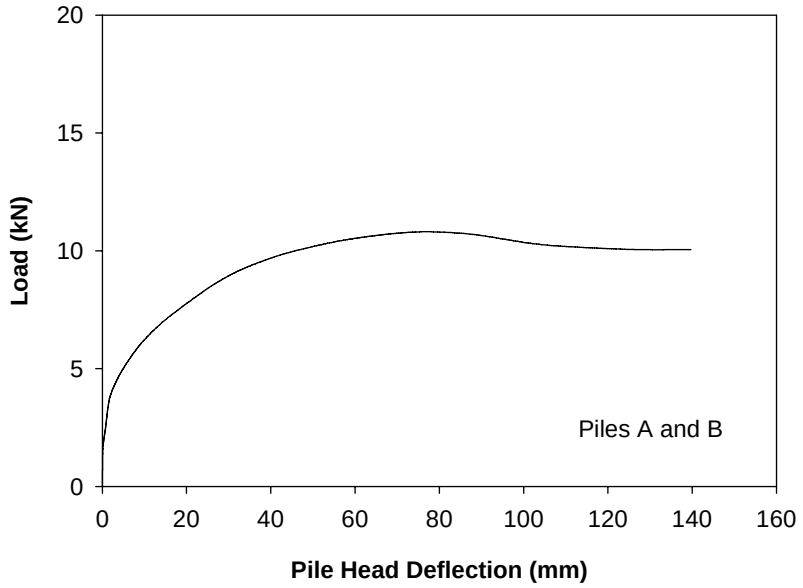

Figure E 7. Pile head load-deflection for loess (Piles 11 A and B)

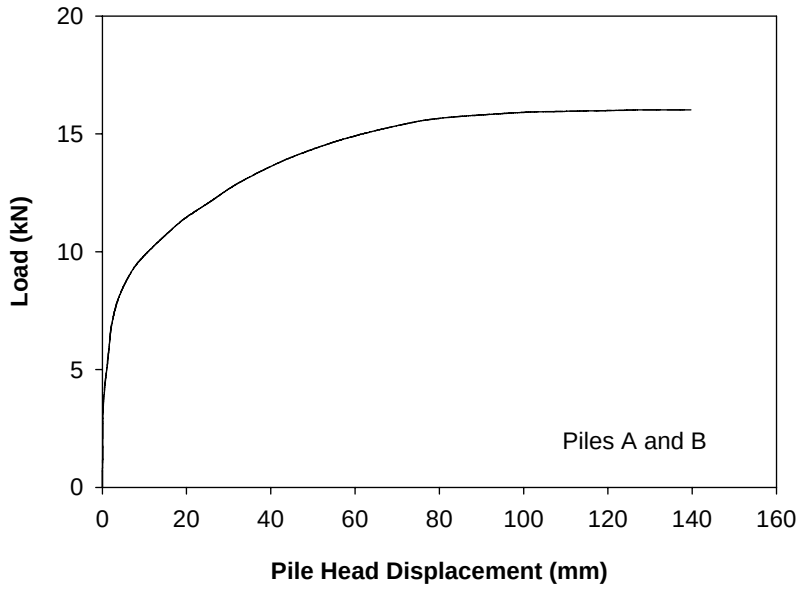

Figure E 8. Pile head load-deflection for glacial till (Piles 13 A and B)

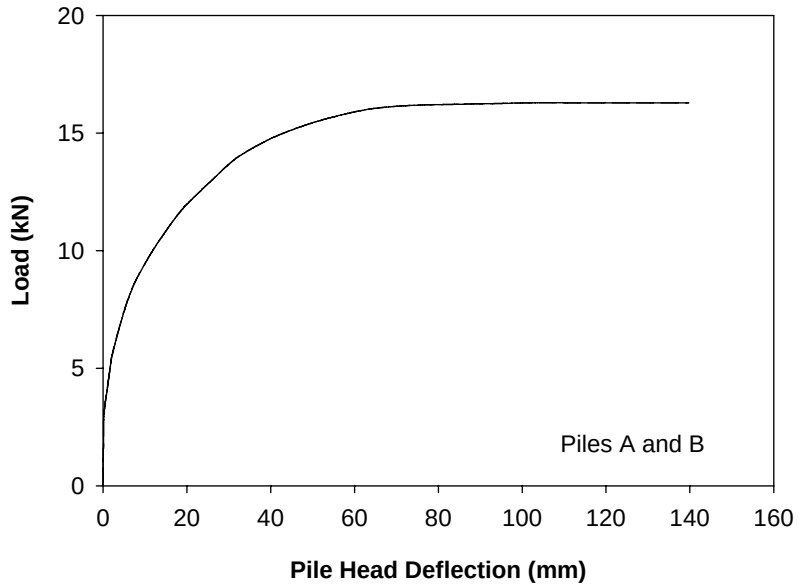

Figure E 9. Pile head load-deflection for glacial till (Piles 14 A and B)

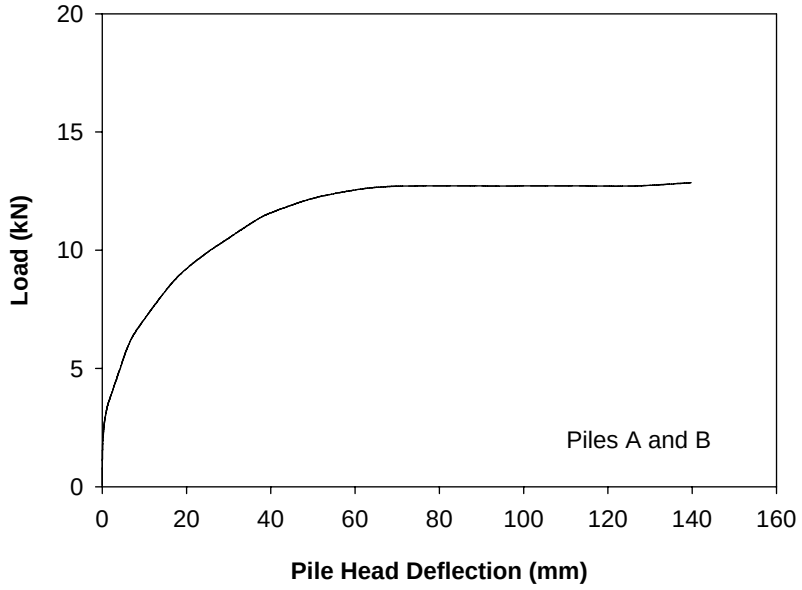

Figure E 10. Pile head load-deflection for weathered shale (Piles 10 A and B)

APPENDIX F: SHEAR BOX ROTATION AND TILT

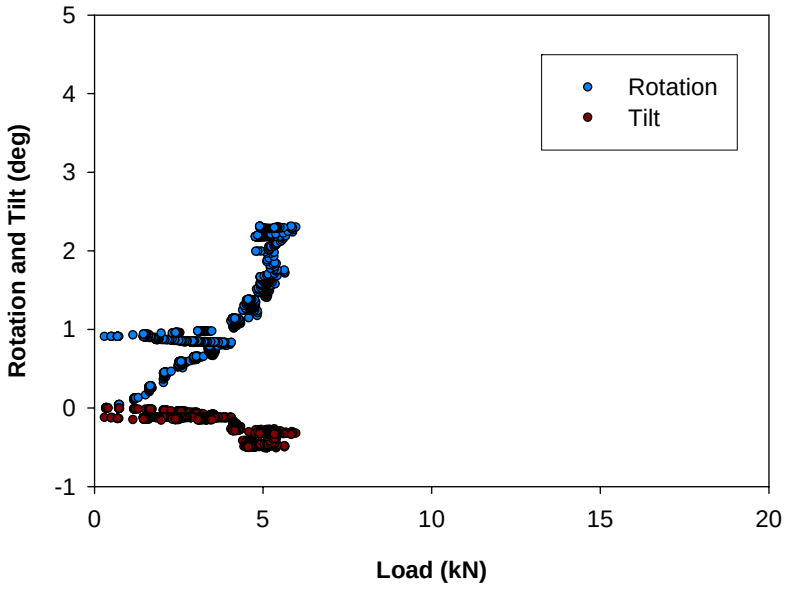

Figure F 1. Box rotation and tilt vs. load for loess (Box 4)

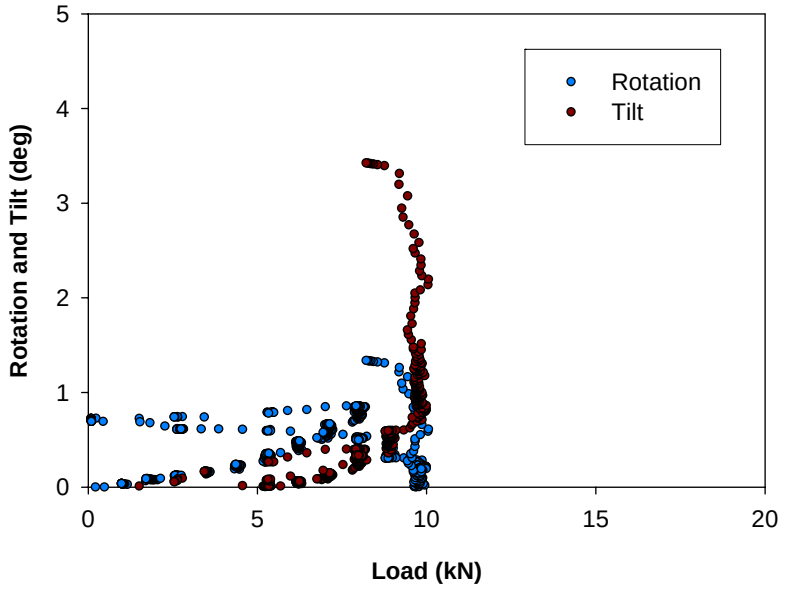

Figure F 2. Box rotation and tilt vs. load for glacial till (Box 5)

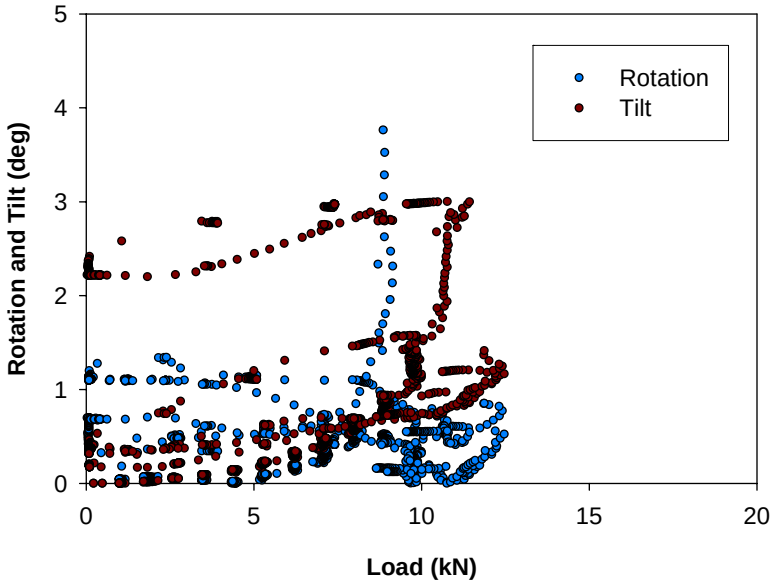

Figure F 3. Box rotation and tilt vs. load for weathered shale (Box 6)

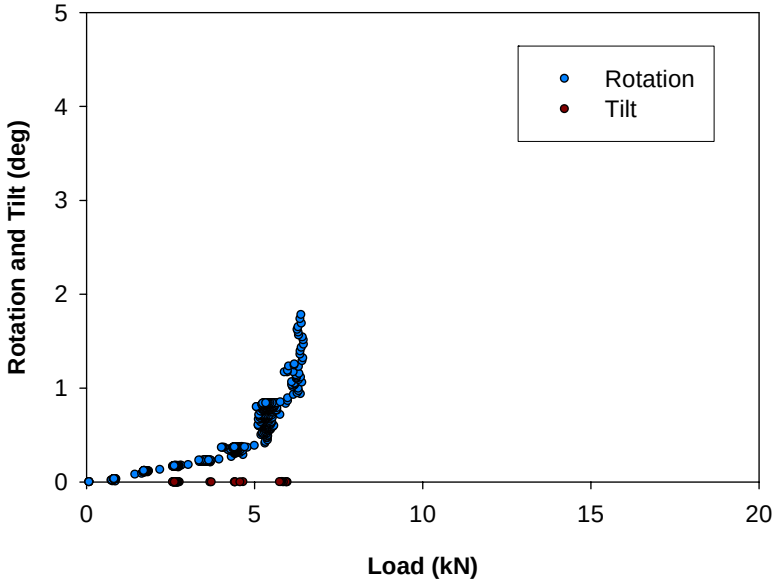

Figure F 4. Box rotation and tilt vs. load for loess (Box 8)

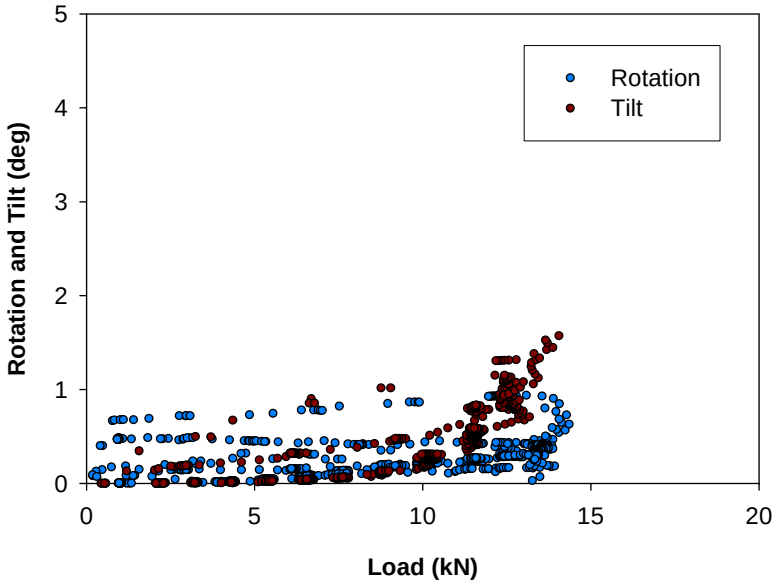

Figure F 5. Box rotation and tilt vs. load for glacial till (Box 9)

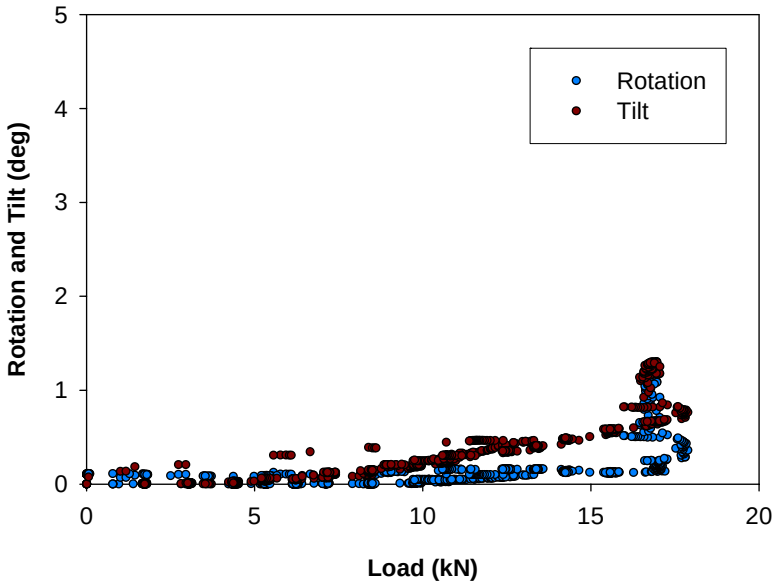

Figure F 6. Box rotation and tilt vs. load for weathered shale (Box 12)

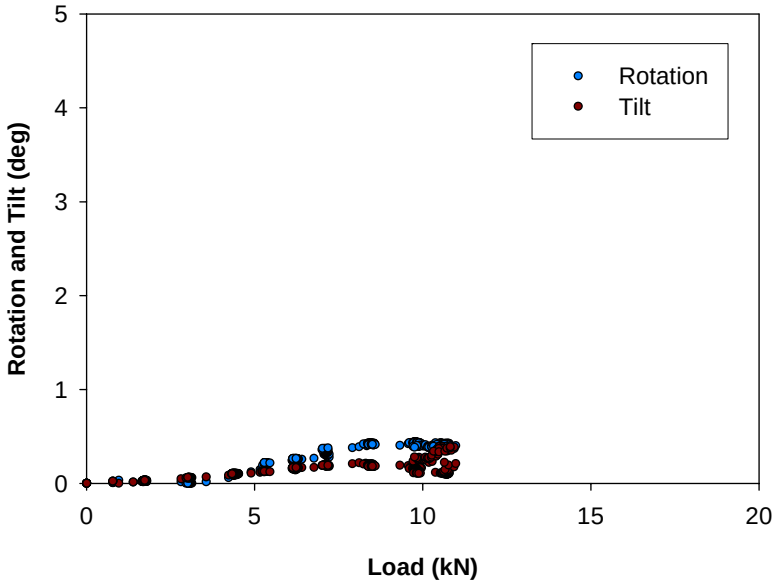

Figure F 7. Box rotation and tilt vs. load for loess (Box 11)

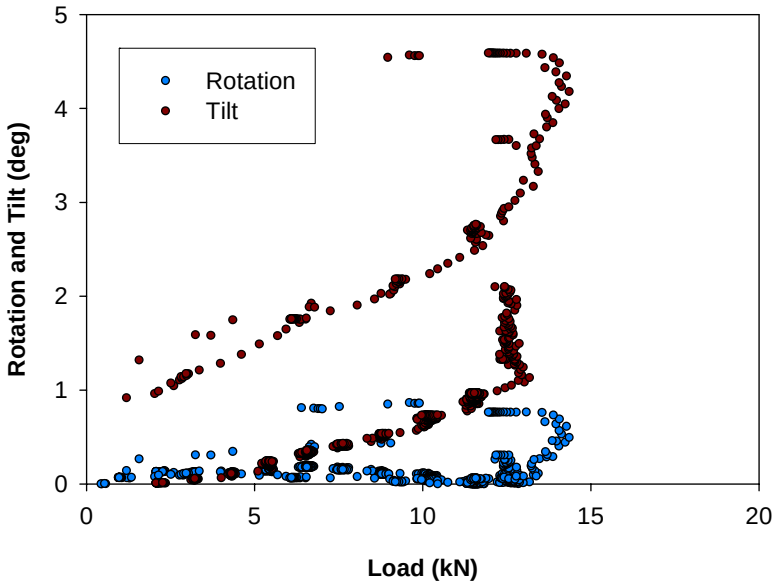

Figure F 8. Box rotation and tilt vs. load for weathered shale (Box 10)

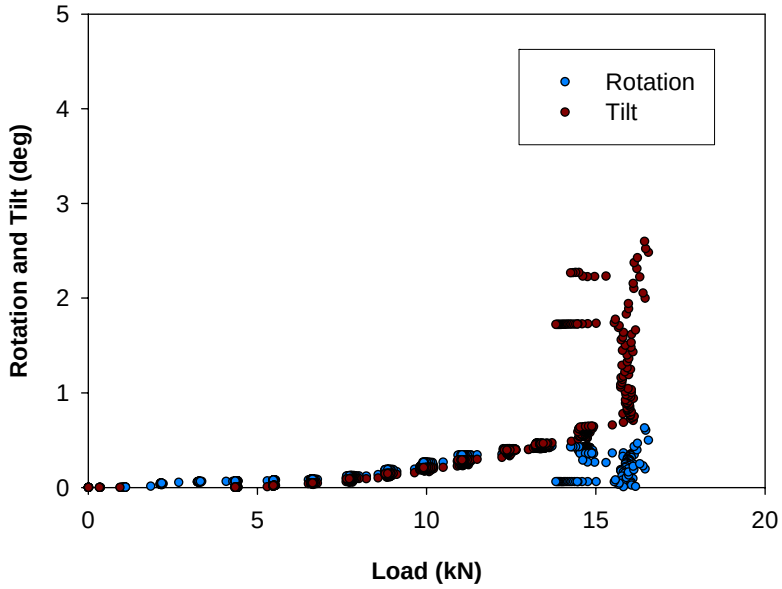

Figure F 9. Box rotation and tilt vs. load for glacial till (Box 13)

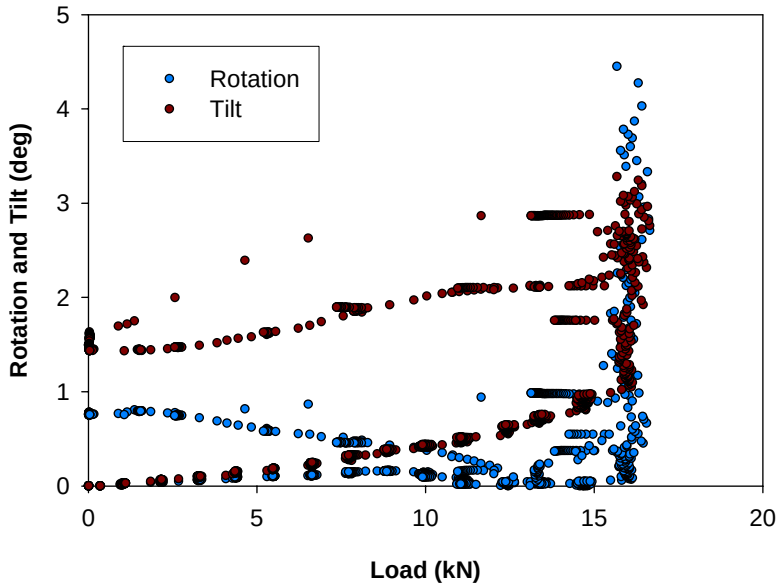

Figure F 10. Box rotation and tilt vs. load for glacial till (Box 14)

APPENDIX G: PILE STRAIN MEASUREMENTS

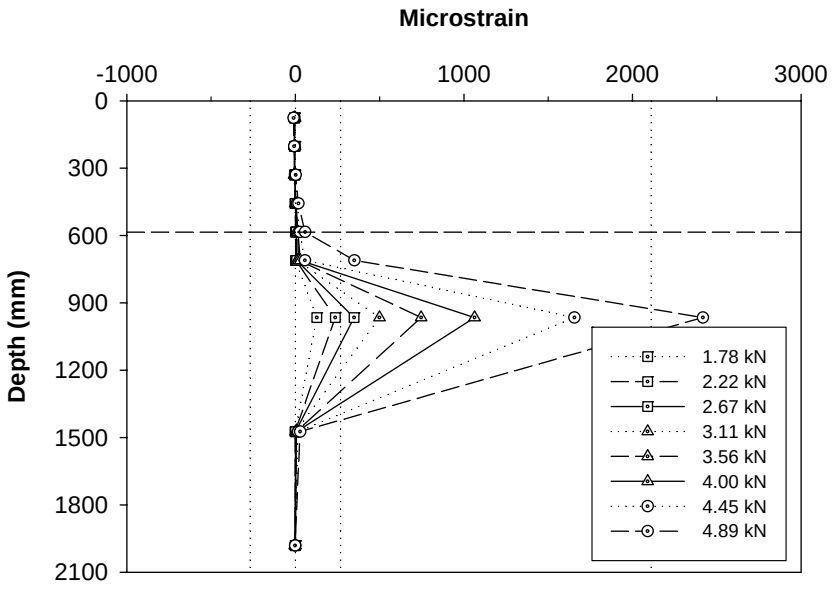

Figure G 1. Strain profiles for pile in loess (Pile 4)

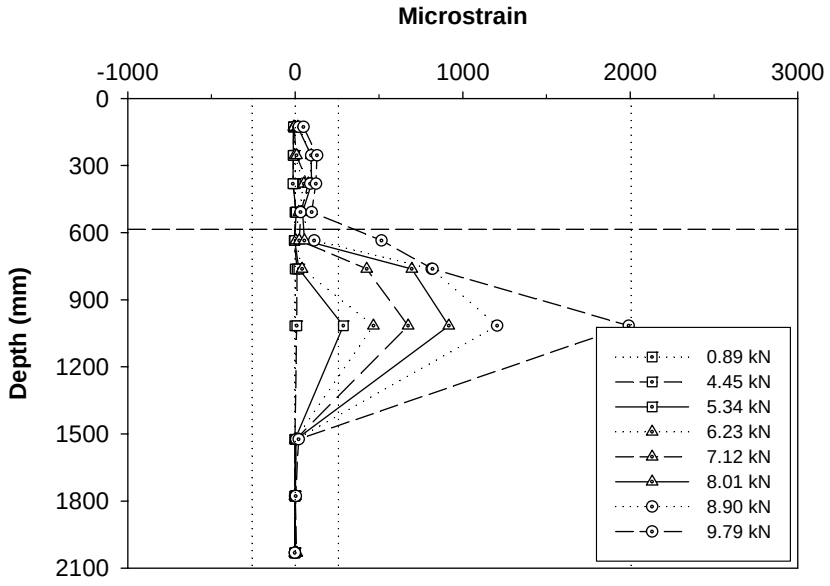

Figure G 2. Strain profiles for pile in glacial till (Pile 5)

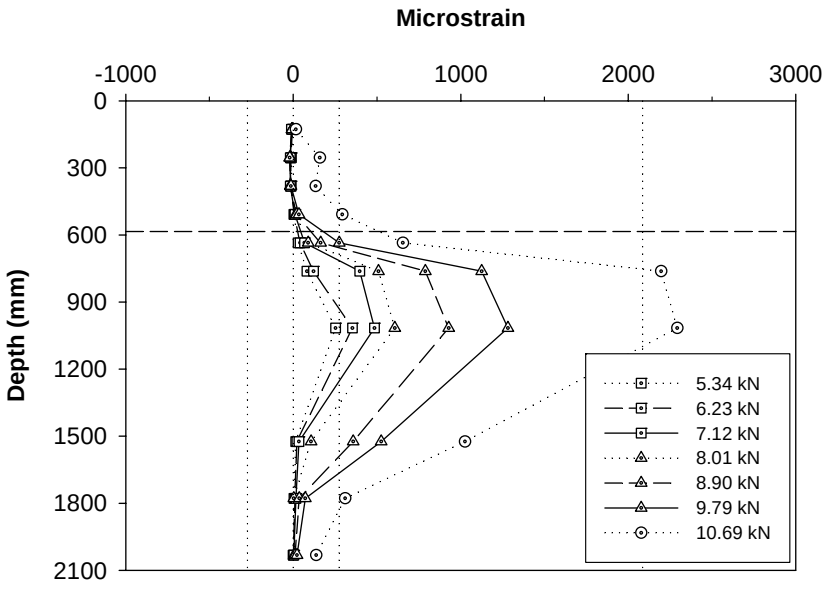

Figure G 3. Strain profiles for pile in weathered shale (Pile 6)

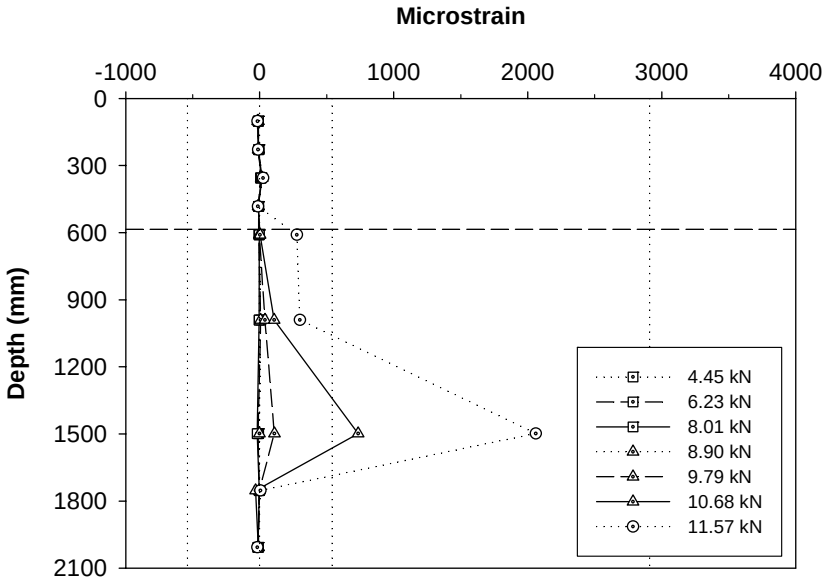

Figure G 4. Strain profiles for pile in loess (Pile 8)

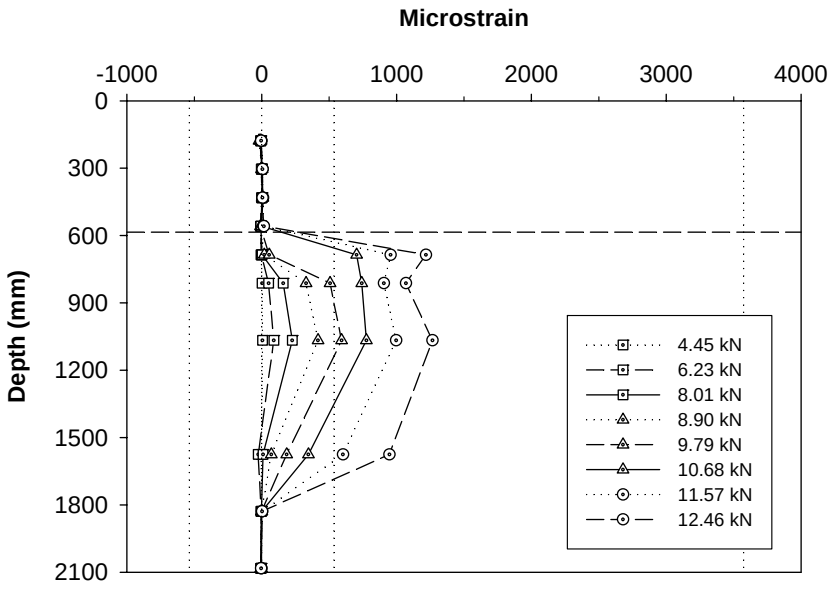

Figure G 5. Strain profiles for pile in glacial till (Pile 9)

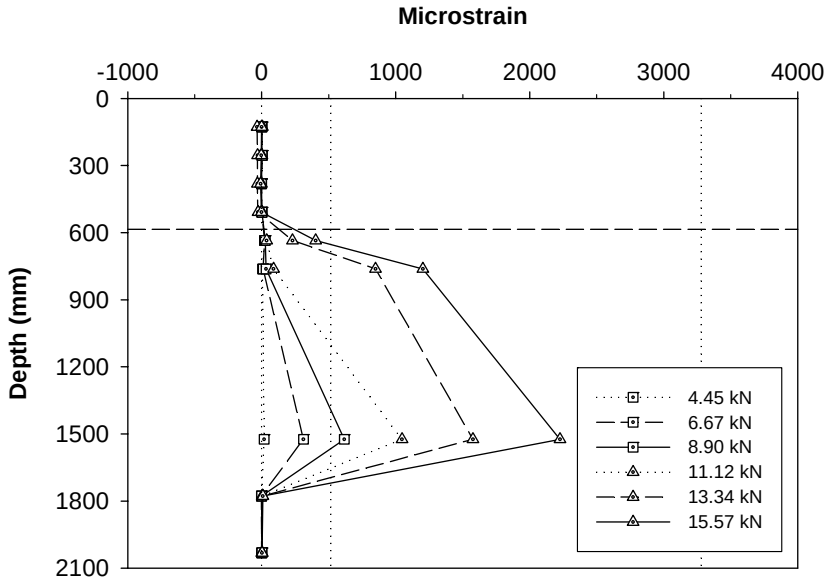

Figure G 6. Strain profiles for pile in weathered shale (Pile 12)

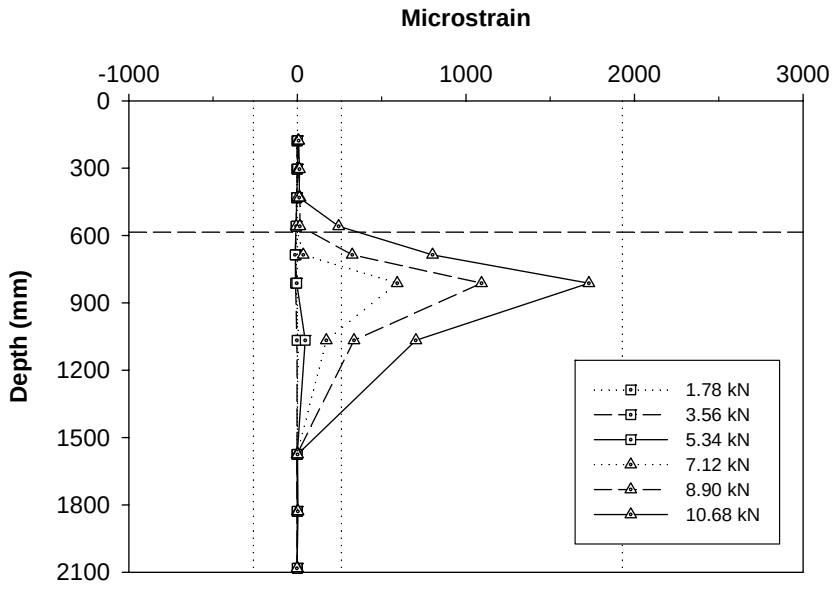

Figure G 7. Strain profiles for pile in loess (Piles 11 A)

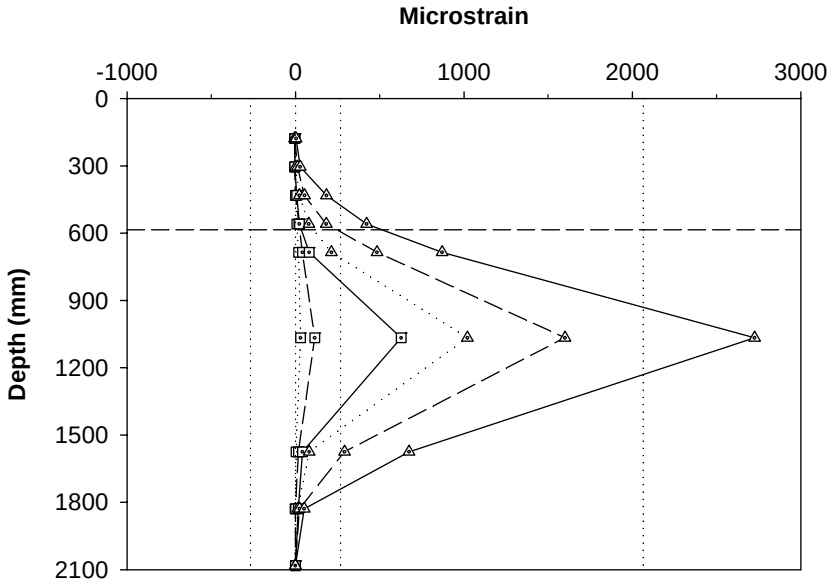

Figure G 8. Strain profiles for pile in loess (Piles 11 B)

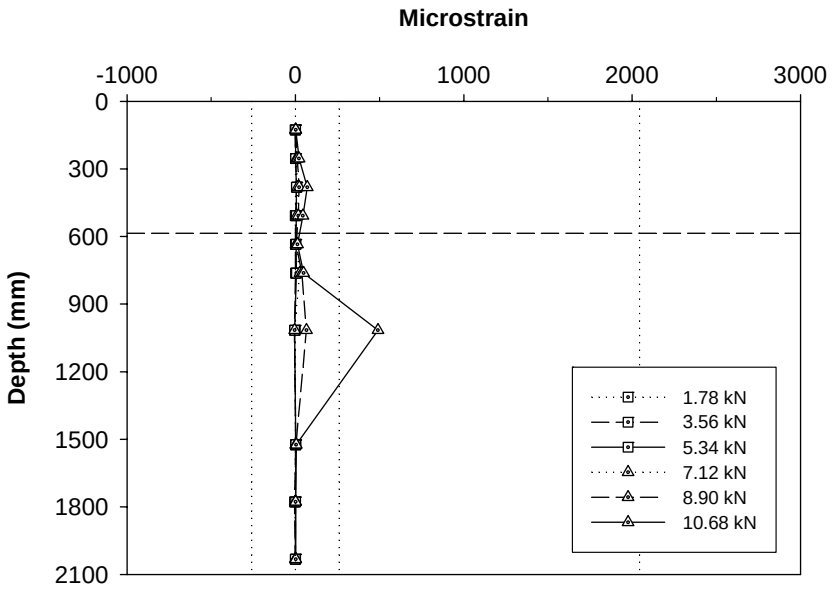

Figure G 9. Strain profiles for pile in glacial till (Piles 13 A)

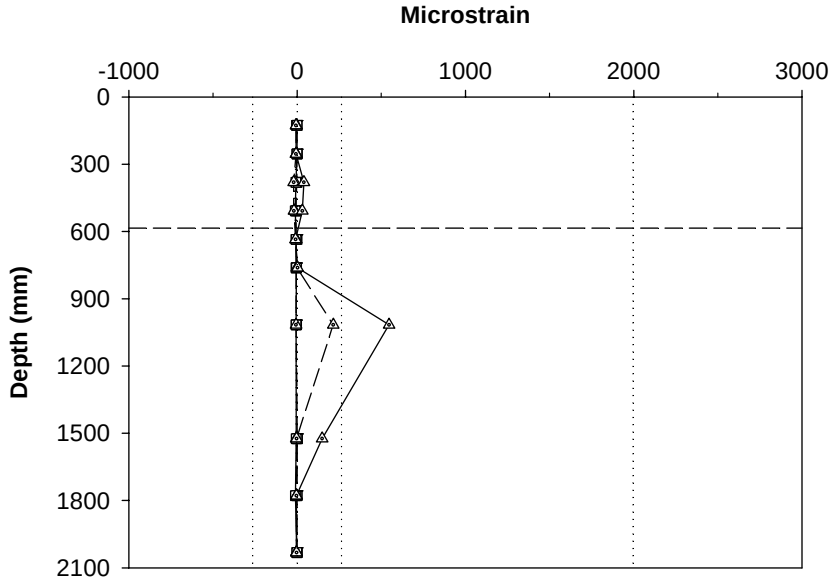

Figure G 10. Strain profiles for pile in glacial till (Piles 13 B)

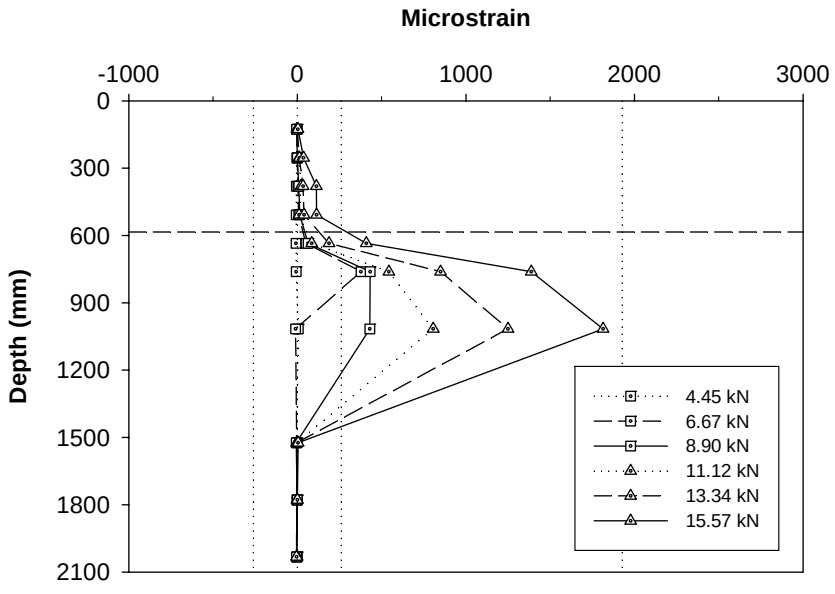

Figure G 11. Strain profiles for pile in glacial till (Piles 14 B)

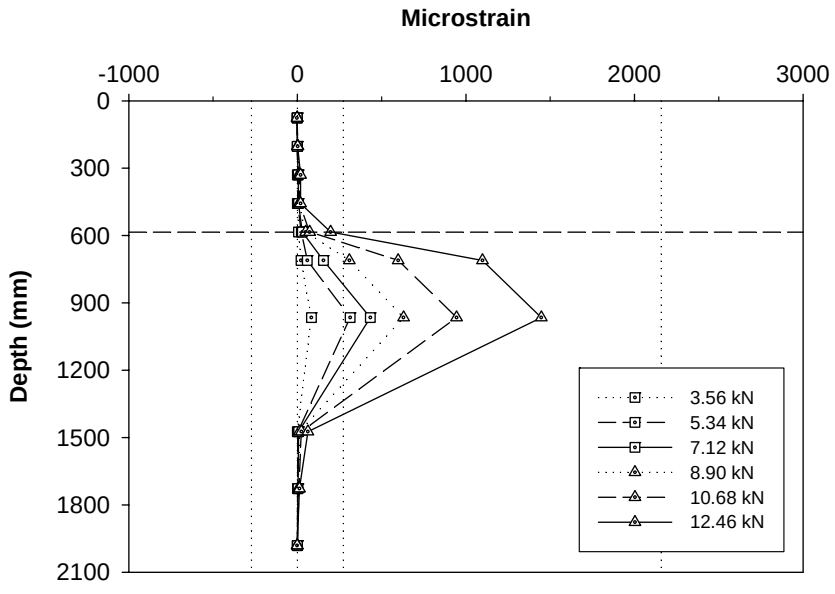

Figure G 12. Strain profiles for pile in weathered shale (Piles 10 A)

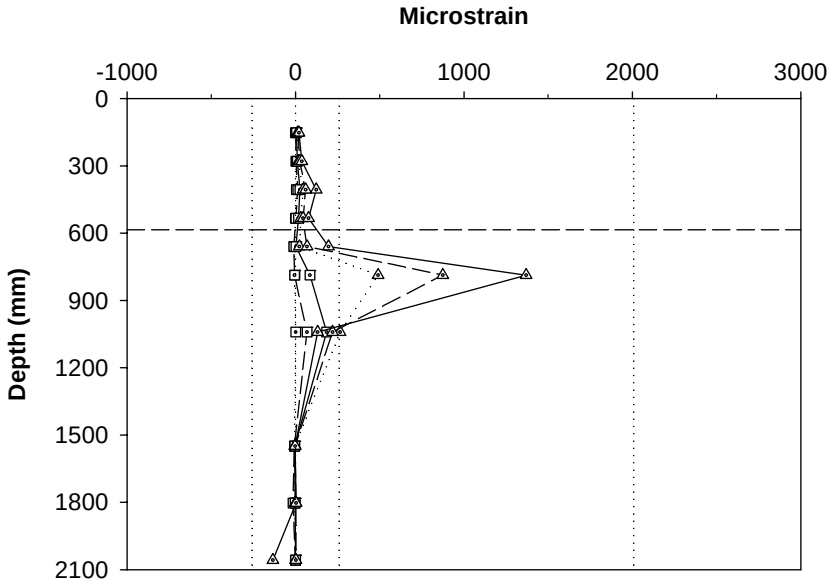

Figure G 13. Strain profiles for pile in weathered shale (Piles 10 B)

APPENDIX H: PILE BEHAVIOR CORRELATIONS PER TEST

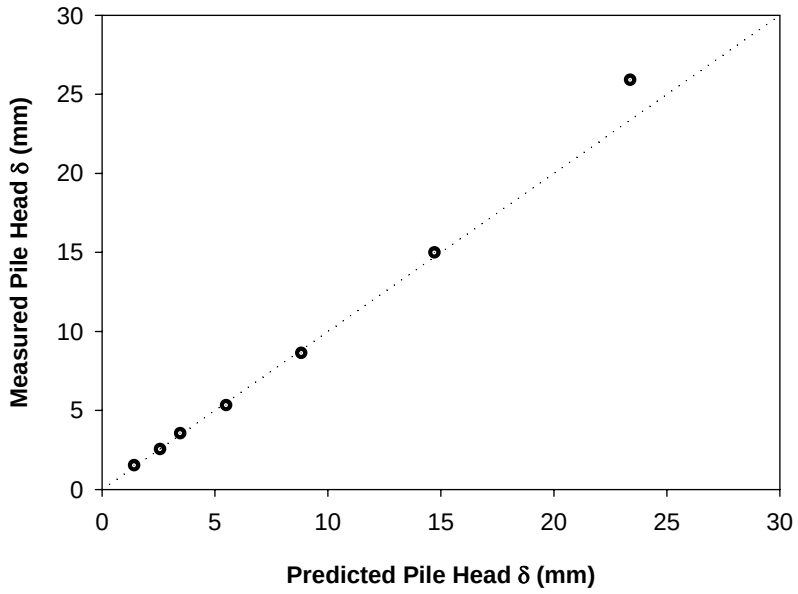

Figure H 1. Pile head deflection correlation in loess (Pile 4)

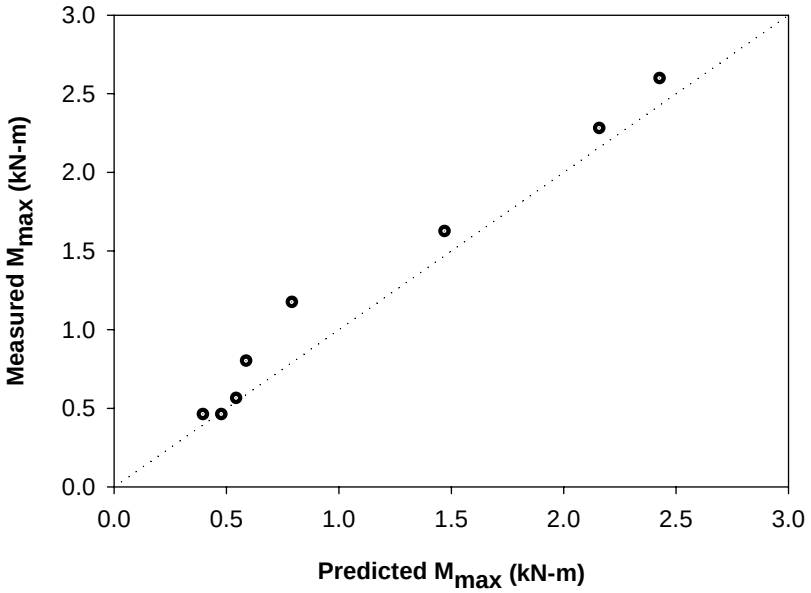

Figure H 2. Maximum moment correlation in glacial till (Pile 4)

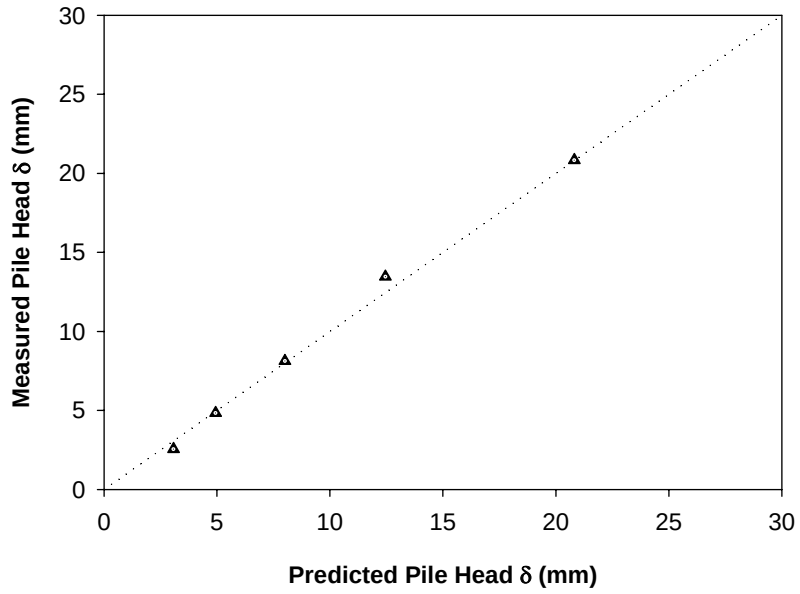

Figure H 3. Pile head deflection correlation in loess (Pile 5)

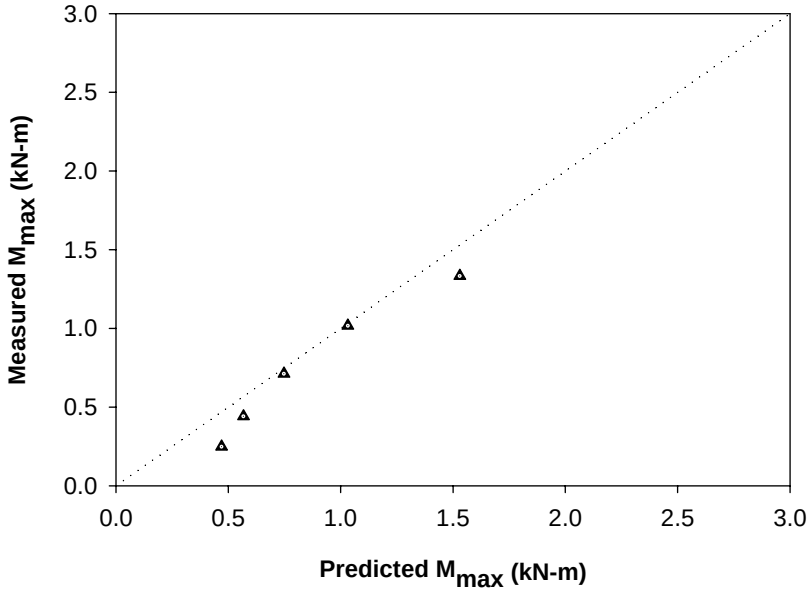

Figure H 4. Maximum moment correlation in glacial till (Pile 5)

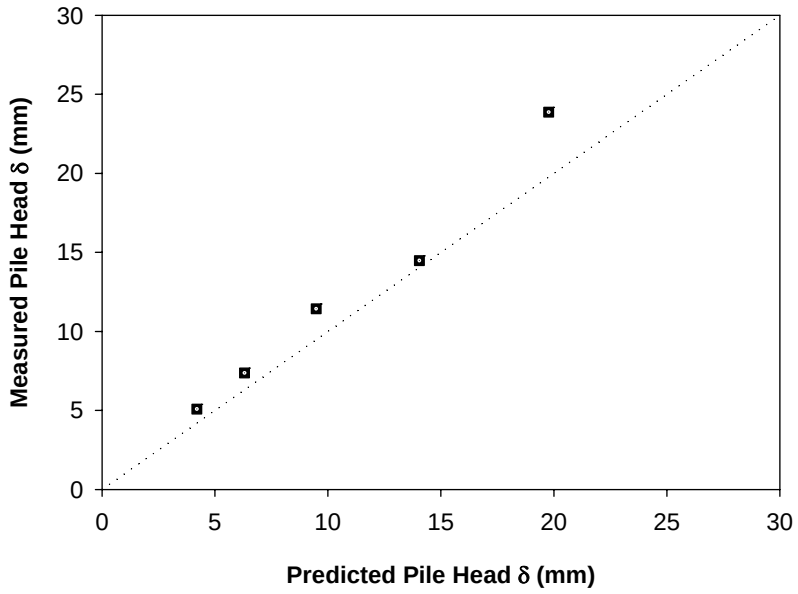

Figure H 5. Pile head deflection correlation in loess (Pile 6)

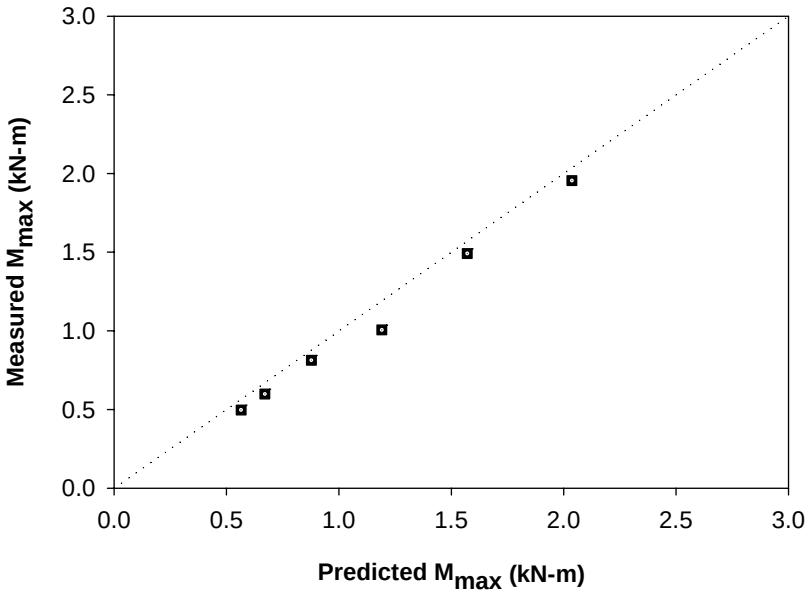

Figure H 6. Maximum moment correlation in glacial till (Pile 6)

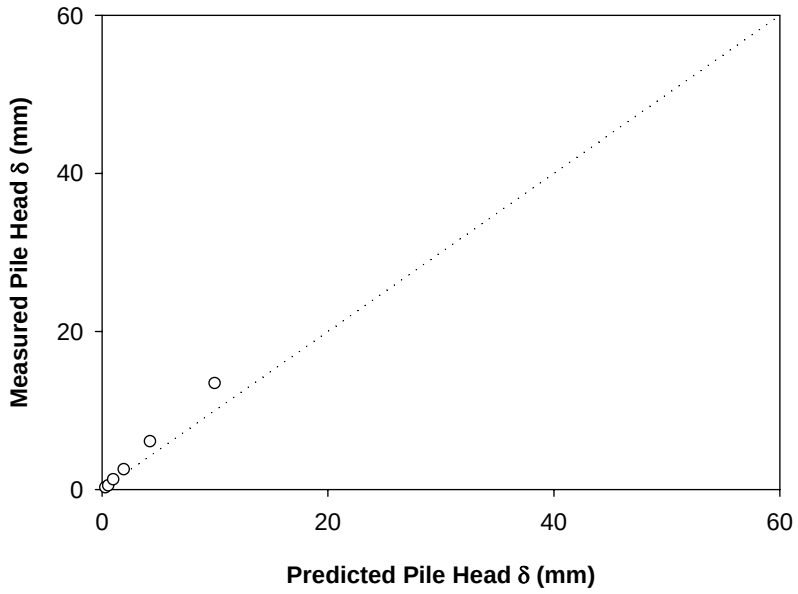

Figure H 7. Pile head deflection correlation in loess (Pile 8)

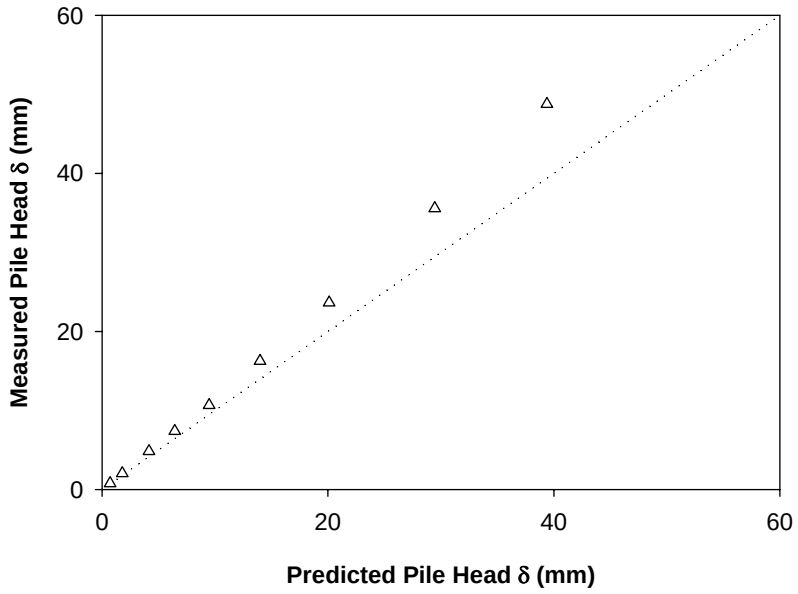

Figure H 8. Pile head deflection correlation in loess (Pile 9)

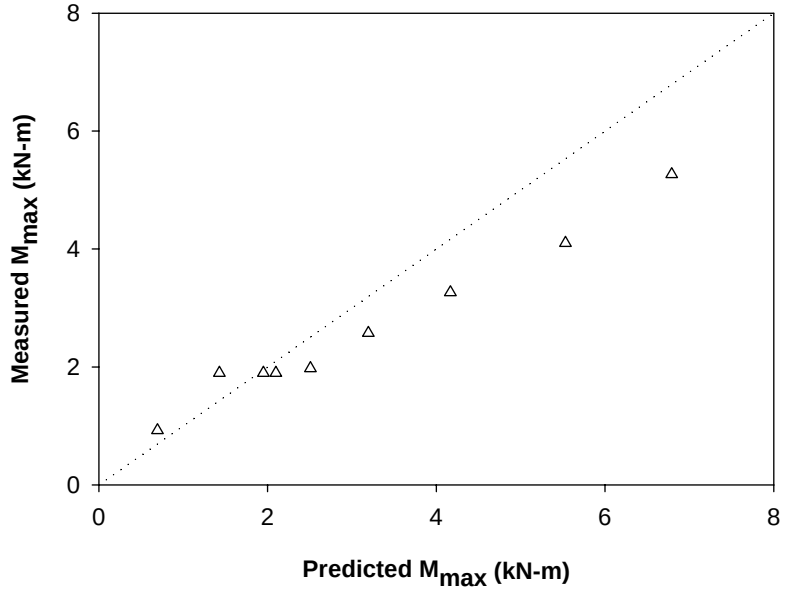

Figure H 9. Maximum moment correlation in glacial till (Pile 9)

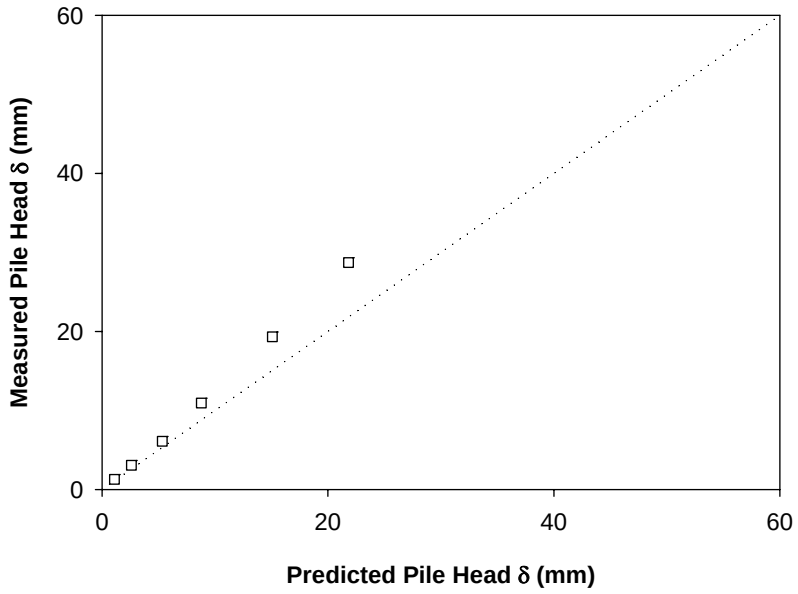

Figure H 10. Pile head deflection correlation in loess (Pile 12)

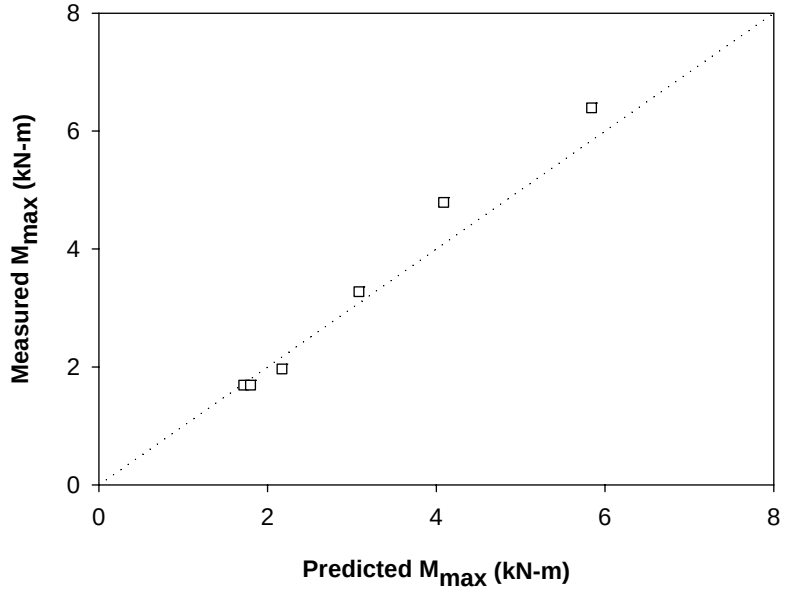

Figure H 11. Maximum moment correlation in glacial till (Pile 12)

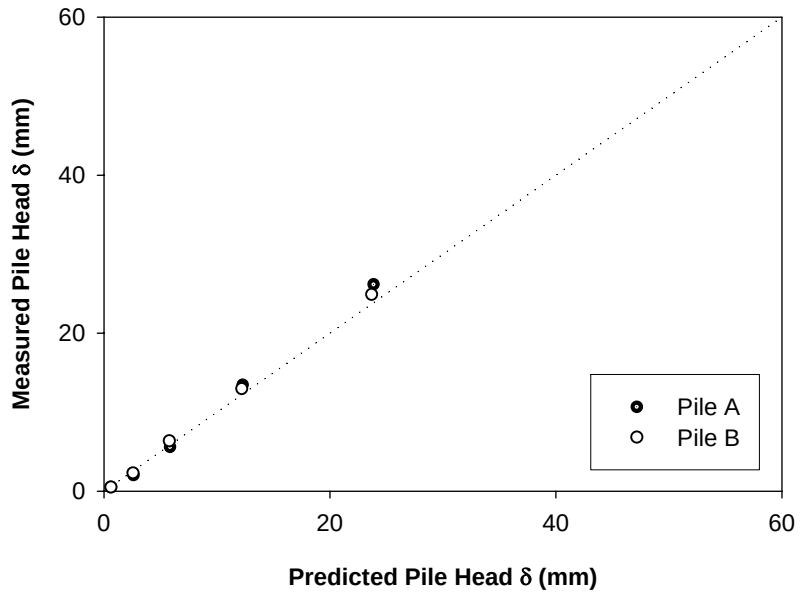

Figure H 12. Pile head deflection correlation in loess (Piles 11 A and B)

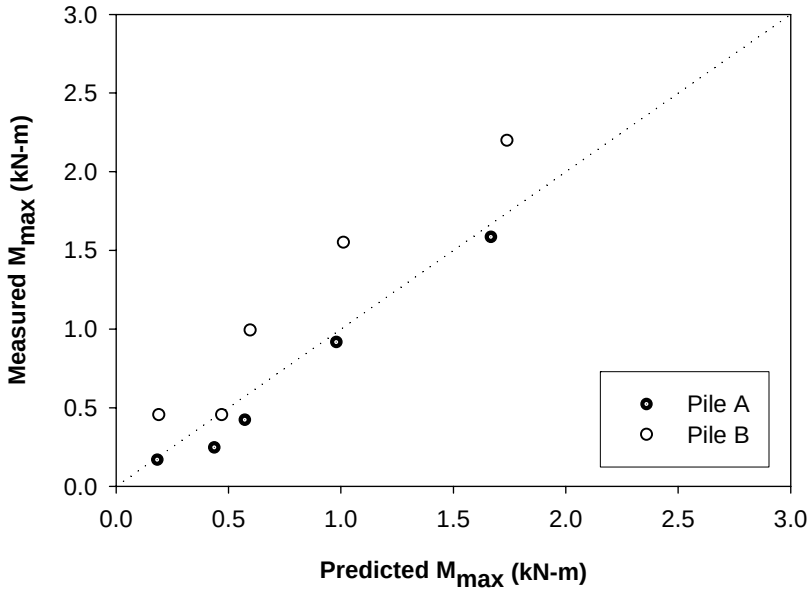

Figure H 13. Maximum moment correlation in glacial till (Piles 11 A and B)

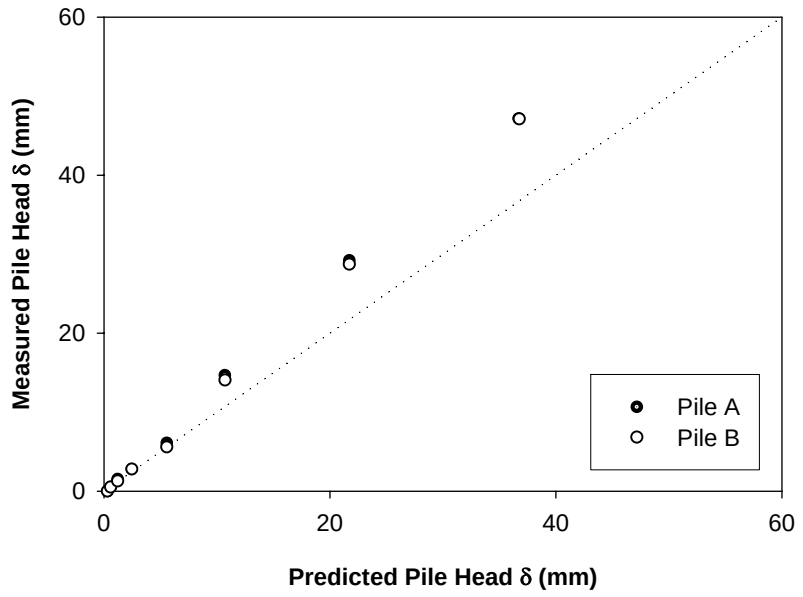

Figure H 14. Pile head deflection correlation in loess (Piles 13 A and B)

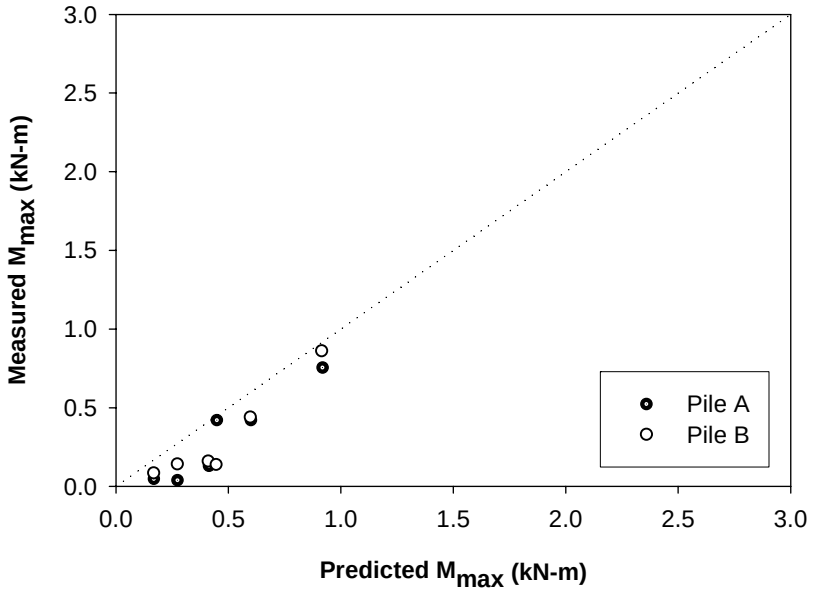

Figure H 15. Maximum moment correlation in glacial till (Piles 13 A and B)

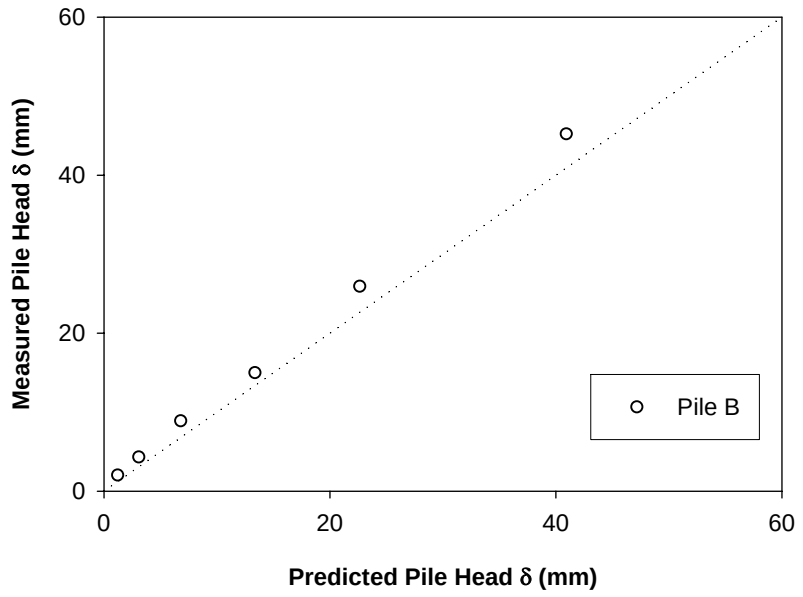

Figure H 16. Pile head deflection correlation in loess (Pile 14 B)

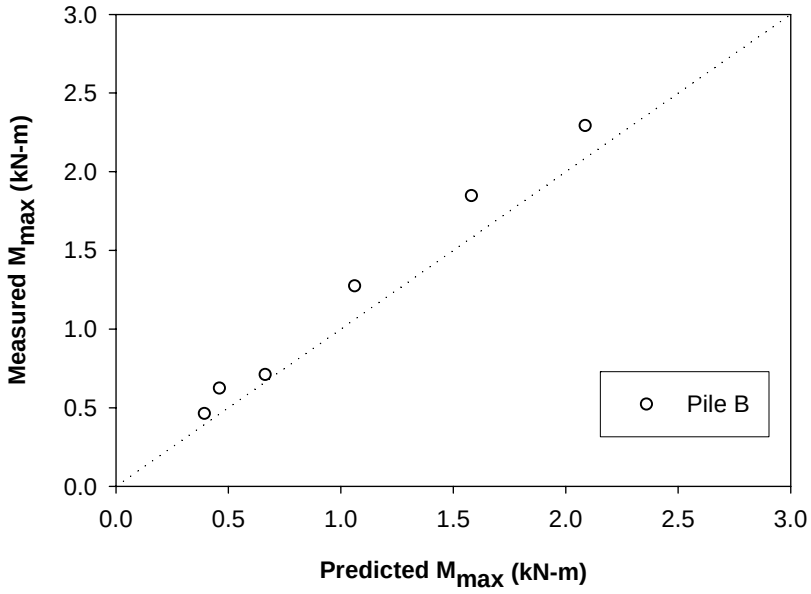

Figure H 17. Maximum moment correlation in glacial till (Pile 14 B)

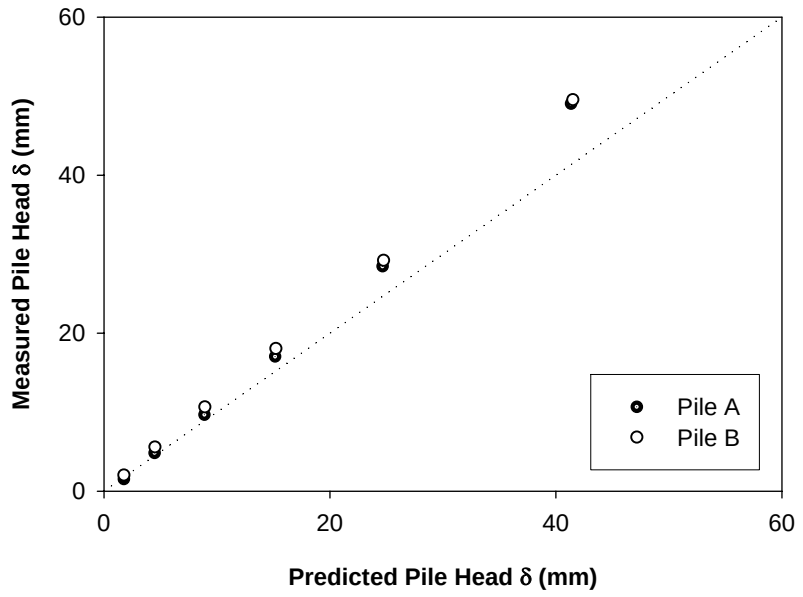

Figure H 18. Pile head deflection correlation in loess (Piles 10 A and B)

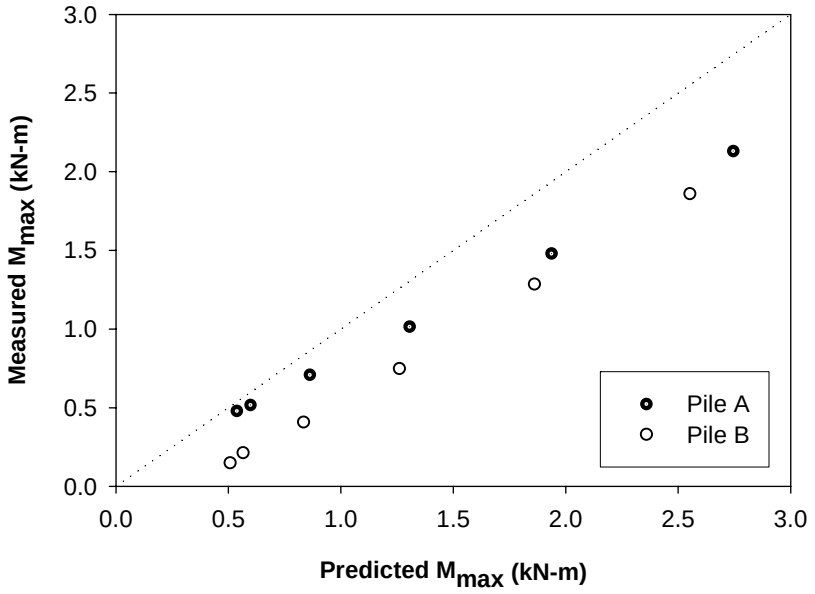

Figure H 19. Maximum moment correlation in glacial till (Piles 10 A and B)